GAS INCORPORATION IN SPUTTERED AND EVAPORATED METAL FILMS

A thesis presented for the degree of Doctor of Philosophy at the University of Keele

by

I. V. MITCHELL B.Sc.

Department of Physics,
University of Keele,
Keele, Staffordshire.

July 1972.

Synopsis

The argon and nitrogen gas concentrations in thin films have been measured for seven different metals. Sputtered and evaporated films are deposited on glass and tungsten substrates in a stainless steel ultra high vacuum system, which is designed to operate at background pressures in the 10^{-8} torr region, and at argon pressures of about $6\ 10^{-4}$ torr. The discharge is maintained by a triode type system and the plasma is confined with the aid of two magnet coils in a helmholtz configuration. The vacuum system is evacuated with ion and liquid nitrogen-cooled sublimation pumps. A second vacuum system is connected to the main deposition chamber by means of a gate valve so that the film samples can be withdrawn for study, using a rack and pinion mechanism, under continuously maintained vacuum conditions. The films are analysed by thorough outgassing in the second system, using an induction coil heater over a glass section of the system, so that desorption from other parts of the system is kept to a minimum. Gas analysis is achieved using a quadrupole mass spectrometer and the results are displayed on an XY recorder. Film thicknesses are monitored using a previously calibrated quartz crystal oscillator and the dimensions of samples and systems are known from careful measurement.

The argon and nitrogen concentrations are measured as a function of gas pressure, film thickness, target voltage, target and substrate species and substrate bias voltage. The sputtered films are always found to contain more argon than the evaporated ones. This may be accounted for partly by the additional process of ion reflection, which takes place at the sputtered target surface but not at the evaporated one. Increasing the bias voltage causes an increase in the argon concentration in most of the films. This can

be related to the noble gas clean-up effect, where energetic ions embed themselves in the film and become trapped by the continuous flux of metal atoms arriving at the surface. The results are in reasonable agreement with a theoretical model proposed by WINTERS et al. A comparison of the theoretical and experimental results makes it possible to derive sputtering yields for the gas. For argon, typical sputtering yields of $\sim$ 10-16 atoms/ion are obtained at high bias ion energies, indicating that the gas release is being brought about by a gas sputtering mechanism. Yields of the same order as those of the metal suggest that gas release by a target sputtering process predominates at lower ion energies. However, the division between mechanisms is not well defined and depends to a great extent on the target species. The results for nitrogen incorporation support Winters proposal that metals can be divided into three classes. The results show that the simple hypothesis that bias sputtering always brings about a reduction in the impurity gas contamination does not hold for all gas/metal combinations. It is shown for nitrogen, that the gas concentration can increase or decrease depending on the class of the metal and on the partial pressure of nitrogen present during deposition. Some of the films have been examined using an electron microscope. A significant change in the surface appearance is observed in some of the outgassed sputtered films which is not apparent in either the non-outgassed films or in the evaporated samples. The reasons for this are not clear at present.

ACKNOWLEDGMENTS

The author wishes to express his gratitude to:

Professor D.J.E. Ingram for the use of his laboratory and research facilities.

Dr. R.C. Maddison for his supervision throughout this work.

Friends and colleagues in the Physics Department, Keele, and in particular, Dr. S. Thomas, for their useful discussions.

Mr. F. Rowerth and his technical staff for their assistance in constructional work.

Mr. Wun Duc Lee and Mrs F. Grundy of the Computer Department for helpful assistance with the computer programmes.

Mrs. B. Haywood for the typing of the thesis.

The Atomic Weapons Research Establishment, Aldermaston, for the provision of a research assistantship and research funds to carry out this work.

My parents for their foresight, and my wife for her forbearance.

CONTENTS

CHAPTER I

1.1 Introduction

Atoms are ejected from the surface of any material under bombardment by ions or atoms of sufficient energy - this effect is known as 'Sputtering'. In the particular case, when an electrical discharge is passed between electrodes at a low gas pressure, the cathode is slowly disintegrated under the bombardment of the positively ionized gas molecules. Here the phenomenon is termed 'Cathodic sputtering'. The disintegrated material leaves the electrode surface either as free atoms (occasionally charged), clusters of atoms, or in chemical combination with the residual gas molecules.

An important parameter in sputtering experiments is the 'Sputtering yield'. This is defined as the ratio of the number of atoms liberated by the bombarding ions to the number of bombarding ions incident on the bombarded surface:

$$S = N_a/N_i$$

where S is the sputtering yield, N_a is the number of sputtered atoms, N_i is the number of bombarding ions.

Much of the early interest in sputtering was devoted to measuring this quantity for different materials under various conditions of ion energy, gas pressure, cathode/anode voltage, etc. BLECHSCHMIDT, for example, in 1926[12] published sputtering yields for over fifteen different metals using different ion species. However, for the reasons pointed out below, little credibility can be attached to these and other early data due to

their unreliability and irreproducibility. When some of the sputtered atoms are condensed on surfaces close to the disintegrating surface they form a thin 'sputtered film'.

Sputtering as a means of depositing thin films, particularly of metals, was noticed from the very beginning and was widely used for such, until the method of thermal evaporation superseded it about the turn of the century[13]. In the following thirty to forty years studies of the sputtering process were mainly concerned with investigations of the physics of ionic bombardment and not the production of films. The method of sputtering to produce films fell out of favour largely because the process had been considered a 'dirty' one (i.e. a large degree of impurity contamination) compared with thermal evaporation techniques. This was due to the early method of producing the bombarding ions in a glow discharge, with the corresponding high gas pressures needed, and the then poor vacuum techniques.

A renewed interest in sputtered films has taken place in the last twenty years, due initially to advances in the micro-electronics industry and its need for refractory metal thin films, semiconductors etc., however such phenomena as;

(a) the discovery of focussed collision sequences in crystals by WEHNER et al[14],

(b) the discovery of a technique by which dielectrics may be directly sputtered[15],

(c) the growing importance of doping and radiation damage in solid state physics[16],

(d) material and surface problems in space research arising from solar

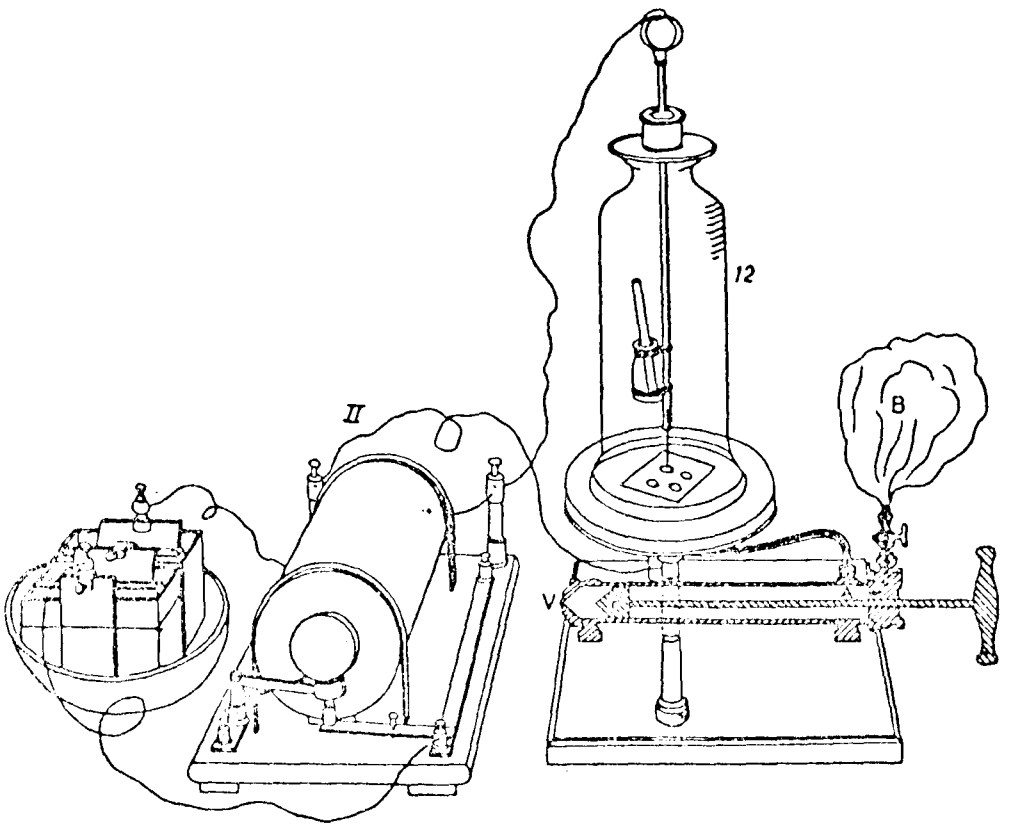

Grove's discharge tube in which sputtering was first observed in 1852.

Figure 1.1

wind and meteorite bombardment, of artificial and natural satellite surfaces[17],

(e) new vacuum techniques using ion pumps[18],

have all played a part in bringing about the renaissance of film production by sputtering.

With the development in the last few years of a host of new techniques both in vacuum technology[19] and ion production[20], the sputtering process has been rendered 'clean', and now compares favourably in this respect with evaporated films.

In this present investigation, now that it is possible to obtain sputtered and evaporated films of comparable quality, the impurity gas content of sputtered and evaporated metal films grown under, as nearly as possible, identical conditions can be compared and contrasted. Variations in gas pressure, film thickness, target species and voltage, and the new technique of voltage biassing of the growing film, are all used to try to ascertain the different processes occurring at the surface of the growing sputtered and evaporated films.

1.2 Early research

The phenomenon of cathodic sputtering was first noted by GROVE[21] in 1852, when he observed the disintegration of the cathode in a glow discharge tube. PLUCKER[22] in 1858 noticed similar effects, as well as the gradual disappearance of gas in a low pressure gaseous discharge tube, and in 1877 WRIGHT[23] specifically used cathodic sputtering as a means of depositing thin films. Figure 1.1 shows schematically Grove's apparatus.

Since then, an enormous amount of research has gone into sputtering

investigations, generating a prodigious amount of literature. Unfortunately, most of the quantitative results obtained up to 1940 must be discarded for several reasons;-

a). Until this time it was not generally realised that the basic apparatus used for sputtering worked at such high gas pressures (10^{-1} to 10 mm Hg) that the sputtered atoms could not escape from the cathode, but diffused back to it. Even at the lower pressure limit of 10^{-1} mm Hg the mean free path of sputtered atoms is about 0.5 mm. This is normally much less than the distance between cathode and collector and under these conditions the transport of sputtered material is essentially diffusion dominated. VON HIPPEL in 1926[24] estimated that the amount of sputtered material diffusing back to the cathode is of the order of 90%. This was demonstrated using a plane electrode arrangement having a cathode as close as possible to the collector (i.e. when the separation is just equal to the cathode dark space) and a gas pressure of 10^{-1} mm Hg.

b). The material having returned to the cathode may be deposited in an unpredictable manner[25,12] thus changing the surface properties and yield of the cathode.

c). The energy and angle of incidence of the bombarding ions is uncertain, since at the high pressures used, collisions occur in the cathode dark space. This creates the possibility of forming new, and multiply charged, ions. This problem was investigated by VON HIPPEL[24] who found most of the bombarding ions arrived at the cathode with very nearly zero kinetic energy.

Due to these and secondary effects such as the questionable purity of the ionising gases and the poor vacuum techniques of the time, the quantitative value of this early work must be considered as poor. One of

the few reliable sputtering experiments performed before the 1950's was carried out by GUNTHERSHULTZE and MEYER[26,27] in 1931 where they measured the sputtering yield of copper. Using an oxide coated cathode and a cylindrical anode they maintained an ion current density of $1mA.cm^{-2}$ on a copper disc 5 cm in diameter immersed in the main discharge, to which a voltage of -1000 volts was applied. With this arrangement the ion bombardment was essentially normal to the copper disc and had an ion energy equal to the full voltage dropped between the target and the plasma.

Reliable basic information on sputtering by positive ions began around 1940 with the work of PENNING and MOUBIS[28] who were the first to realise the importance of the pressure factor and the necessity of reducing it to a point where back diffusion becomes unimportant.

A glow discharge with a high current density cannot be maintained at pressures lower than about 10^{-1} torr because the electrons released from the cathode have such long mean free paths (around 1 cm) that many of them reach the anode without ionizing any gas atoms.

Penning and Moubis overcame this problem by increasing the total electron ionizing path between the electrodes with the introduction of a suitably designed magnetic field. The apparatus consisted of a water cooled cylindrical cathode 2 cm diameter and 25 cm long, surrounded at each end by anode rings. The magnetic field was applied parallel to the axis of the cathode cylinder. It was found possible, with this arrangement, to work at pressures of about 10^{-2} torr and still obtain high deposition rates with ion energies of 500 to 1500 volts and ion current densities of about 20 $mA.cm^{-2}$.

Although many experimental investigations of sputtering were carried out up to 1940 to try and determine the processes of metal removal

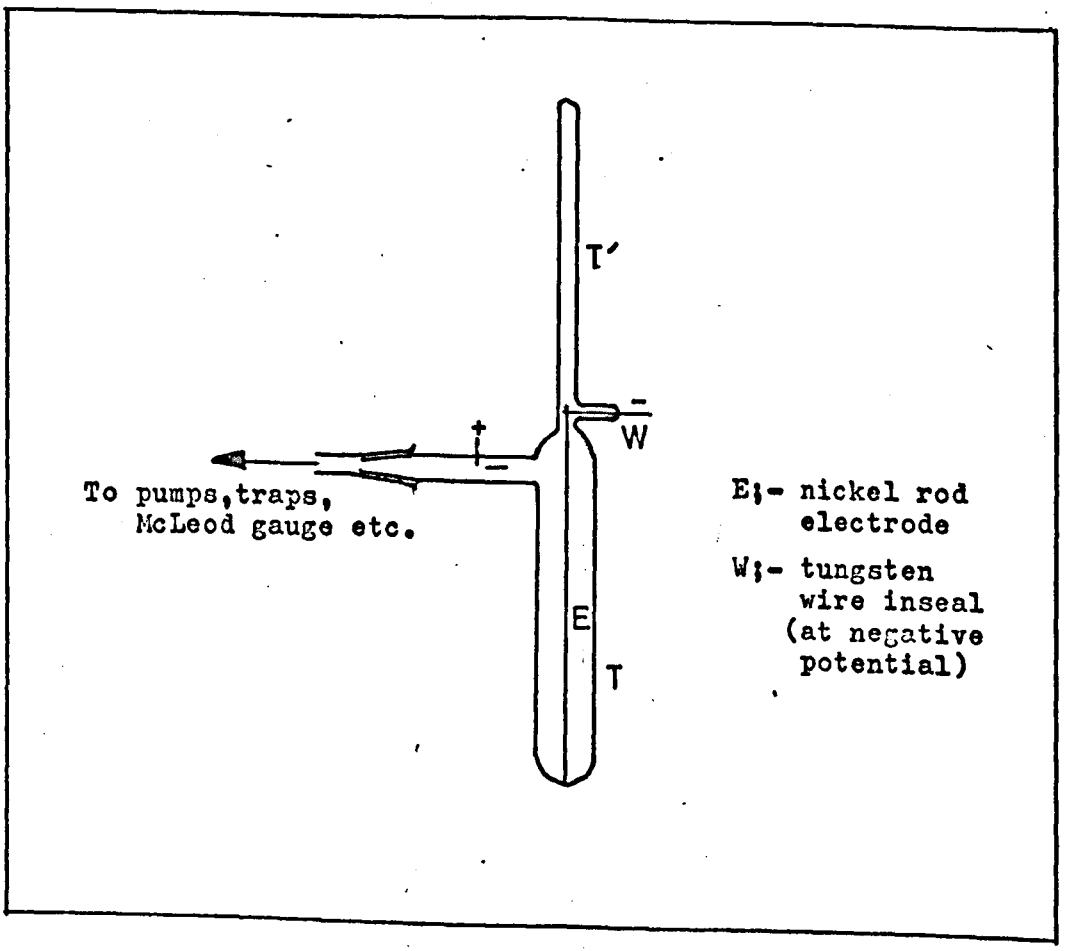

Figure 1.2 Sputtering apparatus of INGERSOLL and HANAWALT.[32]

from cathodes, very little was undertaken in comparing the properties (a) of sputtered and evaporated films and (b) their relative gas contents.

An exception to (a) was the investigation carried out by DITCHBURN[29] in 1933. Knowing from experiments by WOOD and others[30,31] that a critical nucleation density exists during evaporation below which metal atoms will not condense on a glass or metal surface, he both sputtered and evaporated films of cadmium to determine the existence of a similar phenomenon for sputtering. In contrast with evaporation he found no minimum deposition rate below which the cadmium films could not be deposited by sputtering.

An exception to (b) was a series of experiments carried out by INGERSOLL and HANAWALT in the mid 1920's[32]. Their studies on the gas contents of sputtered nickel films and their comparison with evaporated films are of especial interest to the present investigation and are described in greater detail below. It must be remembered, however, that the same restrictions to the reliability and validity of their results apply as to that of the other early workers.

A nickel electrode was mounted centrally along the axis of a pyrex tube, 2.5 cm in diameter. The tube T, Figure 1.2, was joined through a ground glass joint to a vacuum pumping system, and was connected to a McLeod gauge. Nickel was sputtered onto the inside surface of T when a voltage was applied between the cathode and a point anode. By inverting the tube, the nickel electrode could be moved to its other end T', the film could be heated away from the nickel electrode and the gas emission or absorption from it studied. Argon, helium, nitrogen and hydrogen at gas pressures between 0.1 to 2 torr were maintained in T, and with discharge voltages from 700 to 1400 volts, the current density on the cathode was of

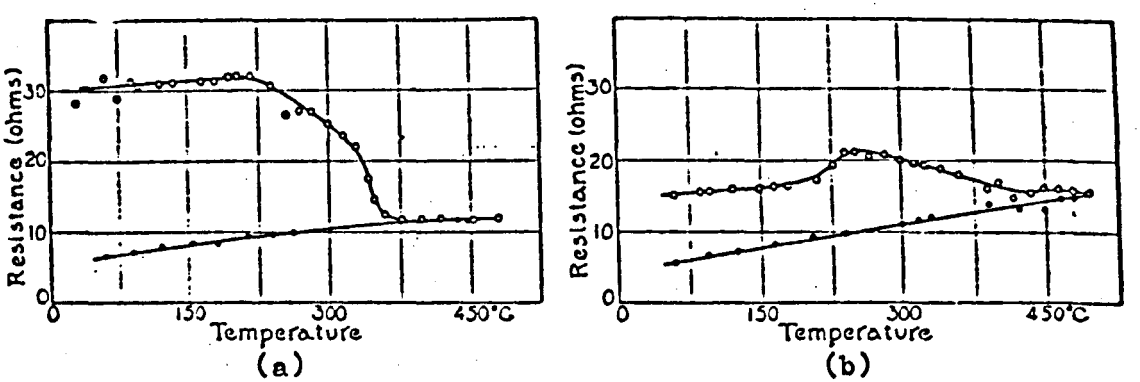

(a) Resistance - temperature curve for nickel film sputtered in 0.5 mm Hg argon.

(b) Resistance - temperature curve for nickel film evaporated in 0.5 mm Hg argon.

Figure 1.3 (a) and (b)

the order of a few milliamps cm^{-2}. After sputtering, the tube was inverted and the system pumped down and sealed off. The pyrex tube and deposited film was slowly baked and the resulting pressure increase measured, minute by minute, with the pressure gauge.

Ingersoll found, with this apparatus, that large quantities of gas were given off from the sputtered films, the most rapid emission being at about 300-400°C. He calculated concentrations of the order of 40 atomic % of occluded gas for films sputtered in argon. He further suggested that the concentrations could rise as high as 100 atomic % if chemical or 'quasichemical' compounds could be formed between the metal and the gas (such as NiA, Ni_2A, ...).

Ingersoll tried also to make a comparison between the amount of gas occluded in sputtered films and evaporated films. For technical reasons he could not do this directly, so he measured the change in resistance that took place when he slowly baked the two films under vacuum. Both films were grown on microscope slides under similar conditions. Making the assumption that the fall in resistance is associated with the escape of gas from the films, he showed that the evaporated films contained much less gas than the sputtered ones, even when the two were produced at the same pressure. Figures 1.3a and 1.3b indicate the results he obtained.

This was unexpected, since at that time the sputtering mechanism was best explained by the 'Evaporation from localized hot spots' theory of VON HIPPEL[33,24]. From this theory it might have been expected that the gas content of both types of film would be comparable. He explained the discrepancy by suggesting that the large gas content in the sputtered films was due to the excitation of the gas atoms accompanying the discharge which

favoured absorption and actual chemical union.

It is unfortunate that he did not use an independently supported discharge such as that described by GUNTHERSHULTZE and MEYER[25], in which case it would have been possible for him to deposit evaporated films in the presence of a discharge. In this way he would have been able to put his suggestion to the test.

Notwithstanding this, the quantitative aspects of Ingersoll's experiments were in doubt for other reasons, such as:

a). The poor vacuum techniques. This made it highly likely that there was a large pressure of chemically active impurities present in the vacuum system during film deposition, which was masked by the high discharge pressures used.

b). The high argon pressure itself made diffusion the predominant factor rather than sputtering.

c). Without the use of any mass spectrometric technique, it was not even certain which gases were coming from the baked films, although it was assumed throughout to be that of the residual atmosphere.

Little advance was made on this topic for the next twenty years or so until the 1950's, when, with the renewed interest in the phenomena of electrical clean-up of gases in cold cathode discharge tubes[34], and improved vacuum techniques, a re-examination of gas incorporation in sputtered and evaporated films became possible.

1.3 Conclusion

Although even from the earliest times a great interest was shown in sputtering, with a view to understanding the mechanism by which it takes place and as a means of depositing thin metal films, it was not until

about 1940 that it was fully realised that the very conditions under which the films were deposited made the understanding of the sputtering mechanism impracticable. In addition, due to the high gas pressures used in the glow discharge, with the correspondingly short mean free path of ions and the uncertainties in their energies, the deposition of thin films with reproducible properties was rendered highly unlikely.

However, although the early work appears to be of doubtful validity in a quantitative sense, these investigations did give an insight into the complexity of the problem, compared for example, with the evaporation technique which was interpreted correctly as far back as the turn of the century. Furthermore, they indicated the lines along which future research had to proceed to achieve a fuller understanding of the sputtering mechanism.

CHAPTER II

2.1 Introduction

Sputtering, in contrast with the simplicity of thermal evaporation, is a complicated process, and the properties of sputtered films are greatly dependent on the numerous, and often competing processes, occurring in the gas discharge. For this reason, the first part of this chapter is devoted to a description of the basic processes occurring in a gas discharge. An understanding of these is necessary if the interpretation of sputtering experiments is to be successful. The middle section of this chapter (2.3) discusses the processes occurring at the target surface, film surface and in the discharge, which go to increase the contamination of the growing film. The final section (2.4) describes the various scattering and adsorption processes taking place at a pure metal target when bombarded by inert gas ions.

2.2.1 Self sustained glow discharge

When a DC voltage is applied between two separated electrodes in a gas at low pressure a current will flow between them providing that the voltage is above a certain minimum value called the breakdown potential. This breakdown potential is also pressure dependent[35].

At a given pressure, above the minimum value, the current flowing will increase with electrode spacing. Consider a single electron leaving the cathode and moving towards the anode, under the influence of the applied voltage. If the energy acquired by the electron is greater than the ionization potential of the surrounding gas atoms, a fixed number of ionizing collisions

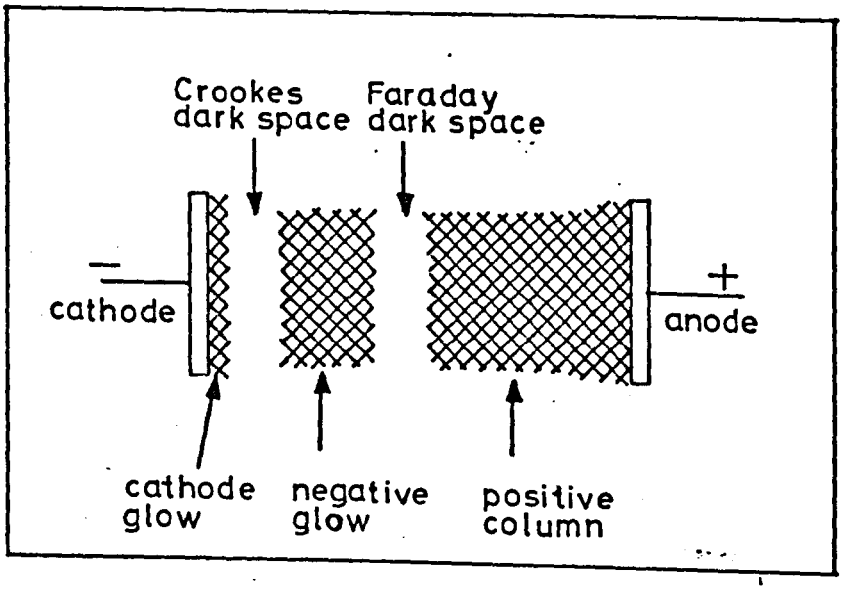

Figure 2.1 CROSS SECTIONAL VIEW OF GLOW DISCHARGE

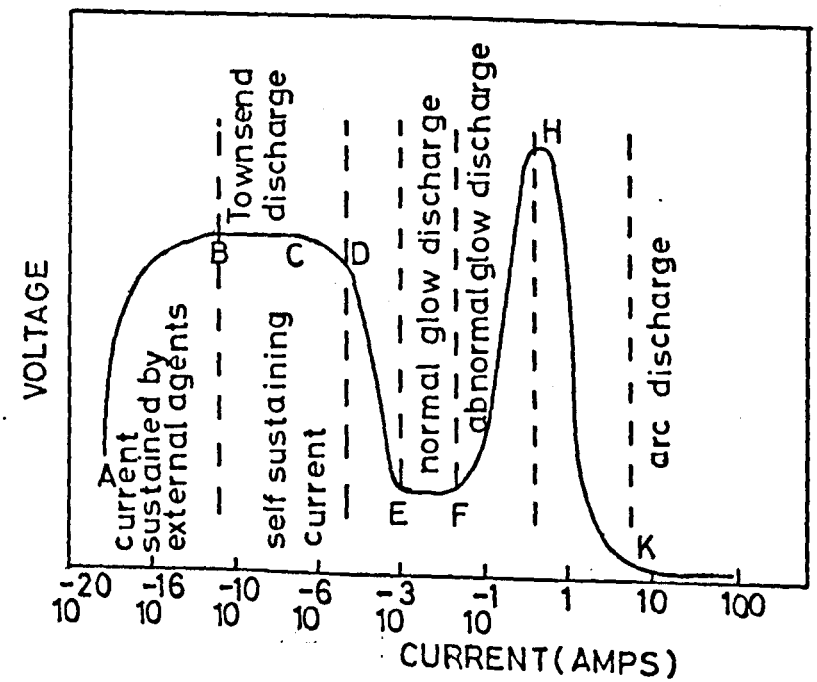

Figure 2.2 CLASSIFICATION OF DISCHARGES

per unit path length will take place. Thus, the greater the electrode spacing the more ionizing collisions take place. The number of generated electrons reaching the anode, will be greater than the original number, (i.e. one, in this case), assuming that no electrons are lost by diffusion out of the inter-electrode space. The ions which are produced at the same time travel towards the cathode. If they acquire enough energy in this journey, they will, on striking the cathode both sputter the cathode material and eject secondary electrons from its surface. These secondary electrons will in subsequent steps collide with further atoms of the gas, generating new ions and electrons in an avalanche type process. Gas breakdown is said to have occurred, and a 'glow discharge' results.

This might imply that the glow would spread uniformly between the electrodes, but this is not the case as can be seen from Figure 2.1. A principal feature of the discharge is the 'cathode dark space', also called the 'Crookes space'. In this region the positive ions have accumulated to form a space charge in front of the cathode. The thickness of this space charge is approximately equal to the distance travelled by an electron from the cathode before it makes an ionizing collision. To the right of the cathode dark space in Figure 2.1 can be seen the negative glow region. This is a region where the ions and electrons are of very nearly equal numbers and is called the 'plasma' of the glow discharge. A voltage - current graph of such a glow discharge, between flat electrodes, is shown in Figure 2.2.[36] In practice, only the 'abnormal glow discharge' mode of operation is of interest in sputtering[37], since this is the only situation where the ion current density and applied voltage are both increasing. In the 'normal glow' mode the current density and the voltage are too low

for useful sputtering rates to proceed[38]. To maintain a glow discharge of the type described, high gas pressures of about 70 millitorr are required and a large voltage of several hundreds of volts must be maintained between the electrodes. In this situation it has been shown[39] that charge transfer , between ions and gas atoms, is a strong effect which will determine the percentage of energetic ions able to achieve the full cathode potential drop on crossing the cathode dark space. In addition the energetic neutrals and doubly charged ions created by the charge transfer effect can bombard the cathode and cause sputtering. Sputtering of the cathode therefore arises from particles of various energies, angles of incidence, and states of excitement[40]. These will in turn affect the deposited sputtered films, often collected on a substrate in the vicinity of the anode, making their properties rather inconsistent. All these problems arise because of the need to use both a high gas pressure, giving a small mean free path, and a high inter-electrode voltage, so that a large number of ionizing electrons can be sustained. If the gas pressure is reduced below 10-20 millitorr, or the voltage below several hundred volts, the glow discharge will be extinguished. To provide sufficient electrons to keep the glow discharge running, whilst at the same time reducing the pressure and voltage, a hot cathode which emits electrons thermionically rather than by secondary emission is substituted for the normal cold cathode. Such a system is called a thermionically supported glow discharge.

2.2.2 Thermionically supported glow discharge

For this type of discharge there is no longer a need for an avalanche type process to provide the electrons, and a stable discharge can

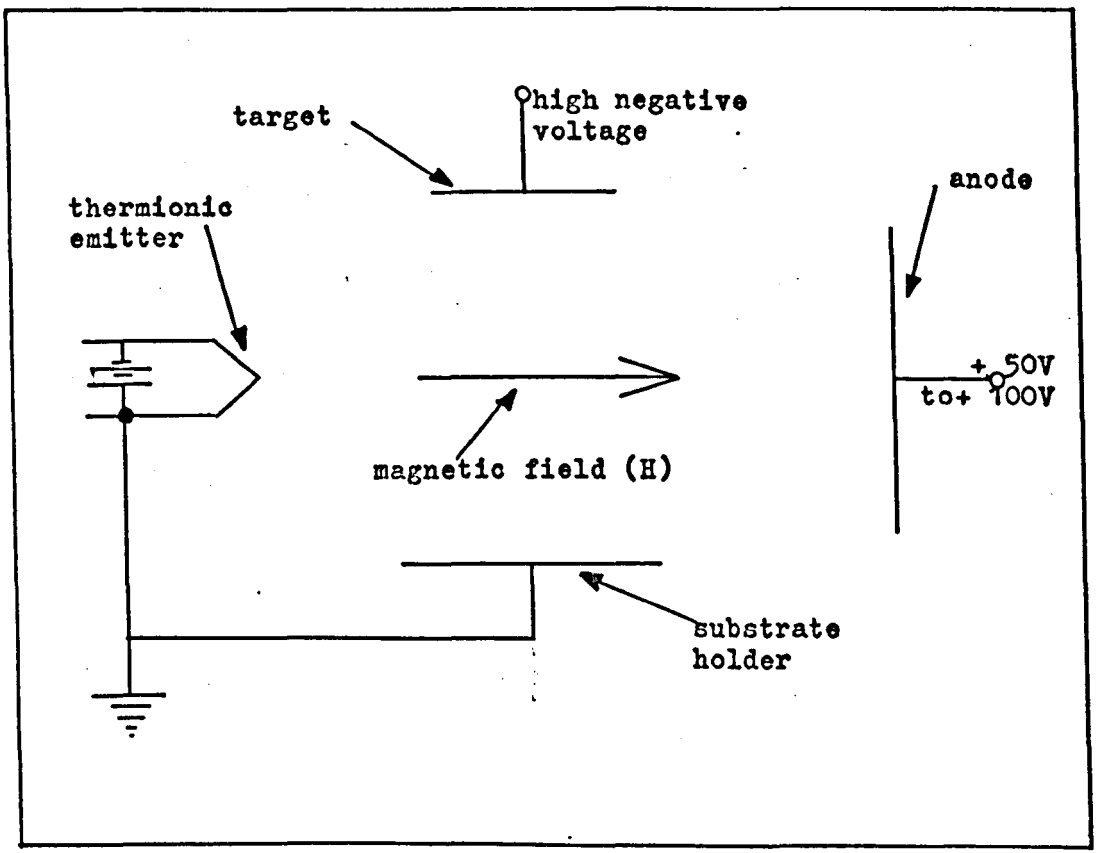

Figure 2.3 Schematic diagram of the thermionically supported glow discharge arrangment (adapted for sputtering)

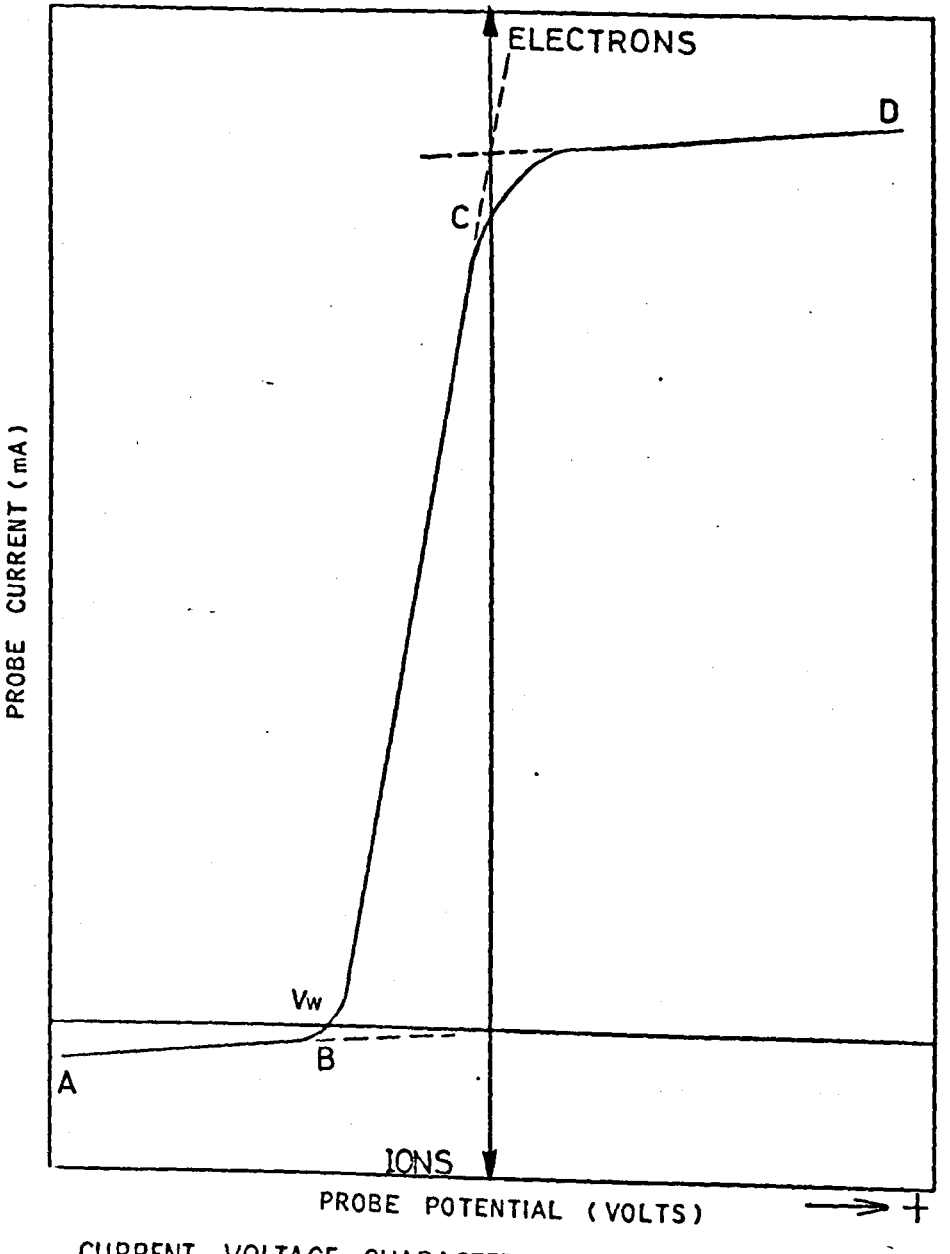

CURRENT VOLTAGE CHARACTERISTIC OF A LANGMUIR PROBE

Figure 2.4

be maintained at pressures as low as 1.0 millitorr with applied potentials only slightly higher than the ionizing potential of the gas[41].

Although the glow looks similar to that of the self supporting discharge it is in some respects quite different. For example, under these conditions the dark space in front of the hot cathode consists of a 'double sheath'. Here, closest to the cathode, is a negative electron sheath and this is followed by a positive ion sheath adjacent to the plasma. The ion sheath not only helps to neutralize the electronic space charge surrounding the cathode, but acts as a virtual anode placed close to the cathode. In this way, even at low potentials, the electron current reaches values closely approaching those obtained in high vacuum and with high potentials across the discharge. The full emission current of the cathode can be drawn at potentials as low as several tens of volts. The material to be sputtered can no longer be used as the cathode, which is now a thermionic emitter at low potential, and consequently it must be inserted as a target, or probe, in the plasma region of the discharge. Figure 2.3. shows a schematic diagram of the general arrangement. To sputter the target, which in this case must be electrically conducting, a negative potential must be applied to it so that ions from the plasma region will be attracted and strike it with energy sufficient to sputter its surface. The target therefore acts as a large 'Langmuir probe'[42], having a current-voltage characteristic similar to that shown in Figure 2.4. Only the region AB is of relevance to sputtering, since B to D is the region for electron collection. At large negative probe potentials, i.e. region AB, the electrons in the plasma will be repelled from the probe, in contrast to the ions which are attracted to the probe. An ion sheath is created in front

of the probe which shields the plasma from it. This sheath appears dark and is known as the 'Langmuir sheath' or the 'positive ion sheath'. The sheath thickness d, the probe voltage relative to the plasma V, and the ion current density, j, to the probe can now be related by the equation[9]

$$d^2 = 4\varepsilon_o/9j(2q/m)^{1/2} V^{3/2}.$$

where m is the mass of the ion, q is the electronic charge, ε_o is the permitivity of free space.

Ions, which arrive at the sheath edge by virtue of their thermal motion in the plasma, are attracted to the target probe and are accelerated across the sheath. The number of such ions arriving per unit area per second is given by:-

$$j = (nqv)/4.$$

where n is the density of the ions in the plasma region and v is the average thermal ion velocity in the plasma. This represents the space charge limited ion current density which should be independent of the magnitude of the negative probe potential, if the probe is small compared with the mean free path of the ion. However, in the practical sputtering situation the target probe is usually large and this condition does not hold. In this case, the boundary of the sheath is diffuse and the ion current varies slowly with probe potential, as seen in Figure 2.4. Because of the existence of the Langmuir sheath, and the low pressures employed, the ions which reach the sheath edge are rapidly accelerated towards the target without any collisions taking place in the sheath itself. These will impinge on the target with an energy equal, or closely equal, to the

total probe/plasma potential[43]. In addition, if a plane target is used which is large compared with the sheath thickness, the ions will strike the target normally. This is not the case, however, at the rim of a plane target[90], a situation which is discussed in more detail in chapter 4. High sputtering rates can be induced since the ion current density on the target can be made large by making the ion density in the plasma large. The independence of the target current and voltage variation from the main current in the discharge also make this type of arrangement ideal for preparing thin films by sputtering[5]. At the low gas pressures used there is a good chance that charge transferal will not take place and that particles sputtered from the target will not collide with other atoms.

If the gas pressure in the discharge is to be reduced still further it may be necessary to introduce a magnetic field, thus establishing a magnetically supported glow discharge.

2.2.3 A Magnetically and thermally supported glow discharge

As the gas pressure is reduced, the number of ionizing collisions made by the electrons also decreases. A point is reached where an electron may reach the anode, from the cathode, without having a single ionizing collision with an atom. In this case the glow discharge will be extinguished. The ionizing efficiency of the electrons may be improved, and hence sputtering proceed at lower pressures, by increasing the time the electron spends in the gas. A magnetic field applied parallel to the electric field between the anode and cathode will achieve this. Two mechanisms operate:- the first causes electrons that are not moving parallel to the magnetic field to describe helical paths around the lines of magnetic force, thereby

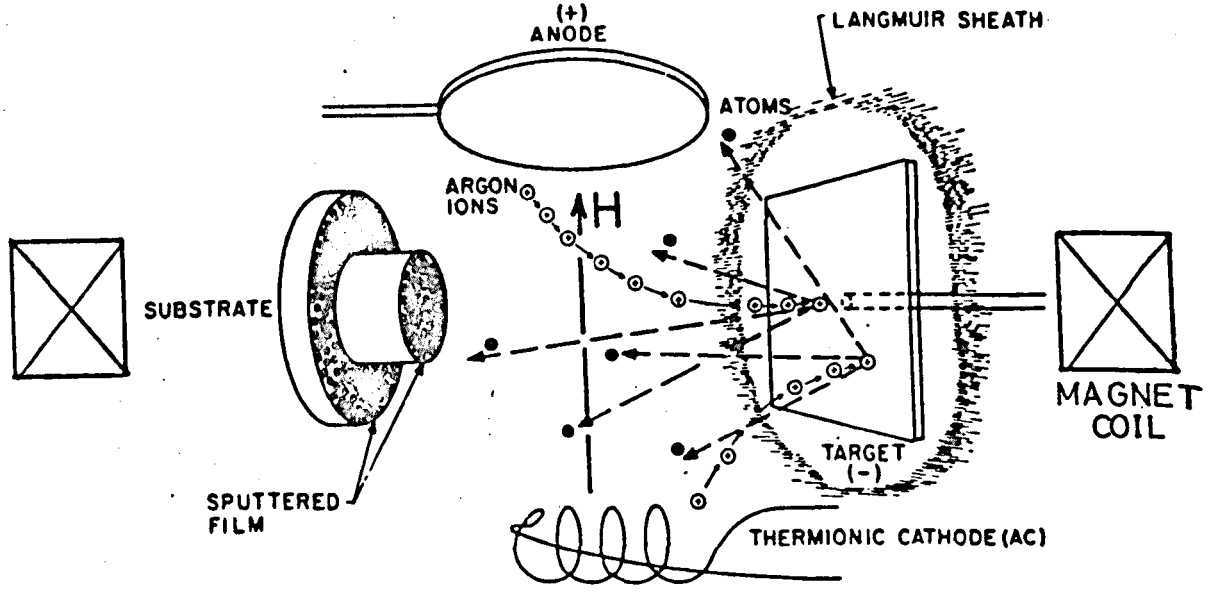

Sputtering Process Schematic

Figure 2.5

increasing the electron path length and hence the time spent in the gas. The second, 'the magnetic bottle'[44] effect, operates by impeding radial diffusion of the electrons out of the glow, so that electrons, which would otherwise be lost, are available for use. Other configurations of magnetic field have been used, such as, transverse[45], and quadrupole[46], but these have not been found to be as useful in sputtering as the longitudinal[9a].

High deposition rates can be produced, even at gas pressures as low as 0.1 millitorr, with a system as schematically outlined in Figure 2.5[47].

2.3 The problem of contamination

2.3.1 Introduction

Sputtering is often referred to as a 'dirty' process as a means of film deposition, when compared with the thermal evaporation method. 'Dirty', here, alludes to the purity of the deposited film which ideally should be composed entirely of the pure source material. This 'dirtiness' may arise for a number of reasons, such as:- high background pressures, the sputtering of extraneous surfaces, for example, vacuum system walls, etc., the gas clean-up phenomena, and the removal of impurities present in the source which find their way into the growing film.

2.3.2 At the source

i. Diffusion

As far as diffusion problems are concerned quite a different picture of contamination arises between thermal evaporation and sputtering processes. The diffusion of gas from within the sputtering target to its surface should be negligible compared with evaporation[7], since the

Purity %	99.995	99.995	99.99	99.99	99.8	99.97	99.7
Material	Al	Cu	Au	Ni	Ti	W	Zr
Impurity (ppm)							
C	15	-	2	50	150	20	40
H	2	1	1	2	30	5	20
O	35	2	10	20	300	25	200
N	5	0.1	3	5	40	10	75

Table 2.1. (taken from MRC handbook page 91 revised edition 1969)

Gaseous impurities found in various pure samples of Marz grade metals.

temperature of the metal target material can easily be kept below 100°C, by external cooling, whilst sputtering is proceeding. This ensures that the diffusion rate of impurity atoms to the surface will be low. On the other hand, in the case of thermal evaporation, the bulk temperature of the metal must generally be raised to a level somewhere near, and, in some cases even above, its melting point if useful rates of vaporization of the metal are to be obtained[48]. In the case of the refractory metals, these temperatures may be as high as 3000°C where the diffusion of impurity atoms to the surface presents a much more serious problem. In this case, in contrast to sputtering, thorough outgassing of the bulk sample is necessary before a pure film can be obtained.

ii. Surface layer contamination

In sputtering, it is from the surface layers of the target that most desorption of unwanted impurities derive, since it is this part which is most directly affected by the incident ions, which often possess considerable energy[49]. When sputtering begins, a fraction of the atoms making up the surface layers of the target, will arrive at the substrate. This includes any impurity atoms which happen to have been in the top layers of the target at the time. The condensation of these impurity atoms on the substrate surface depends on many factors, for example:- the rate of arrival at the substrate[50] and the chemical nature of the system involved[51]. Since many target surface layers have to be ejected to form a film deposit of reasonable thickness this source of contamination can be noticeable. Even the purest sputtering samples available usually contain incorporated gas species. For example, Table 2.1 shows the gas impurity content of some of the purest sputtering samples commercially available.

The amount of impurities at the surface of the target during ion bombardment of the surface may be even higher than in the bulk of the material because a small fraction of the occluded gases beneath the surface layer and within the ion bombardment damaged layers, usually less than 100Å, may be forced into the top layer as a result of internal collisions between the primary and 'knock-on' particles[7].

iii. Alloying

The problem of alloying is relevant only to the evaporation process, since in the sputtering arrangement the target is normally self supporting, and even if not, is usually maintained at relatively low temperatures. With the thermal evaporation technique, however, it is often found necessary to support the source material in a refractory container such as, tungsten, tantalum, molybdenum or carbon. In some cases these might tend to alloy themselves with the source material, especially at the high temperatures encountered in evaporation[52,53].

2.3.3 At the surface of the growing film

In addition to the contamination occurring at the growing film, which arises from the source, contamination may also occur at the substrate surface because of the chemically reactive and inert gases present in the vacuum system.

It should be possible with good vacuum techniques, to reduce the contamination effects of the chemically active gases to about the same level for both processes. On the other hand, the amount of inert gas present during sputtering is always large. For this reason the effects of inert and chemically reactive gases will be considered separately.

i. Compound formation

One of the ways by which it would be possible to incorporate inert gas atoms into the growing film, would be the formation of 'compounds' between the metal and gas atoms in the glow discharge similar to the 'gas compounds' like HeH_2^+ and Ar_2^+ which have been shown to exist in a glow discharge[54,55,56]. It is likely, however, that any 'compounds' so formed would be unstable, and would not remain long in the film[57].

ii. Clathrate formation

These compounds are formed by 'molecular imprisonment' rather than the establishment of valency bonds[58], the combined 'molecules' being held together mechanically by the retention of the inert gas atoms in 'claws' or closed 'cages' provided by the structure of the host. Although complexes involving inert gases are known to exist, such as the gas hydrates[59], they would be highly unstable in a glow discharge[7].

It is nevertheless quite possible for inert gases to be trapped in a thin film without involving themselves in chemical bonding, if the right conditions prevail. Such a condition is that the film deposition takes place in the presence of a glow discharge.

iii. Gas clean-up

This is probably the most dominant of the processes occurring, in the presence of a glow discharge, by which the inert gas finds itself incorporated in the growing film. Before the inert gas can be incorporated in the film it must first be sorbed at or near the film surface[60]. Since this is unlikely to occur with any of the processes mentioned in this section such as, physisorption (at least not at room temperatures)[61], chemisorption, etc. another mechanism must exist.

It is well known that inert gas ions have a significant probability of being sorbed on collision with a surface[62] if they have sufficient kinetic energy. It has been shown that energetic ions approaching a metal surface may be converted into energetic neutral atoms by electronic interactions between the ion and the surface such as Auger neutralization or resonance neutralization followed by Auger de-excitation[63]. As with the colliding inert ions, the energetic neutral atoms created in this way will also have a definite probability of being sorbed on the surface. If, while this prior sorption is taking place, material is being deposited on the surface, there is a definite possibility that the sorbed gas will be permanently buried and trapped in the film[64]. The amount of trapping produced in this way depends on many factors, such as the rate and method by which the metal is deposited on the surface, the potential of the surface on which the metal lands, and the presence of a gas discharge. If no metal film is being deposited, the surface collecting the energetic ions or atoms (if neutralized at the surface) at a uniform 'current' density will have a net clean-up rate of zero after an initial clean-up of a small amount of gas[65]. Resputtering will then take place, liberating the gas at the same rate as it is being cleaned up. The initial clean-up occurs through the imbedding of ions at trapping sites in the surface until saturation results. In the absence of the gas discharge no gettering or clean-up of the inert gas is observed[66]. The effects on the clean-up of gases by metal surfaces of a variation of surface potential under sputtering and evaporating conditions is the main topic of the present investigation, and is treated in greater detail in chapter 6.

If an inert gas atom can be forced into the growing film by some

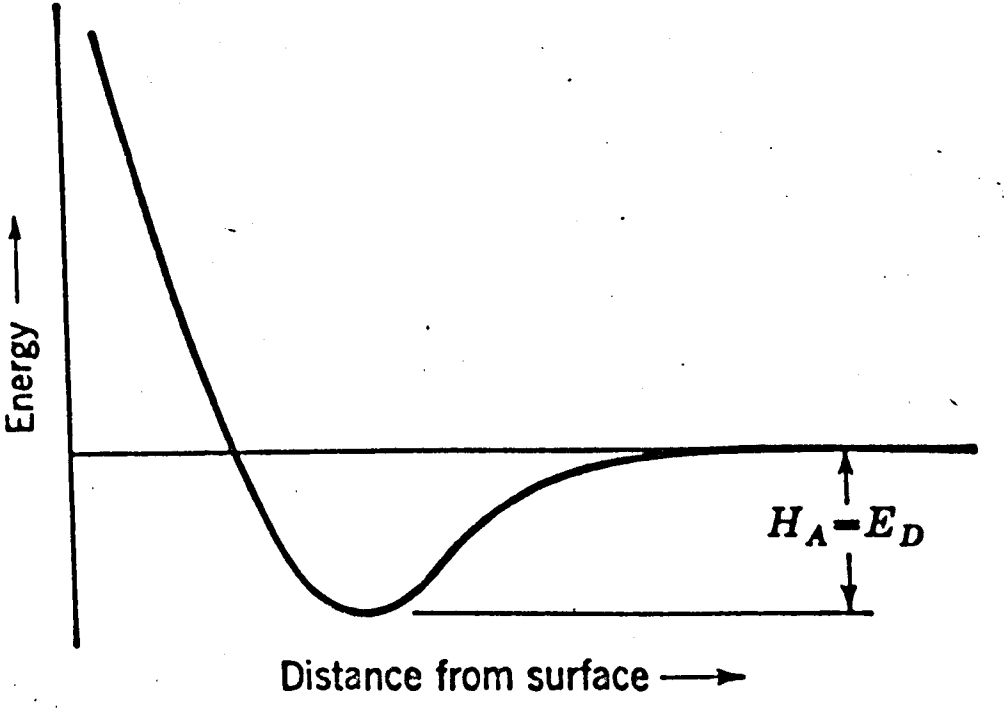

Potential energy of a molecule in non-activated adsorption. H_A is heat of adsorption; E_D is energy of desorption.

Figure 2.6

mechanism, such as the gas clean-up process described above and if the temperature is high enough, diffusion can take place with the possibility that the inert gas atom may migrate to the film surface and escape into the gas phase. The escape however, might be prevented if 'occlusion' occurs.

iv. Occlusion

Since it is unlikely that the inert gas is 'freely' soluble in the metal film[67], or to be sorbed at the film surface, at least not at the temperatures normally encountered in a glow discharge, inert gas atoms already in the film may be permanently trapped on encountering any imperfections or closed 'cells' in the growing film. This trapping, or occlusion, will arise if any of the gas atoms should enter one of these 'cells' whilst diffusing through the film. The gas atoms will continue to accumulate at these defects until, finally, if an excessive pressure is created, a fracture will occur, and the gas escape.

v. Physical adsorption

A gas atom approaching an atomically clean surface experiences a force of attraction due to a potential field shown by the potential energy diagram in Figure 2.6. The shallow potential well arises from weak interactions due to Van der Waal and polarization forces. This state of attraction is called 'physisorption' and is associated with small adsorption energies of less than about 10 kcal mol^{-1}. [68]

Physisorption is a spontaneous phenomenon and takes place, at sufficiently low temperatures, between any surface and any gas. It always results in a decrease in the free energy of the system (ΔF) and consequently is always an exothermic process.

Although physical adsorption can occur between an inert gas and the surface of a metal film if the temperature is low enough, it is negligible for a neutral inert gas at the temperatures normally encountered in sputtering and evaporation experiments[61].

For example, it can be shown[61] that about 1 atomic % of xenon will be found in a film analysed at room temperature, if the film is deposited in 10^{-6} torr xenon environment at a metal deposition rate of 100 monolayers sec^{-1} on a substrate held at 20°K. This result is in keeping with a condensation coefficient of 1 at 20°K and assuming no diffusion of the gas as the film is warmed up to room temperature for analysis. If the same experiment is performed at room temperature, no inert gas is found, regardless of the relative amounts of inert gas and metal atoms arriving at the substrate. In conclusion, since the inert atoms are not sorbed on the surface, nor are they 'freely' soluble in the film, it follows that the film must be impermeable to the inert gas[69].

vi. Chemisorption

In addition to all the previously mentioned processes which apply to film surface contamination by both inert gas atoms and reactive gas atoms, a further contaminating effect may take place for reactive gas atoms and molecules, namely 'chemisorption':-

In contrast to physisorption, chemisorption involves some sharing or transfer of electrons between the solid (adsorbent) and the gas (adsorbate)[70]. For this reason it is highly unlikely that an inert gas will be involved in chemisorption. There are other differences between the two kinds of adsorption, for example, the binding energy (heat of adsorption), activation energy, surface coverage and the range of temperatures and

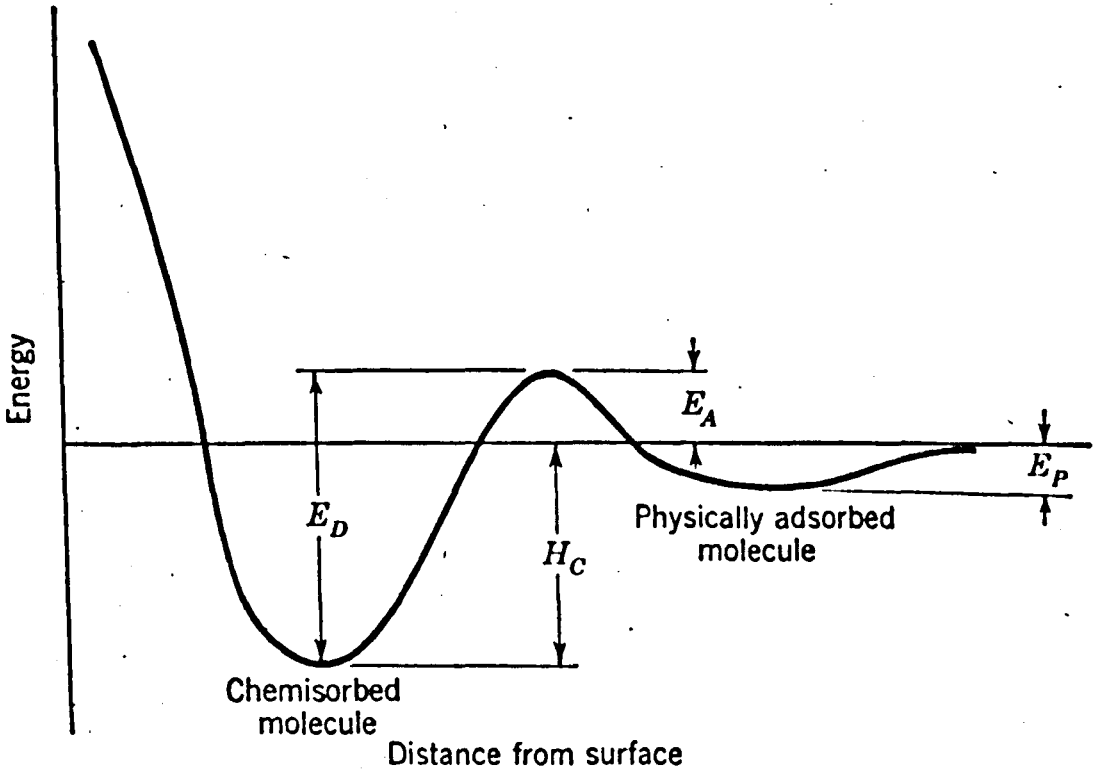

Potential energy for activated chemisorption. Molecular adsorption.

Figure 2.7

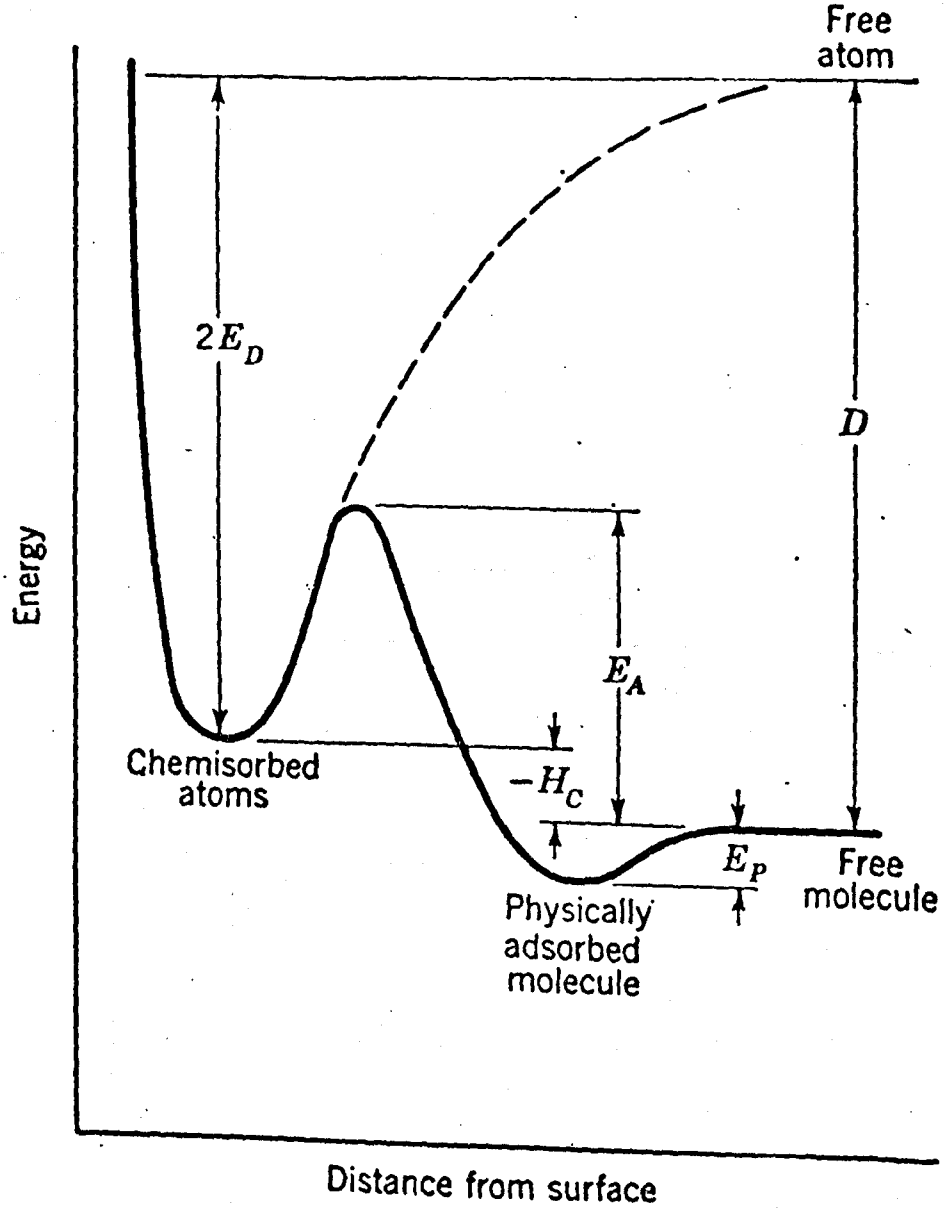

Potential energy for activated chemisorption. Endothermic atomic adsorption of diatomic molecule: $2E_D < D$. (From G. Ehrlich, *J. Chem. Phys.*, vol. 31, p. 1111, 1959.)

Figure 2.8

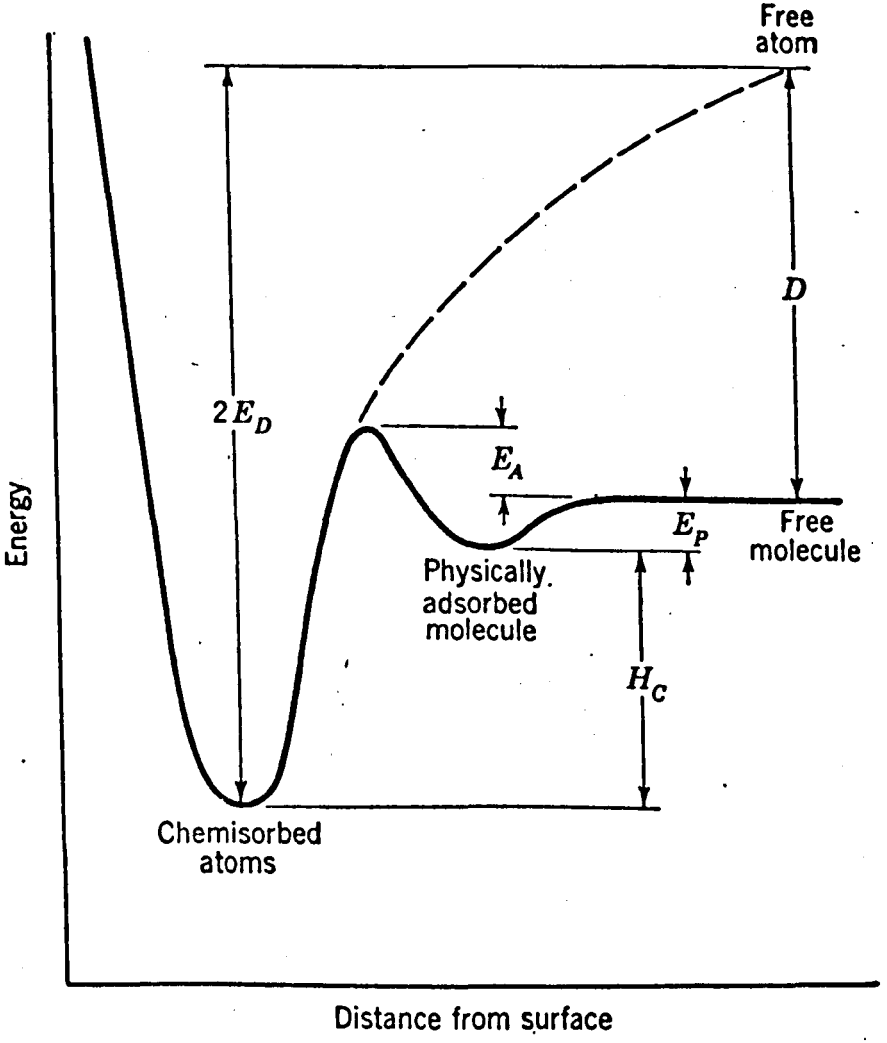

Potential energy for activated chemisorption. Exothermic atomic adsorption of diatomic molecule: $2E_D > D$. (From G. Ehrlich, *J. Chem. Phys.*, vol. 31, p. 1111, 1959.)

E_D is energy of desorption as molecule (a) or atom (b,c); E_P is energy of physical adsorption; E_A, activation energy of adsorption; H_C, heat of chemisorption; D, energy of dissociation.

Figure 2.9

Chemical adsorption of gases on metals at room temperature.

Metal	Gas					
	N_2	H_2	CO	O_2	CO_2	CH_4
Ag	N	N	N,Y*			
Al	N	N	Y	Y		
Au	N	N	N,Y*	N		
Ba	Y	Y	Y	Y	Y	Y
Ca	Y	Y	Y	Y		
Cd	N	N	N	Y		
Co	N	Y	Y	Y		N
Cu	N	N	Y	Y		
Cr	N	Y	Y	Y		Y
Fe	Y	Y	Y	Y		N
Hg	N	N	N			
In	N	N	N	Y		
Mg			Y			
Mn				Y		
Mo	Y	Y	Y	Y		Y
Nb	Y	Y	Y	Y		
Ni	N	Y	Y	Y		N
Pb	N	N	N	Y		
Pd	N	Y	Y	Y		Y
Pt	N	Y	Y	Y		
Rh	N	Y	Y	Y		Y
Sn	N	N	N	Y		
Sr			Y			
Ta	Y	Y	Y	Y		Y
Ti	Y	Y	Y	Y	Y	Y
W	Y	Y	Y	Y		Y
Zr	Y	Y	Y	Y		Y

N = No, Y = Yes, Blank = Unknown, * = Two different investigators.

Table 2.2.

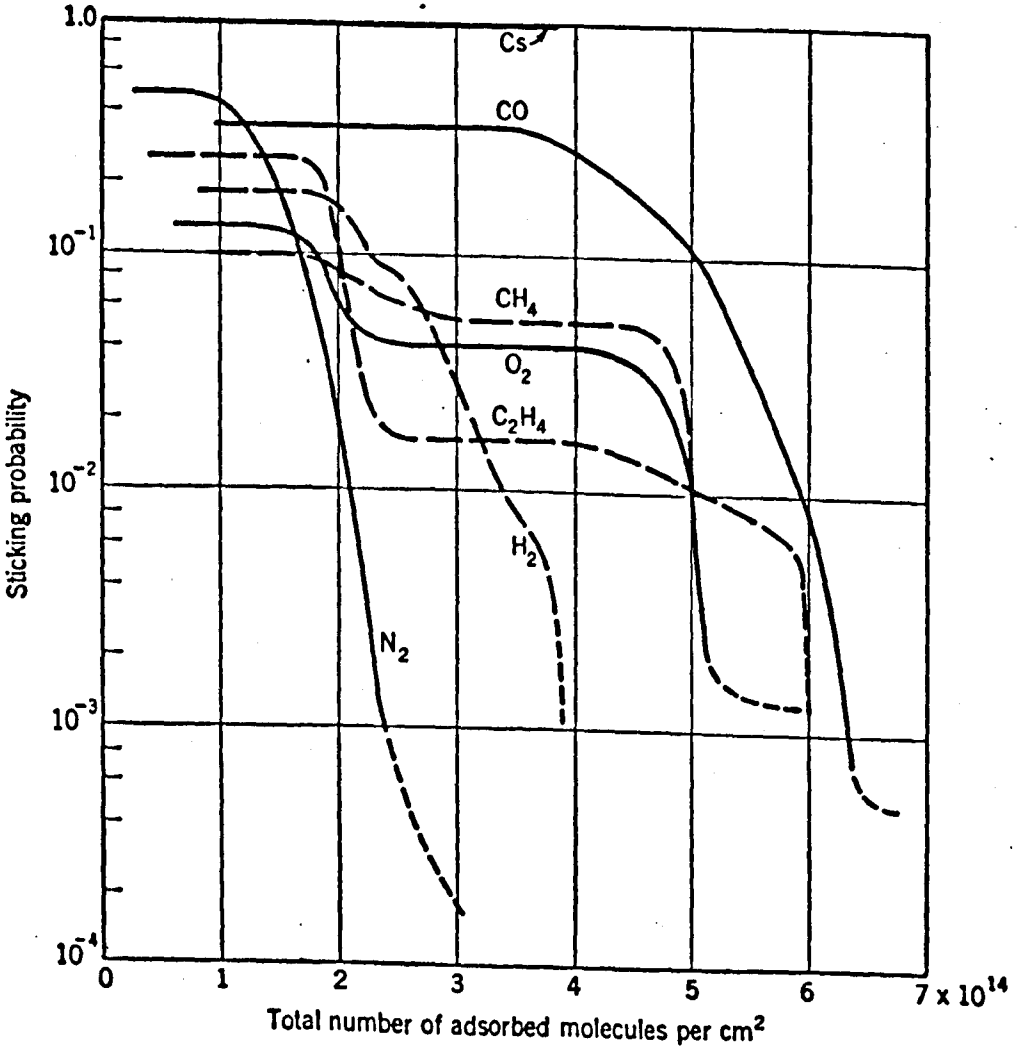

Sticking probability versus number of adsorbed molecules on the 411 plane of tungsten at 300°K. (After J. Becker, "Solid State Physics," vol. 7, p. 379, Academic Press Inc., New York, 1958.)

Figure 2.10

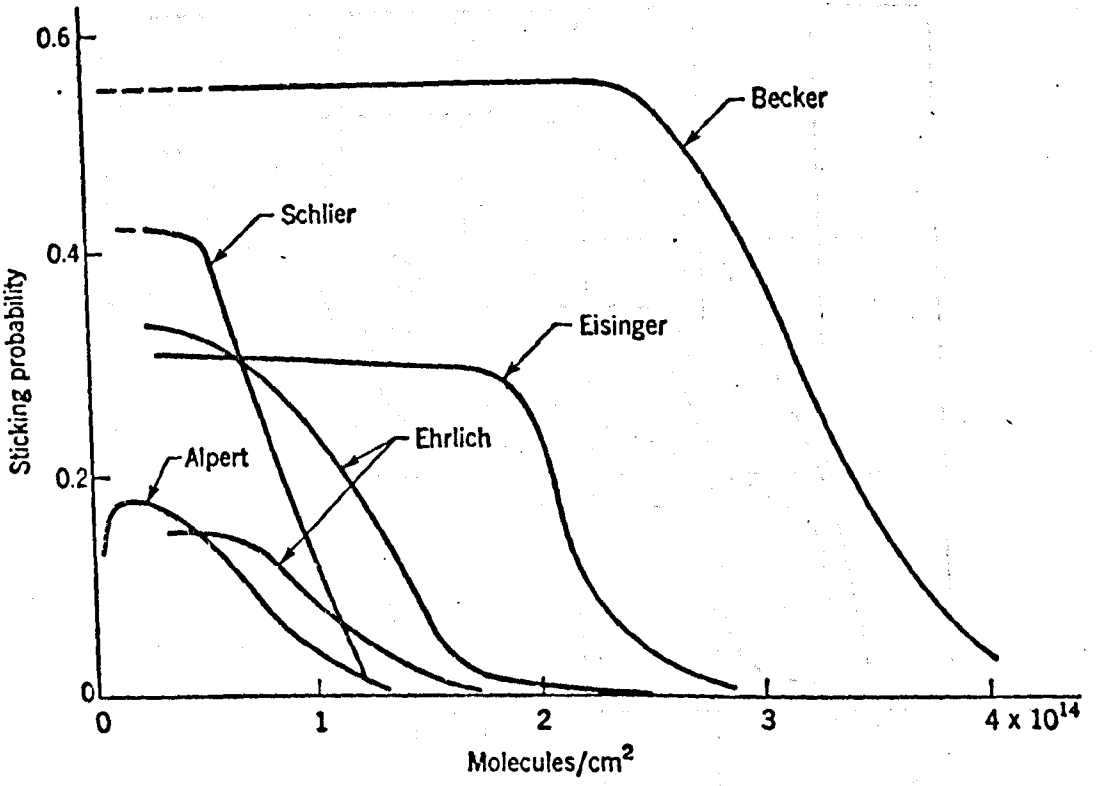

Comparison of the results of various investigators for the sticking probability of nitrogen on tungsten. The two curves given for Ehrlich are for surface temperatures of 290 and 373°K. All others are nominally at room temperature. (After D. Lee, H. Tomaschke, and D. Alpert, 1961 *Vacuum Symp. Trans.*, p. 153, 1962.)

Figure 2.11

pressures involved. Figures 2.7, 2.8 and 2.9[71] show the potential energy diagrams for chemisorption depending on whether the active gas is sorbed as molecules or atoms. Chemisorption may be characterised by a 'sticking probability', which is defined as the probability of adsorption of an atom incident on a surface.

Table 2.2.[72] indicates whether or not chemisorption occurs for various gases on different metals. Figures 2.10 and 2.11[73,74] show the variation of sticking probabilities with surface coverage for various gases on tungsten. It can be seen that there is a wide measure of disagreement between various authors.

Chemisorption, at least by the active gases commonly found in vacuum systems, could be a seriously contaminating feature at the surface of the growing film. The rate at which molecules are adsorbed is given by :-[75]

$$dn_a/dt = s\nu = sP(2\pi mkT)^{-1/2}$$
$$= 3.5 \times 10^{22}\, sP(MT)^{-1/2}\ sec^{-1}cm^{-2}$$

where ,

ν is the number of impinging molecules,

s is the sticking coefficient,

n_a is the number of adsorbed molecules,

P is the pressure of gas in torr,

M is the molecular weight of the gas,

T is the temperature in ^{o}K.

Taking nitrogen as an example, at a pressure of 10^{-6} torr,

ν is $3.9\ 10^{14}$ molecules $sec^{-1}cm^{-2}$

assuming, (a) that every nitrogen molecule which lands on a surface sticks to it, and (b) that it lies at a distance of 3.7 10^{-8}cm from its nearest neighbour (i.e. the nitrogen molecular diameter, calculated from gas kinetic theory), then a monolayer of nitrogen molecules contains 7.3 10^{14} molecules and, for a sticking probability of 1, this monolayer should take about 2 seconds to form. Hence, if no other counteracting processes are taking place, such as thermal desorption or ion bombardment desorption, one would expect that the growing film, whether sputtered or evaporated would contain a noticeable percentage of chemically active gas atoms.

Finally, apart from chemisorption, collisional processes occurring in the gas discharge result in an energetic flux of excited, ionic and atomic species of the chemically reactive gas molecule. Some of these species will be adsorbed at trapping sites on the film surface in which the unexcited gas molecule would not be sorbed[76]. This type of sorption is called 'impact activated sorption'[77].

2.3.4 In the discharge

i. Masking of chemically active gases

The high pressures essentially present in a sputtering system are due to the inert gas, such as argon, used in producing the glow discharge. Whilst there may be reactive gases present at the same time, the problem should be no more serious than in the evaporation case. However, it is more likely that in a glow discharge any reactive gases present will be undetected, by being masked by the much greater quantity of inert gas present. In addition, a fraction of the reactive gas will be ionized

in the discharge, thereby increasing its reactivity and consequently its contaminating ability.

ii. Desorption from walls, etc.

The walls, and all surfaces which are in contact with the discharge, are likely to outgas thereby increasing the number of impurity gas atoms in the system. This outgassing arises for two main reasons:-

(a) the glow discharge plasma tends to heat any surface not shielded from it, and

(b) electrons and ions from the plasma will bombard any unprotected surfaces and tend to remove loosely bound impurity atoms.

The magnitude of this problem may be seen from the following calculation[78]:-

For a cylindrical vacuum system volume 100 litres and diameter 50 cm, the surface area (A) to volume (V) ratio is given by,

$$A/V = 0.12 \text{ cm}^{-1}$$

Considering, in addition, fixtures inside the system, grooves and the surface roughness, this may make the ratio A/V as high as 1 cm^{-1}. If the entire surface area were covered with a single monolayer of adsorbed atoms (N_a), there would be about $5.10^{14}.(A)$ atoms if they are composed of water molecules, methane etc. or about $8.10^{14}.(A)$ if of nitrogen, oxygen. From the universal gas equation the number of free gas atoms in volume (V) is given by (N_g)

$$N_g = 3.24\ 10^{16}.\ (PV) \text{ at room temperature}$$

Therefore the ratio of adsorbed to free gas atoms in a vacuum system with

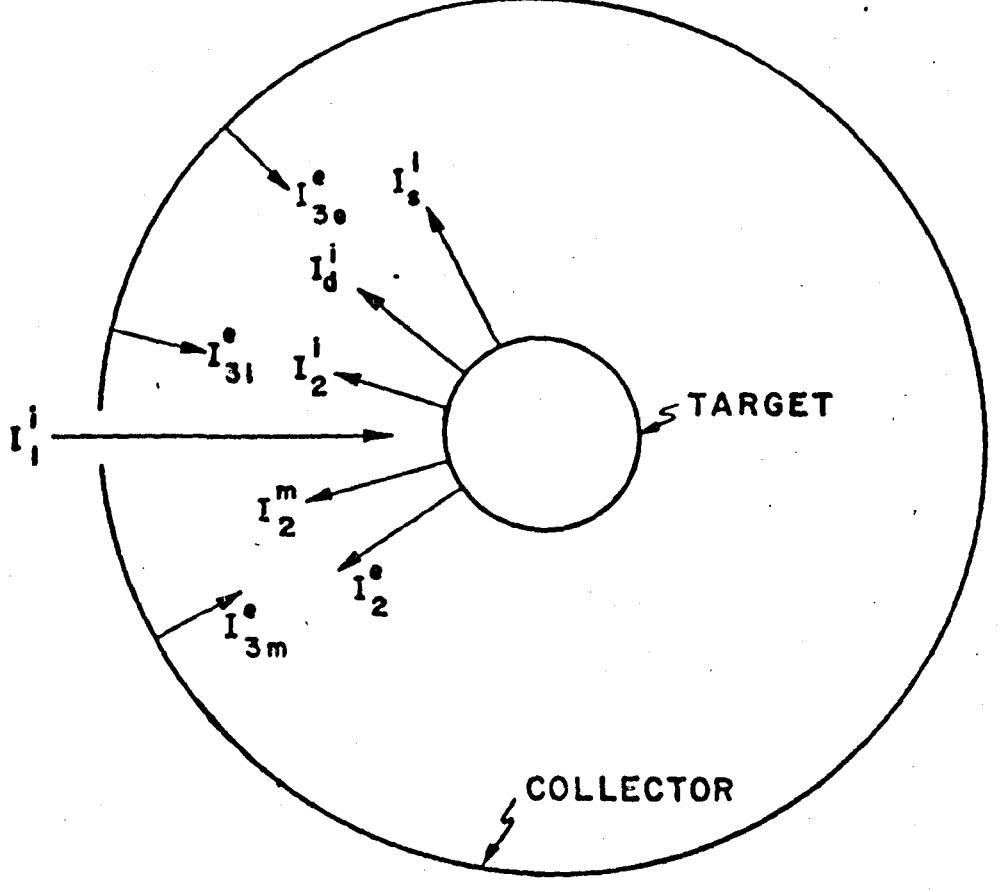

Schematic illustration of various particle currents (ion currents I^i, electron currents I^e, and currents of metastable atoms I^m) which may occur at target and collector when a primary-ion current $I_1{}^i$ strikes the target. The symbols used have the following meanings: $I_2{}^i$ is the current of reflected primary ions, $I_d{}^i$ the current of thermally desorbed primary ions, $I_s{}^i$ the current of target particles sputtered as ions, I_2^m the current of reflected metastable atoms, I_2^e the current of secondary electrons emitted by ion impact, and I^e_{3e}, I^e_{3i}, I^e_{3m} are currents of electrons ejected from the collector by impinging electrons, ions, and metastable atoms, respectively.

Figure 2.12

surface to volume ratio of unity is approximately,

$$N_a/N_g \sim 2.10^{-2}/P \quad \text{where P is pressure in torr.}$$

At a pressure of 1 torr, N_a/N_g is about 1/50, i.e. there are about 50 free atoms for every adsorbed atom, whereas at a pressure of 10^{-7} torr the ratio is reversed, N_a/N_g is about 2.10^5, i.e. there are about 200,000 adsorbed atoms for every free atom.

In other words, when the mean free path of the ions and electrons in (b) become comparable with the vacuum system dimensions, desorption from the walls, etc., may have a seriously contaminating effect.

iii. Charge transfer

The possibility in a glow discharge of charge transfer taking place with little loss of kinetic energy is well known[7]. If it takes place, the contaminating effect of the discharge is increased. The transfer of charge in the gaseous phase may produce both fast and slow moving, inert, reactive and cathode ejected neutrals, as well as ions. However, in contrast to the ions of the various species, the neutrals cannot be controlled either by the electric field created from the discharge voltage or by a magnetic field. Consequently, they can travel unimpeded through the discharge with the possibility of being trapped in the growing film.

2.4 Particle scattering from metal surfaces during ion bombardment

Many different processes can take place simultaneously during ion bombardment of a metal target, amongst them being secondary emission of electrons, gas ions and neutral gas atoms, as well as the surface effects such as sorption and trapping in the target, which were mentioned in the

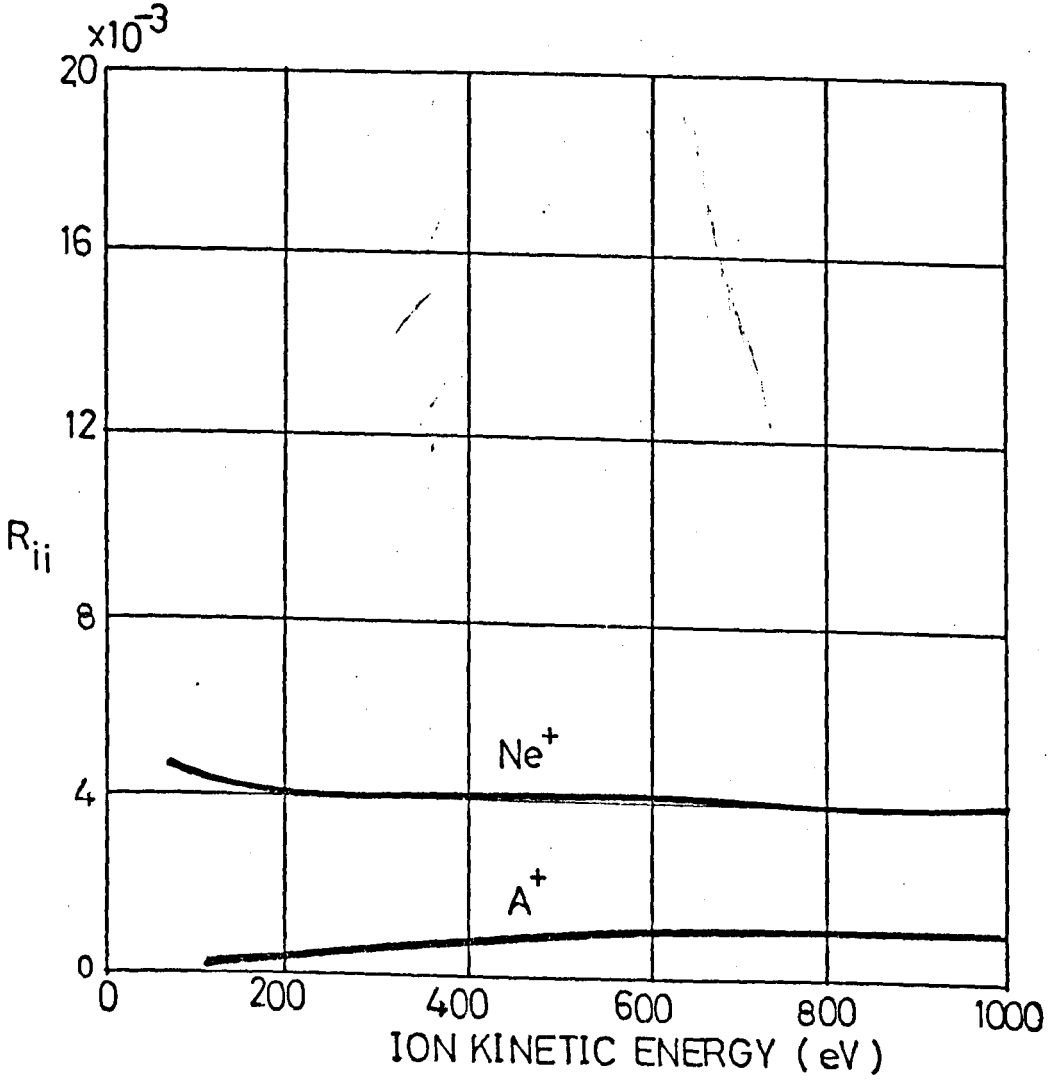

Figure 2.13. Reflection coefficent of incident ions (as ions) versus ion kinetic energy.

previous section. Figure 2.12 illustrates schematically the various processes taking place. For the sake of simplicity only the case when pure inert gas ions bombard the surface is considered.

2.4.1 Reflection and adsorption of incident ions

When positive inert gas ions are incident normally on a metal surface there is a definite probability that the ion will be reflected after collision with the surface[79]. This may take place 'elastically' with no loss of energy during the collision, or alternatively, 'inelastically'.

A reflection coefficient is defined for the ion as,

$$\ell = \frac{\text{current of incident particles ejected as ions}}{\text{ion current striking target}}$$

The reflection coefficient for the noble gases has been found to be relatively independent of incident ion kinetic energies in the range 0 to KeV's[80], see Figure 2.13. However, it does depend, amongst other things, on the angle of incidence[81], target species[82], temperature[83] and "cleanliness"[84] of the target. For the energies of interest in sputtering experiments, that is between 0 to KeV, it has been shown that[85] elastic collisions predominantly occur, between the incident ions and individual 'free' atoms of the target, i.e. binary collisions only take place.

From the classical conservation of energy and momentum, and with ions striking the target at angle Θ to the target normal, the energy of the reflected ions is given by:-

$$E = (1 + M/m)^{-2} (\cos \Theta \pm ((M/m)^2 - \sin^2 \Theta)^{1/2})^2 E_o$$

where m is the mass of the incident ion,

M is the mass of the target atom,

and E_o is the kinetic energy of the ion before collision.

For $\Theta = 0$, i.e. the ion striking the target at normal incidence, this equation reduces to:-

$$E = (m - M)/(m + M).\ E_o$$

For argon ions of 1600eV incident normally on a nickel surface, $M = 58.71\ m_o$, $m = 40\ m_o$, and $E_o = 1600$ (in eV units), where m_o is the mass of a hydrogen atom, then E = 320 eV, i.e. the energy possessed by the reflected ion is about 20% of the incident ion energy. With the large flux of gas ions bombarding the target occurring in sputtering experiments, and a reasonably high reflection coefficient, there exists the possibility of finding a number of high energy reflected ions in the vicinity of the surface of the growing film.

Alternatively, a sticking probability can be defined for the ion approaching the surface and being sorbed:-

$$\lambda = \frac{\text{the number of incident ions sorbed at the surface}}{\text{the number of incident ions striking the target}}$$

On colliding with the surface the energetic ion, or the neutralized ion, if neutralization has taken place at or near the surface (see 2.4.2 below), may penetrate the surface and interact with the individual atoms of the target, losing energy at each collision until finally it comes to rest in the lattice and becomes trapped there. In this way the impinging 'ion' may be locked in the target either as an interstitial, lattice or

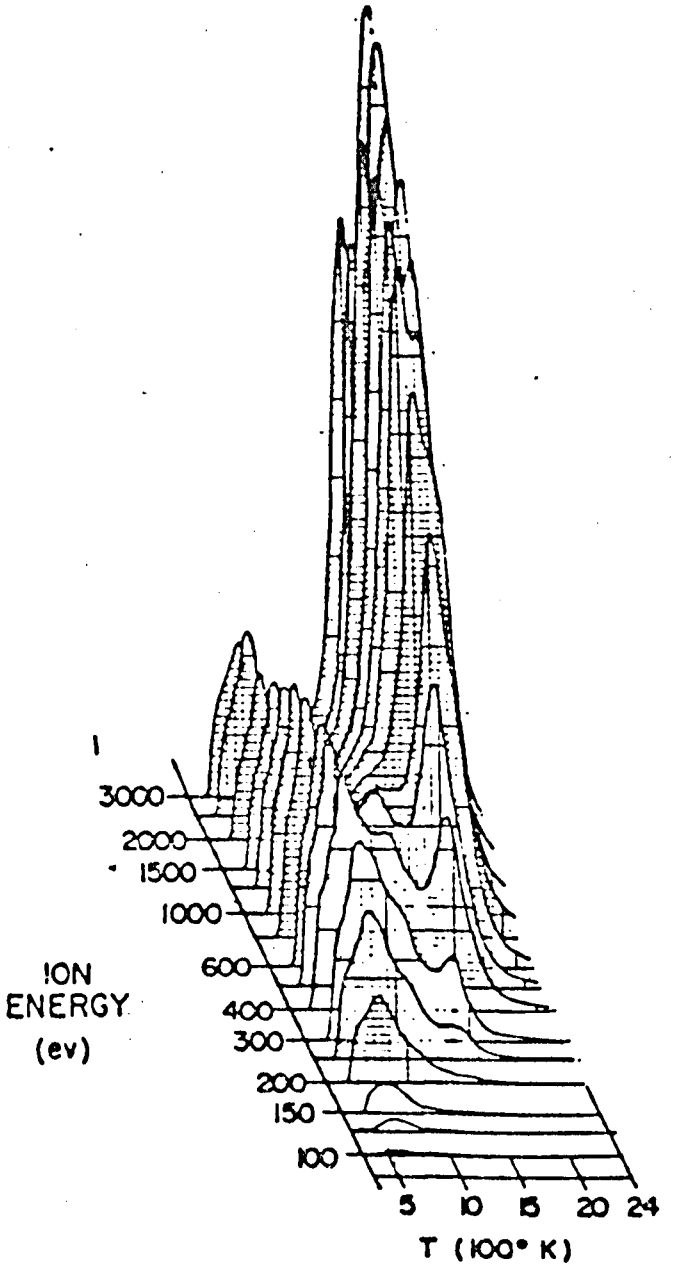

Figure 2.14 Desorption spectra for argon in tungsten at various ion energies. The desorption rate is plotted as a function of temperature.

substitutional particle.

The depth at which these particles come to rest depends on many factors, amongst them being the primary kinetic energy of the ion[86]. However in the case of a monocrystalline target, the energetic ion may be 'channelled' along the axis provided by rows of close packed lattice atoms and in this way may travel large distances into the target without loss of energy to the surrounding atoms[87]. The ions thus trapped in the target may be re-emitted (a) by heating the target, thereby initiating a 'thermally activated diffusion process'[88] or (b) by being struck by further ions or energetic target atoms in a 'bombardment induced re-emission process'[89,90] or (c) spontaneously[91].

a) By heating the target, after ion bombardment, at a linearly increasing rate, a desorption spectrum is obtained which may be interpreted on the basis of the various trapping sites of the ion in the target. Figure 2.14 shows the desorption spectra for argon in tungsten at various ion energies[62].

b) Gas trapped in the target by the initial ion bombardment may be released by the application of a second ion bombardment. This may be investigated most easily if the target is bombarded by one ion species, and released by a second ion species, the gas increase being followed mass spectrometrically.

This is a form of sputtering and can be characterised by a 'sputtering yield' (S_g) for the gas-gas interaction, similar to that for the gas-solid interaction (S_t). However, whereas in the latter case it is assumed that a complete surface layer exists, in the gas-gas case this is not normally so, and the sputtering yield (S_g) must be normalised to that of full monolayer coverage (about 10^{15} atoms cm^{-2} for most inert gases). Values of

Effective gas sputtering ratios of 100 eV ions trapped in nickel[92].

Trapped atom	Bombarding ion	Sorbed gas
He	He	0.6
He	Kr	0.2
Ne	Kr	0.7
A	Kr	0.3
Kr	He	0.2
Kr	He	0.4
Kr	Ar	0.35

Table 2.3

Sputtering coefficient (Gas release efficiency) for inert gas (sorbed at 250 eV) in glass bombarded by other gas ions (at 250 eV)[93].

Sorbed gas	Helium	Neon	Argon	Krypton	Xenon
Helium	5.5	12.0	50.0	40.0	5.0
Neon	9.0	20.5	35.0	33.0	10.0
Argon	10.0	35.0	22.0	18.0	12.5
Krypton	7.5	38.0	12.0	11.5	6.0
Xenon	13.0	24.0	40.0	62.0	63.0

Table 2.4

sputtering yield S_g are given in Table 2.3[92] for 100 eV ions bombarding a nickel target, and Table 2.4, for 230 eV ions bombarding glass[93]. The sputtering yields S_g measured on glass are seen to be as much as an order of magnitude greater than on the nickel. This discrepancy may be explained on the basis of two mechanisms:-

For the nickel case, the results may be interpreted on the basis that the release of the previously trapped gas atoms is dependent on the sputtering, and hence the erosion, of the target by the secondary ion bombardment. This is called the 'target sputtering mechanism'[94,95,96].

In the case of the results for glass, a 'gas sputtering' mechanism must be invoked[97,98]. It can be shown[99] that an ion of energy E_o impinging on a target can produce about $E_o/2E_d$ lattice atom displacements by collisions in which kinetic energy is imparted from the ion. (E_d is the binding energy, in the order of 25 eV). If by this sort of process energy could be transferred to the trapped gas atoms in the target, large S_g values would result. However, large values of S_t for the glass would similarly be expected, which is not the case. Alternatively, if the incoming ion gives up its energy into a small volume of the target, the temperature in the small volume will rise rapidly and the trapped gas might be released by a 'thermal spike' effect[100]. In some respects this shows a similarity to the 'evaporation from localised hot spots' theory of Von Hippel, an early explanation of target sputtering. However, if the energy given to the target and trapped atoms is of the order of 1eV, this will be sufficient to initiate gas atom migration and release, but insufficient to provoke target evaporation. It should be possible for both the target sputtering and gas sputtering mechanisms to occur simultaneously and this will be

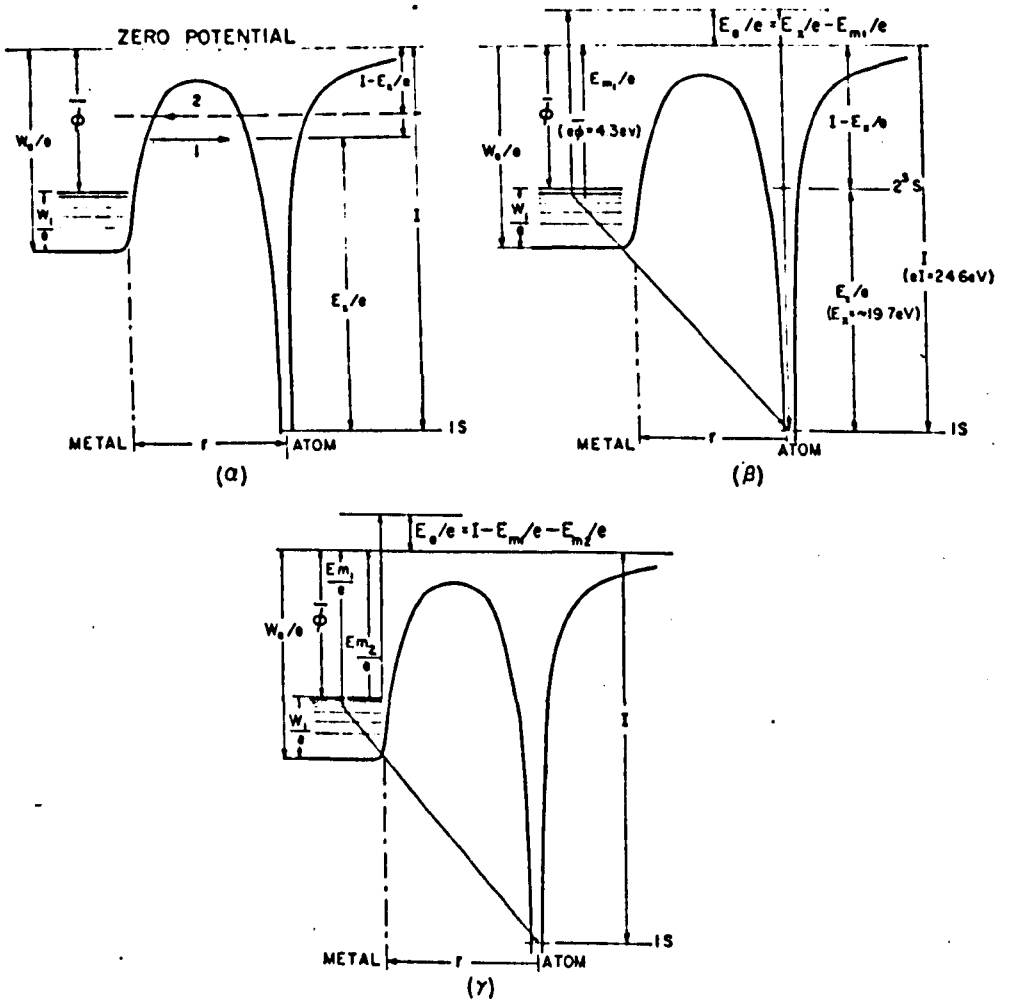

Diagram α: Schematic illustration of the resonance neutralization of an ion (transition *1*) or resonance ionization of an excited atom (transition 2) at a metal surface. Diagram *β*: Schematic illustration of the AUGER de-excitation of a metastable helium atom (2^3S) on a Mo surface. The electron-exchange process is indicated by the full lines. Diagram *γ*: Schematic illustration of the AUGER neutralization of an ion at a metal surface.

Figure 2.15

dealt with in chapter 6.

2.4.2. Ion neutralization and the secondary emission of electrons

The impinging ion may be neutralized and reflected as an energetic neutral atom, often with the release of secondary electrons from the target surface[101]. This can come about through one or more of three processes, involving electronic transitions between ion and surface:-
These are,

a. Resonance neutralization,

b. Auger de-excitation,

c. Auger neutralization.

The presently available evidence[102] indicates that for ions of energies less than about 1000 eV, the electronic transitions involved in these processes are independent of the kinetic energy of the incident ion and only governed by the potential energy it has by virtue of its ionized state. Figures 2.15a,b,c show schematically the potential energy diagrams involved in these processes.

A two step process using resonance neutralization followed by Auger de-excitation may be invoked to obtain the neutral gas atom. This can be represented by the two equations:

$$A^+ + Ne_m^- \rightarrow A^* + (N-1)e_m^- .$$

and then

$$A^* + Ne_m^- \rightarrow A + e^- + (N-1)e_m^- .$$

where, A^+ represents the incident ion, Ne_m^-; all metal electrons,
and A^* the excited atom.

However, it is possible to achieve the same end through a single operation

if Auger neutralization only takes place:-

$$A^+ + Ne_m^- \rightarrow A + e^- + (N - 2)e_m^- .$$

Secondary electron emission can also take place through the influence of the kinetic energy of the incident ion, if certain conditions are fulfilled. The ionization potential of the ion for example, should be less than the work function of the target, and the kinetic energy of the ion should be above a threshold value.

2.4.3. Thermally desorbed primary ions

Primary ions, which have previously been sorbed at the target surface, may be desorbed back into the gas phase as ions if the temperature of the metal is sufficiently high. LANGMUIR[103] derived an expression for the ratio, ε, of ions to atoms leaving a surface:-

$$\varepsilon = \exp((\Phi - V_i)e/kT)$$

where Φ is the work function of the surface,

V_i is the ionization potential of the gas atoms,

e is the electronic charge,

k is Boltzmann's constant,

and T is the target temperature in ^oK.

At room temperature and for $(\Phi - V_i)$ values of -3 to -4 volts, $\varepsilon = 10^{-54}$. This is far less than the experimentally determined values of about 10^{-2} to 10^{-4}, and implies that at the target temperatures normally encountered in glow discharges, thermal emission of ions is not a significant effect. However, at higher temperatures (around 10^4 ^oK) ε can assume greater importance.

.4.4. Sputtering of ions, neutrals and metastables

When an ion approaches a metal surface there is a probability, related to the sticking factor for that ion-surface interaction, that the ion will penetrate the target surface. Many collisions take place between the incident ion and target atoms with energy and momentum being transferred from the ion to the atoms at every impact. If the momentum that was associated with the incident ion can be reversed in direction, particles of the target may be ejected by the initial impact, or through the subsequent collisions in the target.

The ejected particles may be in the form of positive, negative and excited atoms as well as neutral atoms. These will be representative of, although not necessarily proportional to, all the atomic species making up the target (at least up to the depth the ions travel in the target). This includes the very ions which were bombarding the target and have come to rest in it. BRADLEY[105] and others[106] have shown that the ratio of the number of sputtered ions and excited atoms to sputtered neutral atoms is always less than 1%.

CHAPTER III.

Recent work

3.1 Introduction

Since the 1950's, advances have been made ~~both~~ in the theoretical understanding of the sputtering mechanism, the gas clean-up phenomenon, and in the technological aspects of thin film deposition.

Thermal evaporation techniques have been improved hand in hand with advances in vacuum technology. The impurity contamination of the evaporated films has been reduced by the use of increasingly pure sources and as a result of progress in reducing the residual gas pressure. These same advances have also led to purer sputtered films. However, other techniques, such as getter and bias sputtering, have been introduced to obtain sputtered films with purities approaching those of evaporated films, although, it has been shown that, in some cases, bias sputtering may actually increase the impurity contamination in the films. On the other hand, interest has recently been shown in deliberately adding given amounts of gaseous impurities to obtain films with specific properties.

The recent advances in sputtering techniques are treated in section 3.2 and sputtering theories are considered in section 3.3. The evaluation, generation and maintenance of clean surfaces are described in section 3.4. Section 3.5 deals with recent experiments in which correlations have been made between the physical properties of thin films and the environments in which they are grown. Advances in the areas of gas clean-up and ion sticking are also included in this section. Section 3.6 describes the work of Winters and Kay. Gas release and analysis techniques are treated in section 3.6.

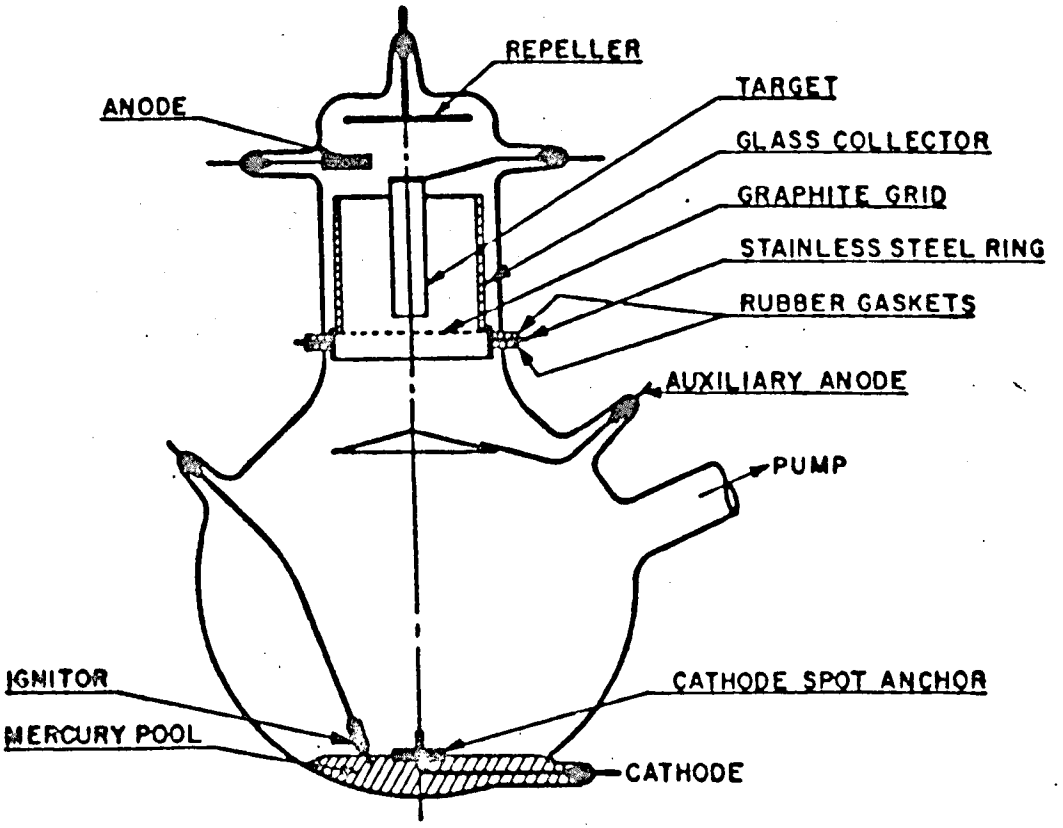

Figure 3.1. Triode sputtering scheme due to WEHNER[107].

3.2 Improvements to the diode sputtering system

i. The triode sputtering scheme

Although the sputtering technique had been used since the turn of the century it was not until the early 1950's that it became possible to use it quantitatively. This very largely came about through the work of WEHNER[107] who designed an efficient and reliable sputtering system using a modified mercury pool rectifier Figure 3.1. Electrons generated by a low pressure mercury arc in the lower chamber are drawn by the anode through the graphite grid into the upper chamber, where they ionize the gas present there. Using a negative repeller electrode increases the effective path length of the ionizing electrons. The material to be sputtered is fixed as a target and is given a negative potential with respect to the main anode. Mercury vapour was used as the sputtering gas in a great number of Wehner's experiments, but other gases could be used by admitting them separately into the top chamber, whilst keeping the partial pressure of the mercury low by cooling the lower chamber. This was one of the first triode sputtering arrangements, so called because of the introduction of the sputtering target as a third independent electrode. Amongst the many advantages of this system over the cold discharge diode technique were :-

(a) little or no back diffusion of the sputtered material (at the gas pressures used, in the order of 1 micron, the mean free path of the sputtered material was comparable with the target-collector distance).

(b) the sputtering rate was high due to the larger plasma densities.

(c) ions hit the target normally with the full target-plasma potential.

Furthermore, Wehner's apparatus combines simplicity of design with versatility of use. Disadvantages of his apparatus lie in the fact that a partial pressure of mercury was ever present to some degree in the sputtering chamber even when the lower chamber was cooled. This was particularly troublesome because mercury vapour could corrode or react with the target material. However, a great deal of useful results were recorded on the sputtering yields of the elements with variation in energy of the bombarding ions by Wehner and co-workers[107-113]. In addition, using a modified version of this apparatus, Wehner was the first person to observe, and explain, the spot pattern distribution of sputtered deposits from a single crystal target[114-119].

ii. Thermionically supported discharge with magnetic field

Since this time, with the advent of all metal and readily demountable vacuum systems, many new designs for sputtering systems have been proposed, e.g. EDGECOMBE, ROSNER and ANDERSON[120], KOEDAM and WEIJENFELD[121,12; and SEEMAN[123]. These have all been shown to have the advantages of Wehner's system (with the possible exception of the simplicity) without the 'mercury' disadvantage. This has been achieved by replacing the mercury arc by a heated filament cathode and using a magnetic field to improve the plasma density.

Further advances have been made in sputtering by the application of new techniques such as :

iii. Tetrode sputtering,

iv. Getter sputtering,

v. Bias sputtering,

vi. RF sputtering.

iii. Tetrode sputtering

A triode system normally operates between 1-10 millitorr. At pressures an order of magnitude lower than this, the stability and operating characteristics become degraded. Improvements at low pressures have been made by MULY and ARONSON[124] by the addition of a fourth electrode, thereby creating a tetrode system. The fourth electrode, in the form of a grid or auxiliary ring anode and bearing a small positive potential, is placed close to and above the electron source so that it lies between the filament and the main anode. This additional electrode greatly reduces the dependence of the discharge operating characteristics on the effect of target voltage and the resulting discharge is stable at pressures as low as 0.2 millitorr.

iv. Getter sputtering

Gettering of chemically reactive gases is known to occur in the presence of a depositing film and this is one of the main causes of impurity contamination in thin films. NEUGEBAUER and EKVALL[125] were some of the first to utilize this gettering action to improve the superconductive properties of sputtered films. This was achieved by making the sputtering gas pass over a freshly evaporated film before reaching the region where the thin film of interest is to be deposited. Another method described by THEUERER and HAUSER[126] to achieve the same result incorporates a second enclosure inside the main vacuum system. The electrode arrangement inside this secondary chamber is of the diode sputtering type. The sputtering gas finds its way into the enclosure through small inlets and joints, and the gettering action is set up due to the internal DC field between the two electrodes. In this way Theuerer and Hauser reduced the partial pressure

of oxygen in the secondary enclosure to less than 10^{-10} torr even with a background pressure in the main vacuum system of 10^{-6} torr. In both these methods it was necessary to keep a shutter over the substrate until the impurities in the sputtering gas had been gettered. Although getter sputtering is very effective for removing impurities brought along by the sputtering gas, it is relatively ineffective in reducing the impurities arriving at the surface of the deposited film from the target or the adjacent walls.

v. Bias sputtering

Films deposited by sputtering are subject to a certain amount of resputtering. This occurs through bombardment by the energetic tail of the sputtered neutrals or by Auger neutralized ions which are reflected with appreciable energies from the target surface towards the growing film.

In addition, the substrate, especially if an insulator, can acquire a significant negative floating potential when immersed in the plasma. Positively charged ions will then be accelerated towards the film growing on the substrate as though the film were a new target. If, instead of leaving the substrate to acquire a negative potential by chance, the film is deliberately given a negative potential with respect to the plasma, the growing film will be continuously bombarded with ions whose energies are related to the magnitude of the applied bias voltage. One of the first descriptions of this technique known as 'bias sputtering' was given in 1942 by BERGHAUS and BURKHARDT[127] who used it to improve the purity of their sputtered films. They mistakenly ascribed the improved purity to the heating effect of the ion bombardment.

Since 1960 this technique has been used by a number of workers

to improve the properties of sputtered films, for example, WEHNER in 1962[128] used it to improve the epitaxial growth of germanium films, GLANG et al[129] in 1965 showed that molybdenum films had a different preferred orientation, depending on whether voltage bias was applied or not, and FLUR et al in 1967[130] observed that bias sputtering had a strong influence on the magnetic properties of thin films.

Throughout these investigations, the improved film properties were thought to be due to the reduction in their impurity concentration, brought about by the bias sputtering. The reasoning behind this is that during the ion bombardment of the film most gaseous and other impurities are preferentially resputtered relative to the target atoms in the film. However, recently WINTERS[131] showed that the occurrence of this depends mainly on the relative strengths of the attractive forces between the metal-impurity atoms and the metal-metal atoms.

Winters, in investigations of the nitrogen concentration in deposited metal films divided the metals into three classes:-
Those which chemisorb molecular nitrogen and form nitrides, those which do not chemisorb molecular nitrogen but form nitrides, and those which neither chemisorb molecular nitrogen nor form nitrides.
From his investigations he showed that the nitrogen gas content in the sputtered films could either increase, decrease or be relatively unchanged with increasing ion bombardment energy (i.e. increasing bias voltage), depending on which class of material was being considered.

The same effect of partial resputtering during film deposition can be achieved by a process first described in 1962 by FRERICH[132] called asymmetric AC sputtering. In this method, instead of applying a negative

DC potential to the growing film as with bias sputtering, an AC potential is applied between substrate and target. With a suitable resistance network it is arranged that a larger ion current flows during the half cycle when the target is negative than when the substrate is negative. In this way a net transfer of material from the former surface to the latter is achieved. During the other half cycle the ion bombardment removes a certain amount of deposited material including adsorbed gas, thereby yielding a purer film.

vi. RF sputtering

Although it had been known for a long time[133] that insulators as well as metals could be sputtered directly by bombardment with energetic ions, it was not possible in practice to maintain this ion current for any period of time because of positive charge build-up on the insulator surface. Several methods were suggested to overcome this charge build-up, such as:-

placing a fine metal mesh over the insulator[134],

making the insulator target small[135], and

simultaneously bombarding the insulator with ions and electrons[136].

However, none of these methods proved very suitable in producing pure uniformly deposited films, and until the 1960's this left only the indirect method of 'reactive sputtering'[137].

In this method, the desired thin film insulator is produced by metal sputtering in a suitable reactive-inert gas mixture. This tends to limit the choice of insulators to types such as metal oxides, nitrides, sulphides etc. In 1955 Wehner suggested the use of an RF field in order to sputter insulators. In 1962, ANDERSON et al[138], and in 1966 DAVIDSE and MAISSEL[139], following this suggestion, introduced a practical method by

which any solid insulator target could be sputtered directly, to deposit insulating films of uniform thickness and at reasonable deposition rates, by the application of a suitable RF voltage to the target.

3.3. Theories of target sputtering

Since the original work of Grove and Plücker many mechanisms have been advanced to explain sputtering. However, up to the present time it has not been possible, because of the number of competing processes and the consequent number of varying parameters occurring at the same time, to describe the sputtering mechanism by a single complete theory. Mechanisms such as:-

physical disruption arising from the expansion of gas accumulating under the target surface during ion bombardment[140];

ejection of atoms due to radiation released when the approaching ions decelerate[141];

volatile chemical formation at the target;

local high temperature hotspot evaporation[142]; and

momentum transferred from the ion to the target atoms[143],

have all been suggested at one time or another to explain sputtering. Of these, only the last two have survived.

The mechanism of local high temperature evaporation spots was first proposed by CROOKES[142] in 1891 and expanded and placed on a more rigorous theoretical footing by VON HIPPEL in 1926[24] and TOWNES in 1940[144]. The theory was based on the concept that the approaching ion gives up its energy to the sputtered surface, producing a rapid rise in temperature in a small hemispherical region of atomic dimensions and thereby causing local evaporation of the surface material. Experiments by SEELINGER and SOMMERMEYER[145] and ROCKWOOD[146] seemed to confirm predictions made by the theory on angular distributions and sputtering yield values of various sputtered materials. Recent experiments, however, using single crystal

targets and low ion energies, and studies on the velocity distribution of the sputtered atoms, have all cast doubts on the universal applicability of this theory, although under certain conditions of high gas pressures and temperatures it may still have some validity[147].

The mechanism of momentum transfer was first proposed by STARK[143] in 1908 and involves elastic impacts between the incoming ions and the atoms of the target material, with transferal of momentum to the solid. Atoms of the target will be ejected if the momentum vector of the incoming ion can in some way be reversed on collision with the target atoms. KINGDON and LANGMUIR in 1923[148] suggested just such a mechanism:-

" A surface atom of thorium is struck by an ion and driven into the underlying tungsten forming a depression. When this depressed thorium atom is struck by a second ion, the ion is elastically reflected and on its way back may strike one of the surrounding thorium atoms and dislodge it".

Another explanation, which is much closer to the one used at present in momentum transfer theory, was suggested by LAMAR and COMPTON in 1934[149]. They postulated that sputtering might occur when an incoming ion penetrated the target surface, was reflected from a lower atomic layer, and recoiled to strike a surface atom in the outward direction.

Since the 1950's mounting evidence by a number of experimentalists and, in particular, Wehner with his studies on sputtering from single crystal targets, has tended to show the pre-eminence of the momentum transfer theory in the explanation of sputtering phenomena.

The evidence for the momentum theory has been summarised by MAISSEL[9] as follows:-

" 1. Sputtering yields depend on the mass of the bombarding ion as well as on its energy.

2. The sputtering yield is very sensitive to the angle of incidence of the bombarding ion.

3. There appears to be a threshold energy below which sputtering does not occur.

4. Sputtered atoms have energies many times greater than thermally evaporated atoms (even for extremely hot sources).

5. Atoms sputtered from single crystals tend to be ejected along directions of close packing.

6. Sputtering yields decrease at very high energies because of ion penetration below the surface.

7. The rate of secondary electron emission by ions is relatively low. If high local temperatures existed, strong thermionic emission would be expected.

8. The sputtering process is rather insensitive to temperature and, in certain cases, there is even a decrease in sputtering yield with increasing target temperatures.

9. There is no sputtering by electrons, even at very high energies."

The most recent theories on sputtering are founded on that of Lamar and Compton, but are complicated by the fact that many collisions of the ion → target and target → target type can take place before an atom is sputtered. This makes the momentum transfer theory a statistical problem and most recent studies such as those of KEYWELL[150] and HARRISON[151] have

treated it as such.

Any modern theory of the sputtering mechanism must take into account the anisotropic ejection of sputtered atoms from a monocrystalline target, that was first observed by Wehner, and more recently by ANDERSON and WEHNER[114], KOEDAM[121], and numerous others[122,152,153].

SILSBEE[154], in 1957, investigated this problem and suggested that the distribution of energy and momentum among the atoms in a collision sequence, during high energy sputtering, may be influenced by the well ordered structure of the monocrystalline target. He showed that 'focusing' of the original energy imparted to the surface was greatest along directions of closest atomic packing, and suggested that this would explain the sputtering deposit patterns from single crystals. 'Assisted focusing' caused by a moving atom, passing through atomic rings[155], and 'channelling' caused by an atom recoiling from either side of widely separated atomic planes[156] have both provided further evidence of the importance of focusing in the sputtering mechanism.

3.4 Target preparation and the generation of clean surfaces

3.4.1 Introduction and definition

In any thin film experiment whether it be by sputtering or evaporation, if reproducible results characteristic of the source material and gases used are to be obtained, the source and substrate surfaces must be 'clean'. An atomically clean surface is said to be "one free of all but a few percent of a single monolayer of foreign atoms, either adsorbed on or substitutionally replacing surface atoms of the parent lattice"[157].

3.4.2 Methods of evaluating clean surfaces

A variety of methods using surface sensitive effects have been employed to evaluate the cleanliness of a surface.
Amongst these methods are:-

Work function measurements[158],

secondary electron yield[159],

low energy electron diffraction[160] (LEED), and

Auger spectroscopy[161].

Pressure change in a known volume during flash heating of a sample may also be used although it cannot distinguish between impurities at the surface and in the bulk of the specimen. The last method is discussed in more detail further on, in relation to the gas analysis techniques required to measure the gas contents of sputtered and evaporated thin metal films obtained in the present investigation.

At atmospheric pressure a clean surface is bombarded by about 3.10^{23} molecules $cm^{-2}sec^{-1}$. A proportion of these molecules will have a sticking probability greater than zero and are therefore adsorbed on arrival at the 'clean surface'. Assuming a sticking probability of 1, it can easily be shown

that in about one second a clean surface will be covered by a monolayer of contaminating gas at an ambient pressure of 10^{-6} torr[162]. It is necessary, therefore, to work at background gas pressures as low as possible if clean surfaces are to be maintained for the length of an experiment..

3.4.3 Cleaning methods

The target source and substrate surfaces may be cleaned by one or more of several methods, principally:-

i. Thermal desorption heating to a high temperature

ii. Vacuum evaporation

iii. Ion bombardment cleaning

iv. Crystal cleaving

v. Chemical cleaning.

i. Thermal desorption is probably the simplest and most easily carried out. For the majority of metals it is accomplished either by electron bombardment, or resistively heating the sample. If the latter is not possible, then it may be inductively heated through its supports. Very recently the promising technique of laser bombardment heating has been used[163,164] and has been shown to have several advantages over the more conventional methods. For example, the vacuum conditions will not be adversely affected by the heat source since it is outside the vacuum system. It is unlikely that impurities will migrate towards the surface since only the surface will be heated, with negligible bulk heating, if only short laser pulses of about 40 nsec are used. Furthermore, the possibility of recontamination by residual gases following the heating cycle is avoided, as the heated surface will also cool off in a few nsecs. Lastly, in contrast with the ion bombardment method (see below), no foreign atoms are introduced

List of temperatures necessary to outgas metal surfaces covered with different gases. The temperature T_s is the melting point of the metal.

System	h (Kcal/mole)	T_d (^oK)	T_s (^oK)
O_2 on W	155	3100	3653
N_2 on W	95	1900	3653
H_2 on W	45	900	3653
C_2H_4 on W	102	2040	3653
N_2 on Ta	140	2800	3303
H_2 on Ta	45	900	3303
C_2H_4 on Ta	138	2760	3303
O_2 on Fe	75	1500	1808
N_2 on Fe	40	800	1808
H_2 on Fe	32	640	1808
CO on Fe	32	640	1808
C_2H_4 on Fe	68	1360	1808
O_2 on Ni	130	2600	1726
H_2 on Ni	31	620	1726
CO on Ni	35	700	1726
C_2H_4 on Ni	58	1160	1726

Table 3.1.

into the sample surface.

Chemically and physically adsorbed impurity molecules may be desorbed thermally if the temperature to which the target is heated, whilst under vacuum, is sufficiently high to overcome their surface binding energies. According to KAMINSKY[10] the highest temperature necessary for desorption, and so adequate cleaning of the surface, is given approximately by

$$T_d = 20h.$$

where T_d is the temperature and h is the binding energy in kcal $mole^{-1}$. of the impurity molecules to the host atoms.

Caution must be used in applying this guide as Table 3.1. shows, for it is possible that the target may melt or even evaporate before the temperature for desorption is reached. No difficulties are experienced in using this method for the refractory metals such as tungsten, molybdenum and tantalum, but it is not possible, for example, to desorb oxygen from nickel since the metal melts before the oxide bond is broken. There is an additional disadvantage in using the thermal desorption method since surface impurities may diffuse into bulk or, on the other hand, impurities in the bulk may tend to diffuse towards the surface. FARNSWORTH et al[165] have observed just such effects when heating nickel under vacuum in a LEED system.

ii. Among the methods of obtaining clean surfaces of the non-refractory metals is the technique of evaporation onto a suitable substrate. Either the electron bombardment or resistive heating methods may be used to achieve the evaporation of the sample to the desired thickness. Initial heating of

the sample to a temperature just below its evaporation point will allow the more volatile of the impurities to thermally desorb. A further slight increase in temperature vaporises the now purified sample, with the added advantage of leaving the less volatile impurities behind.

iii. Another method of cleaning is ion bombardment of the metal surface[166] with inert gas ions of several hundreds of volts energy. This will remove the layers of foreign atoms from the surface as well as layers of the target material itself. This procedure is particularly attractive in the present investigation since the facilities for ion bombardment are already available in the triode sputtering arrangement. Unfortunately the ion cleaning technique also has some shortcomings, the most important being that surface damage can occur at the bombarded surface. Examples are the formation of cones and pits on the target[167] and atomic displacements at the surface of a crystal[168]. The latter physical heterogeneities can, however, be annealled out by using the thermal desorption process in conjunction with ion bombardment. FARNSWORTH et al[169] have established a procedure which, if followed, should lead to atomically clean and undamaged surfaces. This is briefly summarised in the following sequence:-

1. Achieve a vacuum of about 10^{-9} torr,
2. thermal desorption of samples at 500-1000°C for several days,
3. ion bombardment of samples with Ar^+ with energies of about 500 eV and 1 mA cm^{-2} density for 1 hour,
4. annealing of the samples at 500°C,
5. repeating 3. and 4. several times, and finishing with 4.

iv. Cleaving of samples under ultra high vacuum is another technique

for producing a clean surface[170]. In practice, however, it is not much favoured since strain is often introduced into the cleaved sample which may affect its surface. In addition, this method is limited to crystal samples which can be fractured along a cleavage plane and therefore is of no use for polycrystalline samples which have no such planes.

v. Finally, in conjunction with one or more of the above mentioned methods, chemical cleaning and etching is often applied to the sample before it is placed under vacuum. Care must be taken with this type of cleaning to remove all traces of the chemicals used. If this is not done it is likely that traces of hydrocarbons (from which the cleaning fluids are often composed) will be left on the surface when the sample is placed under vacuum. When the clean surface has been prepared it is necessary to maintain it in this 'clean' state and free from all contamination. This can only be achieved by maintaining the surface under ultra high vacuum conditions.

3.5 Gas incorporation in thin films and the effects of ion bombardment

3.5.1 Introduction

During the deposition of a metal, either by sputtering or evaporation, for an average rate of deposition of 500 Å min^{-1}, about 5.10^{15} metal atoms sec^{-1} will arrive at a 1 cm^2 substrate surface. At a residual gas pressure of 10^{-5} torr, the substrate will also be subjected to bombardment by about 4.10^{15} gas atoms $cm^{-2}sec^{-1}$. This suggests that the metal film will be deposited in compound form, or at least will contain considerable quantities of occluded gas, if the residual vacuum includes reactive gases, with sticking probabilities greater than zero.

Many investigators have in the past shown that the physical properties of thin films can often be correlated with the environment in which they are grown. Often a specific property of a particular film has been related to the partial pressure of a particular gas present during deposition. This type of investigation has been carried out for both evaporated and sputtered films, often with comparisons of the film properties being made between the two methods of preparation[171-173].

However, as pointed out by KAY et al[77] "These types of investigations have not primarily concerned themselves with the mechanism of gas incorporation or with the analysis of the gas content of the completed films". Surprisingly few studies had been made of this topic until WINTERS, KAY et al, began investigations during the early 1960's. Since then interest has steadily grown in this field stimulated largely by new techniques which have facilitated the analysis of the gas content of these thin films.

3.5.2 Correlation with the physical properties of the films

MELMED[174], in experiments using a field electron emission

microscope, showed that residual gas pressures as low as 2.10^{-8} torr increase the density of nucleation of Cu on W compared with the nucleation density at ambient pressures of 4.10^{-10} torr. The effect of the adsorbed oxygen and nitrogen on the mobility of Cu on W increases the activation energy for surface diffusion. FRERICH[132] in 1962, aware of the problem of gaseous impurities in the production of superconducting films of tantalum and niobium, was one of the first to use AC asymmetrical sputtering to obtain purer films. CASWELL[175] deliberately introduced specific amounts of particular gases into his vacuum system to investigate their effects on the superconducting characteristics of evaporated tin films, and SOSNIAK and HULL in 1967[176] succeeded in depositing DC diode sputtered niobium thin films with superconducting properties by extensive presputtering, to obtain the required reduction in film impurity content. GERSTENBERG and HALL[173] made comparisons between sputtered and evaporated superconducting films of niobium, tantalum and their nitrides and carbides. The sputtered compounds were reactively produced by adding small quantities of methane and nitrogen to the sputtering argon atmosphere, whereas the evaporated films were deposited by electron beam evaporation.

A number of workers have investigated the resistivities and temperature coefficients of resistance of sputtered films, evaporated films and their bulk materials, and have suggested that the differences between them lie to some degree in the amounts of gaseous impurities they contain. GERSTENBERG[177] found a strong relationship between the residual gas pressure and the electrical properties of sputtered titanium films. Comparison with evaporated films of the same thickness showed that these had a lower resistivity than the sputtered films due to the lower impurity content in

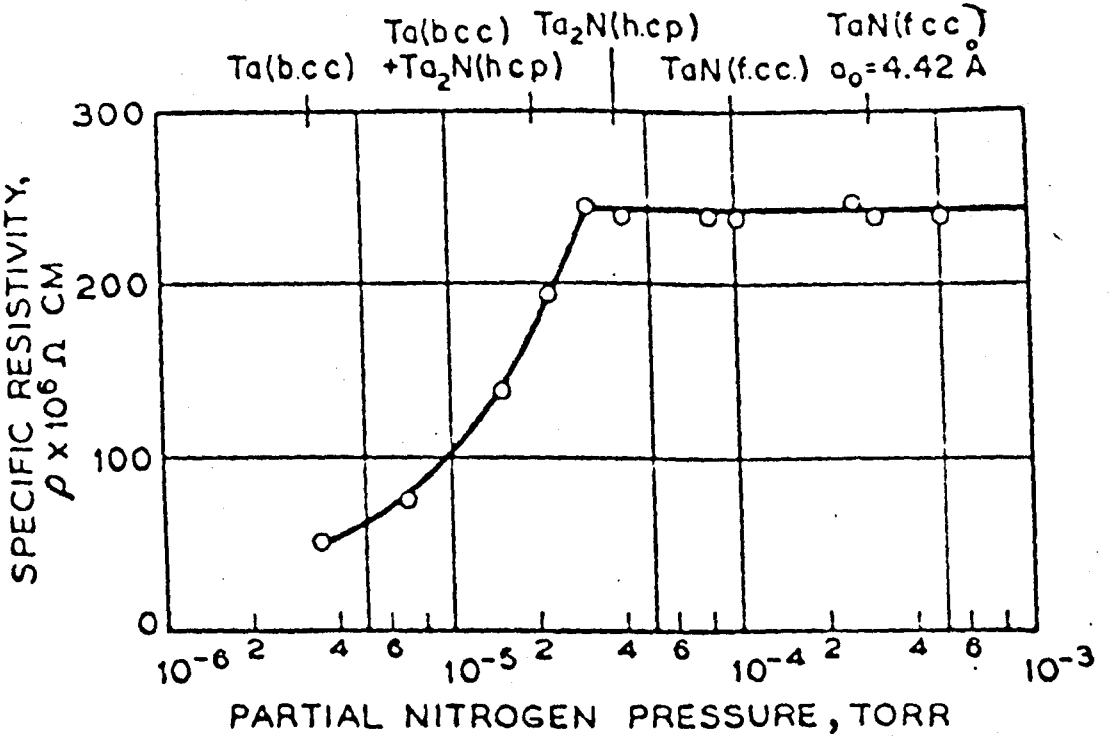

Figure 3.2 The effect of nitrogen on the resistivity of sputtered tantalum films.

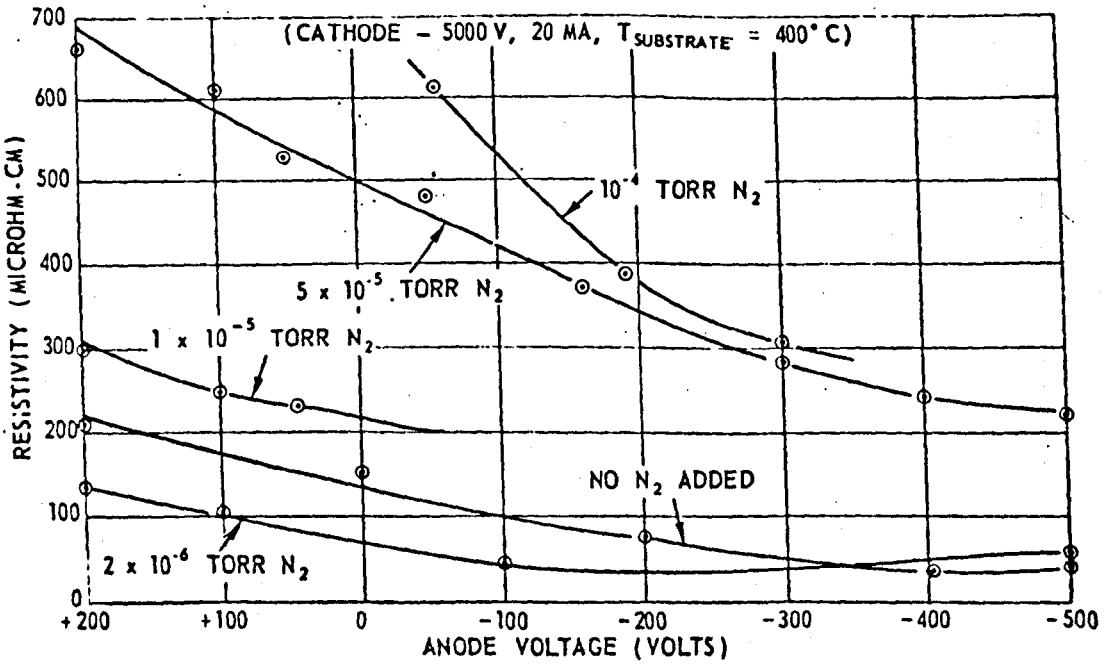

Effects of anode potential on tantalum and tantalum nitride film resistivity.

Figure 3.3

the evaporated films. Similar studies in 1964, by GERSTENBERG and CALBRICK[178] using tantalum, showed that tantalum films, 1000 Å thick sputtered in pure argon, had specific resistivities about four times the bulk value. Additions of small quantities of nitrogen, methane and oxygen all further increased the resistivity, often with the formation of new tantalum compounds, Figure 3.2. Also using tantalum, MICHALAK[179], KRIKORIAN and SNEED[180], and COOK[181] showed that in general, the resistivity of the sputtered films may be reduced by the application of a negative voltage bias to the substrate on which the film is growing. They all ascribed this reduction in resistivity, at least in part, to a lowering of the gaseous impurity content of the growing film, brought about by ion bombardment cleaning when a voltage bias was applied. In addition, Krikorian and Sneed made a detailed study on the effects of the sputtering characteristics, such as target voltage, substrate temperature and film growth rate, on the resistivity of the sputtered films. They showed that in some situations it was possible to obtain lower resistivity values by the addition of small amounts of nitrogen in the sputtering gas (argon) Figure 3.3.

SOSNIAK[182] and SOSNIAK, POLITO and ROZONYI[183] described a mass spectrometric investigation to follow the composition variations in the ambient atmosphere during the sputtering of tantalum films. They not only tried to relate these results to the resistivity of the films but were among the very few, already mentioned, who measured directly the gas content of these films, using the flash discharge technique (described further on).

TOOMBS in 1968[184] measured the resistance of thin triode sputtered gold films. He found that films of greater than 200 Å exhibited a constant resistivity about four times that of bulk gold, up to a maximum of 4000 Å

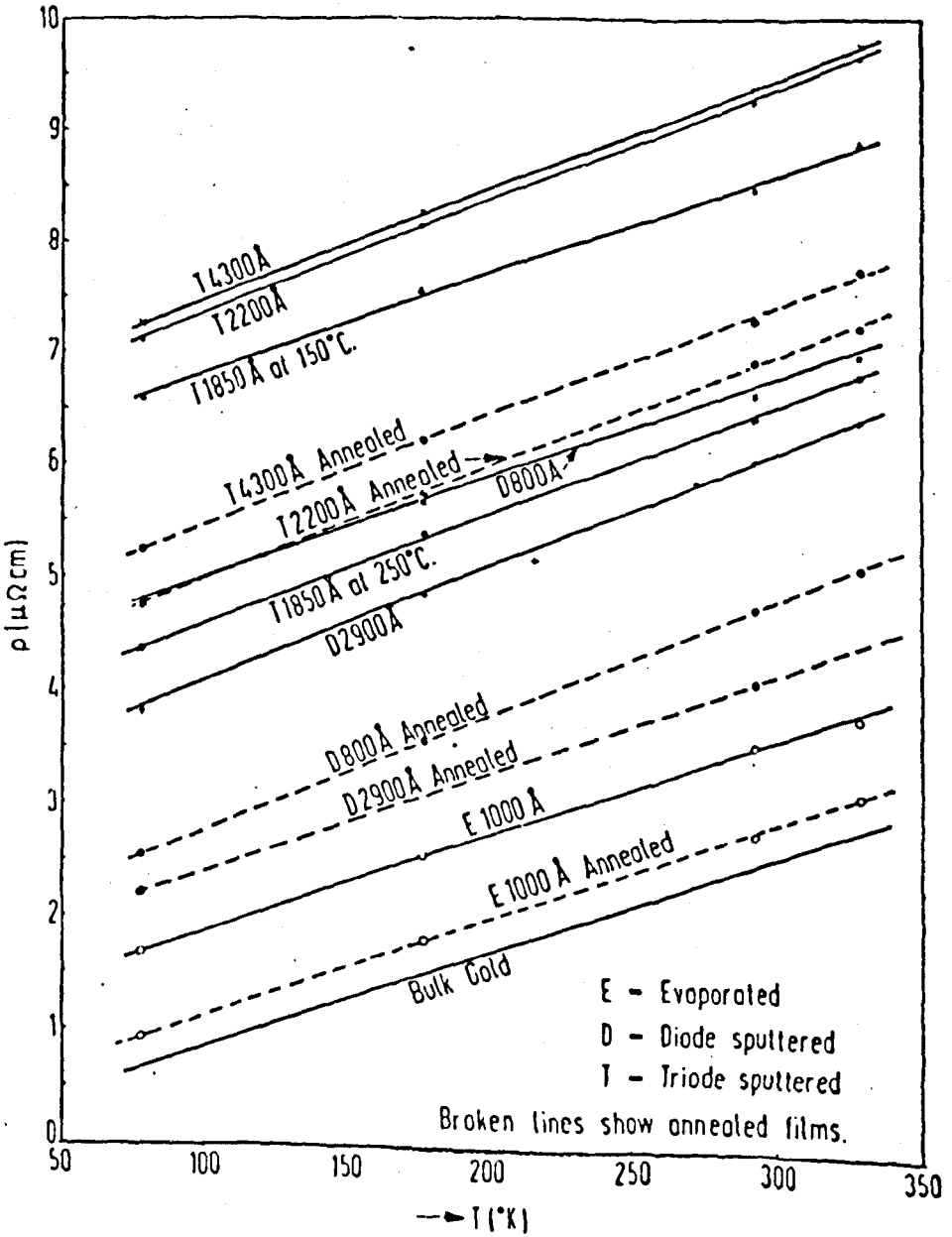

Resistivity vs temperature for thin gold films.

Figure 3.4

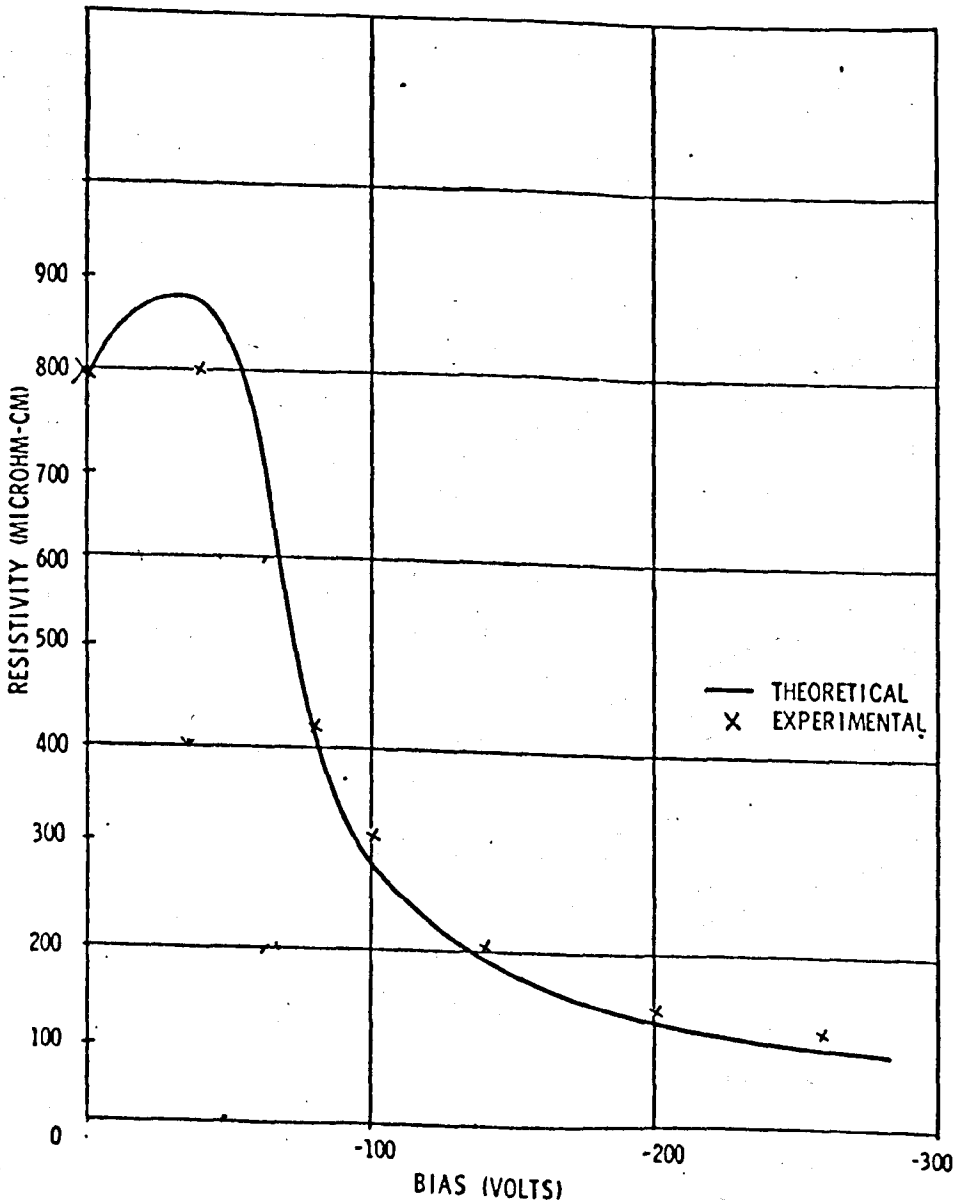

Figure 3.5 (a) Effect of bias voltage on resistivity of sputtered tantalum films.

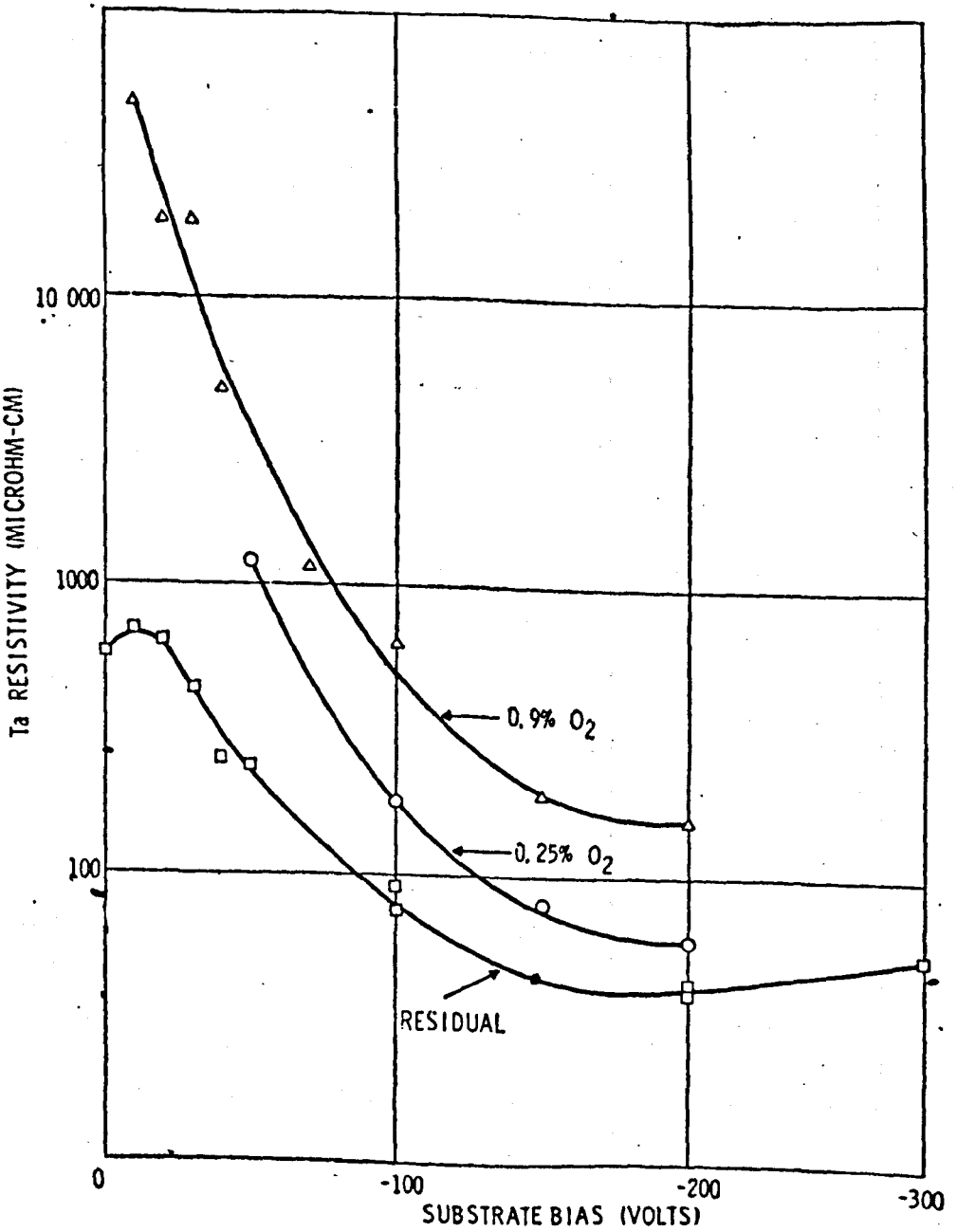

Effect of bias against oxygen contamination.

Figure 3.5 (b)

(the thickest films made). Annealing at 300°C for four hours only reduced the resistivity to about twice that of the bulk. Comparison with evaporated gold films showed that resistivity - temperature values for the sputtered films were always about twice those of the evaporated films, see Figure 3.4. In an attempt to explain these results on the basis of gaseous impurities, he subjected the films to electron microprobe analysis but could find no sign of gases in his films, either reactive or inert, or any other form of contaminants. He therefore attributed his results to electron scattering effects at grain boundaries, and to small crystallites he had observed growing on the surface of the sputtered films. It does seem surprising that Toombs found no sign of any contamination in his sputtered films, since the apparatus, with background pressures of about 10^{-5} torr, argon pressures of about 1.5 10^{-3} torr and the fact that the samples had to be removed from vacuum into the atmosphere before the gas analysis could take place, would have led one to expect active gas impurities, at least , to be found.

MAISSEL and SCHAIBLE[185] in 1965 published a paper in which they described an investigation on the variation of resistivity of tantalum with increasing ion energy bombardment of the growing film. Using an ion bombardment model, which they had suggested, they were able to obtain an expression for the concentration of gaseous impurities in bias sputtered films which was in good agreement except at the very high and very low values of voltage bias, with the experimental results for tantalum films sputtered in argon, containing 1.8 at % oxygen, see Figure 3.5a and b. They did not, however, directly measure the gas content of the films, but used computed values from Gerstenberg and Calbrick's results.

The model used was as follows:-

The concentration of impurities in the film g_i, grown either by evaporation or sputtering in the presence of some partial pressure of a gaseous impurity, is given by:

$$g_i = \alpha_i N_i / (\alpha_i N_i + R)$$

where N_i is the number of impurity gas atoms striking a unit area of film in one second, α_i is the sticking coefficient for the gas atoms on the film, and R is the deposition rate of the film.

For evaporated films g_i can be reduced by increasing R, whereas this is more difficult to achieve in sputtering. Therefore attempts to reduce g_i for sputtered films must depend on reducing α_i and/or N_i. In the presence of voltage bias the above equation is modified to

$$g_i = \frac{\alpha_i N_i - (j/q)(AS - \beta)}{\alpha_i N_i - (j/q)(AS - \beta) + R}$$

and

$$A = \frac{\alpha_i N_i + \beta j/q}{\alpha_i N_i + j(S + \beta)/q}$$

where β is the fraction of the bias current density due to the impurity ions, q is the electronic charge, S is the sputtering yield for the impurities, and j is the bias current density ($= \frac{i}{1+\gamma}$) where γ is the coefficient of secondary electron emission.

OBLAS and HODA[186] in 1969, using an RF spark source mass spectrograph, found considerable amounts of argon in diode sputtered tungsten films. These results were compared with those obtained by an ion induced re-emission

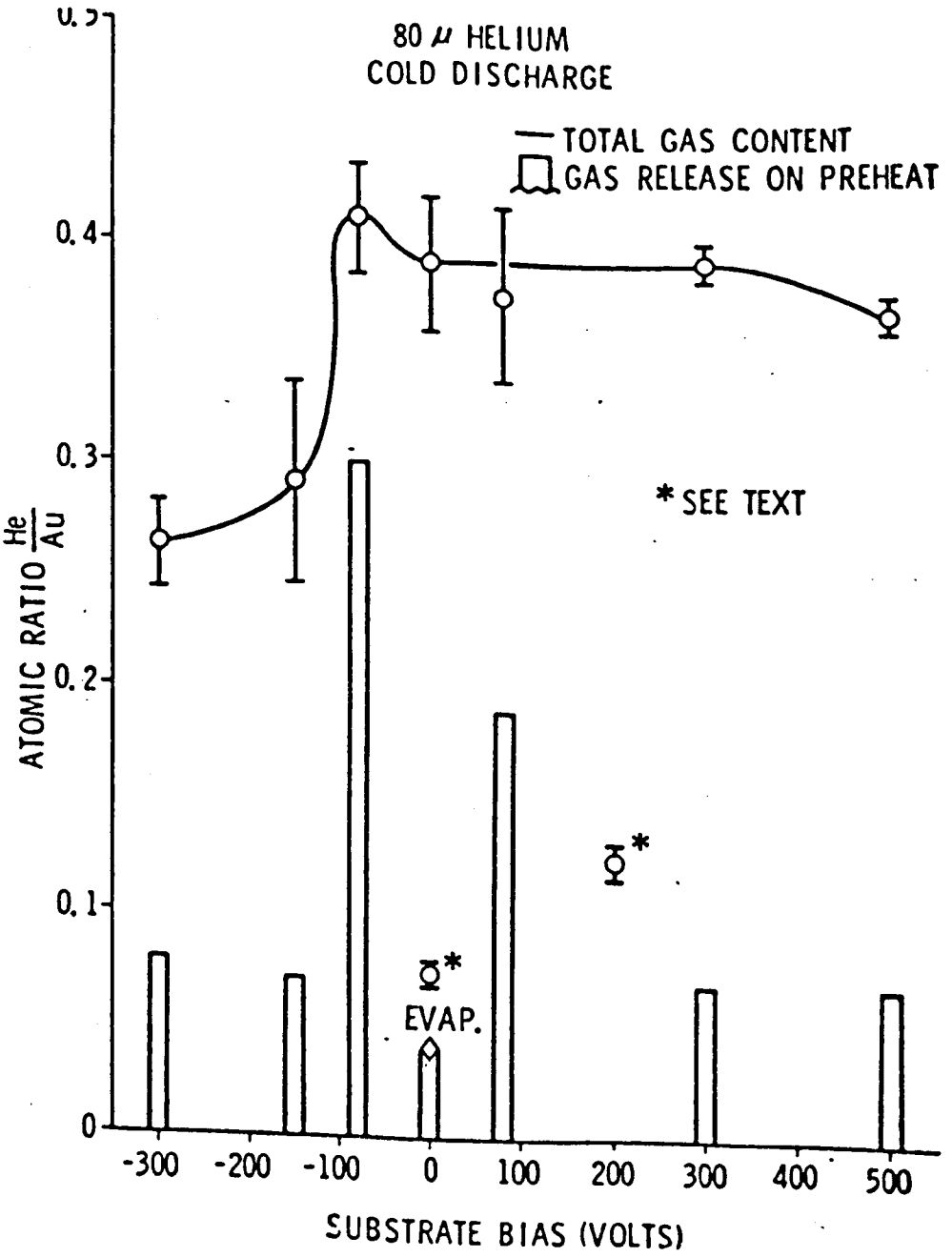

Figure 3.6 The effect of bias voltage on the incorporation of helium in sputtered gold.

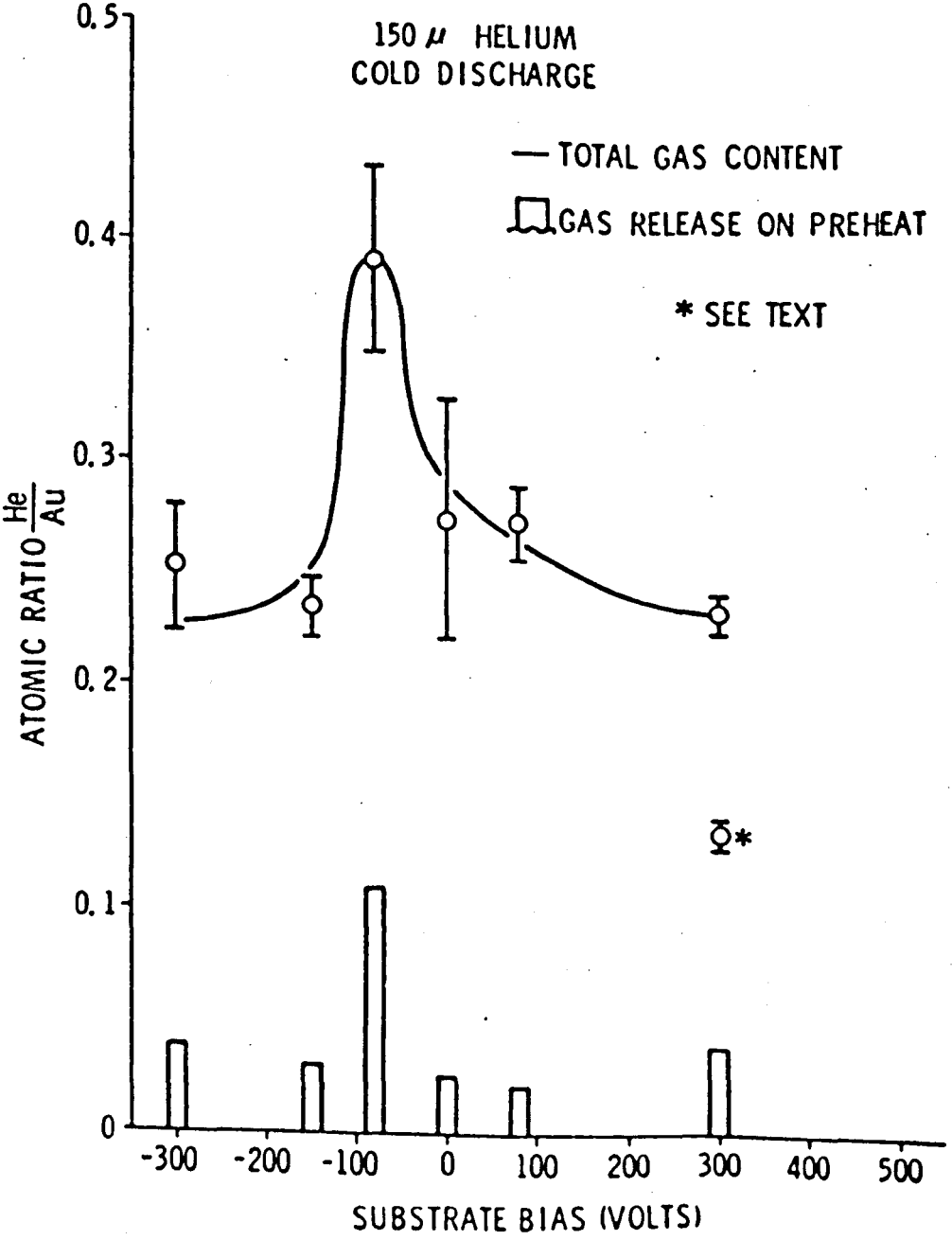

Figure 3.7 The effect of bias voltage on the incorporation of helium in sputtered gold.

method and reasonable agreement between them was found. LEE and OBLAS[187] measured the argon concentration of DC sputtered tungsten films deposited for both the diode and triode sputtering configurations, as a function of argon pressure, target to substrate voltage, substrate bias and target to substrate distance. Measurements of the argon to tungsten ratios were also performed on an RF spark source mass spectrograph and they concluded that, whilst the results for the diode deposited films supported Winters' model (see below), the results for the triode deposited films required an additional mechanism to explain them, involving the entrapment of low energy argon ions originating from the main discharge. SACHSE and NICHOLS[188] measured, by chemical analysis, the stoichiometric variations in sputtered oxide films of copper prepared by triode sputtering. They found it necessary, however, to sputter films of at least 100 cm^2 to obtain sufficient analytical accuracy.

Recently, MATTOX and KOMINIAK[189] in 1970, investigated the incorporation of helium in sputtered gold films, when applying positive as well as negative voltage bias to the growing film. Figures 3.6 and 3.7, indicate the results they obtained for gas pressures of 80 and 150 microns respectively, and for voltage bias from -300 to +300 volts. The 'starred' (*) points in Figure 3.6 refer to experiments carried out in a triode type arrangement, whilst the 'circled' (o) points, refer to a diode system. In contrast with LEE et al[187], they found that the diode sputtered films contained more incorporated gas than the triode ones. Furthermore, for the lower pressure values the positively biased films contained greater concentrations than the negatively biased ones, except for a peak value at about -80 volts. The much greater helium concentrations obtained, compared

Argon concentrations found in films sputtered at zero bias voltage (ZB) by various authors.

Author	Ref.	Deposition Method	Metal	(μ) Pressure	$X10^{-3}$(Å) thickness	Substrate	Argon content Atomic %
KAY	60	D	Ni	70	1.59	W	0.046
KAY	60	D	Ni	120	5.9	Ar	0.027
KAY	60	D	Ni	70	1.74	SiO_2	0.045
KAY	60	D	Gd_3Fe_5	70	3.55	W	0.85
GLANG	129	D	Mo	56	?	SiO_2	0.17
DAVIS	60	D	Ta	?	?	Corning(7059) glass	2.07
LEE	187	D	W	8	3.0	Si	0.10
LEE	187	D	W	20	3.0	Si	0.03
LEE	187	T	W	2	3.0	Si	12.0
LEE	187	T	W	8	3.0	Si	2.0
LEE	187	T	W	50	3.0	Si	0.03
WINTERS	212	D	Ni	70	?	?	0.21
WINTERS	212	D	Ni	70	?	?	0.42
WINTERS	212	D	W	70	?	?	2.27
WINTERS	212	D	Ar	70	?	?	0.28
WINTERS	212	D	Fe	70	?	?	0.061
WINTERS	212	D	Ag	70	?	?	0.10
OBLAS	186	D	W	50	3.0	Si	0.22
OBLAS	186	D	W	2.2	3.0	Si	9.0

D = DIODE T = TRIODE

with the argon concentrations found by Lee et al, can be understood when one considers that helium, being a very light gas compared with argon, has a much lower sputtering yield, even at relatively high ion energies. The reason for the high helium concentrations at large positive biases is not so clear, since it would be thought that a large energetic electron flux would stimulate thermal desorption.

Table 3.2. shows the results obtained by various investigators (including Winters and Kay, see later) for argon/solid concentrations in sputtered films at zero bias voltages. As is seen, a wide measure of disagreement exists between various investigators and the same is found for nitrogen and oxygen concentrations. Reasons for this disagreement must lie to some extent in the various methods of deposition and analysis, as well as in the inadequate knowledge of the 'cleanliness' of the target, substrate and surroundings, and the gases present in the system during film deposition.

Allied to the investigations into the gas incorporation in depositing films with and without the effect of voltage biasing, are the recent studies of the inert gas clean-up phenomena and ion sticking probabilities discussed in the previous chapter.

VARNERIN and CARMICHAEL[190] and YOUNG[191] in 1956 found, using a Bayard Alpert gauge, that a metallic film was necessary for the clean-up of helium and that the clean-up was related to positive ions striking the glass walls of the ionization gauge. BLODGETT and VANDERSLICE[64] found subsequently that the clean-up could not be explained by the simple depletion of available trapping sites at the glass wall. They postulated that the adsorption arose as a result of the interaction between metastable atoms and the surface, and their subsequent burial by sputtered material. In this way

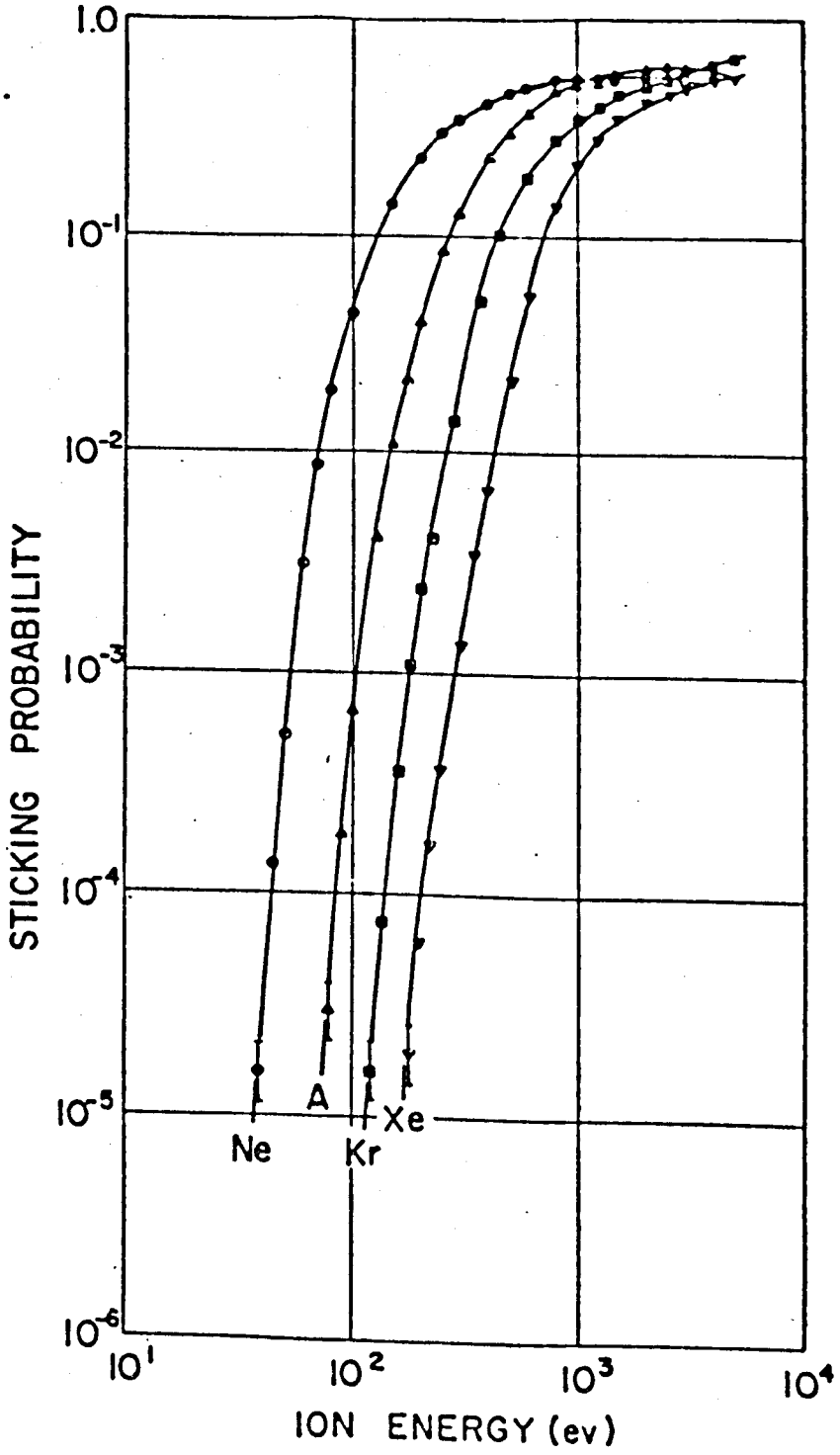

Figure 3.8 The inert gas sticking probability versus ion energy (on tungsten)

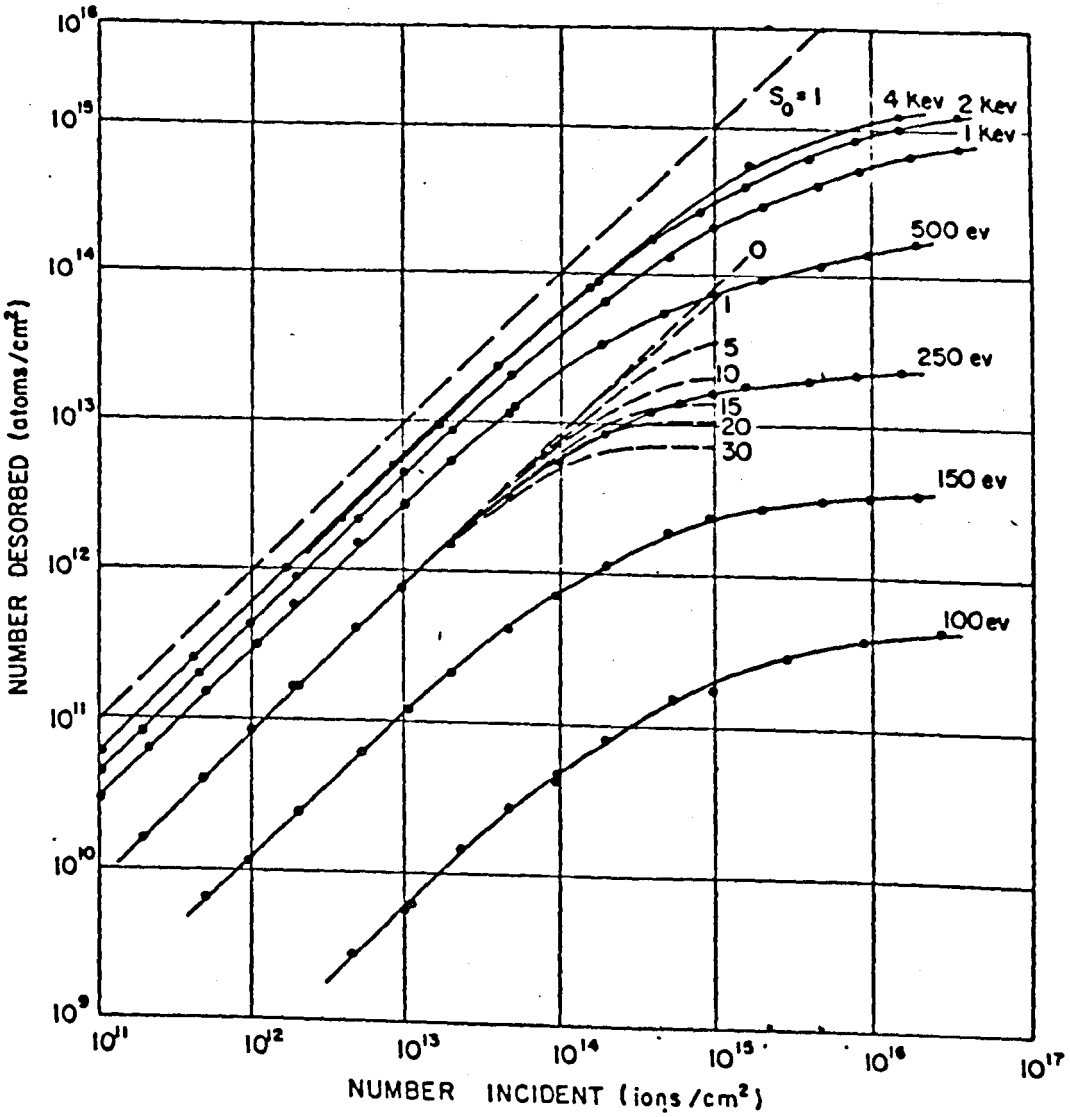

Figure 3.9 Ion bombardment induced re-emission on tungsten (determined from saturation curves).

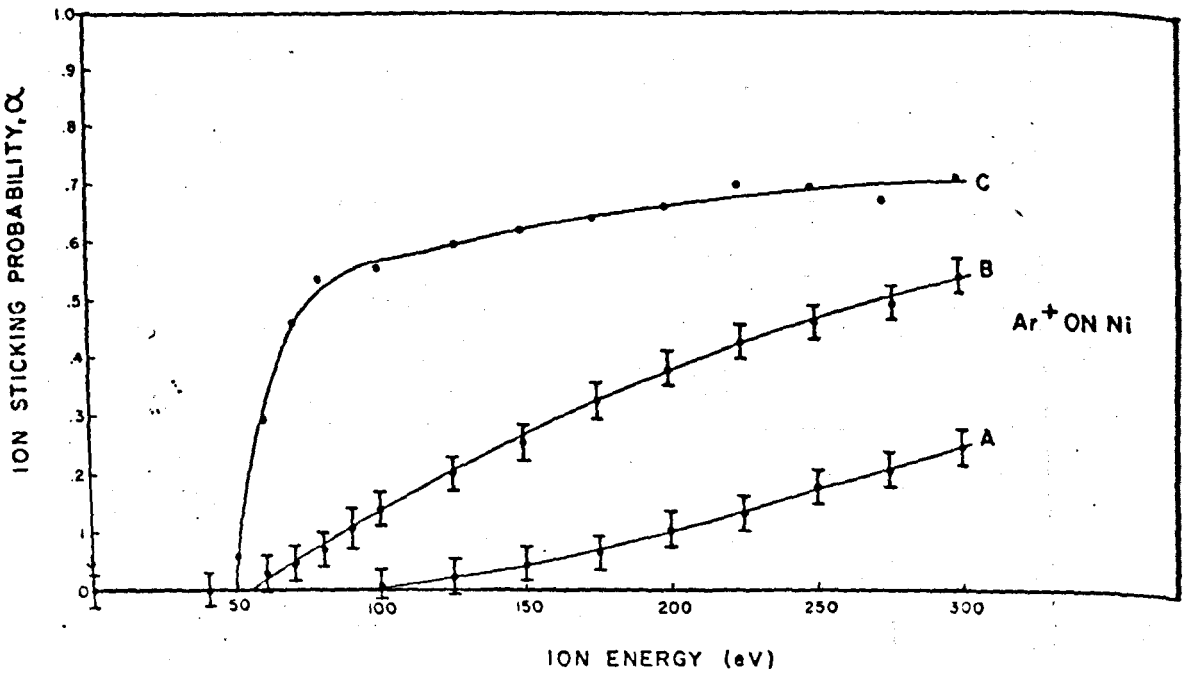

Curve A - on a freshly evaporated nickel film.

Curve B - on an evaporated nickel film after exposure to O_2.

Curve C - on an evaporated nickel film with a complex history of oxygen exposure and induction heating.

Figure 3.10 Sticking probability for argon ions as a function of ion energy.

the gas is distrubuted in the bulk of the material according to some depth function, and desorption takes place through diffusion. WINTERS and KAY[60], however, suggested that Blodgett et al's results could equally well be explained by high energy neutral atoms, colliding with the surface. These atoms are created by the resonance ionized and auger neutralized ions which approach the surface. SMEATON, CARTER and LECK[192], JAMES and CARTER[93] and CARTER and LECK[193], proposed that the noble gases must be adsorbed at or near the surface and that they can be desorbed in single activated jumps from sites of various binding energies.

Numerous investigators[194-197] have measured the sticking probability, i.e. trapping efficiency, for the ion - surface interaction for a variety of gases, targets, surface coverages and incident ion energies. For example, KORNELSEN[198] in 1964 measured the sticking probability for various inert gases on tungsten, as well as the effects of high gas concentrations, as shown in Figures 3.8 and 3.9. The amount of trapped gas was determined by thermal desorption. KAY and WINTERS[60] measured the ion sticking probability of argon on nickel as a function of ion energy and the previous 'oxygen history' of the metal, see Figure 3.10. In their case, the amount of sorbed gas was calculated from the pressure drop in the vacuum system after a given ion bombardment dose.

Gas release efficiencies, i.e. sputtering yields for gases, have also been determined. CARMICHAEL and TRENDELBURG[92] bombarded a nickel target with one inert gas and measured the amount released when the surface was bombarded with a different inert gas. The energy of ion bombardment was about 100 eV in both cases. Table 2.3. indicates their results. They interpreted their results on the basis of the target

sputtering mechanism. On the other hand, see Tables 2.4, JAMES et al[199,200,9] in experiments with glass targets, and CARMICHAEL and WATERS[201] who released He_3 by bombarding with He_4, both found that their results were consistent with gas release by a gas sputtering mechanism. Here, trapped gas atoms are released by an amount of energy from the bombarding ions which is not, however, sufficient to remove target atoms.

3.5.3. The work of WINTERS and KAY

Of great importance to the present investigation were experiments carried out from the early 1960's by WINTERS et al[76,202-210], and later in conjunction with KAY[60,61,77,211-213]. These studies related to the incorporation of inert and reactive gases in sputtered films, with and without ion bombardment of the growing film.

At first, using a relatively simple piece of apparatus, Winters endeavoured to determine the way in which nitrogen and argon were adsorbed at the surface of a growing film. By this means he determined the sticking probabilities for the ions, molecules and atoms of these gases and also their ion induced re-emission as a function of the ion energy of the bombarding species. These measurements were made on films deposited by evaporation. From these measurements, and using more sophisticated equipment, he went on to investigate the effects of ion bombardment during film growth on the structural properties and gas content of sputtered nickel films, and attempted to relate these results with the previously evaporated films.

In a publication in 1967 WINTERS and KAY[60] describe a series of experiments in which they measured the argon and nitrogen gas concentrations in sputtered nickel as a function of film growth, temperature, discharge

Figure 3.11

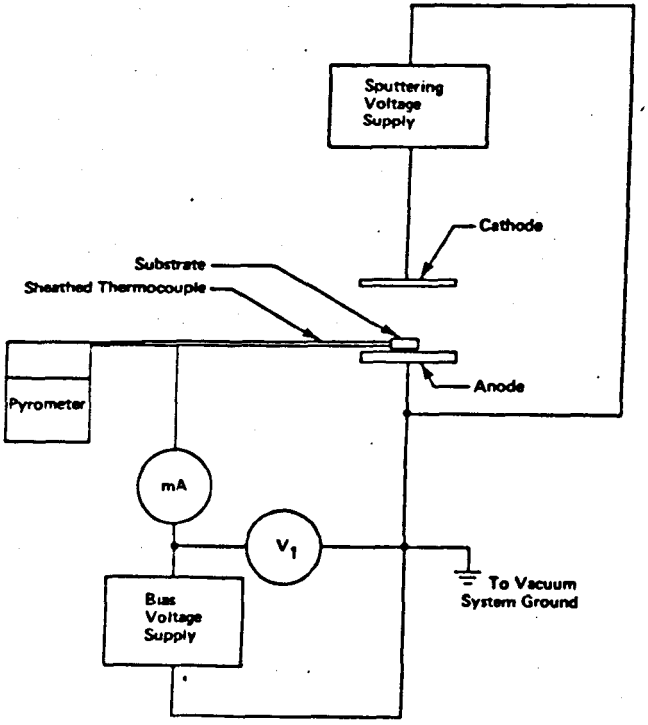

Schematic of sputtering apparatus.

MEANS FOR TEMPERATURE AND BIAS CONTROL FOR SPUTTERING SUBSTRATES

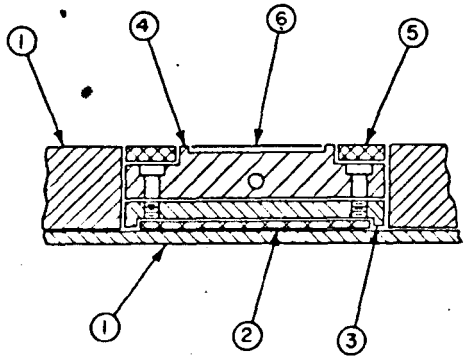

(1) TEMPERATURE CONTROLLED ANODE

(2) BERYLLIA DISC SOLDERED TO (1) AND (3)

(3) CONSIL DISC

(4) CONSIL BUTTON - SCREWED TO (3). TC HOLE IN CENTER

(5) ALUMINUM GUARD RING

(6) SUBSTRATE, GA SOLDERED INTO WELL IN (4)

BIAS IS APPLIED THROUGH THE STAINLESS STEEL SHEATH ON THE THERMOCOUPLE

Schematic of substrate assembly.

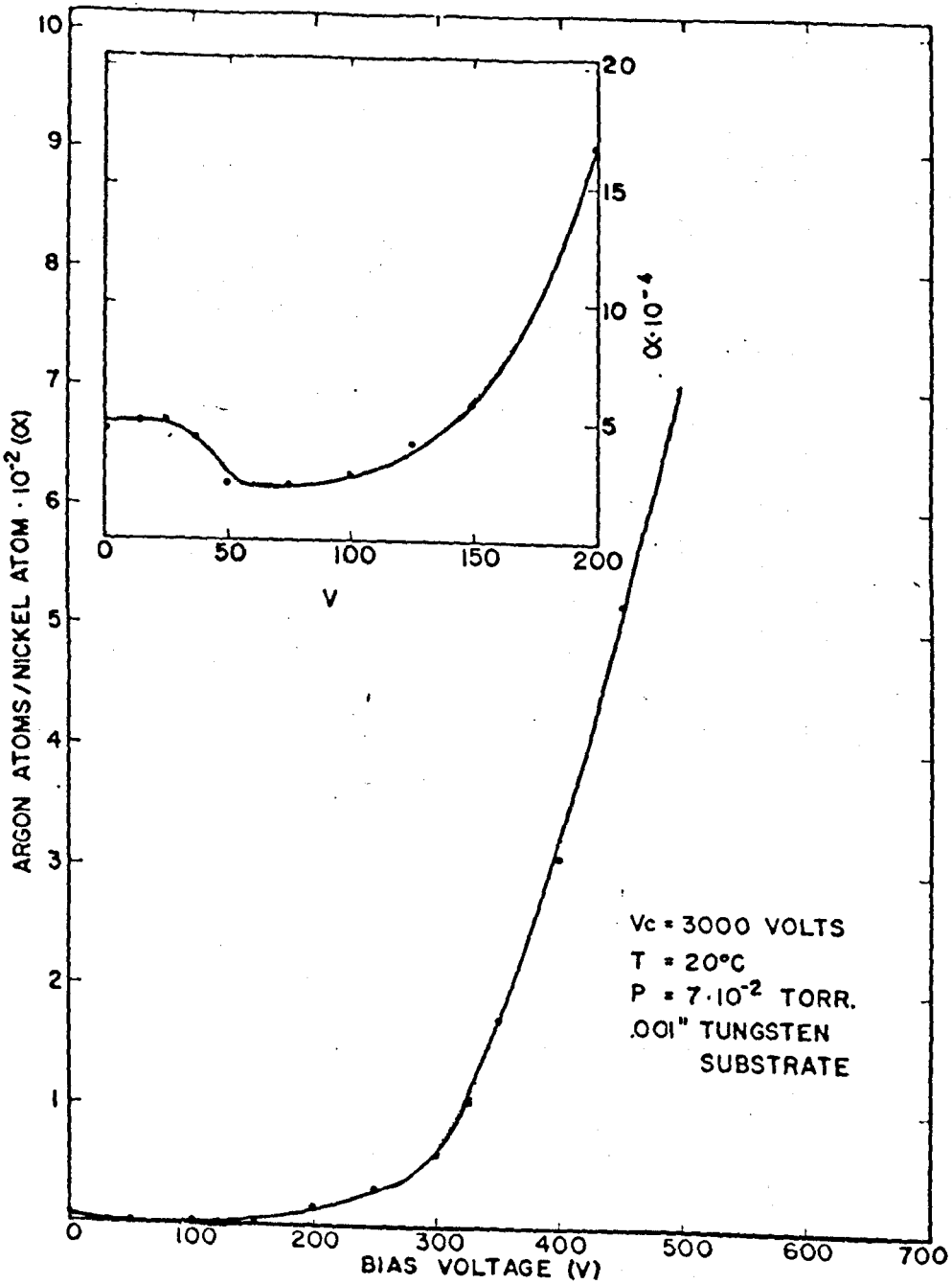

The argon concentration vs bias voltage.

Figure 3.12

pressure and ion energy of the bombarding ions impinging on the growing film. Their experiments indicated that some of the sputtering gas (argon) was incorporated in the film, and they suggested various mechanisms by which this process could occur. Reactive gases (e.g. Nitrogen) in the background pressure desorbed from surrounding surfaces during the experiment, were similarly considered. By applying low energy ion bombardment to the growing film the amount of gas incorporated could be controlled. The procedure was basically that of DC bias sputtering, which was previously used for controlling the physical properties of sputtered and evaporated thin films. The experimental apparatus was a typical DC diode glow discharge with the cathode acting as the sputtering target and the substrates, normally of glass or tungsten, resting on a temperature controlled anode, Figure 3.11. Gas analysis of the films was achieved by one of two methods, both of which involved vaporization of the film with the subsequent release of the gases into the vapour phase. These gases were then analysed by mass spectrometric means. (The gas release methods are described later in the chapter). Both of these methods, however, necessitated the removal of the sputtered films after deposition and prior to outgassing. This could be a serious disadvantage if reactive gas incorporation with chemically active films, such as titanium, is of interest, particularly as no indication was given of the time lapse which must have occurred between removal of the film and its replacement in the outgassing vacuum system. Their results, Figure 3.12, indicate that the inert gas concentration increases with ion bombardment energy, except at low bias voltages between 0-60 V, where there is a slight fall. In addition, they measured the concentrations as a function of argon pressure and substrate temperature. For the former,

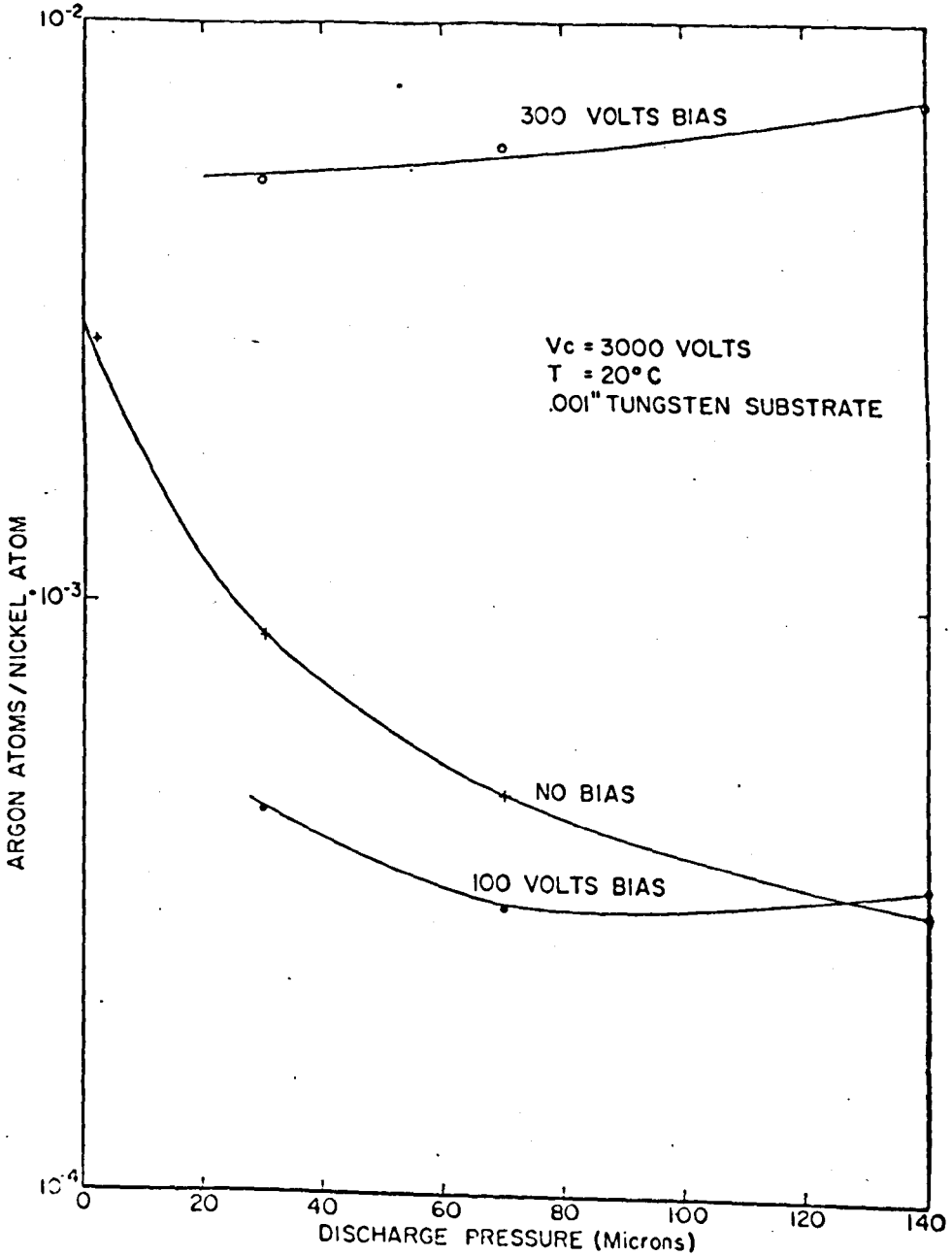

The argon concentration vs pressure.

Figure 3.13

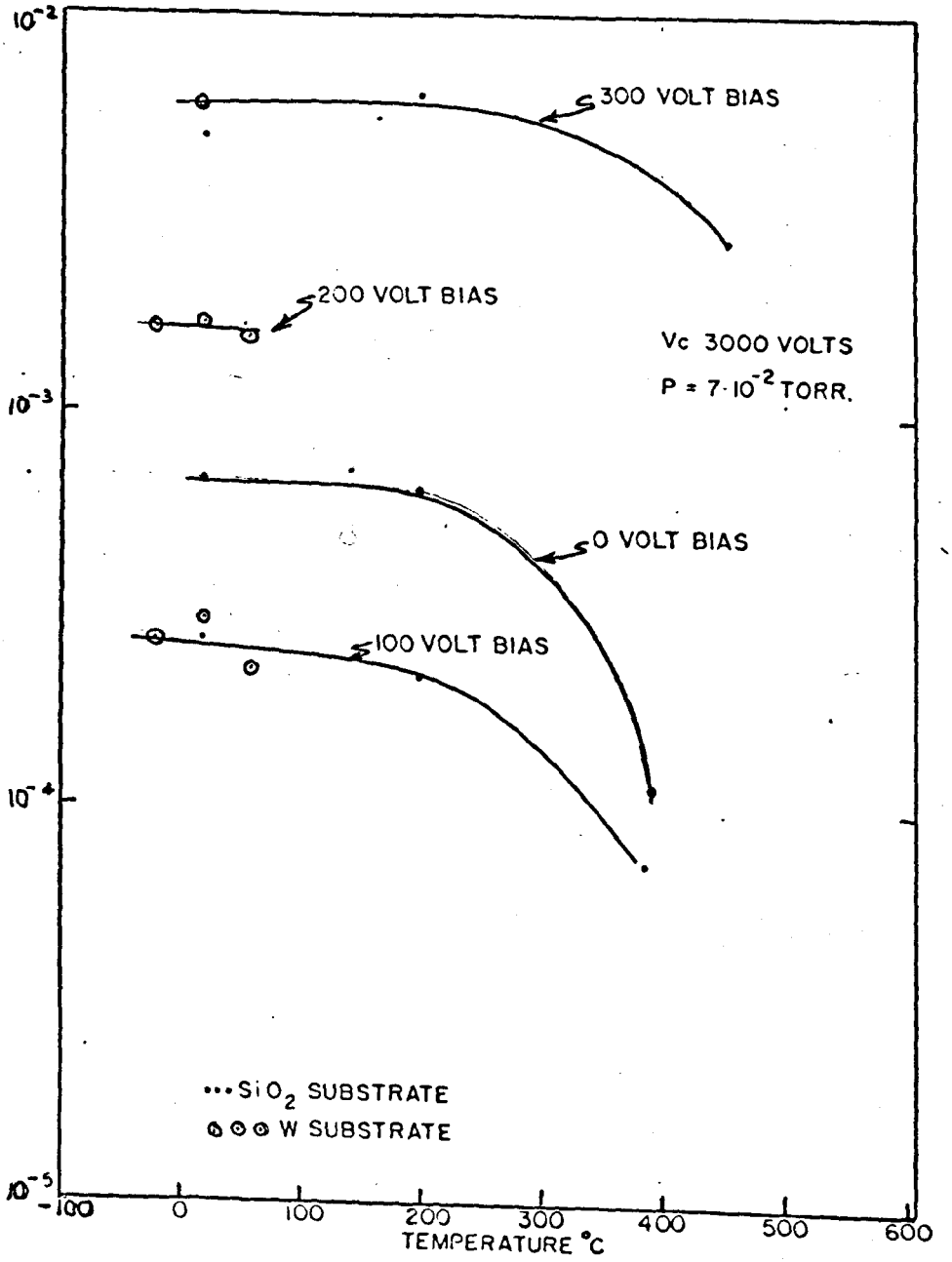

The argon concentration vs temperature.

Figure 3.14

Figure 3.13 shows that the concentration could increase or decrease depending on the bias applied to the film, whilst for the latter, Figure 3.14, the concentration is seen to be relatively unaffected by change in temperature, until about 300°C is reached. The implication is that, if the ion current density bombarding the growing film is kept at a level of about 1 mA cm^{-1}, overheating will not occur and temperature variations at the growing film should leave the concentrations almost unaffected. A detailed explanation of their results was given to show the manner in which the inert gas could be incorporated in the sputtered films. Similarly, although more sketchily, an attempt was made to describe the incorporation for nitrogen.

In 1969 WINTERS, RAIMONDI and HORNE proposed a model for the composition of sputtered multicomponent thin films[205]. This model is used in the present investigation (see chapter 6) to compare the experimental results obtained with those postulated by the theory..

The theoretical model of Winters et al.

The rate of incorporation of a substance into a growing film can be written as the difference between the rate of condensation and the rate of re-emission. If resputtering and evaporation are considered as the only re-emission processes taking place, then:-

$$k_n = R_n - S_n - \mu_n \qquad (1)$$

where k_n is the rate at which the component n is being incorporated into the film, R_n is the rate at which the nth component is condensing, S_n is the sputtering rate, and μ_n is the evaporation rate.

A fraction of the incident material may be reflected from the growing film and, defining a sticking probability for the nth component as λ_n, then the amount reflected is given by

$$(1 - \lambda_n)N_n \quad \text{atoms cm}^{-2}\text{sec}^{-1} \tag{2}$$

where N_n is the incident flux of the nth component. Hence the amount sticking is given by, R_n,

$$R_n = \lambda_n N_n \tag{3}$$

The incident flux will arise from the cathode or from an external source such as a gas leaked into the sputtering system. Under steady state conditions and in the absence of external sources, the material arriving at the growing film mirrors the cathode composition, i.e.

$$C_n^{\text{cathode}} = N_n / \sum_p N_p \tag{4}$$

where C_n^{cathode} is the concentration of the nth component in the cathode. The concentration of the nth component in the film, C_n, is given by:-

$$C_n = K_n / \sum_p K_p \tag{5}$$

$$= \frac{\lambda_n N_n - S_n - \mu_n}{\sum_p (\lambda_p N_p - S_p - \mu_p)} \tag{6}$$

From equations (4) and (5) it can be seen in general that

$$C_n^{\text{cathode}} \neq C_n$$

The concentration in the target will only be identical to the concentration in the film when $S_n = \mu_n = 0$, and when $\lambda_n = 1$. From DUSHMAN[214] and LANGMUIR[215] it can be shown that the rate of evaporation for a single component system is given by

$$\mu = 3.51 \times 10^{19} (M.T)^{-1/2} \times P \text{ atoms } cm^{-2} sec^{-1} \qquad (7)$$

where M is the molecular weight, T is the temperature in ^{o}K, and P is the vapour pressure in microns. Similarly it can be reasoned that

$$\mu_n = 3.51 \times 10^{19} (M_n T)^{-1/2} \times P_n$$

for the nth component in an alloy which is in thermodynamical equilibrium with its surroundings. If RAOULTS law holds then P_n may be related to the vapour pressure, P, measured in a single component system, and to the concentration of the nth component in the alloy. Alternatively, from REDHEAD[216]

$$\mu_n = \nu_n \sigma_n^x \exp(-E/kT) \qquad (8)$$

where σ_n is the surface coverage, ν_n is the rate constant, E is the activation energy for desorption and x is the order of the desorption reaction. Equation (8) is a more convenient form for gases than (7). However, for the situation where only two components are present (μ_1 and μ_2), and where the binding energies of the surface atoms are of the order of several eV, which is the case in most sputtering experiments, no evaporation will take place from the top film layer and so $\mu_1 = \mu_2 = 0$ and may be ignored in the equations derived from (6).

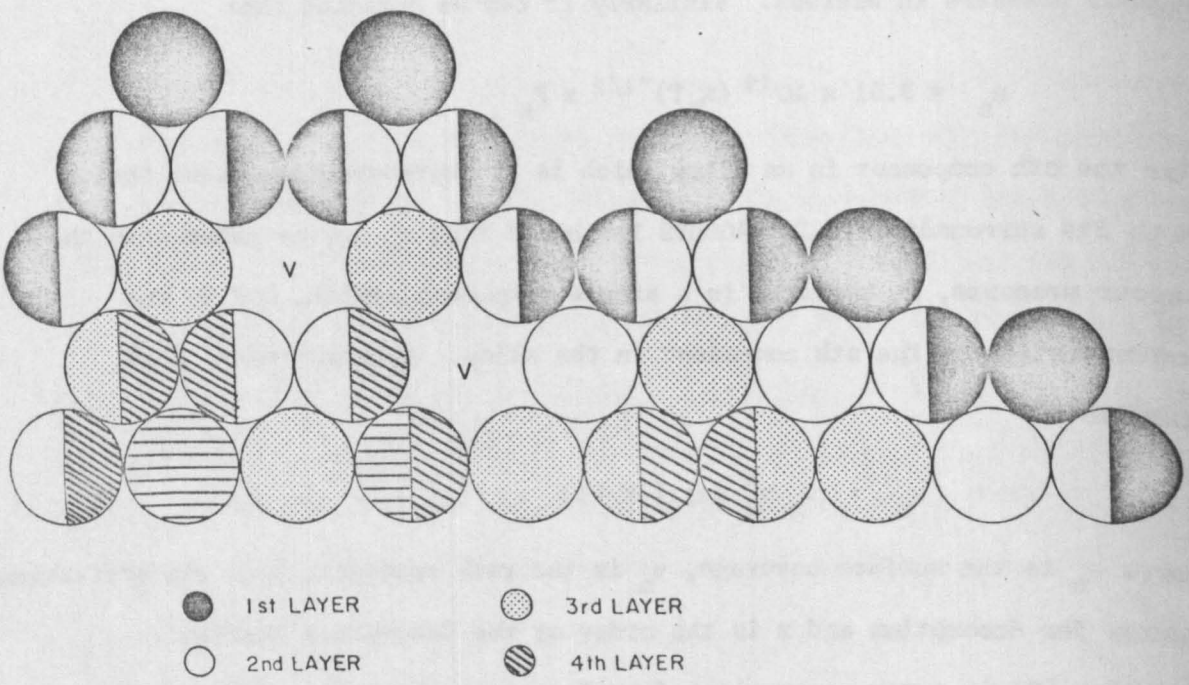

Figure 3.15 Cross-sectional view of the film which schematically illustrates the definition of surface layers used in the model of WINTERS et al [205].

Considering the cross-section of the growing film, illustrated by Figure 3.15, the part of the film that is seen enclosing atoms is defined as the top layer. The atomic layers defined in this way allow the sum of the fractional areas covered by the different components to be set equal to unity,

$$\sum_{n} A_{n,m} = 1 \qquad (9)$$

where $A_{n,m}$ is the fractional area of the mth layer covered by atoms of the nth component. It has been shown [217] that sputtering events due to ion bombardment up to 10 keV only occur in the top four layers, with most of them occurring in the first, surface, layer. Hence if only low energy ion bombardment of about <500 eV is considered, it is reasonable to assume that only sputtering from the first layer is predominant. In this case the number of atoms of the nth component leaving the film as a result of sputtering is proportional to $A_{n,1}$ where the subscript 1 refers to the first layer. Then S_n, the sputtering rate for the nth component, can be written:-

$$S_n = \alpha_n n_i A_{n,1} \qquad (10)$$

where α_n is the sputtering coefficient for the nth component and n_i is the flux of incident ions and energetic neutrals on the growing film. Substituting equation (10) in (1), and putting equation (8) = 0 gives

$$k_n = \lambda_n N_n - \alpha_n n_i A_{n,1} \qquad (11)$$

In general S_n and R_n are both a function of $A_{n,1}$ and temperature. Since it is usually difficult to obtain values of $A_{n,1}$ directly, the model makes the following simplifying assumptions:-

i. atoms leaving or condensing on the film always come from or go to the first layer.

ii. material entering or leaving the first layer causes material to enter or leave the mth layer, and it is further assumed that this is the only way that material enters or leaves the mth layer.

iii. for steady state conditions the composition of a given layer is constant.

One of the important properties of this model is that all layers, including the first, should have the same composition. With these assumptions:

$$A_{n,1} = a_n k_n / \sum_p a_p k_p \tag{12}$$

where a_n is the cross-section area of an atom of the nth component. Substitution of (12) into (11) gives a set of n equations solvable for k_n.

$$k_n = \lambda_n N_n - \alpha_n n_i (a_n k_n / \sum_p a_p k_p) \tag{13}$$

and the concentrations are given by equation (5).

$$C_n = k_n / \sum_p k_p$$

For a two component system equation (13) reduces to

$$K_1 = \lambda_1 N_1 - \alpha_1 n_i \, a_1 k_1 / (a_1 k_1 + a_2 k_2)$$

and

$$K_2 = \lambda_2 N_2 - \alpha_2 n_i \, a_2 k_2 / (a_2 k_2 + a_1 k_1) \tag{14}$$

It can thus be seen from this theory that equations (14) are realistic, only if processes such as exchange of material between layers by diffusion, knock-on collisions, and chemical reactions do not take place.

Gas incorporation into sputtered films.

Cathode material	Ambient atmosphere	R	Comments
Tungsten	Ar	$R_{Ar} \cong \lambda^{t}_{Ar} n_{Ar}$ $R_N \cong 0$	Argon is sorbed only by being embedded in the lattice.
Tungsten	Ar–0.01% N_2	$R_{Ar} \cong \lambda^{t}_{Ar} n_{Ar}$ $R_N \cong \lambda^{1}_{N}(1+\beta\lambda^{1}_{N})7.7\times10^{20}P_N$	The primary source of nitrogen is normal chemisorption.
Tungsten nitride	Ar	$R_{Ar} \cong \lambda^{t}_{Ar} n_{Ar}$ $R_N \cong \lambda^{1}_{N} F(P_N)$	The only source of nitrogen is the cathode. The nitrogen is assumed to be sputtered as atoms.
Nickel	Ar–5% N_2	$R_{Ar} \cong \lambda^{t}_{Ar} n_{Ar}$ $R_N \cong \lambda^{3}_{N} F(P_N) + \lambda^{2}_{N} n_N + \lambda^{t}_{N} n_N$	Nickel does not normally chemisorb molecular nitrogen.

TABLE 3.3

Radii and cross-sectional areas of some metal atoms

	Al.	Cu.	Au.	Ni.	Ti.	W.	Zr.	Ar.	N_2
Atomic radii Å	1.432	1.278	1.442	1.246	1.448	1.37	1.589	1.46	1.57
cross-section area $\times \pi^{-1} 10^{+16}$	2.05	1.633	2.08	1.563	2.1	1.88	2.53	2.13	2.465
cross-section area $\times 10^{+16}$ cm^2	6.44	5.14	6.54	4.92	6.6	5.91	7.95	6.7	7.75
Number of atoms making 1 monolayer $\times 10^{-15}$	1.56	1.95	1.53	2.04	1.52	1.69	1.26	1.50	1.29

Table 3.4

In order to make calculations for gas incorporation in films, values for the R_n's and α_n's must be known as well as n's and a's. This leaves equation (14) as two equations with two unknowns, k_1 and k_2 and is therefore soluble in principle, and hence values for C_n may be calculated.

Prior to incorporation into the growing film, the gas must be sorbed at the film surface. For nitrogen this may result from the sorption of molecules, atoms, ions which dissociate upon collision with the surface, or energetic molecules which penetrate the lattice. It is reasonable to assume that the sort of sorption mechanisms found for nitrogen are also present to some degree for other gases. In this case sticking probabilities can be defined for each of these processes as

$$\lambda_n^1, \quad \lambda_n^2, \quad \lambda_n^3, \quad \lambda_n^4, \quad \text{respectively.}$$

Each of these λ's has a different functional dependence on the surface coverage $A_{n,1}$. In general for a gas, the rate of sorption at the surface is given by:-

$$R_n = \lambda_n^1(1 + \beta\lambda_n^2)X.10^{20}P_n + \lambda_n^2 F(P_n) + \lambda_n^3 n_n + \lambda_n^4 n_n \qquad (15)$$

where β is the probability that an atom sputtered at the cathode reaches the substrate, and X is a constant depending on the gas. One or more of the terms in equation (15) can predominate, such that the others can be neglected. This depends on which gas is involved, the target species, the voltage bias etc. This is illustrated for several different conditions in Table 3.3.

Unfortunately all the parameters necessary to solve equations (14) are not known[210] and therefore reasonable guesses must be made. Values for the cross sectional areas of atoms are obtained from [218] see Table 3.4.

Sputtering yields of various materials in argon (Bombarding Energy of Ar^+ in Volts)

Sputtering Yields in Atoms/ion						
Target	200	600	1000	2000	5000	10k
Ag	1.6	3.4	-	-	-	8.8
Al	0.35	1.2	(1.05)	-	2.0	-
Au	1.1	2.8	3.6	5.6	7.9	-
C	0.05	0.2	-	-	-	-
Co	0.6	1.4	-	-	-	-
Cr	0.7	1.3	-	-	-	-
Cu	1.1	2.3	3.2	4.3	5.5	6.6
Fe	0.5	1.3	1.4	2.0b	2.5b	-
Ge	0.5	1.2	1.5	2.0	3.0	-
Mo	0.4	0.9	1.1	-	1.5	2.2
Nb	0.25	0.65	-	-	-	-
Ni	0.7	1.5	2.1	-	-	-
Os	0.4	0.95	-	-	-	-
Pd	1.0	2.4	-	-	-	-
Pt	0.6	1.6	-	-	-	-
Re	0.4	0.9	-	-	-	-
Rh	0.55	1.5	-	-	-	-
Si	0.2	0.5	0.6	0.9	1.4	-
Ta	0.3	0.6	-	-	1.05	-
Th	0.3	0.7	-	-	-	-
Ti	0.2	0.6	-	1.1	1.7	2.1
U	0.35	1.0	-	-	-	-
W	0.3	0.6	-	-	1.1	-
Zr	0.3	0.75	-	-	-	-

Table 3.5

Sputtering yield values for the solid target species with variation in ion energy have been collected by MAISSEL[9a] from data by WEHNER and others[219, 220] as shown in Table 3.5. Very little data is at present available for the sputtering yields of ion incorporated gases from solids. The available data is collated by CARTER and COLLIGON[11]. Very recently WINTERS[208] derived a value for the sputtering yield of nitrogen chemisorbed on tungsten. He obtained a yield for nitrogen about twice that of tungsten. In addition, data on sticking probabilities, λ, as a function of surface coverage, for the different types of gas particles, are available from various sources. Amongst them being EHRLICH[221], CARTER and COLLIGON[11], KORNELSEN[198] and KAY and WINTERS[60].

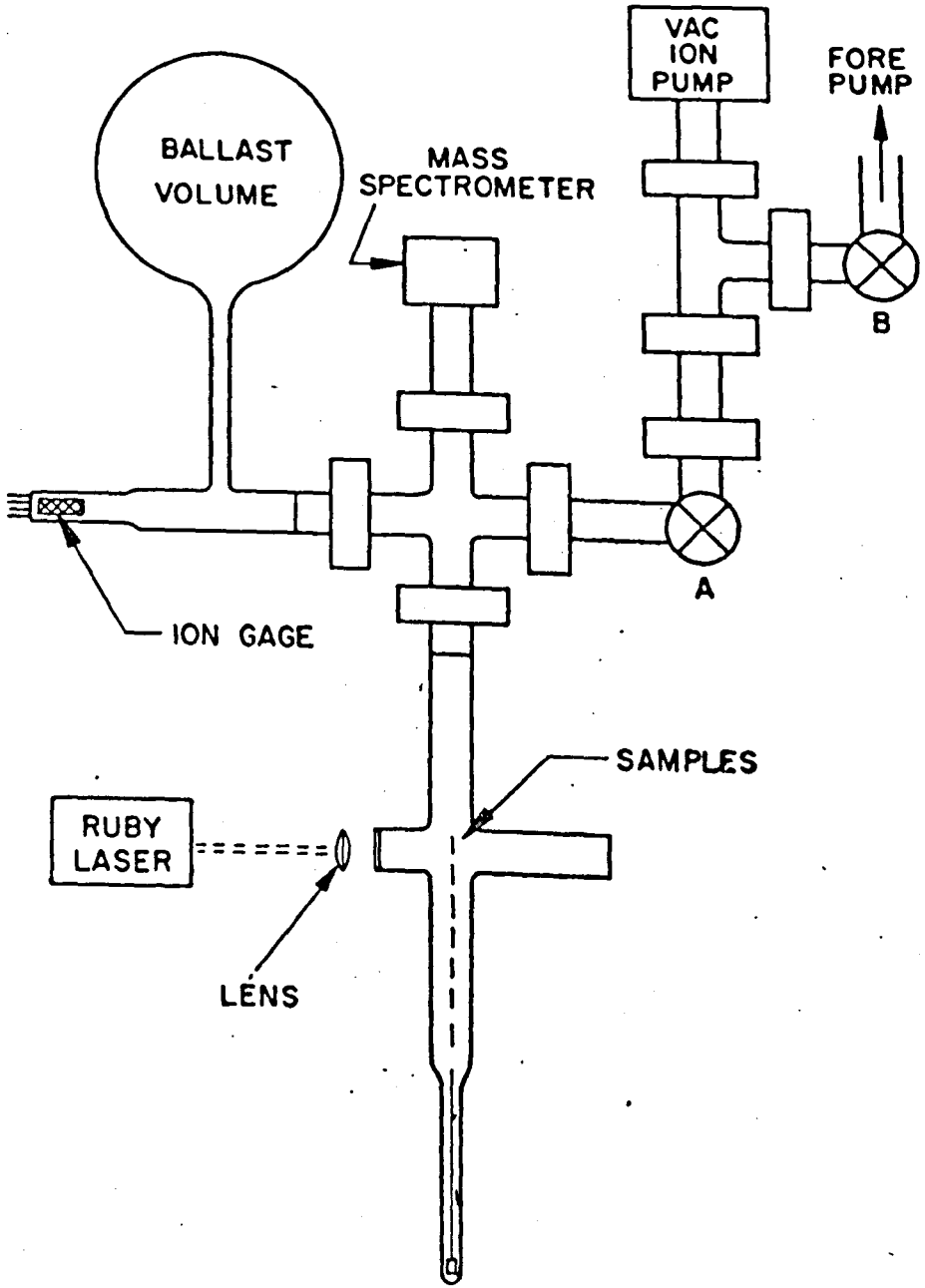

Figure 3.16 Schematic diagram of system used for laser-induced flash evaporation[60].

3.6. Gas release and analysis techniques

i. Conventional analytical methods to determine the gas content of thin films have proved to be inadequate[222] since, (a) it is often difficult to obtain complete chemical dissolution of the films, (b) the amount of material is small, usually less than 10^4 Å thick, and, (c) the methods are insensitive. Recently several techniques have been suggested using flash evaporation of the films, coupled with one of the numerous methods of analysing the composition of the released gases.

ii. GULDNER[223] reported a promising technique called flash photolysis in which the entire film is flash evaporated in an evacuated quartz tube, by a xenon discharge lamp focussed on it. The released gases are analysed using a gas chromatograph. VRATNY[224] used this method to determine the amount of argon trapped in DC and RF sputtered tantalum and tantalum oxide films.

WINTERS and KAY[60] used two methods, both of which required the vaporization of the film. In the first method, a small chip of the film and substrate is wrapped tightly and compressed in a tantalum foil boat. The boat is placed inside a copper coil inside a vacuum system of known volume. The copper coil is connected to an RF induction heater and the film is then vaporized, releasing the gases into the closed volume. These gases are then analysed using a mass spectrometer. The second method involves firing a ruby laser at the deposited film, as illustrated in Figure 3.16. This melts or vaporizes a well defined area of the film, depending on the spot size of the laser beam. This releases the trapped gas from the film which again may be analysed mass spectrometrically. One advantage of the flash evaporation technique described, is that the heating

source is kept outside the vacuum system, thereby eliminating any contaminating effects associated with it. Amongst the non-destructive methods of gas analysis are:-

iii. Electron probe micro-analysis[225], where an electron beam of about 1 micron diameter impinges on the film and excites it to emit primary X-rays, characteristic of the elements present. Elements with atomic number greater than six can be detected, and concentrations as low as 10^{-3} atomic % can be measured. Quantitative analysis, however, requires calibration against standards obtained from pure elements. Wide application of the electron probe method has been found in the analysis, of the composition and the measurement of thickness (up to about 1 micron), of microvolumes of thin films. However the high cost of the equipment, together with the inadequate supply of standards and the long time required for the analysis of each sample add to the disadvantages of this method.

iv. The X-ray milliprobe method[226], where the sample is irradiated by an intense X-ray beam so that the elements in the sample emit their characteristic secondary X-ray spectra, has also been used. HOFFMEISTER and ZUEGAL[227] used this method to determine the argon content in RF sputtered silicon dioxide films.

An added complication arises[228], when using the mass spectrometric method, from the fact that the elements found most commonly in metal films, such as hydrogen, nitrogen, oxygen, carbon monoxide etc. also go to make up the residual gases in most vacuum systems. These background gases contribute to the spectra making the analysis more difficult. It is therefore not surprising that there is often a measure of disagreement between results obtained by different investigators using various analytical techniques.

3.7 Conclusion and introduction to present investigation

Most of the previous studies on gas incorporation have been performed under relatively poor vacuum conditions: using glass systems, rubber 'O' rings and greases, and rotary oil and diffusion pumps. Under these conditions, the target surfaces quickly become contaminated and, not only is the sputtering yield affected, but often the contamination finds its way into the deposited film. In addition, impurities in the discharge gas are ionised and may similarly be incorporated in the growing film. It is not then surprising that there exist large discrepancies in the results, from author to author. Hence, it is essential to perform the experiment in conditions of ultra high vacuum and with very pure gases, if the results obtained are to be reproducible and characteristic of the targets and gases used.

Most previous investigators have performed their experiments in diode sputtering systems where the necessarily high gas pressures result in small mean free paths of the bombarding ions and sputtered atoms compared with the cathode/anode spacing. Consequently the film is not characteristic of the ions and sputtered atoms initially produced.

Relatively few investigators have measured directly the actual gas content of the deposited films, but rather they have measured a particular physical property of the growing film, under various conditions of pressure, ion bombardment etc., and have interpreted the results on the basis of incorporated gas in the film. For example,[185] measuring the resistivity of tantalum films, deposited by bias sputtering and postulating that the decrease in resistivity with increasing voltage bias is due to the preferential removal of gaseous impurities from the growing film. In addition, little

investigation has been made in comparing the gas contents of sputtered and evaporated films deposited under as nearly as possible, identical conditions. Of the experiments that have directly measured the gas contents, some use a total pressure gauge rather than a mass spectrometer to evaluate the gas content. In others, the analysis technique necessitates the removal of the deposited film from vacuum prior to the gas measurements, thereby increasing the possibility of further contamination.

In the present investigation, which forms part of a programme of research on sputtering, thin metal films have been deposited by the triode sputtering and evaporation techniques in a bakeable ultra high vacuum system, under various conditions of voltage bias, film thickness, gas pressure and target voltage. After deposition, the films are withdrawn, via a rack and pinion mechanism, through a gate valve into a small volume analysing chamber, where the gas content of the films is determined from the pressure rise on flash evaporation of the film. In this way the gas content is measured without the need to remove the film from vacuum conditions. The pressure rise is analysed with a Varian quadrupole residual gas analyser (QRGA).

CHAPTER IV

Experimental apparatus and techniques.

4.1 Introduction

In this chapter the apparatus designed to investigate the gas content of sputtered and evaporated films is described. The experimental arrangement involves two distinct sections: firstly, that for the deposition of the sputtered and evaporated films, and secondly, the gas analysis of these films by flash evaporation. The chapter is therefore divided into three main parts; 4.2 to 4.7 describes those parts of the experiment and techniques common to both vacuum systems, such as pumping, baking and pressure measurement. 4.8 describes in detail the deposition chamber and 4.9 the gas analysis system. The experimental procedure is discussed in 4.10. The quartz crystal film thickness monitor, its calibration and difficulties arising from its use, is described in 4.11.

4.2 The use of stainless steel in ultra high vacuum (UHV)

Until very recently, glass has been used in fabricating vacuum systems. However, in the last few years, it has been shown that glass may be a serious source of contamination in UHV[229], particularly if it is required to bake-out the vacuum system to a temperature of the order of $400^{\circ}C$, since decomposition of the glass occurs at these temperatures, emitting gaseous compounds containing Na^{+} and K^{+} ions.

There are a number of reasons why it is preferable to use stainless steel rather than glass in fabricating UHV systems:-

(a) A stainless steel system is both mechanically and thermally robust

in contrast to glass systems.

(b) Stainless steel has a low vapour pressure even at high temperatures.

(c) Stainless steel is relatively chemically inert.

(d) To reduce the residual pressure in a UHV system an evacuated stainless steel chamber can be baked quite safely in air to temperatures of 450°C and by so doing can be thoroughly outgassed. For example, clean stainless steel has an outgassing rate of less than 1.10^{-9} torr litre sec^{-1} cm^{-2} after one hour exposure to vacuum and less than 1.10^{-12} torr litre sec^{-1} cm^{-2} after a 12 hour bake at 450°C[230].

(e) Better ultimate vacuum is obtainable using stainless steel since it is not porous (glass is porous to helium[231]).

One of the few weaknesses in a stainless steel system is the difficulty of seeing into it during evacuation, however, glass viewing ports may be fitted at strategic positions. It is also necessary to make electrical connections into the vacuum system by means of ceramic to metal feedthroughs, and these tend to be fragile to mechanical and thermal shock. A wide variety of mechanical and electrical feedthroughs are available commercially at the present time, which reduce the relative inflexibility of a stainless steel system compared with that of glass. However, the outstanding feature of a stainless steel system is the ease with which it can be dismantled and reassembled in contrast with the glass system, by using annealed OFHC copper gaskets, bolted between Varian 'conflat' flanges. This method of sealing is used throughout, in this investigation, with the exception of the top-plate, the sealing diameter (12") of which is larger than that of the copper gaskets presently available. In this case a gold wire ring (0.025" cross-section diam.) is used as the sealing gasket

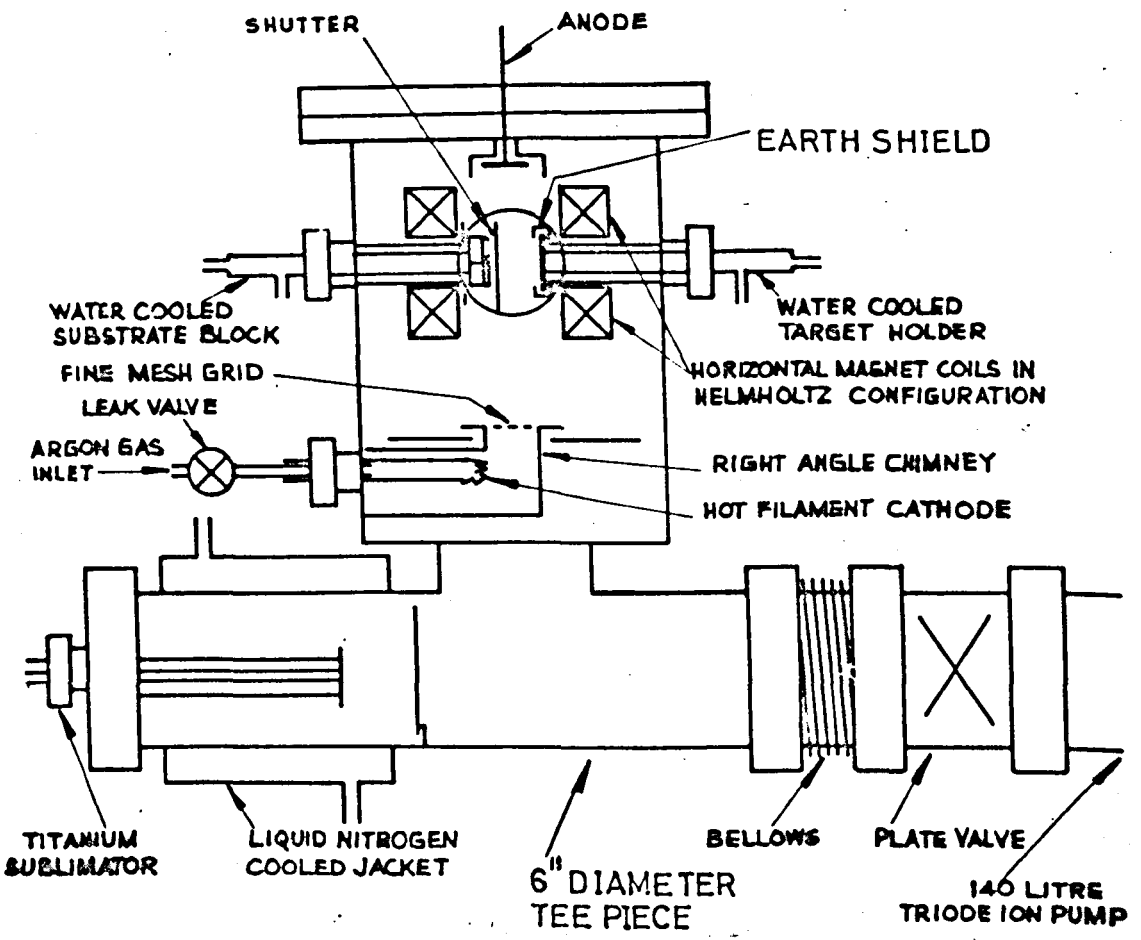

SCHEMATIC DIAGRAM OF THE MAIN SPUTTERING CHAMBER AND PUMPING SYSTEMS

Figure 4.1

and is bolted tightly between the flat and polished faces of the top-plate and vacuum well.

4.2.1 Cleaning of stainless steel prior to use in UHV

Much of the stainless steel vacuum system, e.g. the top-plate, the 6" diam.'Tee'piece, see Figure 4.1, and various other component parts were fabricated in the departmental workshop, and it was necessary for them to be cleaned and leak tested before use on the experimental apparatus.

The stainless steel was chemically cleaned in the following manner:-

(a) Degreasing with carbon tetrachloride.

(b) Hot detergent wash to remove final organic traces.

(c) Hot water wash.

(d) 2 minute dip in saturated sodium hydroxide solution.

(e) Water wash.

(f) 60 sec. dip in 50% (by vol) hydrochloric acid.

(g) A final wash with de-ionised distilled water.

(h) Hot air drying and a light (150^{o}C) air bake.

In 1968, a Guyson shot blaster was purchased and was used to clean the steel by shot blasting with 6 micron glass beads. This was found to give entirely satisfactory results and eliminated the need for the previously mentioned elaborate chemical cleaning. Glass beads are used, in preference to sand particles because of the 'smearing' effect that takes place whon using the latter on stainless steel. This 'smearing', of the metal surface, tends to leave air pockets under the surface of the cleaned steel, which furnish 'virtual' air leaks when the steel is under vacuum. Using six micron glass beads this 'smearing' is found not to take place. The leak testing is performed on a 20th Century leak detector. The probe gas used is helium.

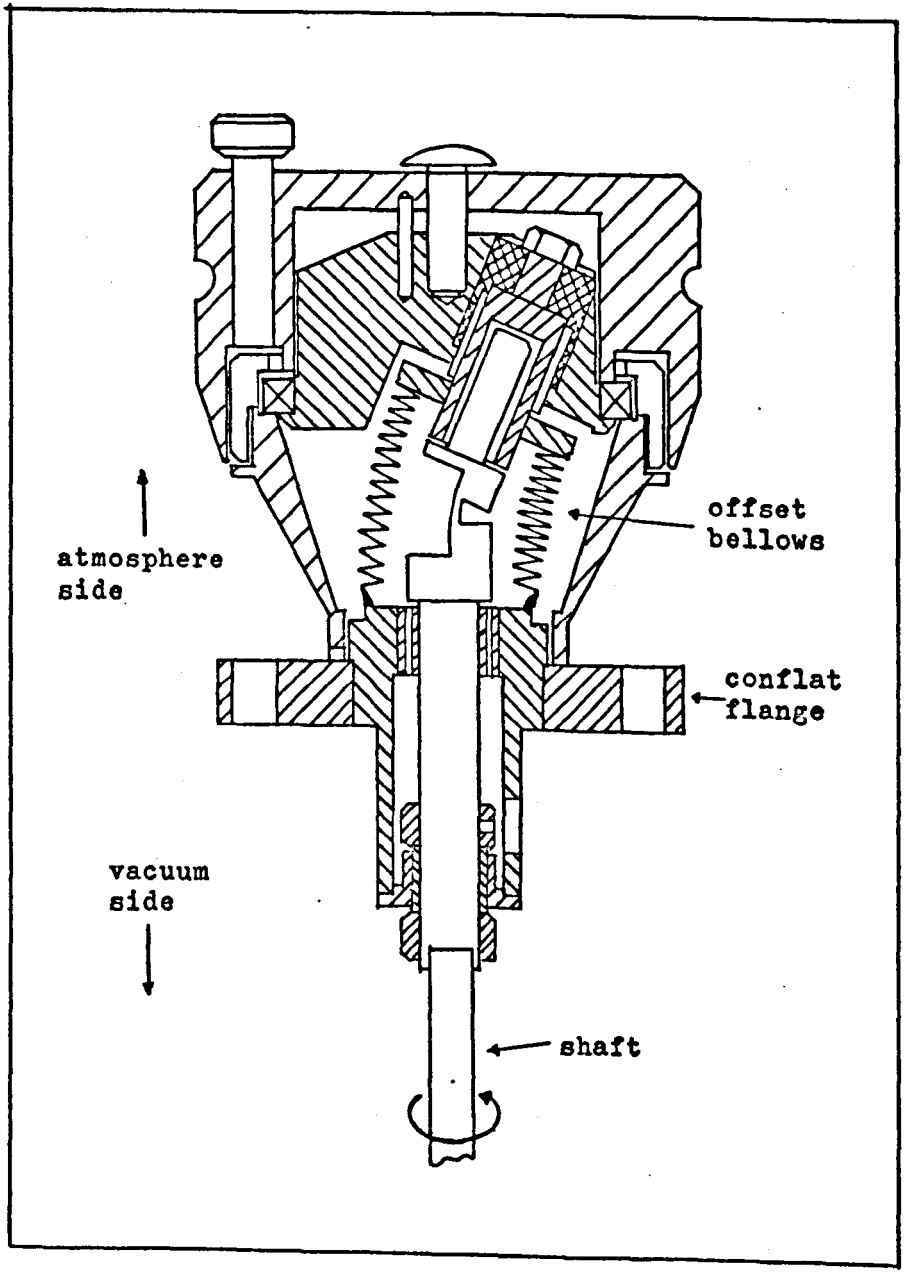

Figure 4.2 The rotary drive feedthrough
(Vacuum Generators R.D.1)

4.3 Electrical feedthroughs

Any electrical power to be used inside the UHV system must be transferred through the walls of the stainless steel vacuum chamber. This is achieved by the use of electrical feedthroughs. They must be able to withstand high bakeout temperatures, have low leakage paths to the system walls, and at the same time make perfect vacuum seals. Several types of electrical feedthrough are used, although they are all based on the principle of metal to ceramic sealing, which necessarily makes them rather fragile. One such type is composed of three copper rods individually brazed into three ceramic collars and mounted on a 2¾" conflat flange. These can withstand currents of up to 40 amps through each copper rod. Another sort consists of 8 nickel wires. These have a rating of about 5 amps per wire.

4.4. Movement in ultra high vacuum

A rather more complex problem is to introduce movement into a UHV system. Direct translational motion, although not through more than an inch or two, is accomplished by compressing or extending a flexible metallic bellows. Rotary motion is obtained by utilizing the 'wobble' effect that occurs when an offset bellows is used in a suitable arrangement, as shown in Figure 4.2.

4.5 Baking

Baking the evacuated stainless steel system to temperatures around 400°C will desorb most gases from the walls. These gases will be continuously pumped by the ion pump and, as the system is allowed to cool, the background pressure may fall by as much as one to two orders of magnitude.

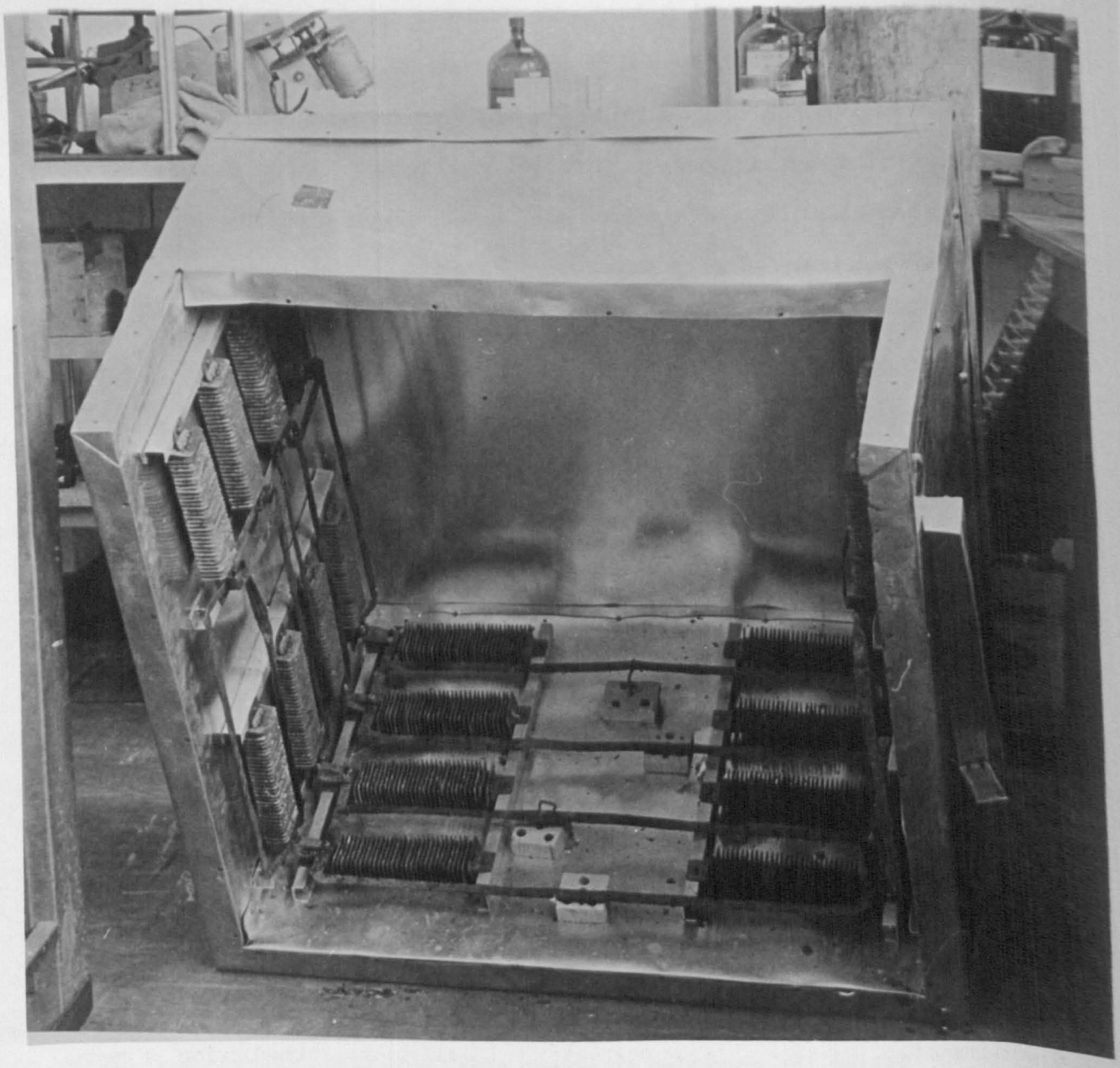

Figure 4.3

Several methods are used to bake the system. A large oven was built from aluminium-asbestos cladding, with strip heating elements fixed to the inside walls Figure 4.3. This oven is large enough to enclose the whole of the deposition chamber. Other parts of the vacuum system are heated within similar, but smaller ovens, or, where this is impractical, with heating tape. The large triode pump was fitted with an internal heater, and had sufficiently high pumping speed, even during high temperature baking, to withstand 'thermal runaway'.

With the vacuum system empty, it is possible to achieve pressures, after a 12 hour bake at 400°C, of better than 10^{-9} torr. However, with the experimental apparatus in the vacuum well, about 10^{-8} torr was more typical. After the system had received several of these 'bakeouts', it was found to be sufficient and more convenient to bake the deposition chamber internally (see section 4.8.iv.) Temperatures in excess of 300°C, measured at the vacuum walls, could be achieved by this means.

4.6 Pumping systems

The quality of the vacuum is of prime importance, if reliable measurements are to be made, and for this reason, several alternative pumping systems were considered. The conventional rotary pumps and diffusion pumps were rejected, since, even when used with a series of liquid air traps and good baking techniques, the problem of backstreaming of contaminating vapours still remains to some degree[232]. Ideally, the introduction of such contaminants into the vacuum system should be avoided in the first place. This is achieved with the use of fluid-free pumps, i.e. pumps which contain no oils, greases, etc. and preferably have no moving parts.

In the present work the sorption pump replaces the rotary pump, and the diffusion pump is supplanted by the ion pump and/or the sublimation pump.

The sorption pump evacuated the system from atmospheric pressure down to about 10^{-3} torr. It has no moving parts and pumps by the physical sorption of gas molecules onto pre-chilled molecular sieve, consisting of pellets of zeolite. The chilling medium used is liquid nitrogen. Further advantages of the sorption pump are that after pumping to 10^{-3} torr, release of the sorbed gas can be achieved by warming to room temperature. Sometimes, it is necessary to bake the zeolite to 200°C for about 30 minutes. Not only does the sorption pump contain no oils, but it is also free from vibration and noise, and requires no power supplies.

The diode getter ion pump is also free from pump oil and any moving parts. It consists of a titanium anode of honeycomb construction, mounted between two titanium cathode plates, fixed to the pump walls. Its pumping action is initiated by applying a large D.C. voltage between the cathode and the anode, whereby a Penning-type cold cathode discharge is formed between the electrodes. To confine the discharge and to improve the pumping efficiency, a strong magnetic field is applied between the electrodes. This has the effect of increasing the path length of the electrons in the discharge, by forcing them to spiral up the parallel magnetic field. At the same time the magnetic field helps to confine the discharge. Both these effects increase the ionization probability of the electrons. Sputtering of the titanium cathodes takes place, when the gas ions created collide with the cathodes, producing active sputtered titanium. The permanent removal of reactive gas atoms and molecules from the system, and the ensuing

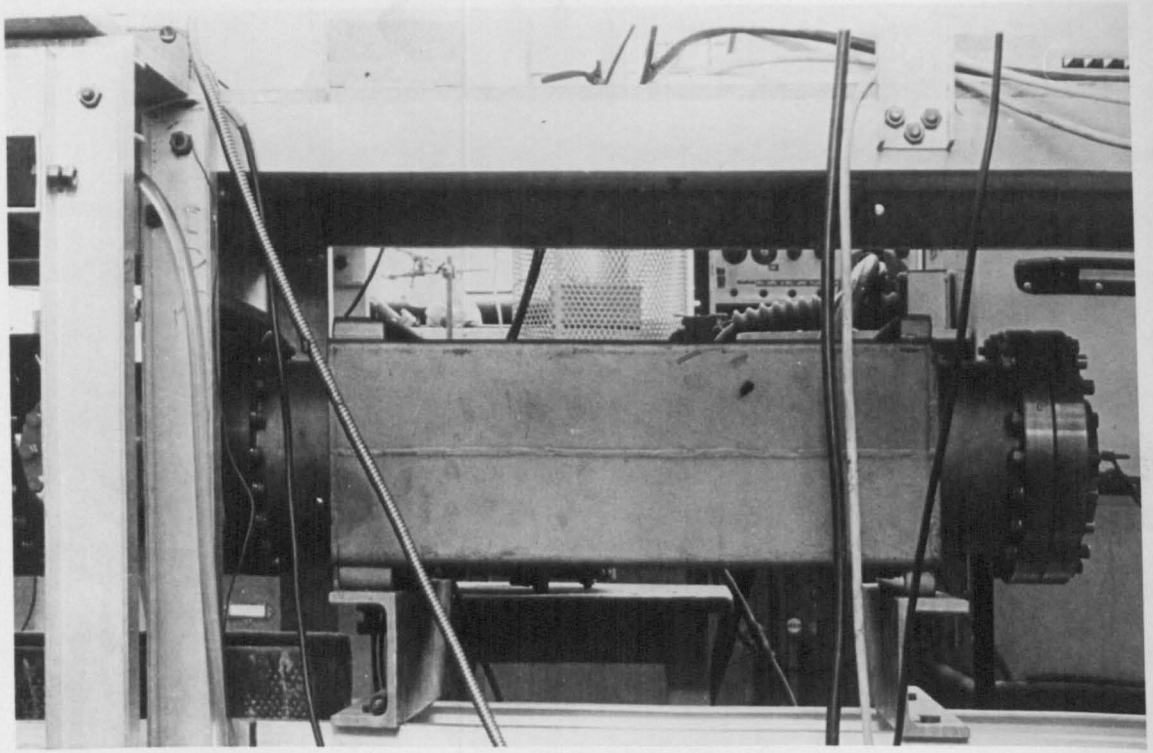

Figure 4.4

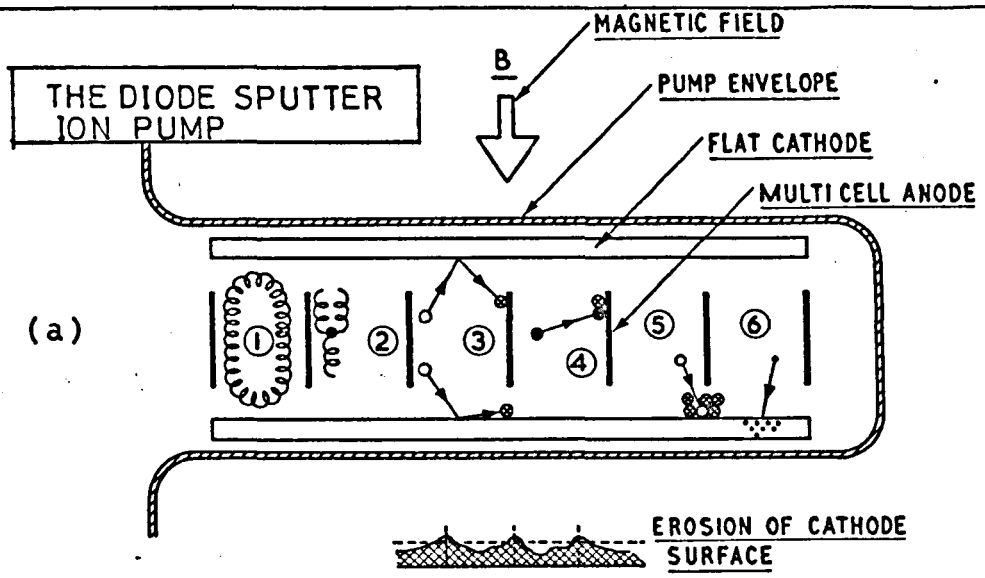

The diode sputter ion pump consists of

(a) Stainless steel pump envelope at earth potential

(b) A pair of flat titanium cathodes at earth potential

(c) A multicell anode assembly of close packed stainless steel cylinders at 7 kV positive

(d) Shielded insulators (not shown) to separate the anode from the cathodes and to produce a rigid pumping element assembly

(e) A magnetic field of some 1200 to 1500 Oersted produced by external bakable permanent magnets

(f) A high voltage feedthrough and connector assembly (not shown) to bring the 7 kV positive potential onto the anode assembly

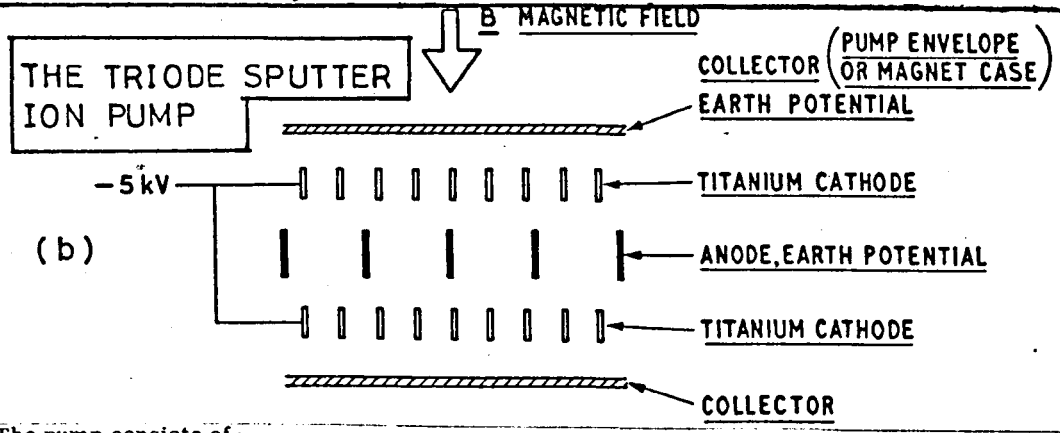

The pump consists of:

a. Stainless steel pump envelope or collector at earth potential. Titanium is sputtered uniformly over the surface of the collector to getter active gases and bury inert gases.

b. A pair of open structure titanium cathodes operating at 5 kV negative.

c. A stainless steel multicell anode assembly at earth potential.

d. Shielded insulators (not shown) to separate anode and cathodes and produce a rigid pumping element assembly.

e. A magnetic field of about 2000 Oersted produced by bakable magnets.

f. A high voltage feedthrough and connector assembly (not shown) to bring the -5 kV supply onto the cathodes.

Figures 4.5(a) and (b)

reduction in the gas pressure, is achieved by the combination of these particles with the freshly sputtered titanium, to form chemically stable compounds on the walls of the pump. To a much lesser extent, the inert gases are pumped by ion burial at the titanium cathode walls[234].

Originally a Ferranti 140 litre diode pump was used, but with the constant need to pump large quantities of argon, it was found unsuitable. In late 1968, a Ferranti 110 litre triode ion pump was purchased and used in place of the diode pump (see Figure 4.4.) The triode pump has a pumping speed for argon of about 30% that of nitrogen, i.e. about 30 times better, in this respect, than the equivalent diode pump. It also has much better starting characteristics than the diode, since it is possible to start the pump at pressures as high as 10^{-2} torr, compared with the 10^{-3} torr required by the diode pump. The triode pump works by striking a cold discharge between cathode and anode, but the configuration and shape of the electrodes are different from those of the diode pump, see Figure 4.5. A cathode grid, made up of thin strips of titanium, is mounted on either side of the centrally placed honeycomb-shaped anode, and electrically isolated from the walls of the pump, which themselves are covered with sheets of titanium. The anode and titanium sheets are earthed, and a large negative voltage is applied to the grid, -5kV for the 110 litre pump, making it into a cathode. As with the diode pump, a large magnetic field is applied parallel to the electric field. Gas ions, produced by collision of electrons with gas molecules in the anode cells, are accelerated towards the cathode grid. They often strike the grid at a glancing angle. The pump wall is not bombarded by the ions, since they are attracted to the negatively charged grid. Hence the pump wall serves as a large area for net titanium build-up.

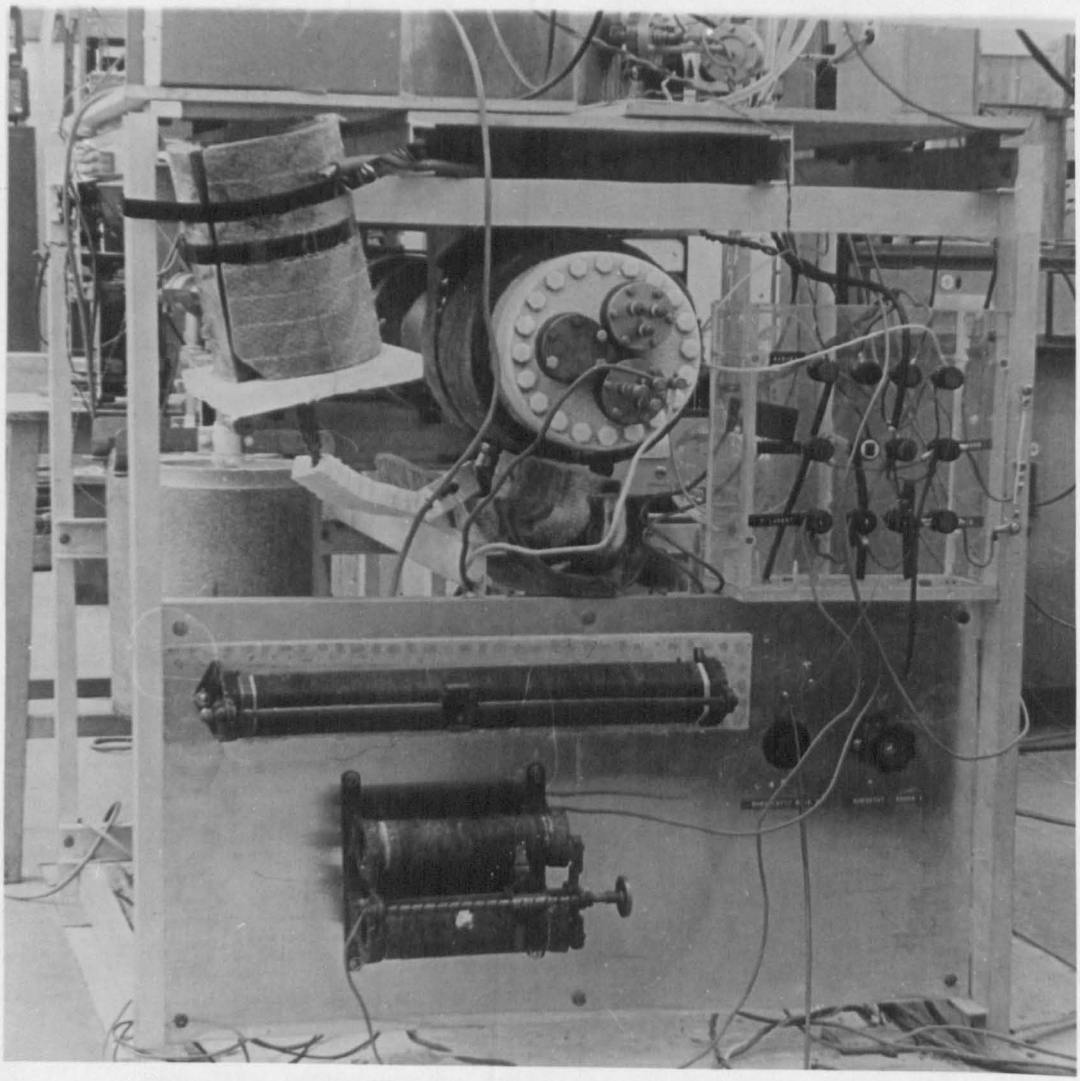

Figure 4.6(a)

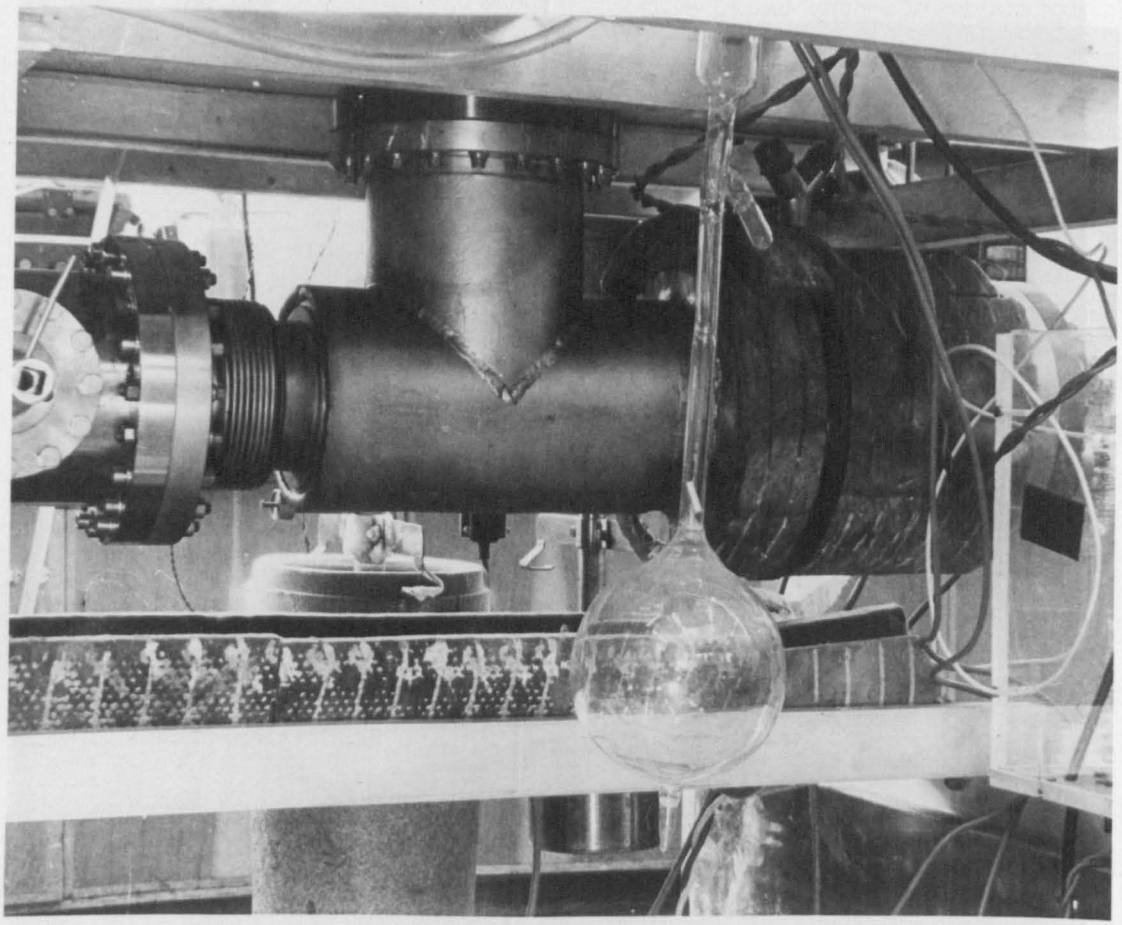

Figure 4.6(b)

This is necessary for permanent inert gas burial. The enhancement of inert gas pumping takes place at the expense of the simplicity and robustness of the ion pump. The life of the titanium cathode elements is less than that of the diode pump.

In the triode pump used, a problem often arose which was not encountered with the diode arrangement. Because of the flimsy nature of the grid cathodes, when the pump had to be run hot for any length of time, i.e. when pumping at high pressures, the grid buckled slightly and electrically shorted to the pump walls, thereby extinguishing the discharge and the pumping action. It was necessary to allow the pump to cool down before it could again be started.

A liquid nitrogen cooled titanium sublimator is also used in conjunction with the ion pump. This pump, as its name suggests, operates by evaporating a fresh film of titanium, from a resistively heated filament, onto the walls of the vacuum system. There, it reacts with the active gas molecules impinging on it, to form stable compounds of titanium. To avoid sublimating titanium over the feedthroughs, etc. in the deposition chamber, the sublimator is fitted in a 6" diam.'Tee'piece which is bolted to the base of the system, see Figure 4.1. The sublimator only has a useful pumping speed if the walls, on which the evaporated film falls, are maintained at a low temperature. This is achieved by welding a thin stainless steel jacket to the outside of the sublimator chamber. Liquid nitrogen is poured into the space enclosed by the jacket and keeps the walls of the sublimator system at a temperature around 77°K. The sublimator system is shown in Figures 4.6a & b

The sublimator used consists of three straight titanium filaments, mounted at one end on a 2¾" 40 amp electrical feedthrough flange, and at the

other, clamped to an earthed rod. Difficulty was experienced with the filaments, which often fractured from strain after only a short time in use. This problem was cured by making a 'kink' in the titanium filaments before they were fitted to the flange. This gave them a small amount of free movement when they expanded on resistive heating.

This type of pump will only remove the reactive gases, since the pumping speed for the inert gases is effectively zero[235]. Advantage is taken of this pumping selectivity, by running the pump during the sputtering experiments. This keeps the background gases low whilst leaving the high sputtering argon pressure unchanged[236].

4.7 Vacuo and pressure measurement

A Pirani gauge measures the degree of vacuum on the roughing side of the vacuum system. Due to its insensitivity at pressures below about 5.10^{-3} torr its only use is to indicate when to start the ion pumps, on initial evacuation of the system. When the ion pumps are in operation the ion current flowing to the pump cathode is very nearly proportional to the gas pressure in the pump, and so can, itself, be used as a pressure gauge. However, since the ion pumps are some distance from the deposition chamber and often isolated, a nude Varian hot ionization gauge (UHV 14), mounted on a $2\frac{3}{4}$" conflat flange, is used to measure the pressure in the deposition chamber. This is capable of pressure measurement in the range 10^{-5} -10^{-11} torr.

The gauge consists of three elements; a filament, a grid (at negative potential), and a collector wire (at positive potential), in a Bayard-Alpert configuration. Electrons from the filament pass back and forth through the grid structure several times before being collected at the grid. During their journey, the electrons ionise gas molecules at a

rate which is proportional to the gas density, and the ions produced are accelerated towards and collected at the collector wire. The gas pressure, P, in torr, is described by the relationship:-

$$P = i_c/S.i_g$$

where i_c is the ion current in amps at the collector, i_g is the electron current in amps at the grid and S is a constant, known as the sensitivity, for the gauge. For the UHV 14 gauge, S is given as 25 $torr^{-1}$ for nitrogen.

For the sidearm system when isolated from the deposition chamber, low pressures are measured with a GE triggered penning gauge. This instrument utilizes a cold cathode discharge in a magnetic field (similar in action to the diode pump) to provide a measure of pressure in the range 10^{-5} -10^{-13} torr. The gauge features a momentarily energised hot filament to trigger the discharge under UHV. The tube itself is rigidly constructed in stainless steel with ceramic-to-metal feedthroughs, bakeable, when the magnet is removed, to 450°C. Unfortunately the tube is not demountable, and during use, the hot filament, without which it is very difficult to start the gauge, burnt out. This made it more or less useless at high vacuum.

The accurate and reliable measurement of the gas pressures encountered during sputtering, between about 10^{-4} -10^{-2} torr, is much more difficult. Originally, an Edwards model 6 Penning gauge was used for this purpose, capable of measuring pressures between 10^{-6} -0.5 torr. However, the meter had a non-linear scale and a poor range between 10^{-4} -10^{-2} torr, making it difficult to take accurate readings from it. Furthermore, it was necessary to make the gauge head entirely bakeable rather than the "O" ringed version supplied by Edwards.

Late in 1968 the opportunity arose of changing this gauge for a Varian millitorr gauge (MIG 10). This has a linear scale for pressure measurement from 10^{-6} to 1 torr. The mode of action of this gauge is similar to the UHV 14, except that the electron path lengths are very short and the emission current from filament to grid must be very low. A thoria-coated iridium filament permits operation of the gauge with active gases at pressures as high as 1 torr. The sensitivity for this gauge is given as 0.5 $torr^{-1}$. The only problem with this gauge is that which occurs with all hot filament gauges, i.e. that of gassing from the hot filament. With thorough outgassing by electron bombardment over several hours this degassing was minimised. This gauge was found to be very suitable, both for measuring the sputtering gas pressures in the deposition chamber and the gas pressure increase from the outgassed films in the sidearm analysing chamber.

Allowance was made for the fact that the predominant gas in the vacuum system was often argon rather than nitrogen, the gas for which the gauge had been calibrated. Since the ionization cross-section for different gases is not necessarily the same, the gauge reading is multiplied by a sensitivity factor, determined by the manufacturer and obtained from the Varian handbook[237]. The table is reproduced herewith:

Gas	multiply by (Nitrogen = 1.0)	Gas	multiply by (Nitrogen = 1.0)
N_2	1.0	CO_2	0.73
Air	1.11	CO	0.95
O_2	1.22	Ar	0.85
H_2O	1.11	Kr	0.53
H_2	2.0	Xe	0.37
He	6.22	Hg	0.29
Ne	4.22		

4.7.1 Partial pressure measurement

A residual gas analyser (RGA) is used to obtain detailed knowledge of the quantities of each gas species found within the vacuum system. Originally a glass encapsulated Omegatron mounted on a conflat flange was used for gas analysis, but this unfortunately broke and proved impossible to repair.

It did however, become possible to purchase the much more suitable Varian quadrupole gas analyser (QRGA) head with an electron multiplier attachment. This QRGA was chosen because all the necessary instrumentation for the analyser was available within the laboratory. The QRGA head arrived in 1968 and all results presented here on gas analysis were obtained with it. The physics of the quadrupole is described in Appendix A and it is sufficient here to describe the basic structure and operational techniques.

The QRGA consists of four parallel stainless steel rods of circular

cross-section very accurately aligned with each other. The rods are about 10cm long, and arranged so that they are at the vertices of a square section tube, about an axis parallel to the rods, as shown in Figure A1 (see Appendix). Ions are created in the quadrupole space by electron bombardment and are accelerated up to 120 V at the entrance aperture, which is positioned on the axis of the rods. Ions which enter this aperture normally will move along the axis undeviated only if they have the M/e ratio determined by the D.C. and A.C. voltages applied to the rods. Such ions will then pass through the exit aperture and be collected, either directly in a Faraday cup or, to improve the sensitivity, at the first dynode of an electron multiplier, where the ion current signal may be magnified into an electron current up to 10^5 times larger.

In contrast with other forms of mass spectrometer no magnetic field is required. A linear mass spectrum of the gases within the vacuum system may be displayed on an oscilloscope or pen recorder, depending on the sweep rates chosen for the D.C. and A.C. voltages. The QRGA can also be used as a total pressure gauge by switching off the D.C. voltage to the rods, in which case all the ions entering the 'filter' will be collected at the exit aperture, regardless of their M/e ratio.

4.8 The film deposition chamber

4.8.1 Introduction

For the purpose of the present experiments both sputtered and evaporated metal films are deposited under, as nearly as possible, identical conditions. The gas content of sputtered films depends on ion species, ion energy, direction of incidence of the ions on the bombarded surface, target species, gas pressure, target and substrate temperature, bias voltage on growing film, residual gas pressure, film thickness and target voltage. There is a similar dependence for evaporated films with the exception of target voltage.

In the apparatus described here most of the above parameters are independently variable. In addition the apparatus satisfies the following conditions:

(a) The pressure of the sputtering gas (typically about 6.10^{-4}torr) is low enough to ensure that the mean free path of the sputtered and evaporated particles is long compared with the target to substrate distance (about 10 cm to 5 cm).

(b) The ion current density to the target of about 0.5 - 1.0 mA cm^{-2} is sufficiently high to maintain a clean surface at the target.

(c) The residual gas pressure is low (about 5.10^{-8} torr) compared with the sputtering gas.

The deposition chamber vacuum system consists of a 12" diameter, 16" deep stainless steel well, sealed at the top by a 14" diameter stainless steel top-plate with a gold wire gasket. The top-plate can be replaced by a 12" diameter bell jar and viton gasket. There are thirteen flanges of various sizes arranged arround the well for appendages to be

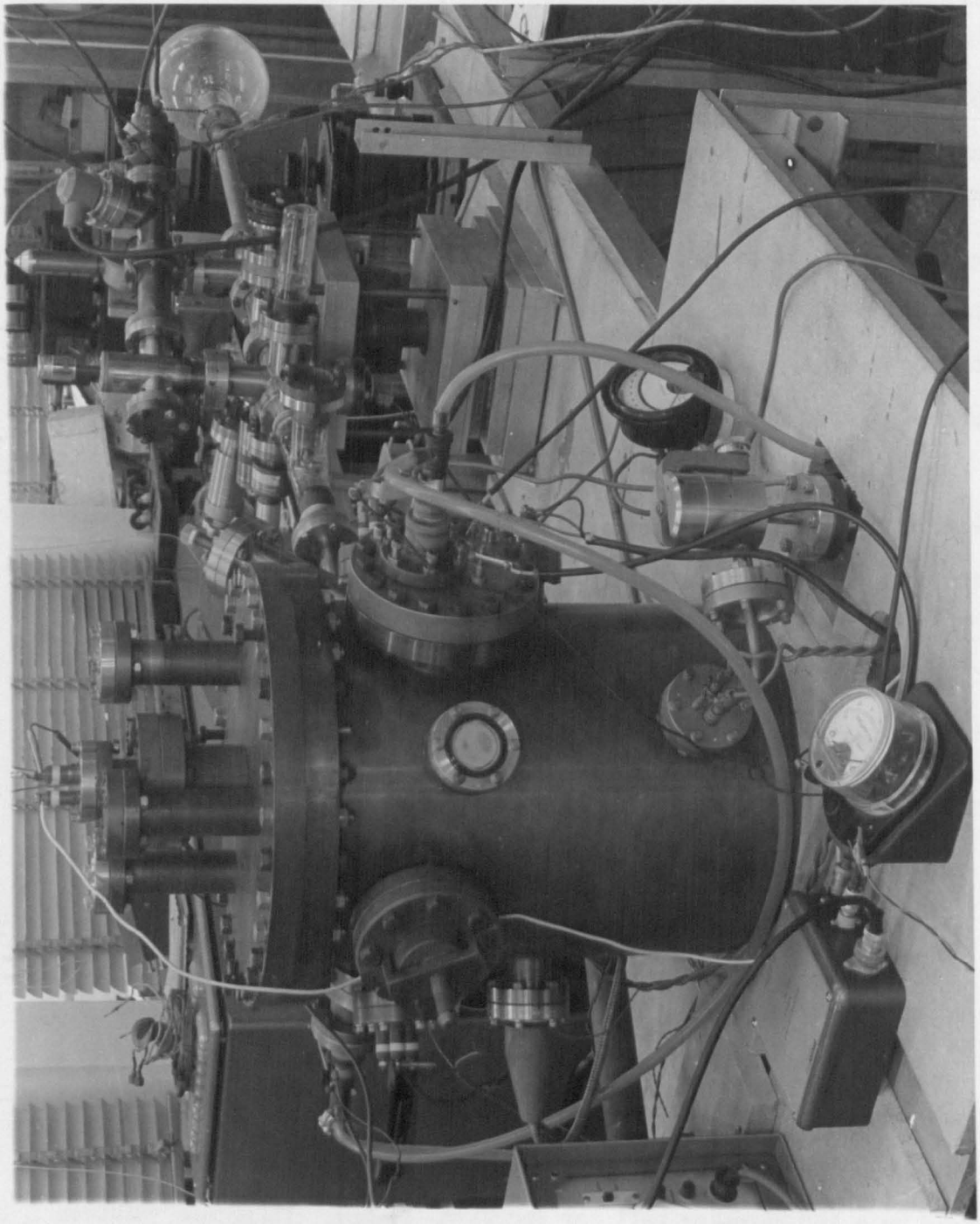

Figure 4.7

Sputtering samples	Source	Cleaning process
NICKEL (sample 1)	(A W R E)	CCl_4 degrease, Nitric Acid dip, distilled water, Alcohol.
NICKEL (sample 2)	Johnson Matthey (Grade 1)	
GOLD	Johnson Matthey (Grade 1 purity)	CCl_4 degrease, Aqua Regus dip, distilled water, Alcohol
TITANIUM	EMI	CCl_4 degrease, HF 4% in H_2O plus 4% per 100 vol H_2O_2 dip for 5 min., distilled H_2O, Alcohol.
ZIRCONIUM	EMI	(as for TITANIUM)
TUNGSTEN	Johnson Matthey (Grade 1)	CCl_4 degrease, H_2O_2 3% in H_2O dip for 30-90 secs, distilled water, Alcohol.
COPPER	Johnson Matthey (Grade 1)	CCl_4 degrease, rapid HNO_3 dip (10-15 secs) distilled H_2O, Alcohol.
ALUMINIUM	Johnson Matthey (Grade 1)	CCl_4 degrease, fuming HNO_3 47% and HCl 50 cc, 60 sec. immersion, followed by distilled water, and alcohol.

Table 4.1.

added. A further 8" diameter flange at the base of the well joins the 110 l/s ion pump, through a P100 plate valve and 6" diameter Tee piece, to the deposition chamber, see Figure 4.1. The whole of the deposition chamber (and the sidearm system) sits on a thick maronite board on the top of a frame work made up from 1"x 2" aluminium channeling. This structure provides rigid support for the vacuum system and pumps, which weigh in the order of 200 Kg. Figure 4.7 shows the general layout of the system in Summer of 1970.

4.8.2 Sputtering assembly

i. Target

The targets are prepared from high purity sheet, between 0.010" to 0.020" thick, and are fitted onto an OFHC copper backing block which is fixed to a water-cooled electrical feedthrough. They are cut and then pressed into shape using a forming machine, fitted with a 2" o/d die. This gives the sheet a 2" diameter flat face, with an edge curving away to form a lip about $\frac{1}{4}$" deep. This lip is bent back so that the target sheet fits tightly and firmly against the backing block, thereby ensuring good thermal contact. Often a nickel wire is wound tightly around the edge to make quite sure of the contact. To measure the temperature of the target a chromel-alumel thermocouple is added under the rim. The sputtering targets used, and the cleaning procedure carried out are shown in Table 4.1.

Special care was taken with the design of the earth shield surrounding the target assembly. This is mainly to reduce 'the rim effect' which arises from changes in the ion trajectories, at the rim of the target. These changes occur because:

(a) The dark space surrounding the target has a focusing effect on ions

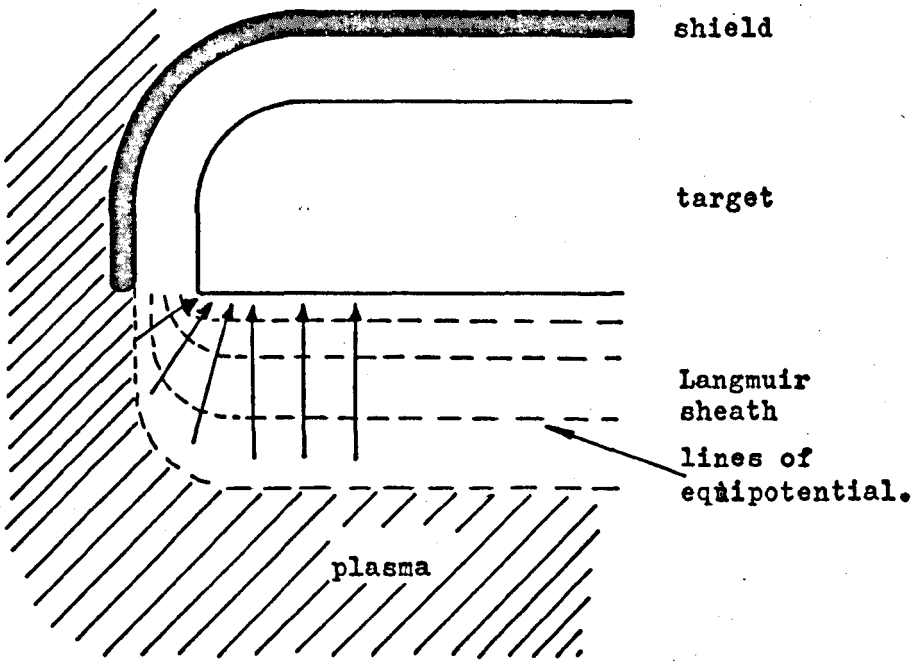

(a) Electric potential around target and shield

(rim effect)

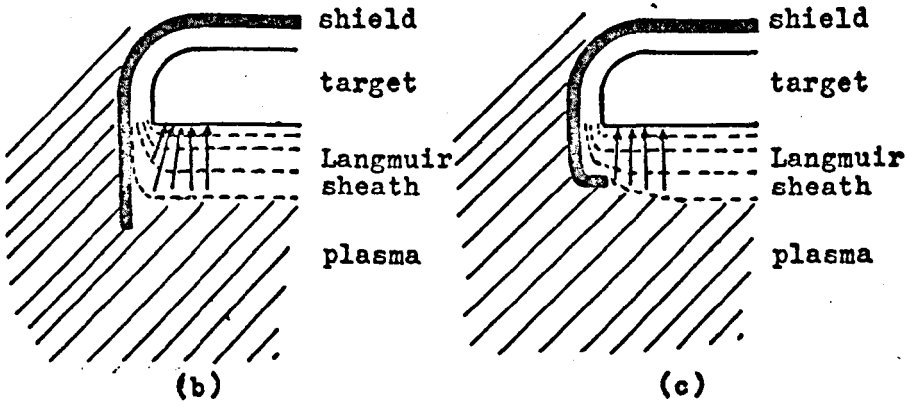

Reducing rim effect by:- (b) extending target shield.
(c) wrapping shield around edge of target.

Figures 4.8 (a),(b) and (c).

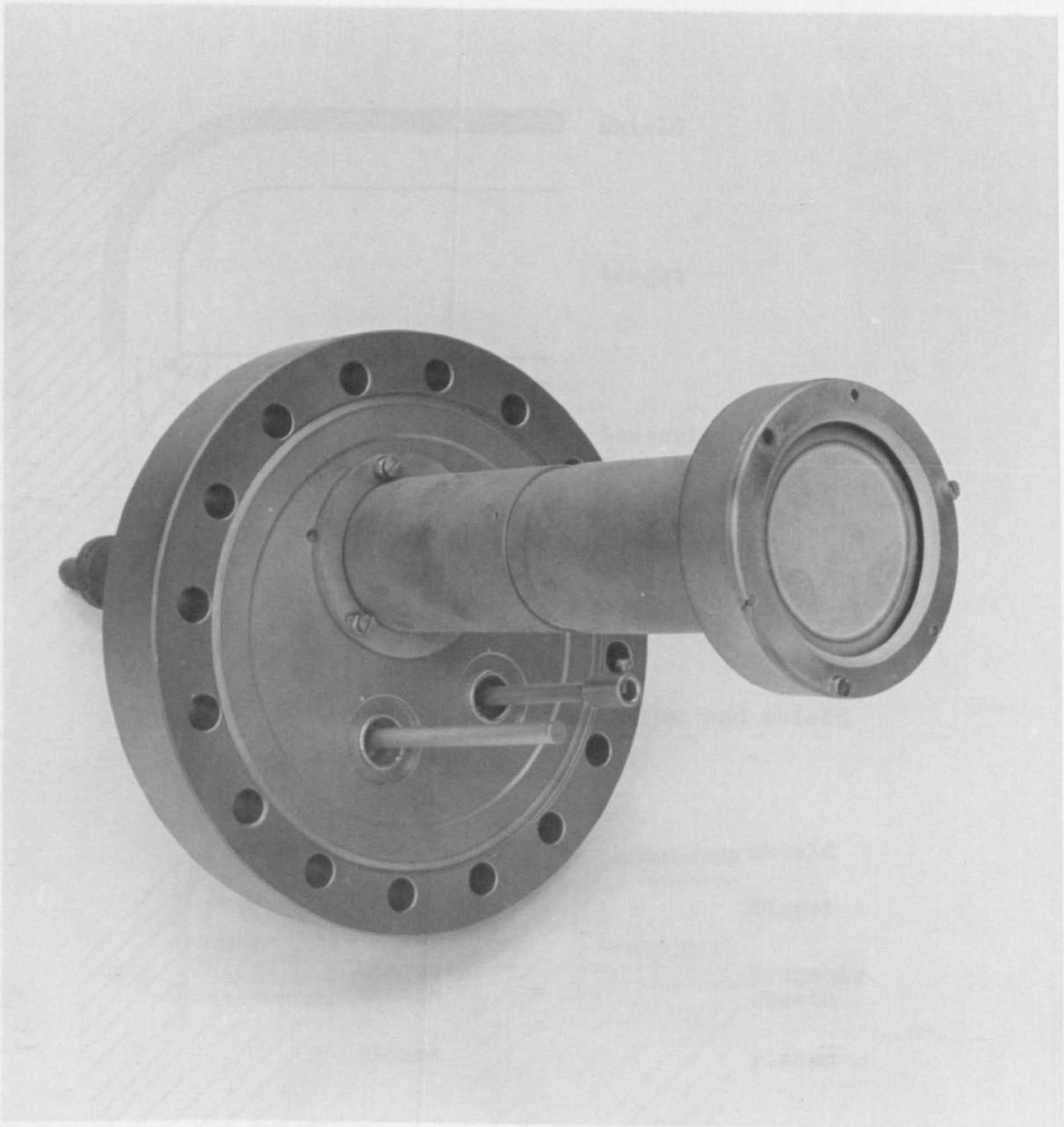

Figure 4.9

Figure 4.10

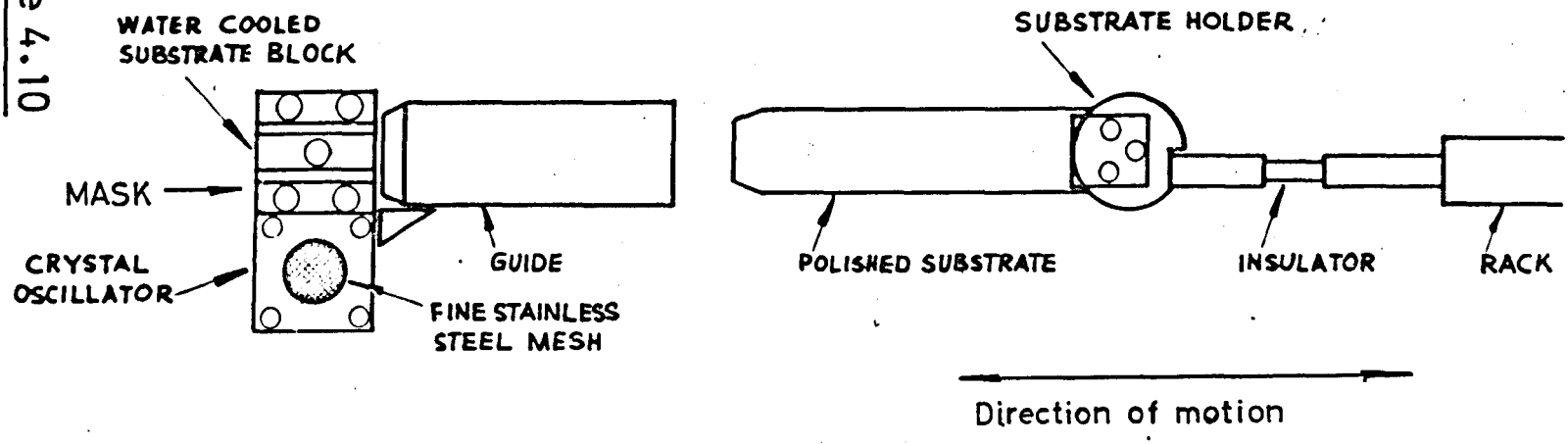

SCHEMATIC DIAGRAM OF WATER COOLED SUBSTRATE BLOCK & SUBSTRATE HOLDER ON RACK

near the rim, which increases the ion current density at the edge of the target[9a].

(b) Ions arrive at the edge of the rim at large angles of incidence, and, as a result, their sputtering yields are considerably greater than those of ions arriving nearer the centre of the target at normal incidence[5].

Figures 4.8 indicate these effects and how they are overcome with a suitably designed earth shield, and Figure 4.9 shows the completed sputtering target assembly used in the present investigation. The earth shield is also used to prevent sputtering from the back of the target and the water-cooled feed-through. This is achieved by adjusting the shield so that it is at a distance less than the 'Crookes dark space' from the target mounting[6].

For a target voltage of 1000 v, the sheath thickness is calculated to be about 5 mm, see Appendix B, in which case the earth shield is placed about 3-4 mm from the target. Increasing the target potential increases the sheath thickness, making it unnecessary to change the shield dimensions. WEHNER[5] has shown that, when the target diameter is large compared with the sheath thickness, the ions will strike the target perpendicularly, which is a situation fulfilled in this experiment.

ii. Substrate mounting holder

The general design of this holder is shown in Figure 4.10. An OFHC copper block was milled, so that the top half could accommodate a 1 cm wide substrate in a good fit. Springy tantalum clips held the substrate firmly against the block to achieve good thermal contact, and, at the same time, supported the substrate face in a vertical plane. A chromel-alumel thermocouple was spot welded to one of the tantalum clips and was used to monitor the temperature of the substrate during film

deposition. Facilities for heating the copper block and substrate were incorporated by inserting a tungsten helix, insulated with a glass sheath, in a hole drilled through the copper block.

A mask, in the form of two, parallel, bevelled copper strips was screwed to the front of the copper block at a separation of 0.7 cm. In addition, a stainless steel guide on one side, and a movable, stainless steel, shutter fitted to a linear motion feedthrough on the other side of the copper block, formed the vertical sides of the mask. By adjusting the position of the movable shutter, a given area of the substrate could be exposed. The guide, shutter and copper strips, which make up the mask, were all electrically isolated from the copper block by Sintox ceramic spacers. This prevented sputtering from these component parts when a negative bias voltage is applied to the substrate through the copper block and eliminated the danger of material being sputtered from the mask, onto the target.

Film thicknesses were measured using a quartz crystal monitor fitted in the bottom half of the copper block at the same distance from the target as the substrate. A $\frac{1}{4}$" diameter hole was drilled in the metal can, enclosing the crystal, to allow some of the depositing material to land on it. To prevent charged particles from hitting the crystal, since it is known that the crystal can be over-stressed by electrically charging it[238], a fine tungsten mesh (about 95% transmissivity) was placed over the hole. The calibration and other problems concerning the thickness monitor are discussed in more detail in section 4.11. The copper block and attachments are mounted on a water-cooled electrical feedthrough, which is bolted to a 6" diameter flange. The substrate bias voltage is applied through this feedthrough. All other electrical connections are made via an 8 way A.E.I.

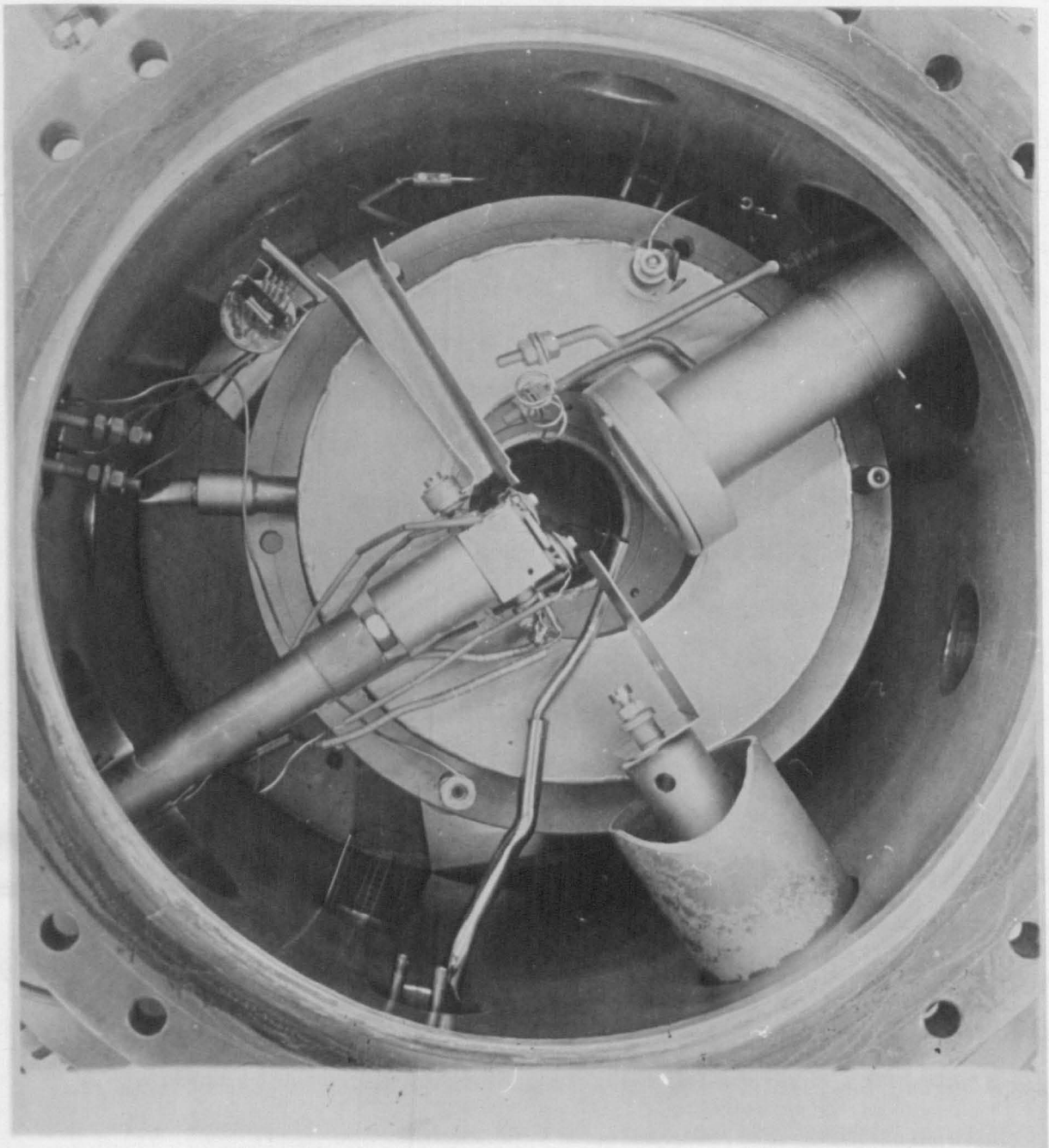

Figure 4.11

electrical feedthrough, also fixed to the 6" flange. Figure 4.11 shows the general arrangement of the target and substrate holder in the vacuum well. The substrate to target distance is 6 cms.

iii. Filament/Anode arrangement

Ions are created by energetic electrons colliding with, and ionizing the gas atoms present in the vacuum system. The electrons are supplied from a heated tungsten filament. Two essential criteria were required of the filament. The first and most important was that a useful electron emission should be obtained from it. The second was that the filament should have a reasonable life, in view of the length of time required to break the vacuum and replace it. A further requirement, although of lesser importance, was that the filament should not generate too much heat during use, otherwise problems of thermal gas desorption from surrounding areas might arise, since there were no facilties for cooling these areas. This restriction prevented the use of very thick filaments running at 100 Amps or more.

The filament chosen was a tungsten wire 3 cm long and 0.075 cm diam. It was bent into a U shape and its ends clamped to a two-way 40 amp copper feedthrough. Preliminary experiments were performed in an Edwards high vacuum plant with different filament diameters, before this one was chosen as the most suitable. From JONES and LANGMUIR[239] and BACHMAN[240] it was calculated that at a temperature of about 2600°K, an electron emission of about 70 mA/cm length of filament could be achieved by passing about 32 A through a tungsten wire 0.075 cm diam. (see Appendix C.) The second criterion was also satisfied since at 2600°K the estimated life of the filament is about 1000 hours[240]. The power generated by this filament was found to be

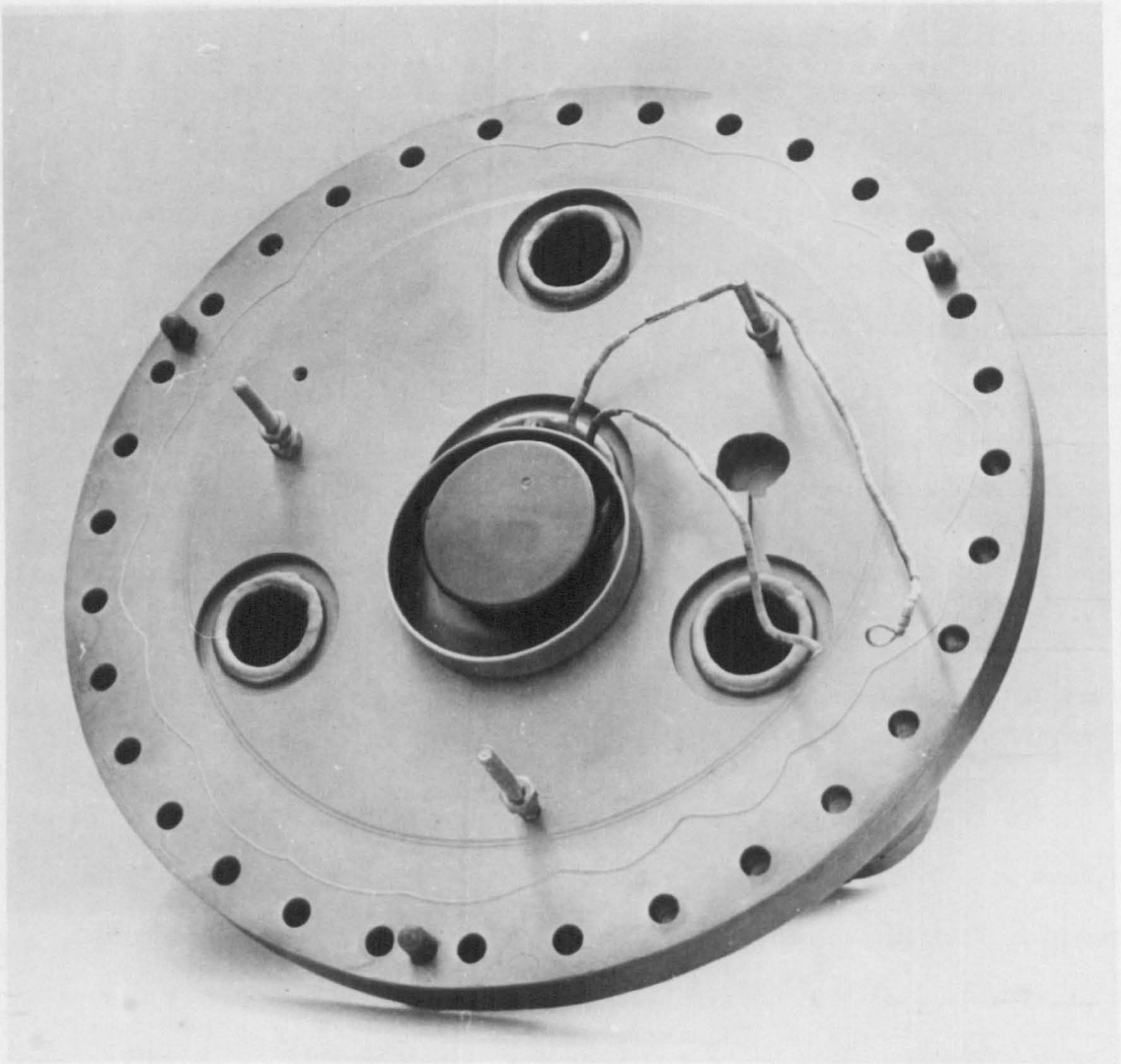

Figure 4.12

about 100 watts. Although the filament was 3 cms long, the ends close to the terminal junctions were cooled by conduction, due to the close proximity of the copper feedthroughs. As a result only about 1 cm of the centre part of the filament was actually at 2600°K.

The filament was situated close to the bottom of the vacuum well and was surrounded by a stainless steel right angled cylinder. This was designed as a heat shield for the rest of the system. In addition, by allowing it to float electrically with respect to the filament, it was used as an electron repeller, retaining the electrons in the cylinder, rather than allowing them to impinge and be collected on the earthed walls of the vacuum system[122].

A fine stainless steel mesh grid was placed horizontally over the open end of the cylinder and insulated from it with ceramic spacers. A positive voltage was applied to the grid, typically of the order of 20 volts, which drew the electrons towards and through it. This helped to initiate the discharge, which otherwise was difficult to achieve at the low pressures used of about 6.10^{-4} torr. It also helped to maintain the discharge, once it had been initiated.

The main anode was made of a polished stainless steel disc 7.5 cm diam. and 0.5 cm thick, fitted to an electrical feedthrough in the top-plate of the vacuum system. The anode edge was surrounded by an earthed shield, screwed directly to the underside of the top-plate, as shown in Figure 4.12. Typical values of +96 volts at pressures of about $6.8\ 10^{-4}$ torr were used to obtain electron currents of about 1 amp at the anode. At pressures of $6.8\ 10^{-3}$ torr only +36 volts were needed to obtain the same conditions.

iv. The magnetic field assembly

The bombarding ions are created by a beam of electrons in the gas. KOEDAM[121] and others[5] have shown that divergence of this beam can be prevented and an improvement in the ionising ability of the electrons achieved by the use of a properly designed magnetic field. Following their reasoning, the magnetic field in this case is obtained by means of two cylindrical coils, placed in a Helmholtz configuration[241], with the magnetic field parallel to the electron beam.

Vacuum-wise the simplest solution to fabricating these coils would have been to wind then on 'formers' and place them horizontally outside the deposition chamber. However, to place then in a Helmholtz configuration and achieve magnetic fields of even tens of Gauss, inside the vacuum system,would have required annuli of about 35 cm inside diameter and hundreds of metres of insulated wire. It was therefore decided to place the coils inside the vacuum system. To prevent the obvious problem of outgassing of many metres of wire and the probably impossible task of finding an insulating coating for the wire that was of reasonable cost and a good vacuum material, it was necessary to encapsulate the whole of each coil in a non-magnetic jacket which had also to exhibit good vacuum properties. The material chosen was EN58E non-magnetic stainless steel. Two identical stainless steel 'cotton-reel bobbins' were fabricated, inside diameter 9.0 cm, outside diameter 18.5 cm, and width 3.6 cm, all joints being argon arc welded. Anodal aluminium wire 16 swg with Al_2O_3 coating for electrical insulation was used instead of copper wire for the following reasons:-

(a) The aluminium insulation was bakeable to over 600°C without any

deterioration, whereas most copper insulation coverings were of low melting point plastics.

(b) Although the electrical conductivity of the aluminium was two thirds that of the same diameter copper wire, its density was only one third that of copper, so thicker diameter aluminium wire could be used with little increase in weight.

(c) The aluminium wire was cheaper than an equivalent amount of copper.

The coils were wound 18 turns in each layer and 16 layers deep, giving a total of 288 turns on each coil. The first and second attempts at winding these coils failed when shorting occurred between layers wound on the coil. This probably arose due to the thinness of the insulating coating (about 0.001"), and the pressure applied on the inner-most layers by the weight of the outer layers. To prevent this it was found necessary to separate each layer with glass fibre tape (100% purity), $1\frac{1}{2}$" wide and 0.003" thick. Output connections were made by removing the oxide coating from the ends of the wire and clamping them to two 30 amp Ferranti copper-to-ceramic electrical feedthroughs, which had previously been welded into the 'bobbins'. When the coils had been satisfactorily wound and tested, a metal sheet, 3.8 cm wide, was welded to the outside of the 'bobbin', completely enclosing the coil. To leak test the coils a stainless steel-to-copper pump-out tube was welded into this outside sheet. Leaks were detected twice in the welds of the coils, but after further rewelding the coils were found to be leak tight. The coils were sent to Ferranti Ltd at Manchester, where they were baked for several days and further leak tested. They were then back-filled with helium to a pressure of about 1 torr and the copper pump-out tube

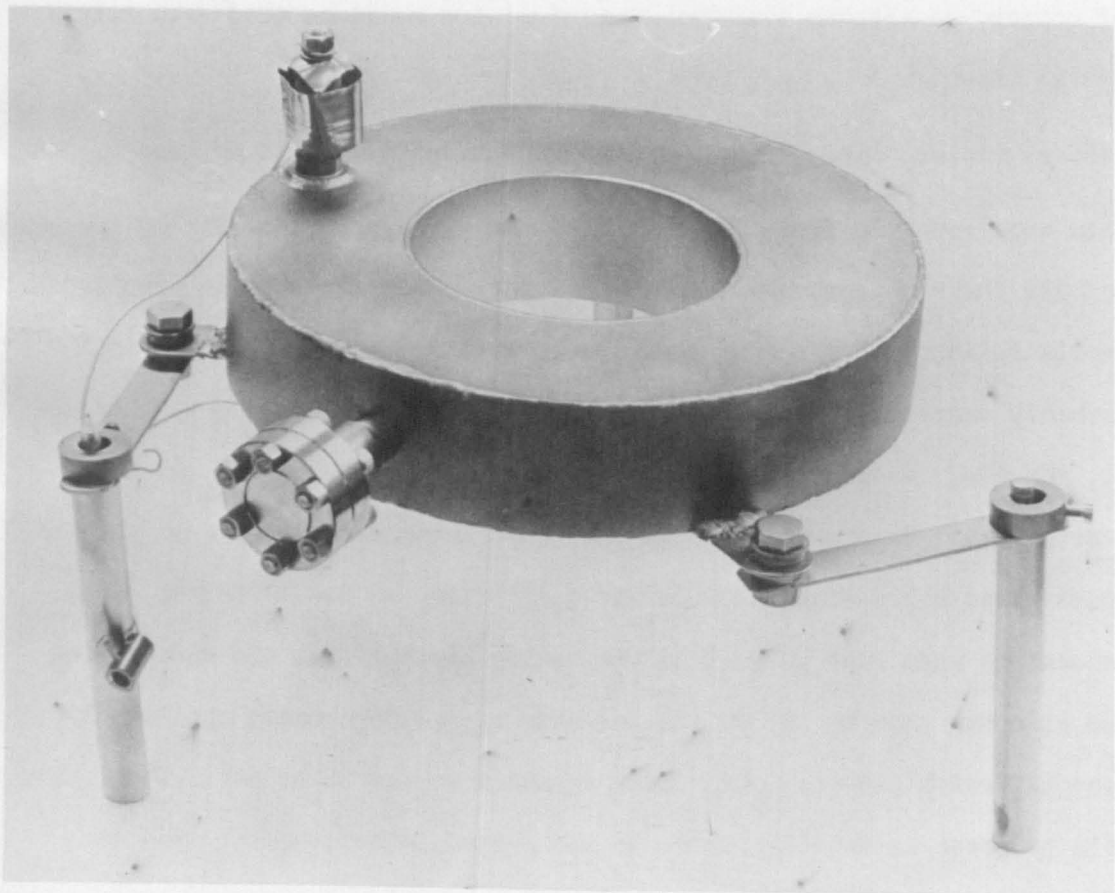

Figure 4.13

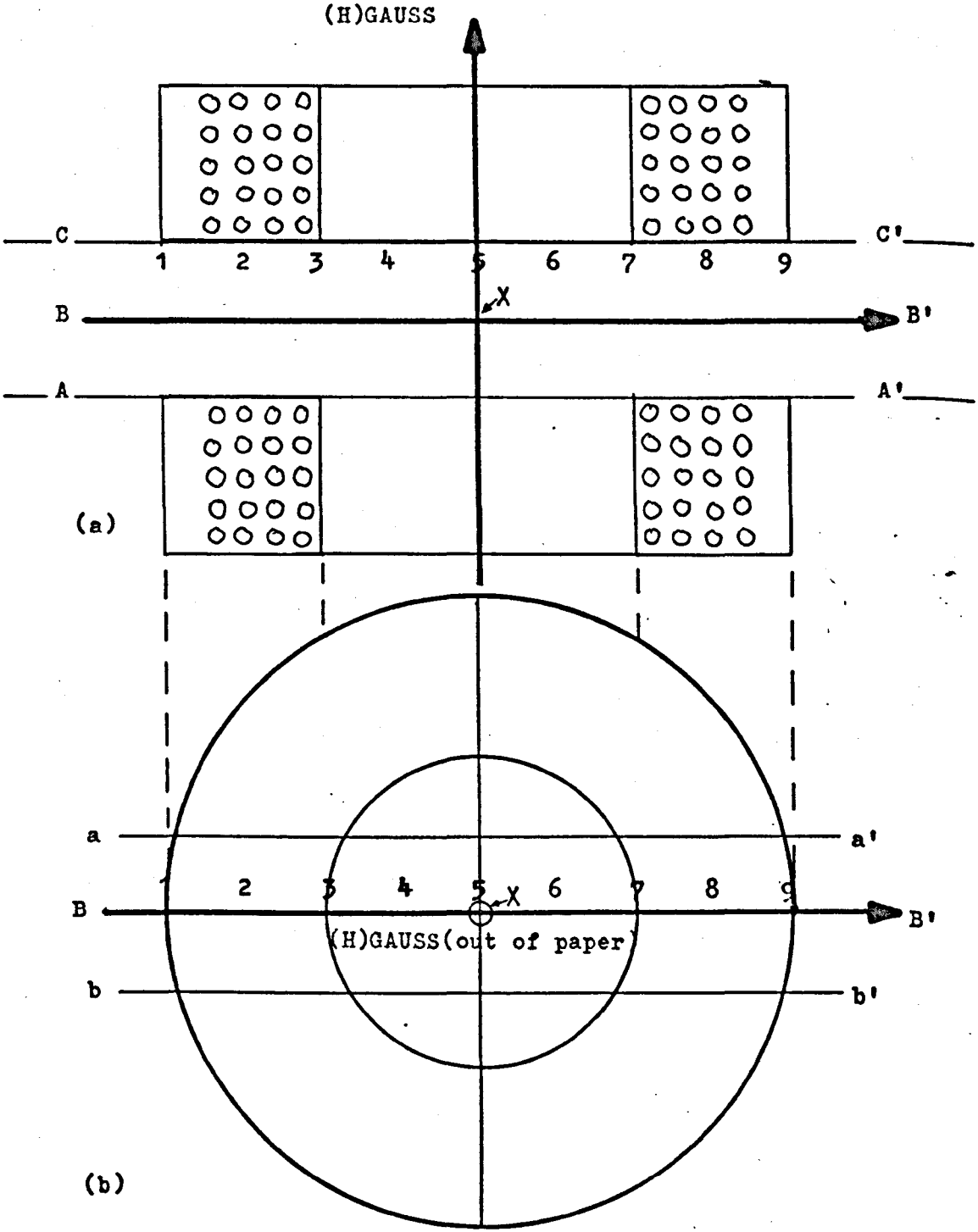

figure 4.14 (a) & (b) SECTION AND PLAN OF MAGNETIC COILS IN HELMHOLTZ CONFIGURATION SHOWING POSITIONS FOR MAGNETIC FIELD MEASUREMENT.

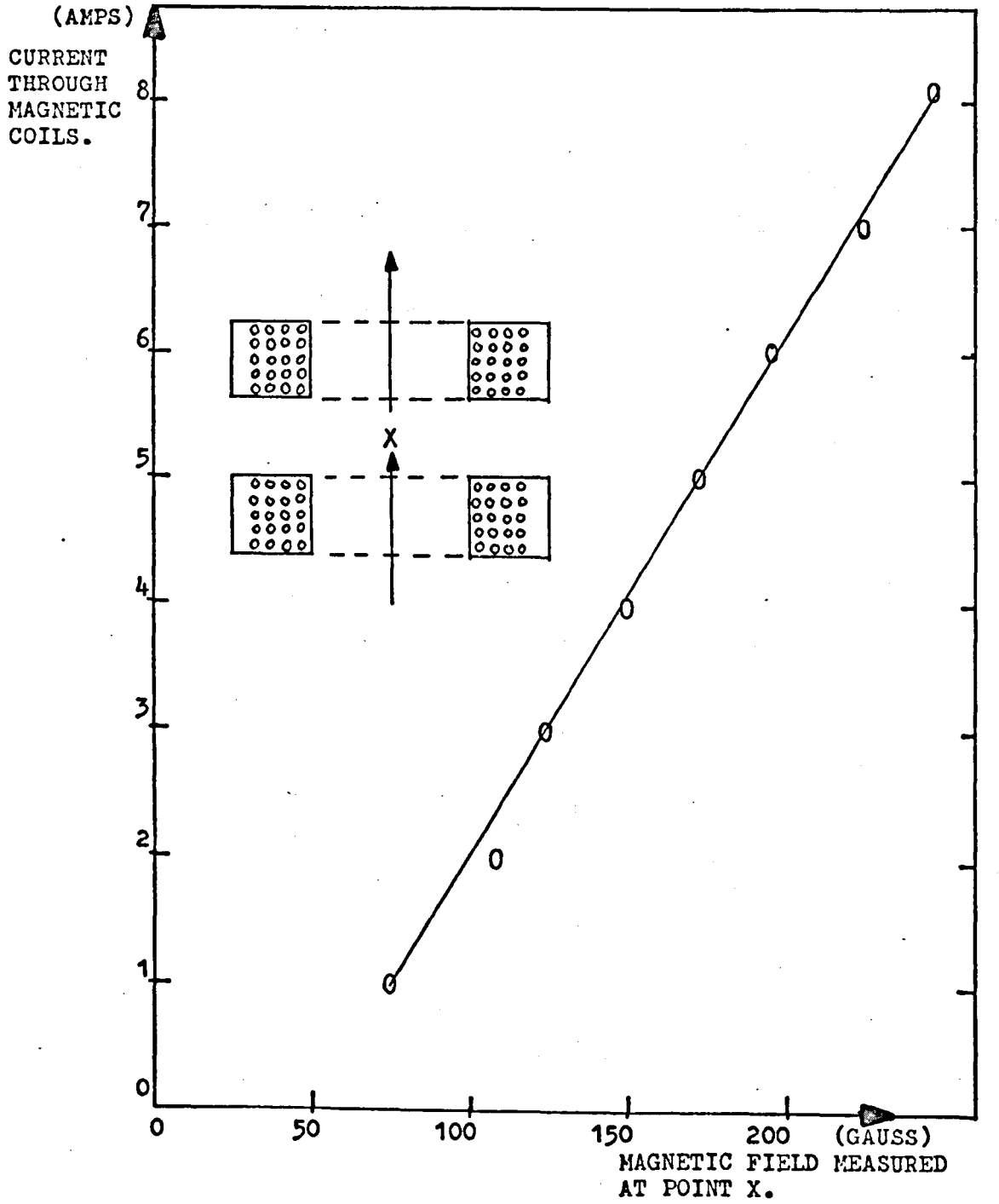

figure 4.15 VARIATION OF MAGNETIC FIELD AT CENTRE OF COILS (X) WITH CURRENT THROUGH COILS.

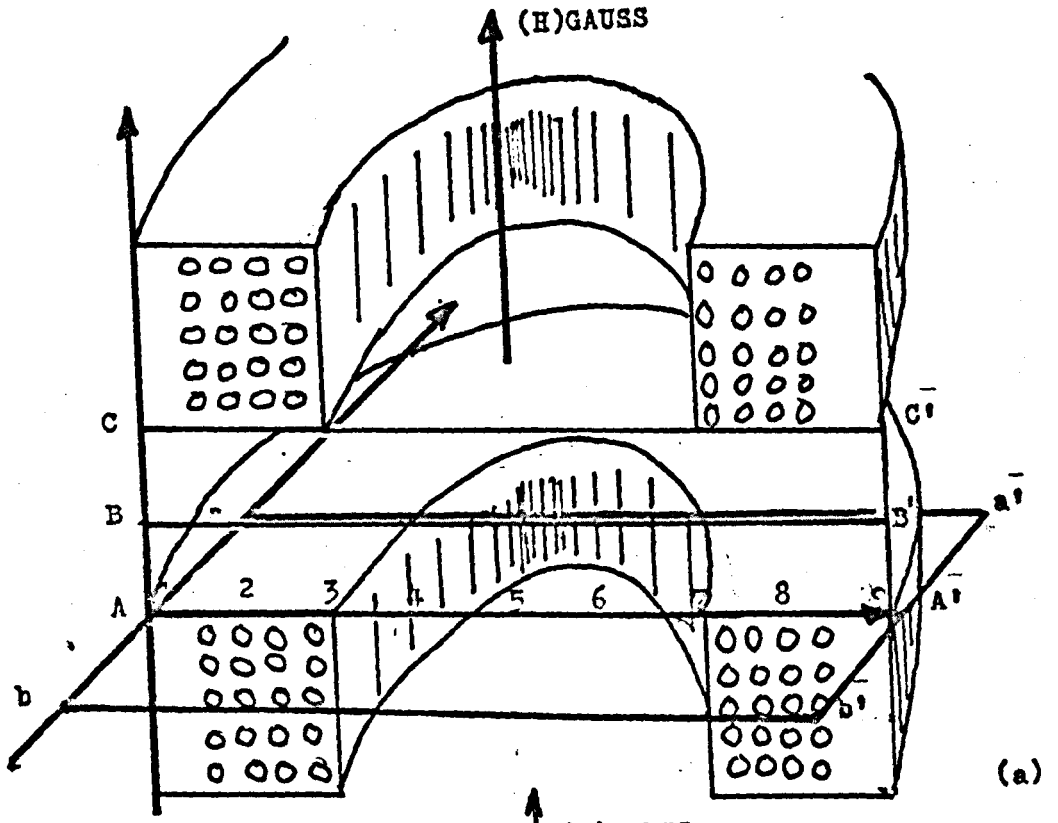

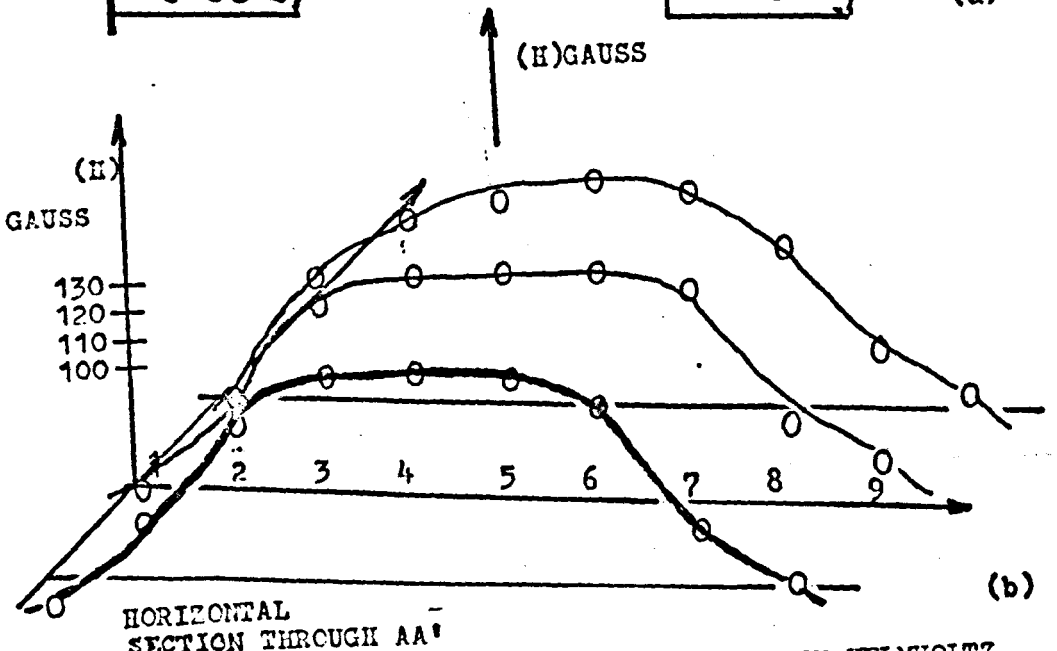

figures 4.16(a). SECTION OF MAGNETIC COILS IN HELMHOLTZ CONFIGURATION

(b). MAGNETIC FIELD PLOT MEASURED IN THE PLANE OF AA'

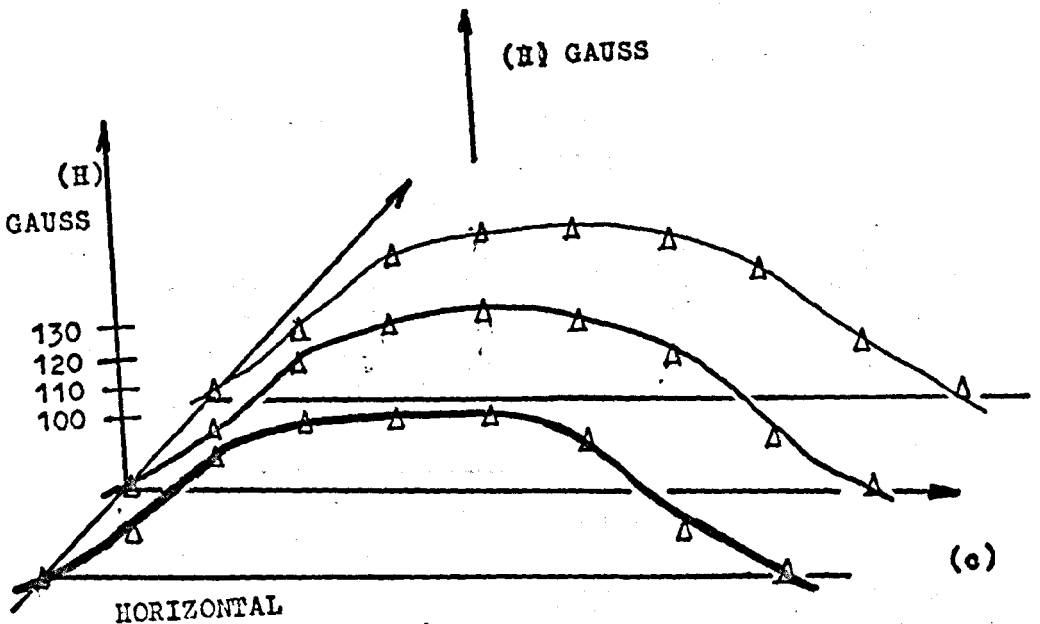

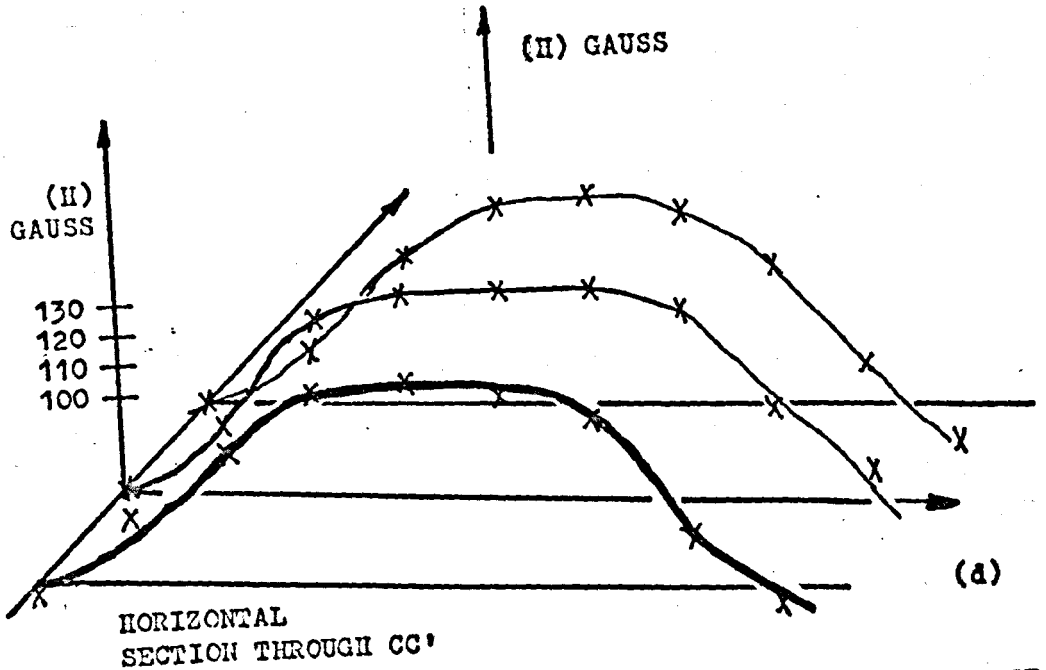

figures 4.16 (c). MAGNETIC FIELD PLOT MEASURED IN PLANE OF BB'

(d). MAGNETIC FIELD PLOT MEASURED IN PLANE OF CC'

sealed off with a special compression instrument. This had the effect of cold welding the copper tubulation. There were several reasons for filling the coils with helium:-

(a) If any leak developed in the coils whilst inside the vacuum system, this would show up as a large He^+ peak in the spectrum of the QRGA. Without the helium, it would not be clear whether a true air leak had occurred or a 'virtual' leak from one of the coils inside the vacuum system. After about 1½ year's use the top coil did develop a leak through the pinched-off tubulation. By this time 'mini conflat' flanges had become available and when the offending tubulation was replaced by one of these, no further trouble was experienced.

(b) The helium helped to conduct the heat, generated in the windings, evenly through the coils, preventing any hot spots developing in the wire. A general view of the top coil is shown in Figure 4.13. The magnetic field was measured with a transverse Hall probe placed at various positions in the space between the coils, when they were in a Helmholtz arrangement. The Hall probe had a sensitivity of 150 Gauss microvolt^{-1} and a probe area of about 2 mm^2. The measuring positions and results are shown in Figure 4.14, Figure 4.15 and Figure 4.16a, b, c, d. It can be seen that the magnetic field, within the space enclosed by the inside diameter of the coils varies by less than ±10%. RUARK[241] suggested the approximate equation: $H = 0.9\ ni/r$ Gauss. to calculate the magnetic field between the coils (H). n is the number of turns of wire per coil, i is the current in amperes through the coils, and r is the mean radius of either coil. Reasonable agreement is found between this equation and the experimentally determined values as shown in Table 4.2.

Current through coils	Calculation of magnetic field from Ruark	Experimental values of magnetic field
amperes	Gauss	Gauss
1	35	75
2	70	108
3	105	123
4	139	150
5	174	172
6	208	195
7	244	225
8	278	247

Table 4.2

The two magnetic coils were mounted horizontally, one above and one below the substrate block/target assemblies, and at a separation of 6.5 cm. This distance is dictated by the requirement that the separation of the coils should be half the mean diameter of either coil[241]. The lower coil is placed on a circular stainless steel ring, mounted on a jig, which rests on insulating ceramics. The top magnetic coil was bolted between ceramic spacers fixed to the underside of the top-plate by threaded rods, as shown in Figure 4.12. The electrical connections were attached to a three-way feedthrough in the top-plate, to which the anode was also connected. With this arrangement it was possible for both magnet coil cases to be electrically floating with respect to the filament. The magnetic field was created by joining the two coils in series to a stabilized D.C. supply. This created a magnetic field in a direction parallel to a line joining the anode and grid. An adapter was made, to enable the top magnetic coil to sit on the ring and jig, when the bell jar was in use.

v. Gas handling arrangement

Spectroscopically pure (BOC grade X) argon is used as the sputtering medium in the present work. It is leaked from a one litre Pyrex bottle, initially at slightly above atmospheric pressure, through a (Vacuum Generator) M.6. bakeable leak valve, seen at the bottom centre of Figure 4.6(b) The leak valve is connected to the deposition chamber by a small bore stainless steel tube, welded into the specially made filament flange. This permits the gas to flow across the filament, thereby improving the chance of a discharge occurring at the grid.

Before the argon bottle could be used it was necessary to pump all the air from the glass tube, connecting the bottle to the leak valve. Whilst

Purity of B.O.C. grade X Argon on leaking into vacuum system

Gas species	A.M.U.	Calculated p.p.m.	Published values (B.O.C.Handbook) p.p.m.
Hydrogen	(2)	~ 10	< 0.05
Oxygen	(32)	not detected	< 0.8
Carbon Dioxide	(44)	~ 2	< 0.55
N_2 , CO	(28)	~ 10	< 3.5
Hydrocarbons	(14, 15, 16)	~ 5	< 0.5

Table 4.3.

Material	Purity	gaseous contaminants p.p.m.			
		C	H	O	N
Gold	99.99%	2	<1	10	3
Nickel	99.99%	50	1	20	5
Copper	99.99%	-	2	2	0.1
Aluminium	99.99%	15	30	35	5
Titanium	99.7%	150		350	40

Table 4.4

pumping, the leak valve was opened fully, giving it a conductance of about 1 litre sec^{-1} [242]. Pumping continued for about two days. Heating tape was then wrapped around the tubing and the glass baked overnight at 400°C. Finally the heating tape was removed and the tubing allowed to cool. The leak valve was then closed. An iron magnet was placed outside the glass tubing to raise a magnetic stainless steel plug, which had been added inside the tubing before evacuation. By manipulation of the magnet and plug, the 'pigs tail' seal above the bottle was broken, allowing the argon to fill the evacuated volume up to the leak valve. The purity of the argon could now be checked by leaking a small quantity into the deposition chamber whilst scanning with the quadrupole mass spectrometer. The purity of the argon, determined by this means, is shown in Table 4.3, where it is compared with the manufacturer's analysis. Assuming the manufacturer's analysis is reliable, the discrepancy between the two sets of values may be attributed, in part, to gaseous impurities arising in the glass connecting tube.

4.8.3 Evaporation assembly

The evaporated films are produced in the same deposition chamber described for the sputtered films. The only difference is that the evaporation source replaces the sputtering target.

Two of these evaporation targets are set up on a 30 amp electrical feedthrough, next to, but shielded from, the front of the sputtering target assembly. The gold, nickel, copper, and aluminium evaporation targets were all prepared by melting pure wire samples onto previously flashed tungsten filaments, the gold on a tungsten loop, the others on tungsten helical baskets. This preparatory work was carried out in an Edwards high vacuum evaporation unit.

Great difficulty was experienced with the preparation of the nickel evaporation targets. As the nickel melted on the tungsten it began to etch away the basket, which often resulted in its fracture. After many attempts, it was found possible to obtain satisfactory samples only if the tungsten used for the basket was made up of at least three wires twisted together, and, in addition, only a very small amount of nickel was melted onto the basket (less than 5% of the weight of the basket).

The titanium evaporation target consisted of a 3 cm length of rod, 1.8 mm diam., cut from a sublimator filament. This was not in fact pure titanium but an alloy of titanium and molybdenum in the ratio 85/15. However, since their melting points are widely different (1660°C and 2620°C) it is presumed that the evaporated films were mainly of titanium. No zirconium evaporation targets were prepared, and attempts at evaporating tungsten resistively proved fruitless. Table 4.4. indicates the purity of the metal samples used, as quoted by the manufacturers.

Figure 4.17

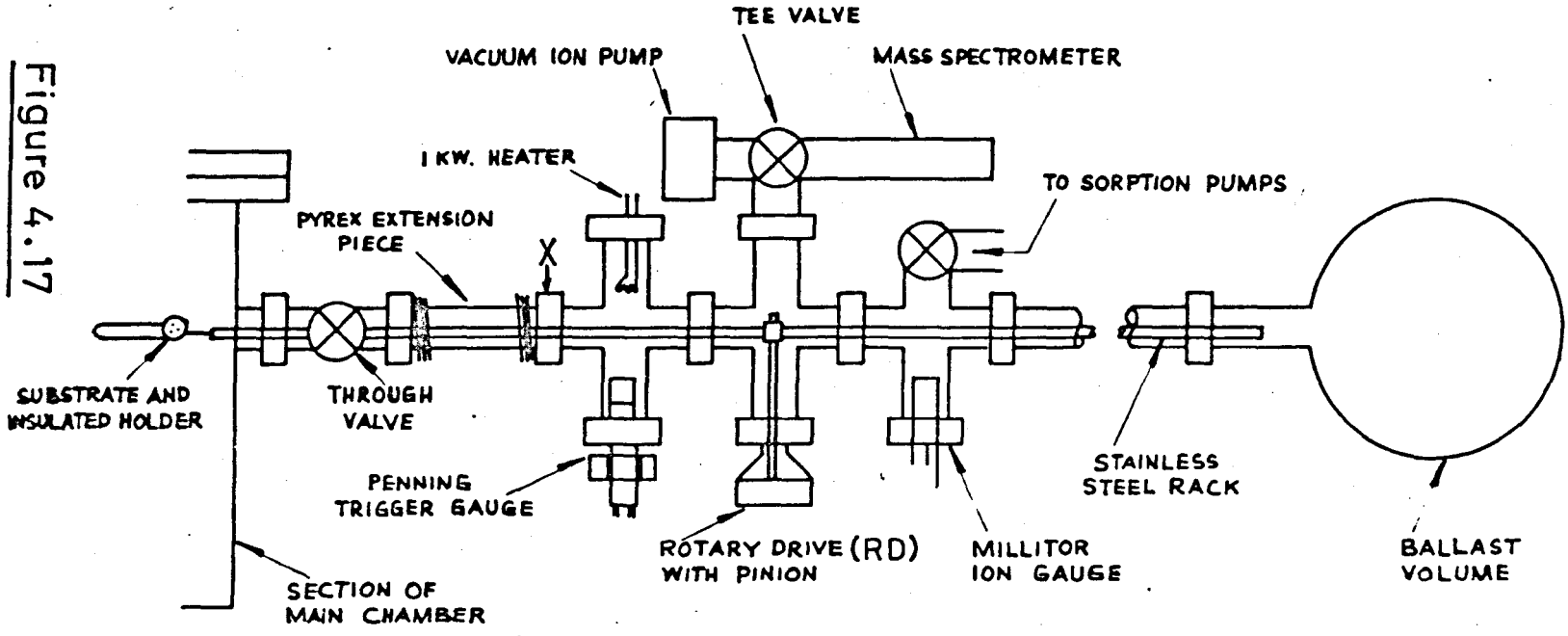

SCHEMATIC DIAGRAM OF THE SIDE ARM OF VACUUM SYSTEM SET UP FOR ANALYSIS USING INDUCTION HEATING UNIT. (N.B THE AXIS OF RD IS SHOWN DRAWN VERTICAL FOR CLARITY, BUT IS ACTUALLY HORIZONTAL)

4.9. The gas analysis system

4.9.1. Introduction

The analysis of the gas content of films produced in the deposition chamber, is made in a separate vacuum system, connected via a gate valve to the deposition chamber. When the gate valve is closed, the samples are in a fixed volume of 5.65 litres, which contains the QRGA and a millitorr ionization gauge. The film (typically of area about 0.7 cm^2) is flash evaporated within the glass section of the vacuum system, using a RF induction heater. This causes the release of gases, trapped in the film, into the closed volume. The amount of released gas is obtained from the mass spectrum measured by the QRGA, and the total pressure increase measured by the ionization millitorr gauge.

From a knowledge of the number of gas atoms released, and the number of metal atoms constituting the film, the concentration of gas atoms of any species in the metal film can be determined.

i. The sidearm vacuum system

This vacuum system is connected to the deposition chamber by a bakeable gate valve (CSD 25). This valve provides a straight clear bore of 25 mm when fully open. The general design of the vacuum system is shown in Figure 4.17. It is made up primarily of extension tubes, several fourway crosspieces and a six-way crosspiece, all joined with copper gaskets between conflat flanges. At various points are connected the GE trigger gauge, Varian millitorr gauge, 10 l/s triode pump, a rotary drive, several electrical feedthroughs and two bakeable valves, one leading to the roughing pump, the other, connected to an 8 l/s diode pump and the QRGA. In this way the QRGA is always maintained under vacuum. In addition, at the far end (seen

to the right, in Figure 4.17, is added a 3 litre pyrex flask, glass-blown onto a glass to metal flange. This acts as a ballast volume. At the gate valve end, a glass Tee piece, fitted with stainless steel bellows, is included.

The whole of the sidearm vacuum system is rigidly mounted on a support made from aluminium and brass (see Figure 4.7). The support is adjustable, and is capable of moving back and forth, and being raised and lowered. It could also move in an arc, swept out from a point at the bellows on the glass Tee piece. These adjustments allow accurate positioning of the end of the rack, carrying the substrate, when entering the substrate mounting block.

ii. Substrate drive arrangement

The films were deposited on substrates in the deposition chamber and analysed in the sidearm, at the glass Tee section. The problem, therefore, was to move the substrate more than 50 cm whilst maintaining vacuum conditions. This was achieved with a rack and pinion arrangement. A small pinion was screwed to the shaft of a rotary drive feedthrough (RD1). When the drive was rotated, a 90 cm long stainless steel rack, of $\frac{1}{4}$" square cross-section, could be propelled back and forth between both vacuum systems, through the open CSD 25 valve. The rotary drive shaft was set above the axis of the rack by the addition of a double-sided conflat flange, with the knife edge of one face slightly off axis. To ensure easy movement of the rack, and to maintain the accurate positioning that was necessary for the substrate to enter the substrate block cleanly and smoothly, the rack has a groove $\frac{1}{8}$" wide milled along the length of its underside. At four points along its run, aided by guides and lead-ins, the rack was made to roll over miniature, greaseless, stainless steel bearings. The bearings were each set in a jig which only

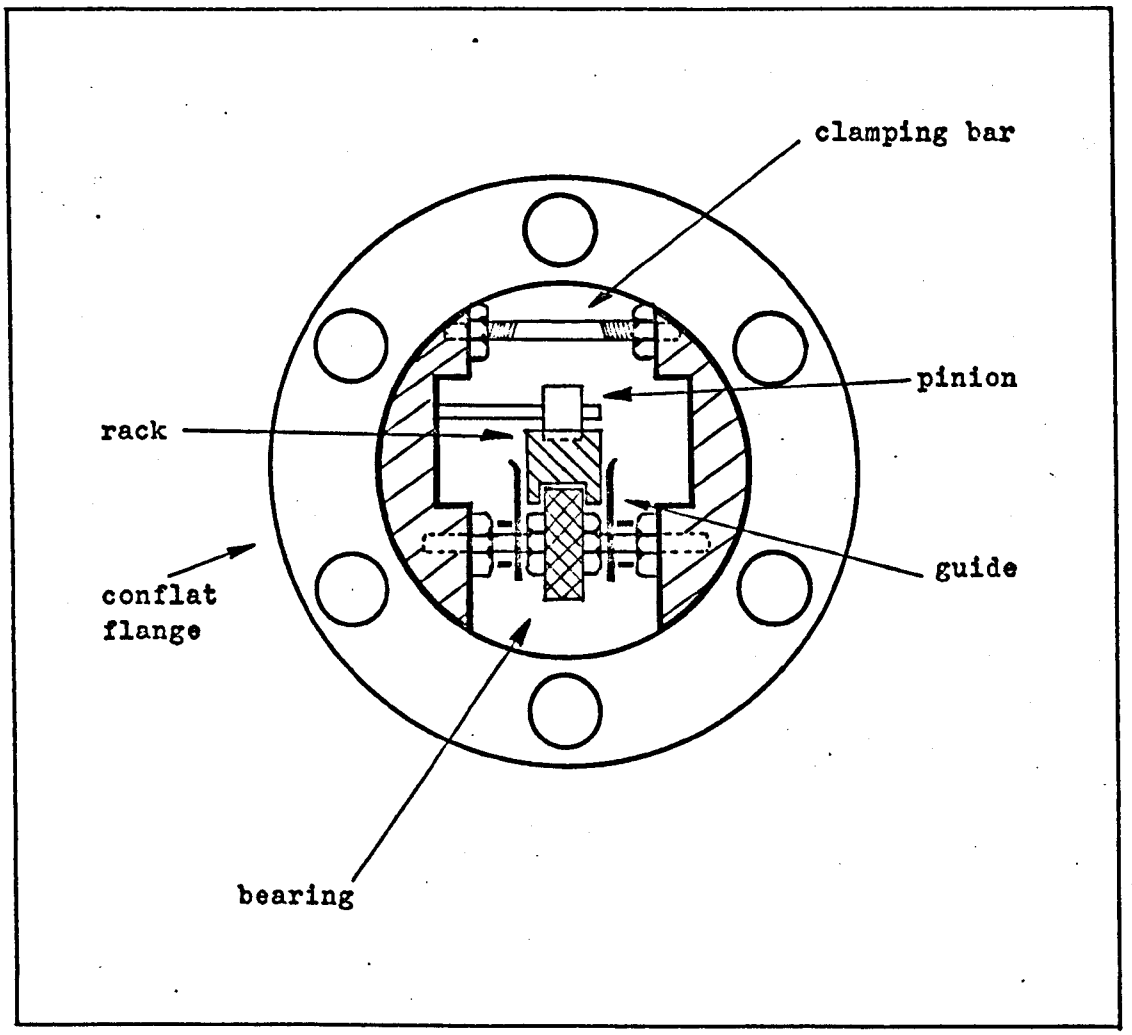

Figure 4.18 Cross-sectional diagram of guiding arrangment for rack. (N.B. the off axis position of the pinion)

Figure 4.19(a)

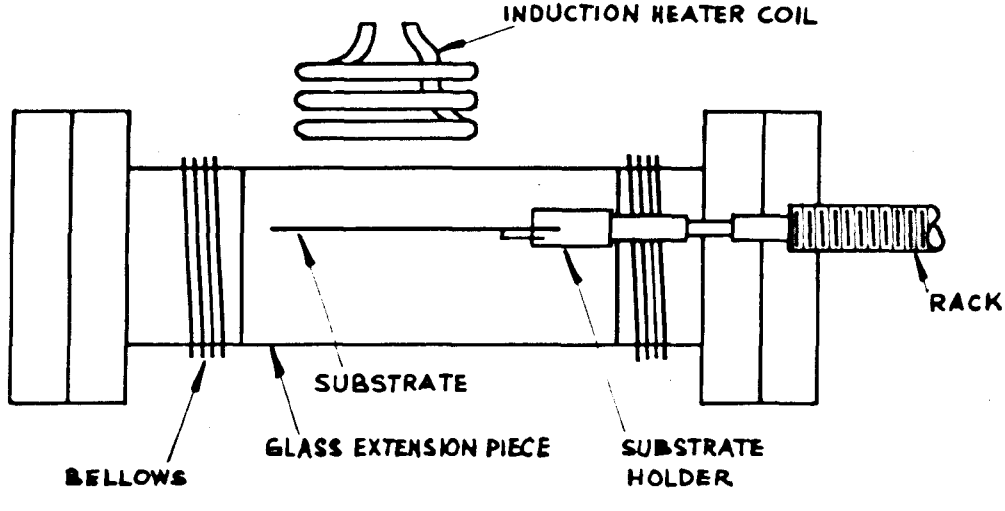

SCHEMATIC DIAGRAM OF VACUUM SECTION SET UP FOR GAS ANALYSIS BY INDUCTION HEATING COIL

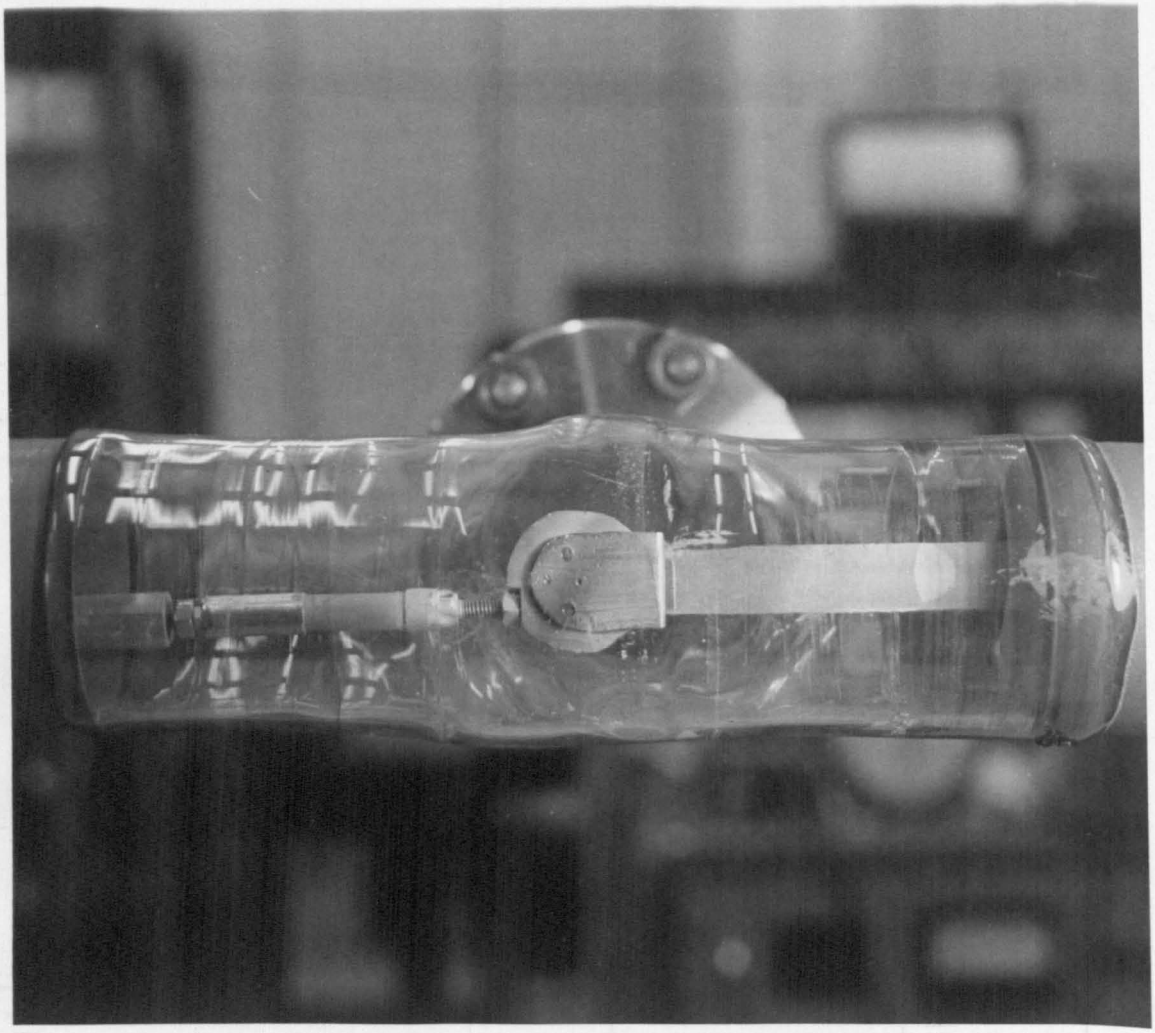

Figure 4.19(b)

allowed them freedom of rotation in a vertical plane, (see Figure 4.18). The substrate was fixed firmly to a small substrate holder. This was connected to the rack by an electrically insulated section modified from a Ferranti 5 amp electrical feedthrough. The arrangement is shown in Figure 4.19(a) and (b)

The substrate could be removed and/or replaced by winding back the rack, until the substrate was in the glass Tee section, closing all valves, and breaking the vacuum in the sidearm at the point marked X in Figure 4.17. The freed section of the sidearm, including the rack and substrate, was then moved away from the deposition chamber, by sliding the sidearm support along closely aligned aluminium angle-runners. With a gap of about 15 cm, the substrate was exposed. An advantage of this technique, is that the deposition chamber and QRGA are maintained under ultra high vacuum during this operation, and it is only necessary to repump out the sidearm system.

iii. Substrates

Substrates of tungsten, stainless steel, soda glass and corning 7059 glass are used in the present experiments. Dimensions are typically about 0.8 cm wide and between 2.5 cm and 10 cm long. Their thickness depends on the material used: for example, tungsten, 0.15 mm ± 2%, soda glass 1.28 mm ± 0.5%, corning glass 0.81 mm ± 6%, and stainless steel 0.95 mm ± 1%.

The cleaning processes for the substrates are briefly as follows:-

Material	Cleaning
Tungsten	Mechanically polished with DP diamond paste and wheel. CCl_4 degrease, H_2O_2 3% in H_2O dip for 60-90 secs., distilled water, alcohol.
Stainless steel	As tungsten to degrease, then 2 min. dip in saturated sodium hydroxide, 1 min. dip in 50% HCl followed by distilled water and alcohol.
Corning glass (7059)	Detergent wash, conc HNO_3 (it was found that chromic acid attacked this glass too strongly) distilled water, alcohol.
Soda glass	As for Corning glass but with chromic acid instead of HNO_3.

In all cases, when the substrates were under vacuum in the system, they were pre-heated at the glass Tee section with the aid of an R.F. induction heater. The problem of outgassing the glass substrates by this method was partially solved by conduction heating, using a tungsten strip pressed closely to the back of them. The heating was continued until no further gas came from the substrates. This was ascertained by operating, at the same time, the quadrupole residual gas analyser. The tungsten substrates were found to be best from the point of view of outgassing and were used for most of the gas content experiments, whereas the glass were better suited to the electron microscope studies.

Time required to sputter a 1000 Å film of various metals (at zero bias voltage)

Metal	Time (mins)
Aluminium	13.5
Copper	8.5
Gold	8.0
Nickel	13.9
Titanium	15.2
Tungsten	19.2
Zirconium	13.0

TABLE 4.5

4.10 Experimental procedure

Beginning with the baked vacuum system at a background pressure of about 10^{-8}torr, the titanium sublimator pump is chilled with liquid nitrogen and the filament cycled at about 38 amps. The cycle time used, is 15 seconds on and one minute off. The thermionic cathode and magnetic coils are switched on and allowed to reach an equilibrium temperature. The ion pumps are then isolated and, if no air leaks are present, the sublimator maintains the system pressure in the low 10^{-8} torr region.

The leak valve is opened slightly and argon, from the one litre bottle, allowed to flow into the main chamber until the desired sputtering pressure is reached (typically about 6.8 10^{-4} torr). This pressure is read from the calibrated millitorr gauge. Periodic checks on the gases present are made using the QRGA. On achieving the required gas pressure, the leak valve is closed and a voltage of about +30 V applied to the grid. This initiates the discharge, as evidenced by the large ($\sim$ 500 mA)current drawn to the grid. Following this, the anode potential is switched on and adjusted to give an electron current of about one ampere. The discharge appears as a confined column reaching up to the anode. The grid voltage may now be reduced to about +15 volts.

For a sputtering deposition, a large negative potential ($\sim$ 1600 V) is applied to the metal target through the water-cooled feedthrough. Presputtering of the target is allowed to take place, for between 10 to 30 minutes, depending on the sputtering yield of the metal. During this period the substrate is shielded, in the guide, from the condensing material. At the same time the deposition rate for the sputtered metal is deduced from the crystal monitor reading. Table 4.5. shows the times required to deposit

a 1000 Å film of the metals studied in the present investigation. The deposition rate is also determined for the situation where a negative voltage bias is applied to the substrate, through the substrate block, thereby introducing a certain amount of resputtering of the deposited film. In this way the additional time required to obtain a 1000 Å film is determined. Having determined these deposition rates, the substrate is moved into the substrate block and the film deposited on it.

For an evaporated film, a similar procedure takes place, but without the target voltage. The current through the support filaments is adjusted to give similar deposition rates to those of the sputtered metals.

A maximum of three deposition may be made, spaced about 3 cm apart, on a single substrate by suitable movement of the substrate. However, one or two depositions per substrate are more usual.

After deposition all the power supplies are switched off. The predominately argon pressure is reduced by opening the plate valve to the 110 l/s triode ion pump. The substrate is removed into the sidearm vacuum system by manipulation of the rack and pinion mechanism. Pumping continues for, from one to two hours, until the residual pressure is down, once again, into the 10^{-8} torr region.

The emission of gas from the deposited films is brought about by flash evaporation, with the aid of an R.F. induction heater, see Figure 4.19(c).

Various differently shaped water-cooled work coils were tried and the most suitable one was found to be of 4.5 cm diameter with ten turns of $^{1}/_{16}$" copper tubing (see later, Figure 5.4). With the substrate withdrawn into the glass Tee piece, the pumps in the sidearm switched off and the CSD 25 valve closed, the films on the substrate are flash evaporated

into a fixed volume, which is measured to be 5.65 litres. The gas desorption is achieved by placing the work coil of the induction heater against the glass section (hence, the importance of the glass Tee piece), so that a well defined area of the substrate is in the field of influence of the circular work coil. Eddy currents, induced in the metal substrates by the RF field from the coil, raise the temperature of the substrate very rapidly, i.e. in the order of seconds. The temperature reached depends on the type of substrate, its thickness and area. Normally, using the 0.15 mm tungsten substrate, the temperatures reached are in excess of 1500°C. Although it is difficult to measure directly this temperature with a thermocouple, since, if pressed against the substrate it also has Eddy currents induced in it, the high temperatures created are indicated by the colour of the tungsten itself, and with the aid of an optical pyrometer. The deposit that often appears on the walls of the glass Tee section after flashing the film is further evidence that temperatures higher than the evaporation point of most of the metal films used, are reached. This condensation on the glass walls is one of the sources of error in the partial pressure analysis for the outgassed active gases, particularly when chemically active metals such as titanium and zirconium are deposited, because of the gettering effect of the redeposited film.

With practice, it is possible to flash desorb only the area of interest. This made it possible, as previously mentioned, to deposit, on a substrate, more than one film during an experimental run. Checks were made to ensure that gas is not being emitted from more than one film at a time, by repeating the experiment with only one film on the substrate and, by reversing the positions of the deposited films.

The major advantage of the induction heater method is that the heater itself is not in the vacuum system and that, whilst flashing the film, it does not heat the surrounding glass or vacuum system. In this way the desorbed gas, as measured by the QRGA, is only representative of the film and not of its surroundings. However, a correction is made for the general increase in the residual gas pressure when the pumps are off. This is achieved in a trial experiment of about ten minutes duration. With the pumps isolated, the partial pressure increase is measured, minute by minute, with the QRGA, and displayed on the XY recorder. After the flash desorption and after repumping, a second trial experiment is carried out, similar to the first. In this way it is possible to separate the partial pressure of any gas species, due to the flash desorption process, from that due to the natural outgassing in the vacuum system.

The amounts of gas released from the film are determined from the partial pressure increase, which in turn, is obtained from the mass spectra, measured by the QRGA, and the millitorr total pressure gauge. It is often found necessary to flash the film several times until there is no further increase in the total pressure. This, in turn, indicates that there is no further gas in the film, or at least, that no further gas is being released by the film. Since, however, there is usually no sign of the film on the substrate after flashing, the former supposition is more probable. Furthermore, if, on flashing, it appears that a large amount of gas will be liberated, so that the total pressure will rise above 2.10^{-4} torr, then the period of flashing is reduced. This is done to ensure that the QRGA is always working in its linear region; i.e. where the partial pressure of any gas, measured by the QRGA, has a linear relationship to the ion current collected, as

given by the manufacturer[243], see Chapter 6. A spectrum is taken at this pressure, and the sidearm then pumped down once more with the 10 l/s ion pump. The pump is switched off and the process of flashing repeated, as before until no further rise in pressure occurs. The number of sputtered or evaporated metal atoms in the film, N_m, is given by:-

$$N_m = \frac{W_s - W_g}{M_m} \times 6.02 \times 10^{23} \text{ atoms.} \quad (1)$$

where $$(W_s - W_g) = W_m \quad (2)$$

and $$W_s = A_s T_s \ell_s \quad (3)$$

where W_s is the weight of the film in gm.

W_g is the weight of the gas in the film in gm.

W_m is the weight of the metal in the film in gm.

M_m is the molecular weight of the metal.

$6.02\ 10^{23}$ is Avogadros number in atoms gm $mole^{-1}$.

A_s is the area of the film in cm^2.

T_s is the thickness of the film in cm.

ℓ_s is the density of the film in $gm.cm^{-3}$.

For the situation, normally encountered, where $W_g << W_s$

then $$W_m \simeq W_s \quad (4)$$

and (1) can be rewritten;

$$N_m = (A_s T_s \ell_m / M_m) \times 6.02 \times 10^{23} \text{ metal atoms} \quad (5)$$

The number of gas atoms of the ith species, N_g^i, in the film is given as follows:-

$$N_g^i = (pp_g^i - bp_g^i) \times 3.24 \times 10^{16} \times V \times \nu_i \qquad (6)$$

where pp_g^i is the pressure of the ith gas from the outgassed sample.

bp_g^i is the residual pressure of the ith gas in the analysing system.

V is the volume of that part of the vacuum system into which the gas is released.

$3.24\ 10^{16}$ is Loschmidt's number suitably modified to one torr pressure and a temperature of $300^{o}K$.

ν_i is the number of atoms/molecule for the ith species. (e.g. for N_2, $\nu_i = 2$, for Argon $\nu_i = 1$)

From equations (5) and (6) the concentration of the ith gas in the film, $C_{i/m}$, may be determined. This is found as follows:-

$$C_{i/m} = (N_g^i/(N_g^i + N_m))\ 10^2 \text{ atomic \% (at \%)} \qquad (7)$$

Expected errors

The area of the deposited film, A_s, is well defined and is known from the size of the mask (typically 70 mm^2). It may be further checked in a preliminary experiment, by removing the film before outgassing and measuring its dimensions with a low power travelling microscope. The area of the film is determined by the position of the movable shutter, which is one of the vertical sides of the mask, and whose position is known to within ± 1 mm. This introduces an error in the area of ± 7 mm^2. For

a 70 mm^2 film this is a percentage error of about 10%. The mean thickness of the film, as determined from the crystal monitor, depends on the accuracy in calculating the relationship between the frequency shift and film thickness by an optical interferometric method. For a film of mean thickness 1000 Å an uncertainty of about ± 100 Å is introduced, i.e. about ± 10%. If W_g, the weight of gas in the film, is ignored, only a small error is introduced into the calculation, since a pressure increase as high as 10^{-4} torr into the closed volume, V, only produces a weight of gas in the film of less than 1% that of the metal in the film. The error in the measurement of the closed volume, V, calculated by the physical measurement of the vacuum system as 5.65 litres, is ± 2%. The accuracy of the partial pressure is dependent on the reading accuracy of the total pressure millitorr gauge and the analysis of the QRGA spectrum for the pressure increase due to (a) the outgassed sample, and (b) the residual gas pressure increase. Assuming the spectrum peaks are corrected for variation in ionisation cross-section for different gases, the error will lie in reading the calibrated millitorr gauge only. This is, at most, ± 0.05 of the meter reading, giving an error of about ± 5% when reading 1.00 10^{-4} torr, and ± 0.5% when reading 10.0 10^{-5} torr. Hence calculating $(pp_g^i - bp_g^i)$ introduces an error of, at most, ± 10%, if $pp_g^i \approx bp_g^i$. Usually, however, $pp_g^i \approx 100\ bp_g^i$ and therefore the error is limited to about ± 5%. The number of gas atoms can therefore be determined with an error of about ± 7%. The error for the number of metal atoms is about ± 20%. This gives an overall expected percentage error in the calculation of the concentration of about ± 27%.

4.11 The quartz crystal thickness monitor

Various methods are available for measuring film thickness, by chemical, physical and optical means. A recent review of these methods has been given by GREENLAND[244], BERNDT[245], and GREAVES[246]. The advantages of the oscillating quartz crystal method over other techniques are numerous:- The former is straightforward to use and gives a continuous determination of the thickness of the growing film; the deposited film of interest need not be exposed to air and is left undamaged, since it is not directly used by the crystal in the thickness measurement. For thickness measurements, the quartz crystal monitor, in common with most of the other methods assumes that the film density is the same as that of the bulk material, and that the film itself is uniformly deposited. It also requires calibration against a standard optical method before it may be used.

The quartz crystal thickness monitor, as its name suggests, employs a quartz crystal, vibrating in the shear mode at a frequency of 6.0 MHz. The frequency is lowered, as the crystal is mass loaded by a condensing film landing on the crystal. The change in frequency is a measure of the mass of the film deposited.

The quartz crystal is calibrated by comparing its thickness reading, given in cycles per second of frequency change, with the thickness, measured by multiple beam interferometric techniques, in Angstroms. The films used for calibration are deposited, by evaporation on glass substrates, in an Edwards high vacuum plant. The substrate and the crystal are placed at the same distance from the evaporating source, as in the UHV system. An opaque film is deposited onto half the substrate, the other half being covered with

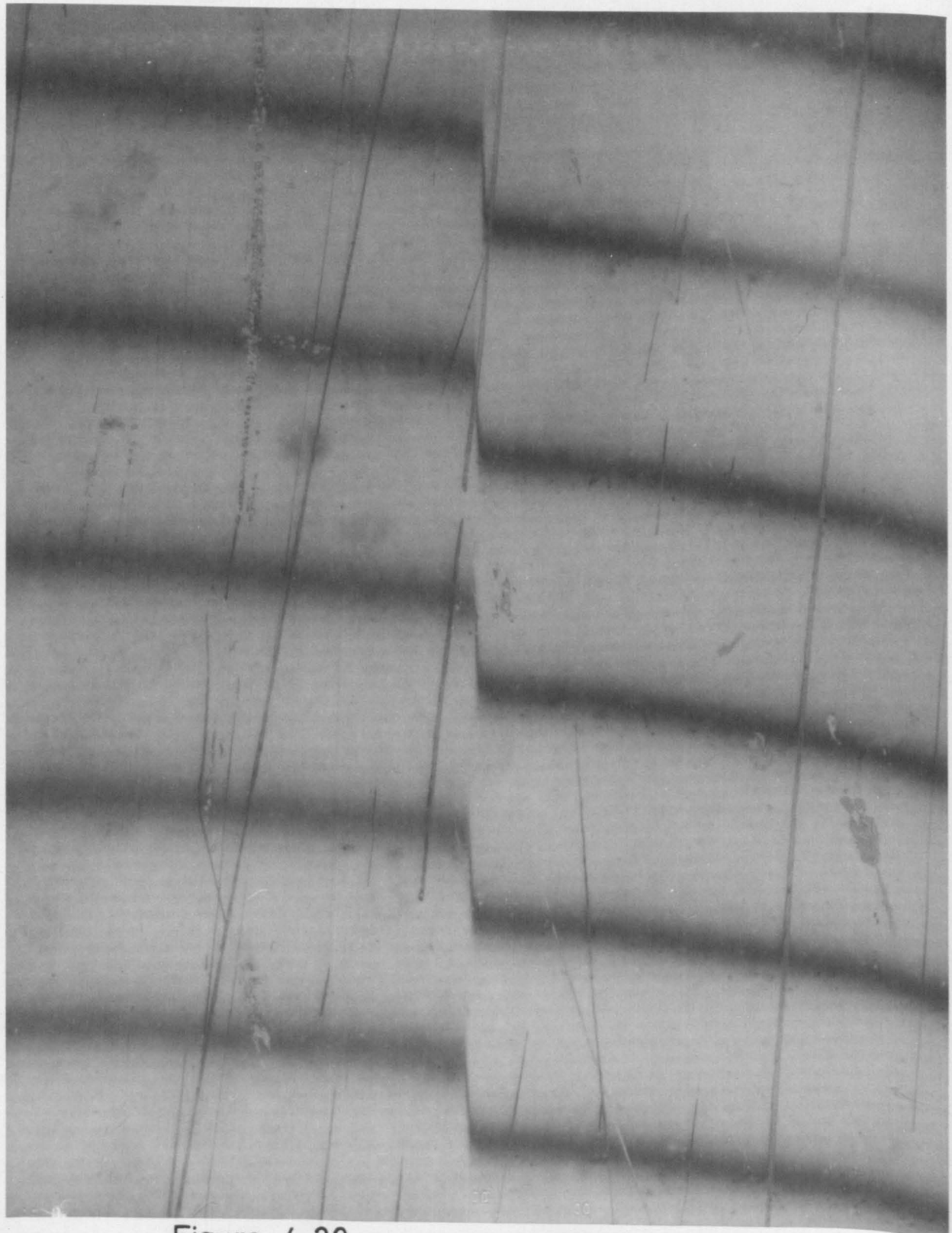

Figure 4.20

a glass slip. This slip is then removed and a silver film deposited by evaporation over the step film. Multiple beam fringes are observed when this substrate and a partially reflecting surface are pressed tightly together and viewed with a sodium light source. The fringe step and fringe width are measured with a micrometer eyepiece, fitted on a Vickers projection microscope. Figure 4.20 shows the fringes obtained by this method. The crystal monitor is calibrated for films of nickel, aluminium, gold and copper and the calibration factors are given in the Table below.

Metal	Calibration factor 1 c/s = x Å
Aluminium	1.38
Copper	0.47
Gold	0.21
Nickel	0.43
Titanium	0.93*
Tungsten	0.21*
Zirconium	0.72*

* calculated.

The calibration factors depend on the mass of deposited material landing on the crystal, which, in turn, is dependant on the diameter of the hole in the metal can surrounding the crystal, and the distance of the crystal to this hole. The error in measuring the fringe step for a 1000 Å film is about ± 10%.

Problems with the monitor

In some ways the crystal oscillator proved difficult to use in the sputtering system. Even with the protective mesh in front of the crystal,

the crystal face would often charge up to high potentials. On connection to the oscillator unit, the first imput transistor (VR205) would break down. Several attempts were made to overcome this problem:

(a) A high resistor was inserted between the transistor base and the earth. This usually prevented the crystal from oscillating at all.

(b) Adding a reverse biassed zener diode in place of the resistor. If any voltage greater than 9 volts appeared at the transistor the zener diode would conduct to earth, so shorting across the crystal. This was not entirely successful.

(c) The final arrangement, in 1969, was to exchange the crystal control unit for one more recently designed by Edwards Ltd. This was designed to allow the front face of the crystal to be at earth potential. In this situation, no charge build-up could occur at the crystal.

Another problem arose from the manner in which the electrical connections to the crystal were made. With prolonged use, the gold connectors lost their springiness and a bad contact resulted. A partially successful solution was to paint over the connections with liquid bright gold (Johnson Matthey).

CHAPTER V

Instrumentation and Sputtering Discharge Characteristics.

5.1 Introduction

In this chapter a description is given of the instrumentation used and its operation in the present investigation. A number of power supplies, monitoring devices and control units are used. These are shown in Figures 5.1, 5.3, 5.4, 5.6 and 5.8. Those instruments purchased commercially will be described briefly and only in terms of their use in the experiment, whereas those designed and constructed at Keele and A.W.R.E. will be described in more detail. (5.2 - 5.10). 5.11 describes the typical operating characteristics of the sputtering arrangement. A brief description is given in 5.12 and 5.13 of the optical and electron microscopes used to study the surfaces of the targets and films.

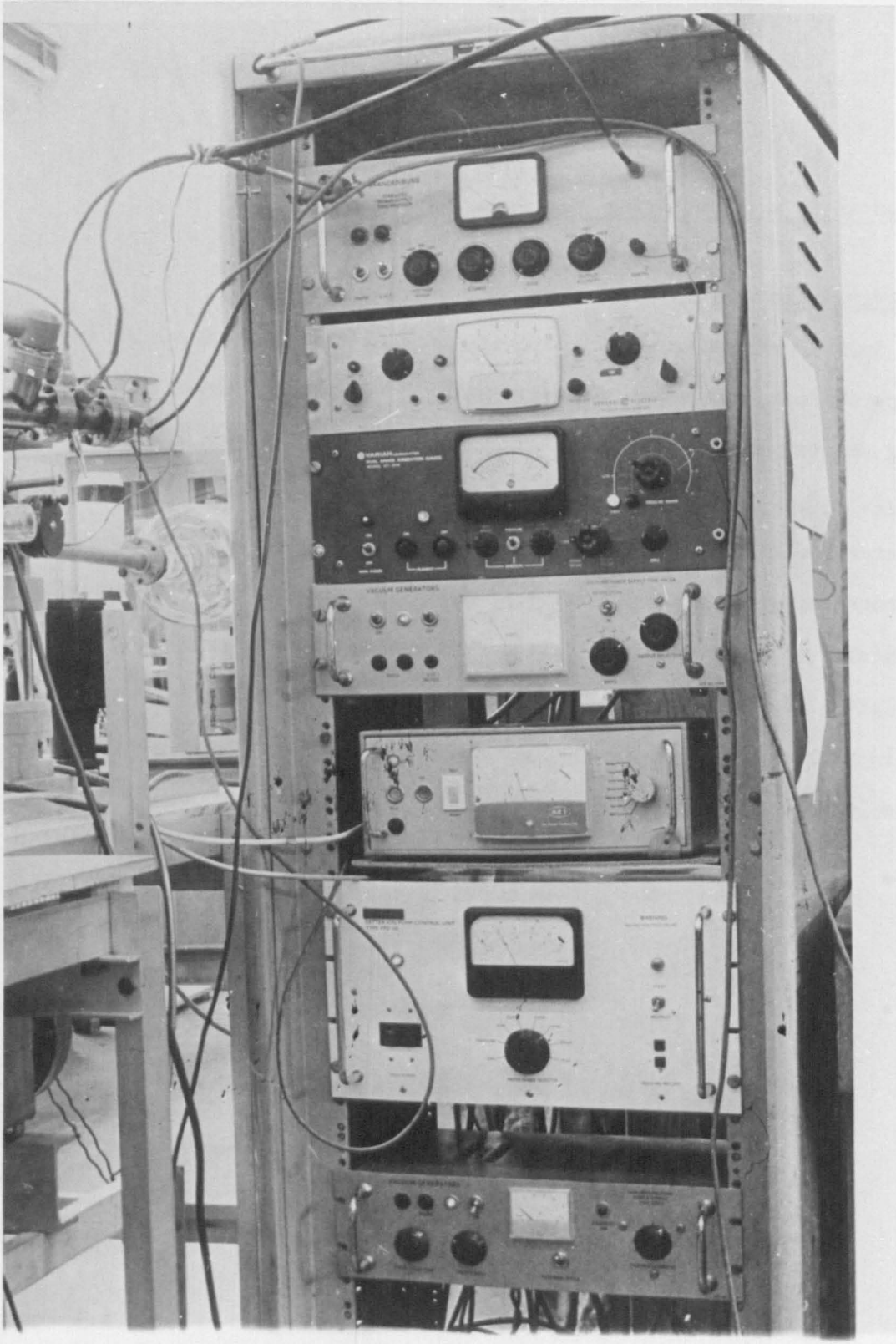

Figure 5.1

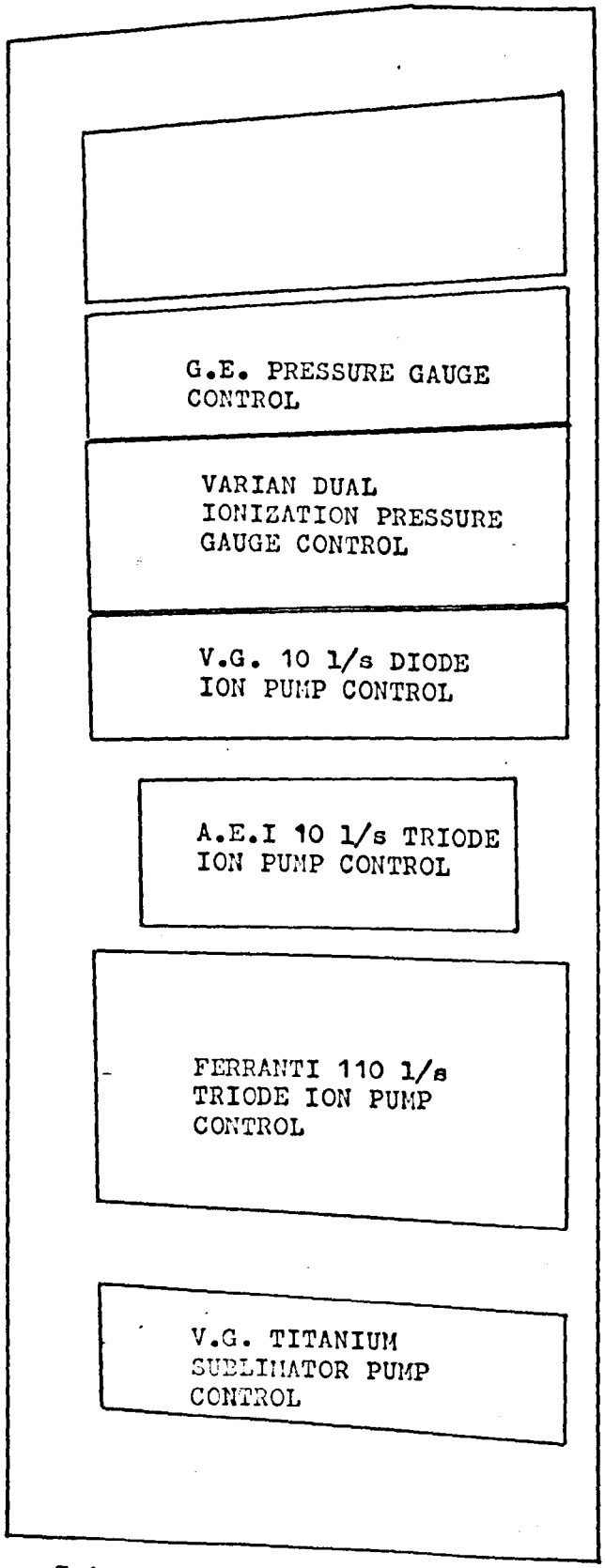
G.E. PRESSURE GAUGE CONTROL
VARIAN DUAL IONIZATION PRESSURE GAUGE CONTROL
V.G. 10 l/s DIODE ION PUMP CONTROL
A.E.I 10 l/s TRIODE ION PUMP CONTROL
FERRANTI 110 l/s TRIODE ION PUMP CONTROL
V.G. TITANIUM SUBLIMATOR PUMP CONTROL

Figure 5.1

5.2 Pump controls

Each of the three ion pumps used requires its own control unit (see Figure 5.1). For the triode pumps, the control units supply a stabilized -5 kV to the pump cathodes. Both units are current limited so that, on starting, an excessive current can not be drawn across the pump electrodes. For the 10 l/s pump this is 50 mA and for the 110 l/s pump, 500 mA. The 8 l/s diode pump power supply is similar to the 10 l/s triode pump control, except that it delivers a stabilized +3 kV to the pump anode.

Each control unit has a meter on the front panel which may be switched to read either log-scale pressure (for nitrogen), electrode voltage, or decade ranges of the discharge ion current from 500 mA to 5 μA. The ion currents may be converted to pressure equivalent values by reference to the pressure/current graph supplied with the pump.

The titanium pump power supply (type SPS 1) provides a maximum of 50 amps, at 7 volts, through the titanium pump filament. In normal use, about 38 amps is drawn from the power supply, providing an evaporation rate from the filament of about 1 Å sec^{-1}. The current can be continuously varied with a Variac on the front panel. Furthermore, the duty cycle of the filament may be varied by using the automatic cycling timer. The filament will be turned on and off for predetermined time periods, until over-ridden by the manual control.

5.3 Pressure gauge controls

The GE gauge control provides a -2 kV supply for the gauge head, and when required, a heating current to the triggering filament. An electrometer circuit amplifies the collector ion current, which may be

read on a meter, calibrated in nitrogen equivalent pressure values. By switching the input resistors on the front panel, the ion current may be multiplied in units of ten. In this way, pressures between 10^{-4} torr to 10^{-13} torr are measurable. The sensitivity of the GE gauge is given as 2.5 amps $torr^{-1}$.

The Varian gauge control may be used with both the hot ionization gauge and the millitorr gauge, although not simultaneously. It supplies +175 V to the grid and +45 V to the filament. The electron emission current is variable, depending on which gauge is in use. Typically, this is 25 μA for the millitorr gauge and 4 mA for the UHV gauge. The meter on the front panel is graduated in a logarithmic pressure scale and a linear pressure scale. The latter, like the GE control, may be scaled up in units of ten, by changing the pressure range switch to the right of the meter. The millitorr gauge can measure pressures between 1.0 torr and 1.10^{-6} torr, although it is found to be unreliable at the low range, always reading higher than either the GE or the UHV ion gauge. The high pressure end is calibrated against a McLeod gauge in a subsidiary experiment. The control unit has a facility for outgassing the ionization gauges by electron bombardment. The Pirani gauge control has a double output for fitting two Pirani heads. The meter display is in pressure readings from 760 torr to 10^{-3} torr on a non-linear scale.

5.4 Quartz crystal thickness monitor unit

A 6 MHz oscillating quartz crystal is positioned in the deposition chamber, so that material is deposited on a well defined area of the crystal surface. A reference quartz crystal with an oscillating frequency of 6.5 MHz

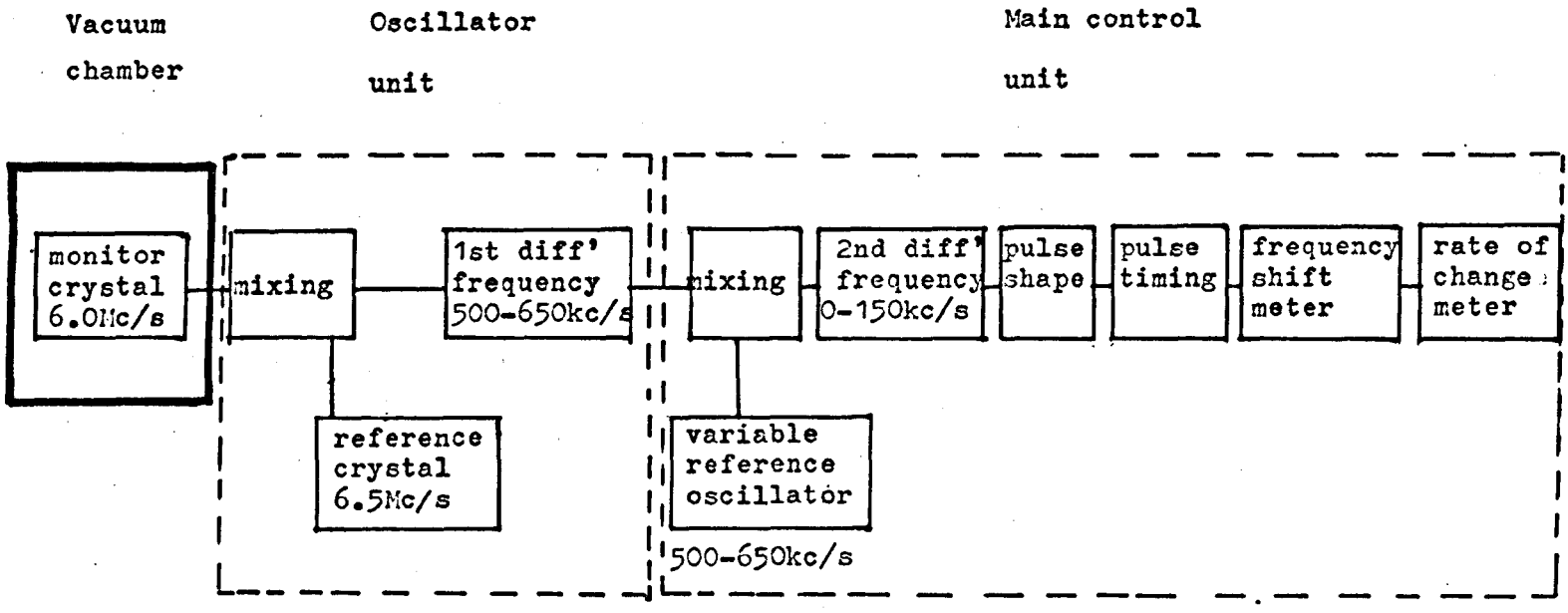

figure 5.2. Block diagram of the film thickness monitor.

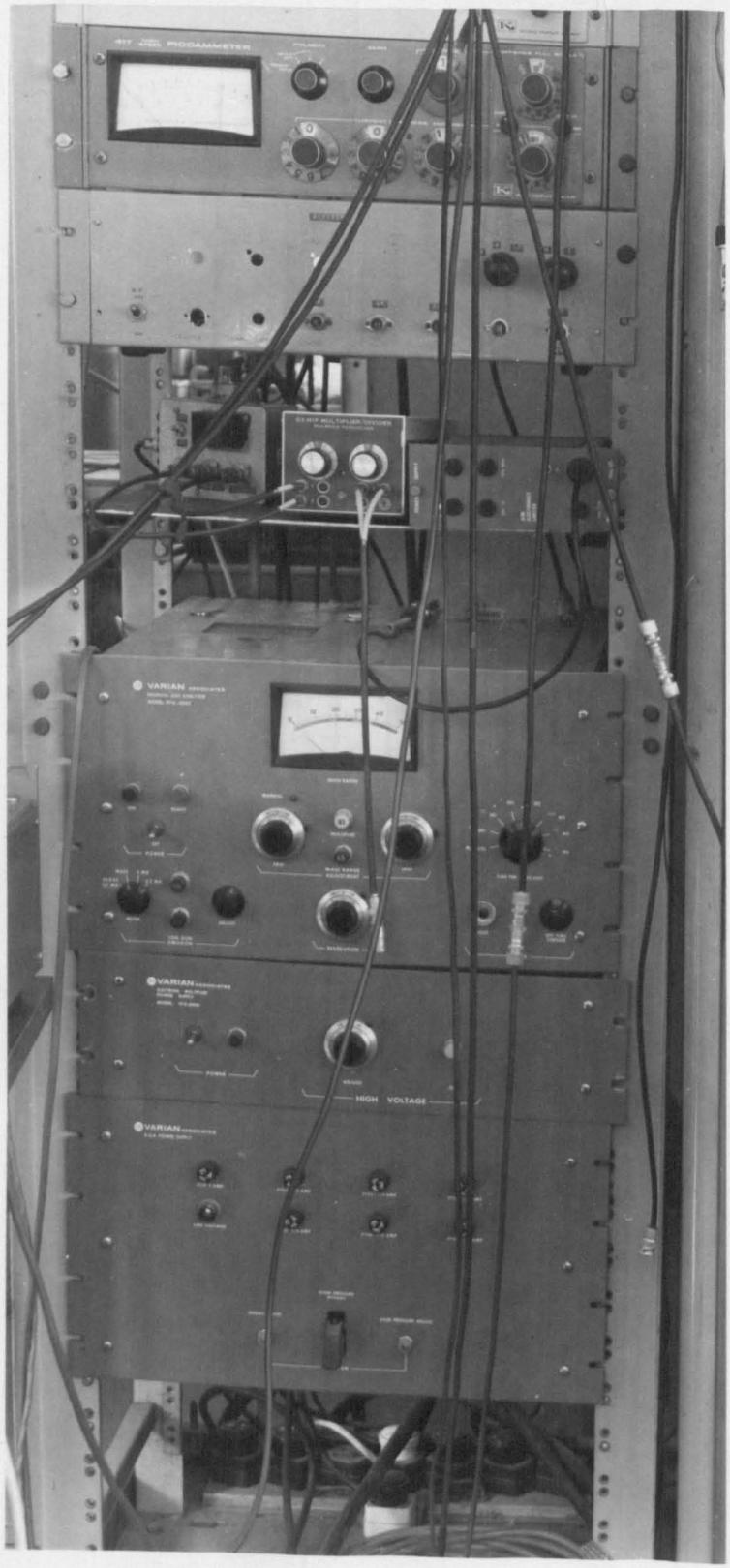

Figure 5.3

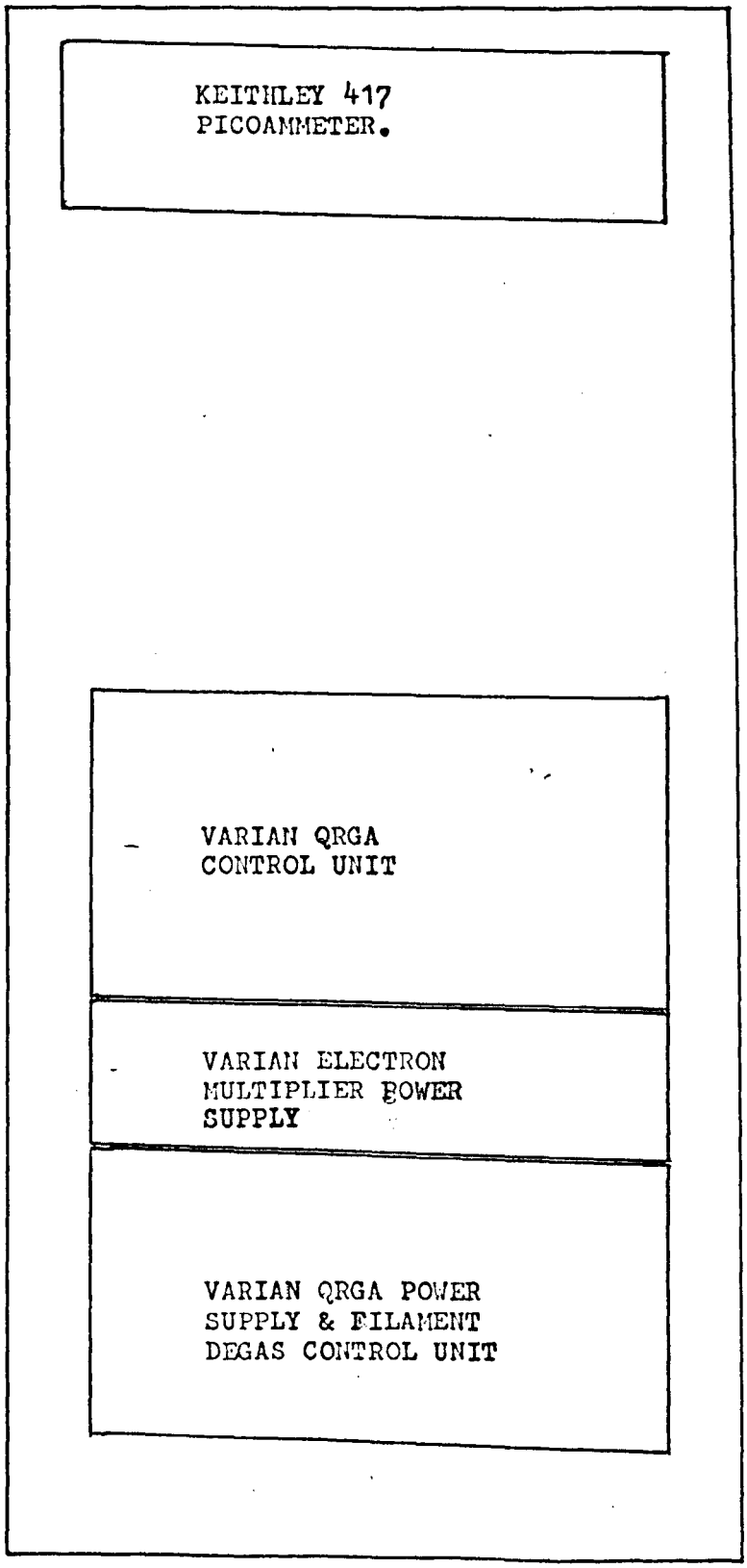
KEITHLEY 417
PICOAMMETER.
VARIAN QRGA
CONTROL UNIT
VARIAN ELECTRON
MULTIPLIER POWER
SUPPLY
VARIAN QRGA POWER
SUPPLY & FILAMENT
DEGAS CONTROL UNIT

Figure 5.3

is mounted in an oscillator unit outside the vacuum system. This unit amplifies the difference frequency between the two crystals and feeds the result into the main control unit, where it is mixed with a variable oscillator to produce a difference frequency between 0 and 150 KHz. Mass loading of the first crystal causes an increase in this last difference frequency, which, when converted to a d.c. signal, is indicated on a frequency shift meter and rate meter. These meters are displayed on the main control unit, together with a frequency range switch, giving a choice of four ranges, 1, 5, 10 and 50 kHz f.s.d., and a zero frequency reset switch. A block diagram of the circuit is shown in Figure 5.2.

5.5. QRGA supplies

The quadrupole power supplies and control unit are in three separate chassis, see Figure 5.3. The power supply as well as containing all the necessary electronics to provide the correct voltages to the control unit and analyser head, has an adjustment on the front panel varying the electron emission to the thoria-coated iridium filament, up to a maximum of 30 mA, so that the ion source may be degassed.

The power supply for the electron multiplier attachment on the analyser head provides a stabilized negative voltage of 1000 to 2500 volts. The voltage is continuously variable by means of a potentiometer on the front panel. It may be measured with a valve voltmeter at the output voltage terminals (1 V per 1000 V ± 2%) located at the rear of the unit. The potentiometer is normally set to give an output voltage of -1350 V, and a measured gain of about 10^3. The main control unit has a meter on the front panel scaled up to 50, which follows the spectrum as it sweeps out one of two ranges:- either 0 to 50 atomic mass units (a.m.u.) (the X1 scale)

or 10 to 250 a.m.u. (the X5 scale).

The latter range is only used, here, to establish that the vacuum system is clean and uncontaminated. This is discussed in more detail in the following chapter. The mass scan is completely automatic with a choice of seven rates. It has fully variable limits for each mass range, from 1 m sec to 30 sec. per a.m.u. so that any group of peaks may be selectively observed. In addition, a manual scan is provided if a single a.m.u. is to be followed. The scan may be made to repeat its sweep at any point by pressing the reset button. The resolution of the analyser, and hence its sensitivity, (see Appendix A) may be varied by adjustment of a ten turn potentiometer at the bottom of the control panel. To the left of this are the controls to the ion source filament, which are normally set at 1 mA of emission current, but, for the purposes of degassing, may be set as high as 30 mA.

5.6 The Picoammeter

To measure the electron current from the quadrupole (or ion current, if the electron multiplier is disconnected) a Keithley 417 picoammeter is used. This is shown above the QRGA control unit in Figure 5.3. It can be switched to measure currents in the range 10^{-13} to 3.10^{-5} amps fsd. To reduce noise at low currents, a filter network is incorporated. An output of 3V is provided at the rear of the unit for connection to a pen recorder.

5.7. Pen recorders

A Japanese XY recorder, made by Yokogawa (Model PRO 12), is used to plot the spectrum from the QRGA. The X axis imput is connected to the sweep output located at the rear of the quadrupole control unit, and the Y axis imput to the Keithley 417 picoammeter output. The control unit

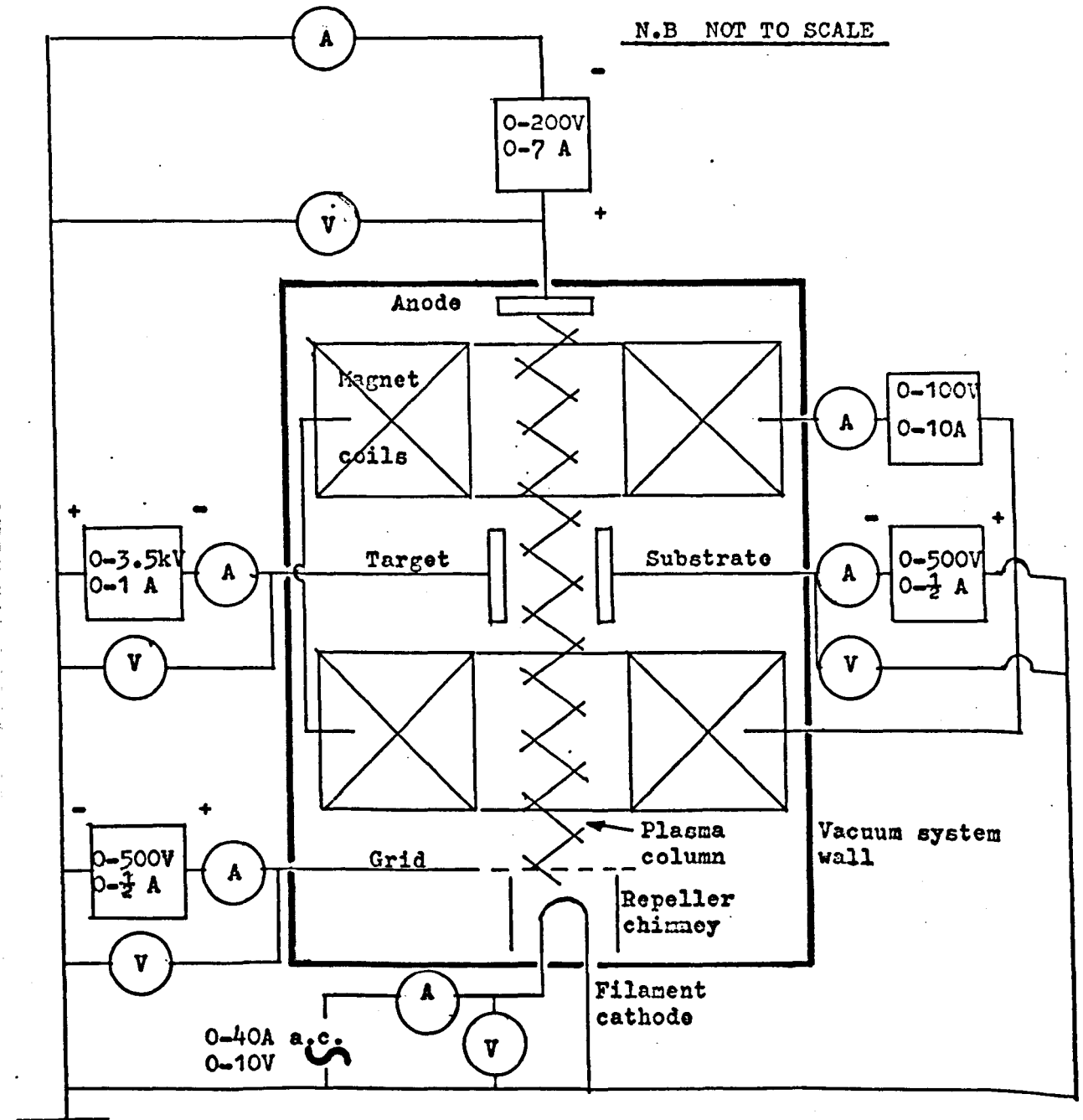

figure 5.5 . Schematic circuit diagram of sputtering system.

sweep output is 0-100V for both the 0-50 and 10-250 a.m.u. ranges. The recorder has a wide voltage range, from 0.5 to 20 $V.cm^{-1}$ for both the X and Y axis. It is normally used with 200 $mV.cm^{-1}$ on the Y axis and 5 $V.cm^{-1}$ on the X axis. This provides the recorder with an imput impedance of 800 kΩ and 2 MΩ, respectively.

In addition, a Moseley Autograph 680 M is used both as an all-purpose recorder, e.g. for recording film thickness deposition, and for recording the mass spectra when the time dependence for an individual peak is required. The Autograph has the advantage of an event marker. It also has a wide range of paper speeds and sensitivity, and an imput impedance greater than 2 MΩ.

5.8 Temperature measurement

Temperature measurement is carried out using chromel-alumel thermocouples and a Croydon thermocouple potentiometer type P.6. This gives direct readings in degrees celcius, when the correct interchangeable scale is fitted. The cold junction is compensated for within the instrument.

5.9 Outgassing supply

To flash evaporate the films, an RF induction heater (Radyne model C9/A) is used with a 4.5 cm diameter water-cooled work coil, (see Figure 5.4.). This operates at a nominal frequency of 450 kHz, giving a current penetration in the order of 0.1 - 0.25 mm.[246a] The output power is continuously variable up to a maximum of 1 kW with a Variac type transformer.

5.10 Voltage supplies and the sputtering system

The triode sputtering arrangement, requires a number of D.C. and A.C. power supplies for its operation. Figure 5.5. gives a schematic

Figure 5.6

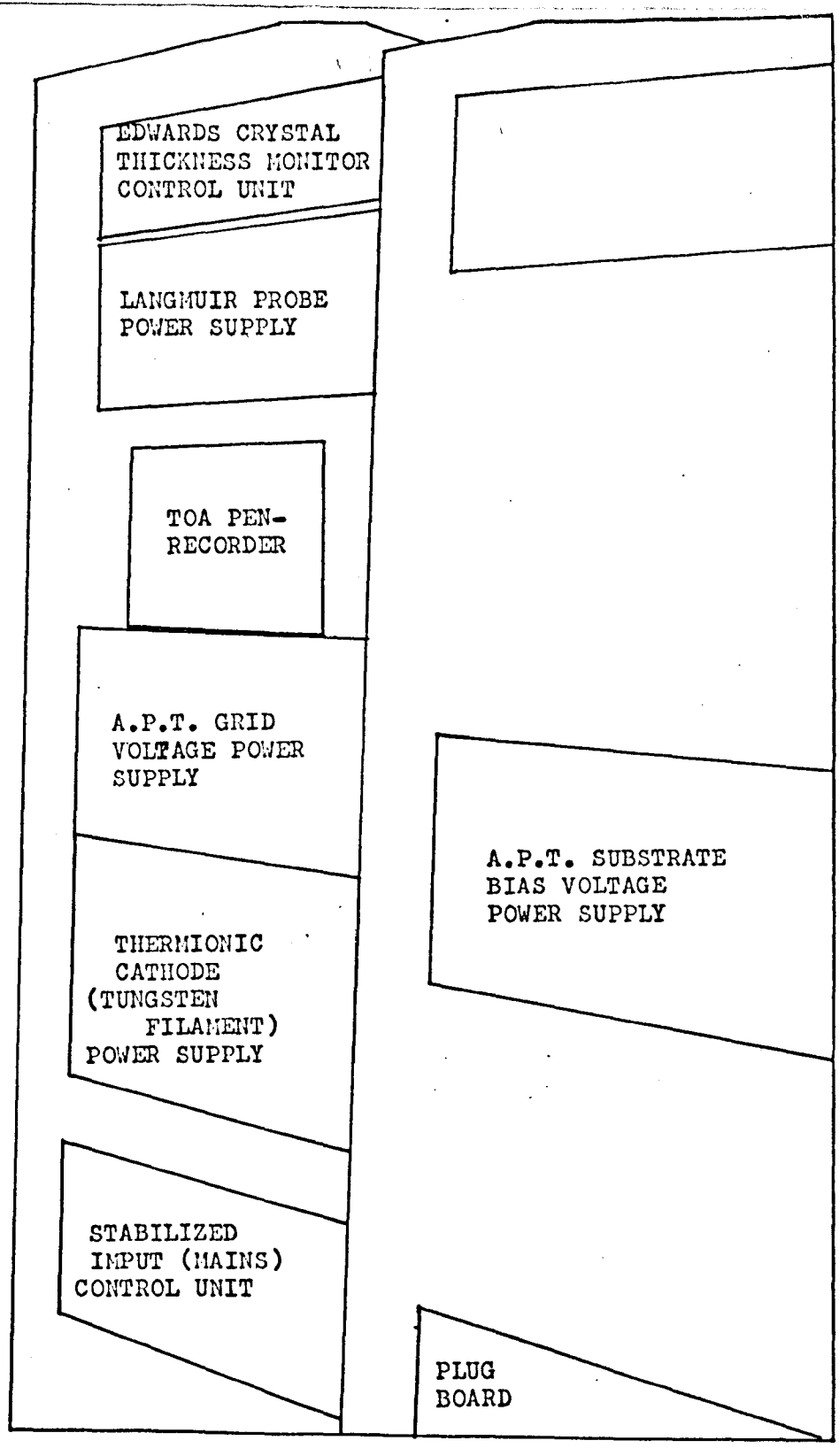
EDWARDS CRYSTAL THICKNESS MONITOR CONTROL UNIT
LANGMUIR PROBE POWER SUPPLY
TOA PEN-RECORDER
A.P.T. GRID VOLTAGE POWER SUPPLY
THERMIONIC CATHODE (TUNGSTEN FILAMENT) POWER SUPPLY
STABILIZED IMPUT (MAINS) CONTROL UNIT
A.P.T. SUBSTRATE BIAS VOLTAGE POWER SUPPLY
PLUG BOARD

Figure 5.6

(a)

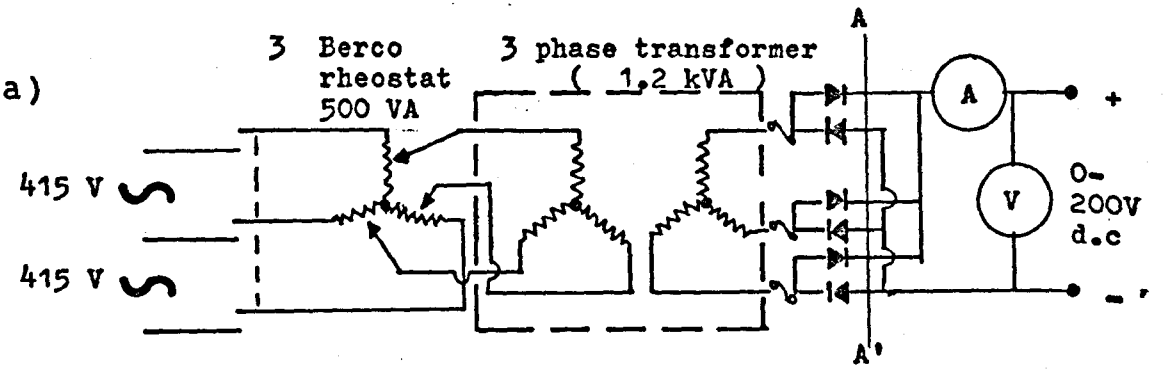

d.c output		a.c secondary RMS			a.c primary			power factor	volts fluct'n
E_o	I_o	V_s	I_s	VA	V_p	I_p	VA		
200V	10A	86V	4.1	1.05kVA	270V	1.3	1.05kVA	0.95	14%

(b) As above up to AA'

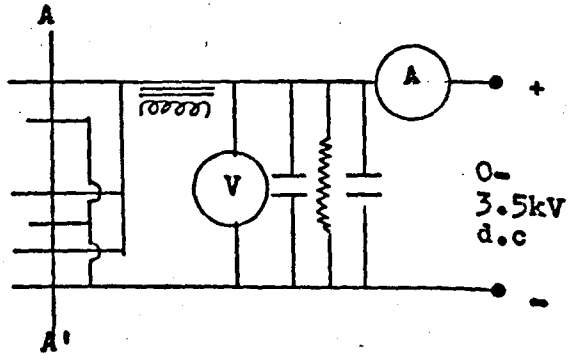

d.c output		V_s phase	V_s line	I_s	N_s/N_p	V_p phase	V_p line	VA phase	VA line
E_o	I_o								
3.5kV	1A	1.5kV	2.6kV	0.82A	6.3	415	240	3.7kVA	3.7kVA

figure 5.7 (a) circuit diagram of anode power supply.

(b) circuit diagram of target power supply.

diagram of the circuit used. Figure 5.6 shows the filament, grid and substrate power supplies together with, at the top of the rack, the main crystal monitor control unit and, directly beneath this, the Langmuir probe control.

5.10.1 Filament supply

A simple Variac/transformer arrangement is designed to provide a maximum of 40 amps A.C. at about 10 V. A stabilized 1:1 power supply is inserted between this arrangement and the imput, to stabilize any variations in the mains supply. A similar arrangement is used for the evaporation filaments.

5.10.2 Grid supply

An A.P.T. regulated power supply (Model 512) is used to give the grid a positive voltage with respect to the filament. It can provide a maximum of 500 V at 500 mA.

5.10.3 Substrate bias supply

An A.P.T. supply identical to the one just mentioned, provides the substrate with a voltage which is either positive or negative with respect to the filament.

5.10.4 Anode and target supplies

For supplying the positive voltage to the anode and the large negative voltage to the target, a power supply, designed and built at A.W.R.E. is used. The circuit diagrams for each are shown in Figure 5.7(a) and 5.7(b). The anode supply will provide up to 7A at 200V D.C. with a voltage fluctuation of about 14%, whereas the target supply is capable of 3.5 kV D.C. at 1 amp. These two power supplies come in one unit, shown

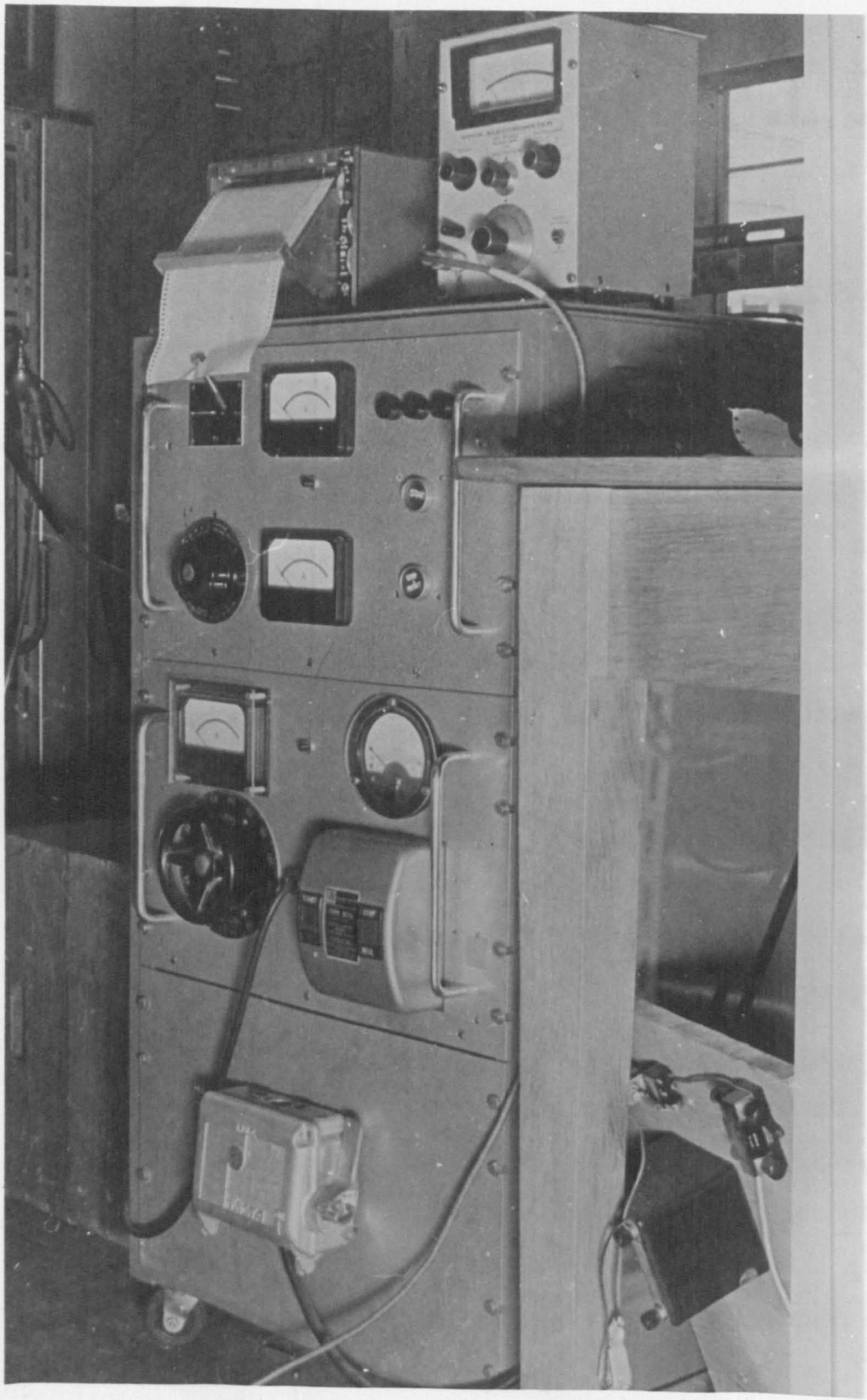

Figure 5.8

in Figure 5.8.

5.10.5 Magnet supply

A Newport stabilized power supply, giving up to 100 V. D.C. at 10 amps, is used to produce the magnetic field between the coils. High stability, about 1 part in 1000, is attainable in the current, and hence in the magnetic field, with this unit.

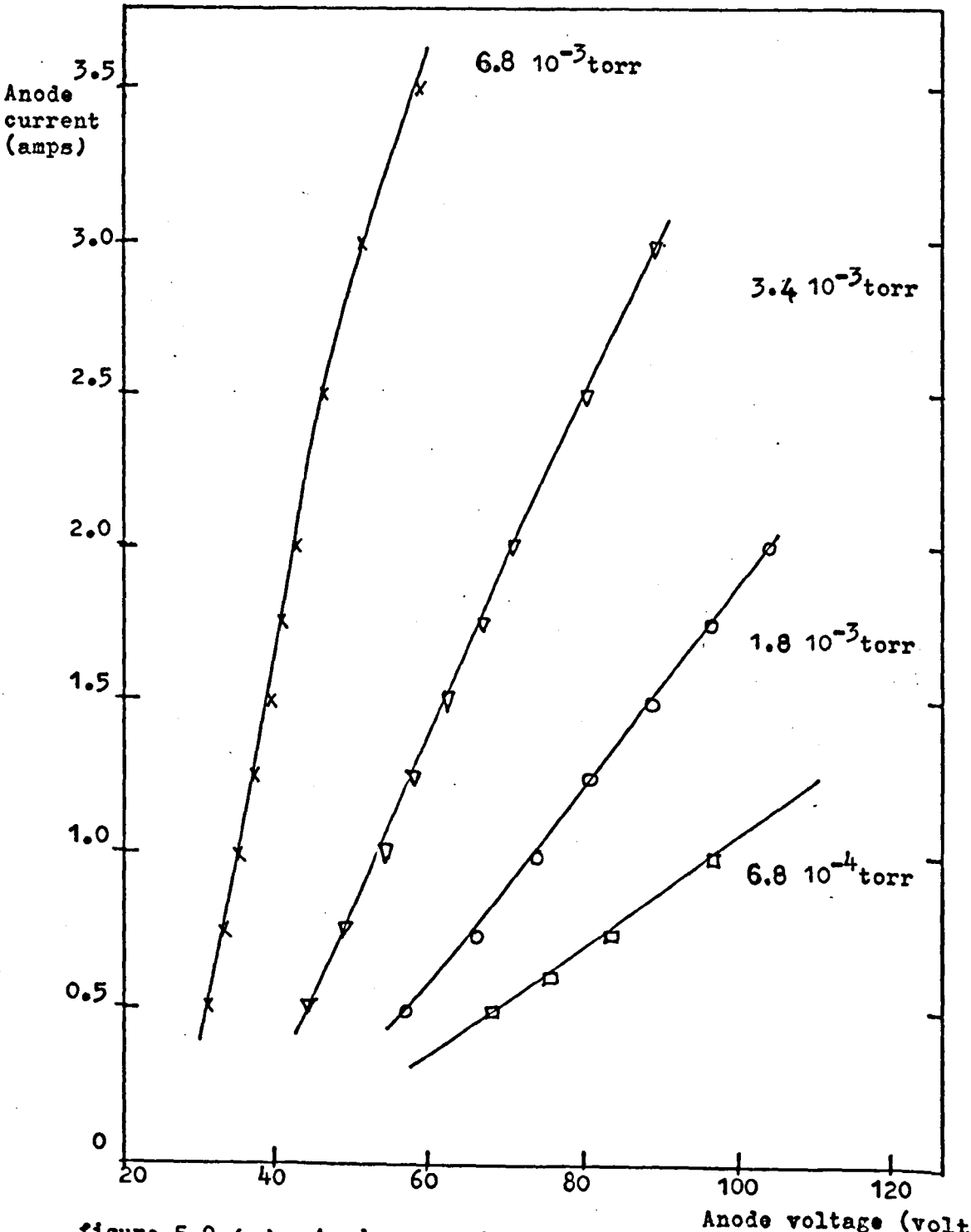

figure 5.9 (a.) Anode current versus anode voltage with variation in argon gas pressure.
(with constant magnetic coil current= 7.0 A)

5.11 Operating characteristics

In the triode sputtering arrangement, a gas discharge may be made to occur, using argon, at pressures as low as 2.10^{-4} torr. However, the discharge is not very stable at this low pressure and is frequently extinguished. Normally, sputtering pressures of about 6.10^{-4} torr (argon) are used. Table 5.1 shows a typical set of values, used to obtain a stable discharge at $6.8.10^{-4}$ torr.

Table 5.1

Parameter	Value	Parameter	Value
Anode voltage	96 V	Residual gas pressure	4.10^{-8} torr
Anode current	1.0A	Argon gas pressure	$6.8\ 10^{-4}$ torr
Filament cathode current	32.0A	Target voltage	- 1600 V
Filament cathode voltage	14 V	Target current density	$+0.8mA.cm^{-2}$
Magnet coil current	7.0A	Target temperature (watercooled)	less $100^{o}C$
Magnet coil voltage	20 V	Substrate voltage	from +50 V to -500 V
Grid current	10 mA	Substrate current	from -250 mA to +1.25 mA
Grid voltage	-15 V	Substrate temperature (watercooled)	less $100^{o}C$

Figure 5.9(a) shows the variation of anode current with anode voltage, for increasing gas pressure. As expected, the anode voltage required to maintain a given anode current, falls as the argon pressure is increased.

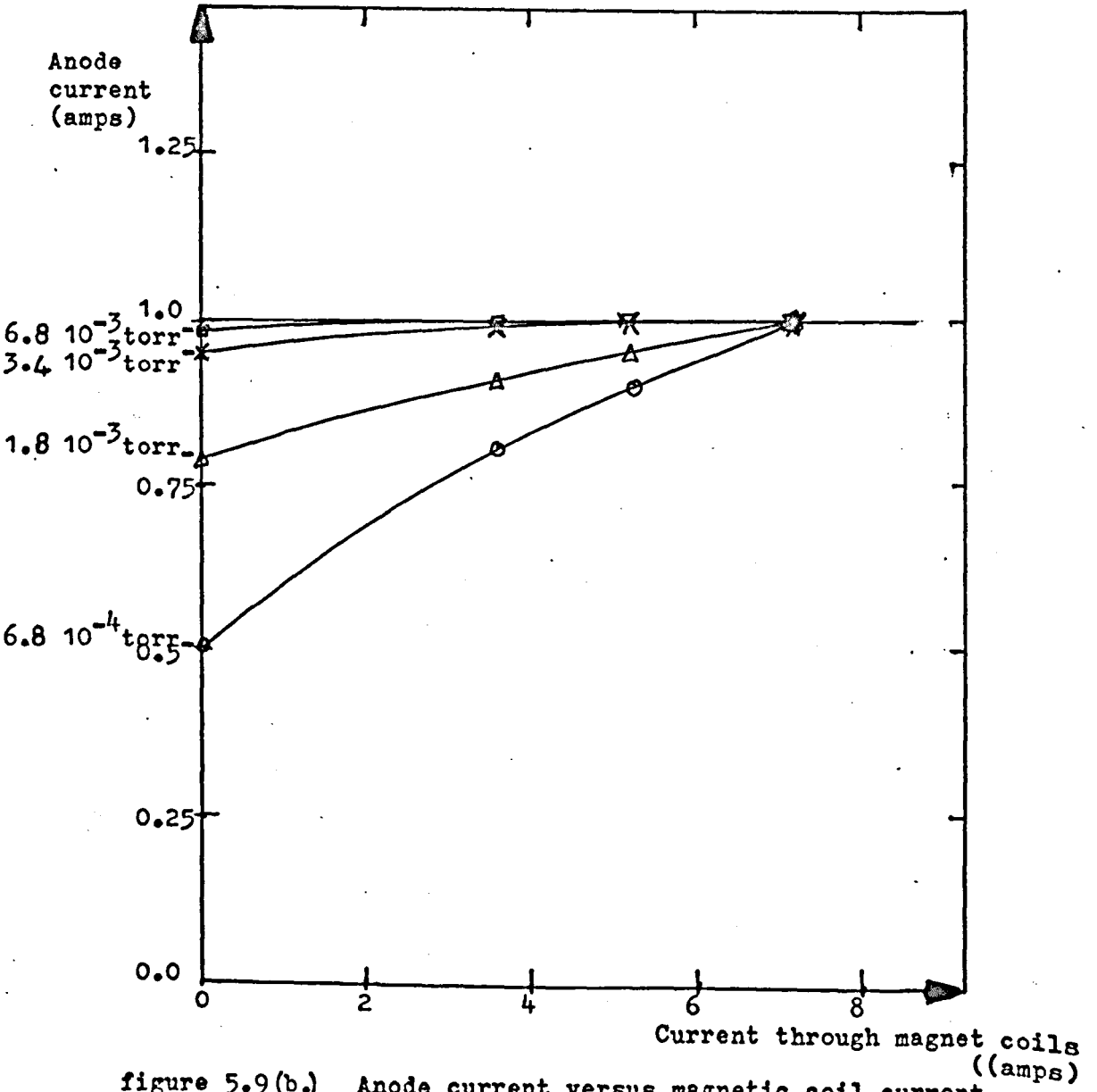

figure 5.9(b.) Anode current versus magnetic coil current with variation in argon gas pressure. (with constant value of anode voltage)

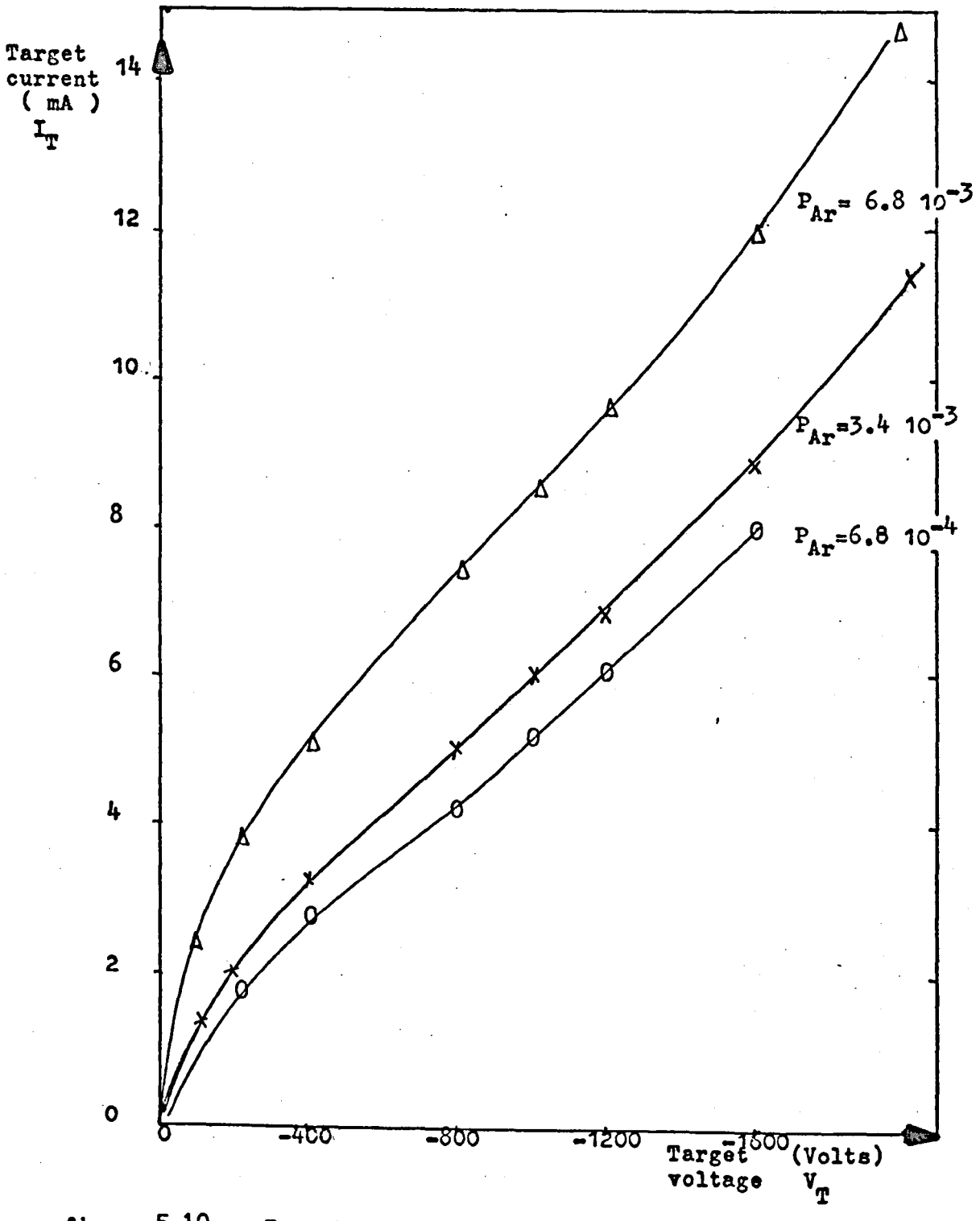

figure 5.10 . Target current versus target voltage with variation in argon gas pressure (P_{Ar} torr) (subtracting the residual ion current at V_T=0)

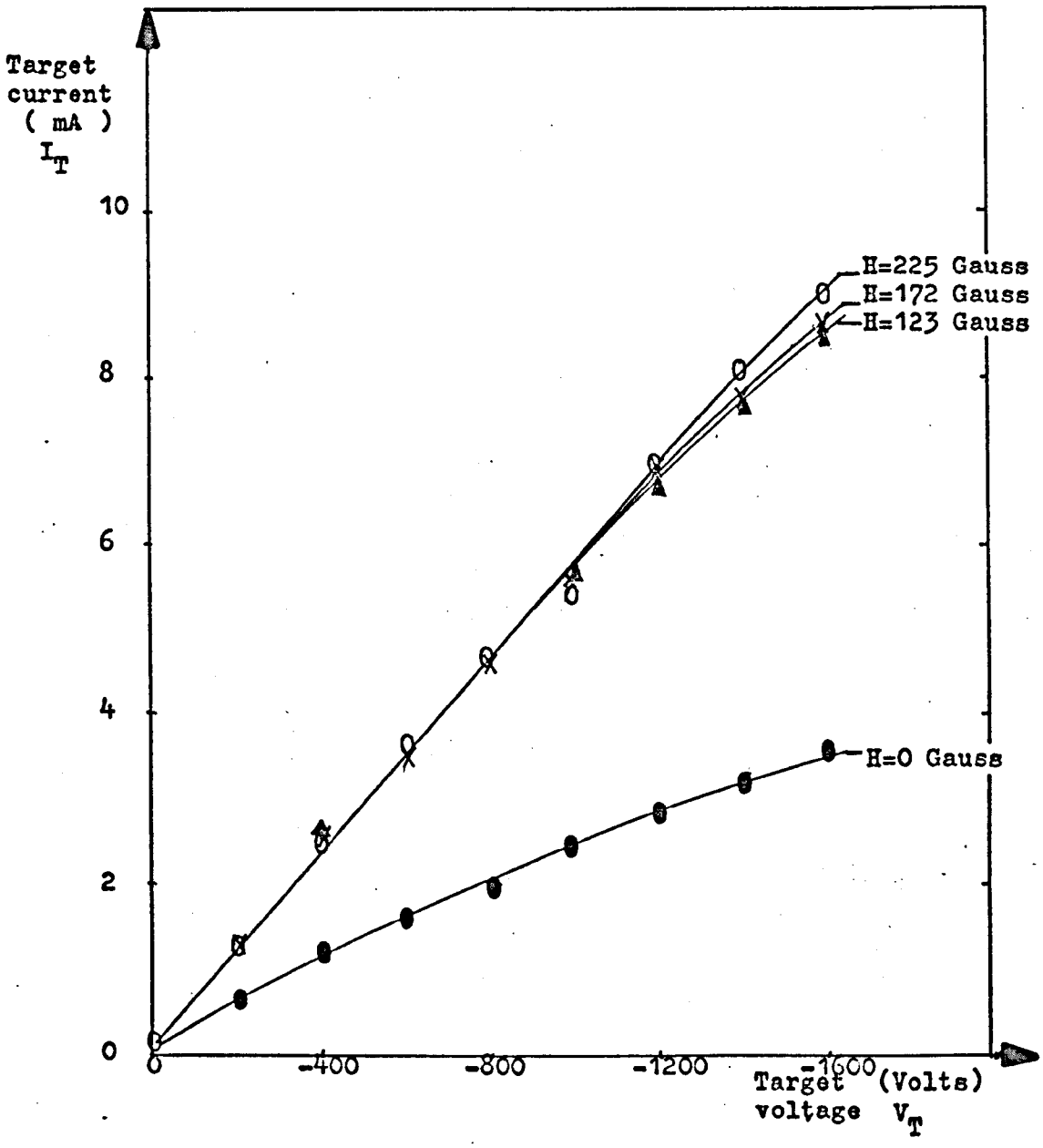

figure 5.11 Target current versus target voltage with variation in magnetic field strength. (H Gauss).
(subtracting the residual ion current at V_T=0)

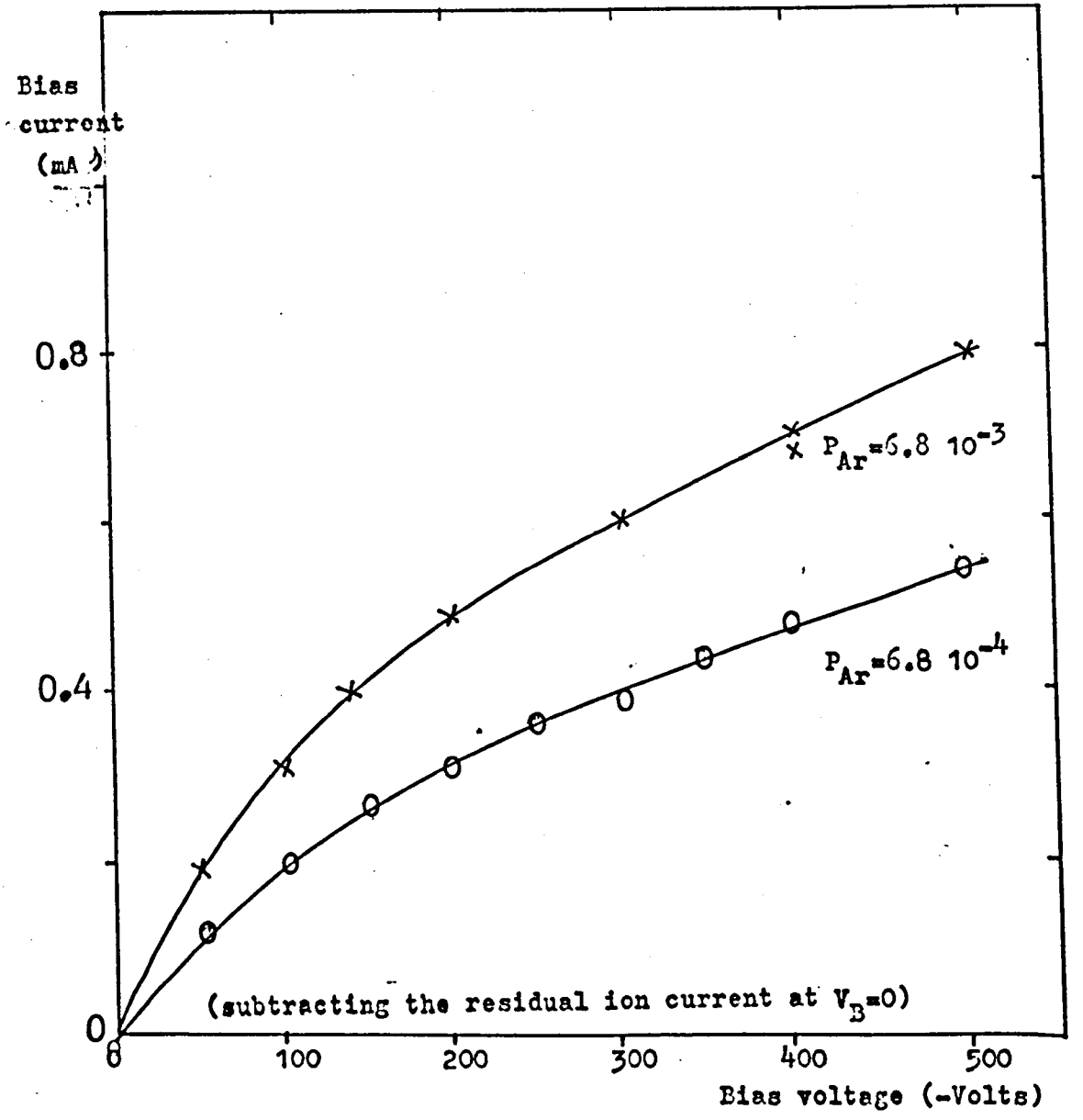

figure 5.12 . Bias current versus bias voltage with variation in argon gas pressure (P_{Ar} torr)

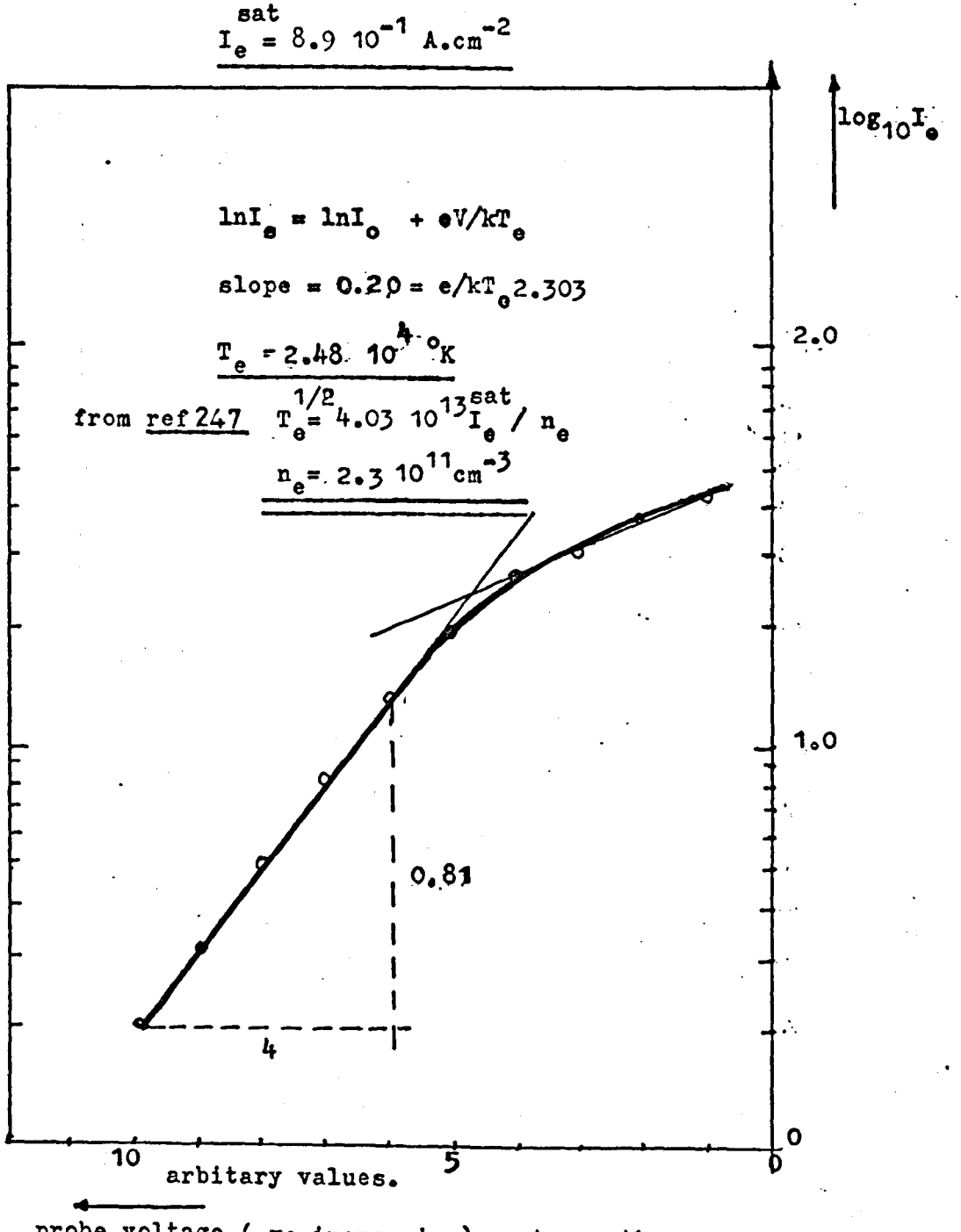

figure 5.13. Langmuir probe measurment of current versus voltage. gas pressure=$6.8\ 10^{-4}$ torr.

The magnetic field has little effect on the anode current at the gas pressures investigated, except at the pressures of $6.8\ 10^{-4}$ torr and $3.8\ 10^{-3}$ torr, where the anode current is reduced, when varying the magnetic coil current from 0 to 7 amps, as indicated in Figure 5.9(b). The effect of increasing gas pressure and magnetic field on the target current, with variation in target voltage, is shown in Figures 5.10 and 5.11. There is a residual ion current at V_T=0 because of the strong confining effect of the magnetic field on the electrons, but not on the ions, in the plasma column. The filament cathode is running in its, more or less, saturated region, for electron emission, so that small variations in the current through the filament will not affect the electron densities in the plasma. The dependence of substrate bias current on gas pressure and substrate bias voltage is shown in Figure 5.12.

A Langmuir probe measurement is taken along the axis of the plasma column, using a fine tungsten wire 0.015 mm diameter and 0.55 cm long. This is to determine the electron and ion current densities in the plasma region, between target and substrate. The power supply for the probe consists of dry H.T. batteries across a variable rheostat. Double pole switches are provided so that the voltage polarity to the probe may be reversed, and so that an ion current, as well as an electron current, will give a positive response on the meter.

From the theory[247], the measurements are only applicable in the absence of a magnetic field, so the values of probe current and voltage are taken with the magnetic coils disconnected. The result is shown in Figure 5.13. An electron density is calculated of about 2.3×10^{11} cm^{-3}. For a field-free space a similar value is deduced for the ion current density. At a pressure

of 6.8 10^{-4} torr of argon there are about 2.10^{13} atoms cm^{-3}. Hence, it appears from the probe measurement that only about 1% of the available gas atoms, in the vacuum system, are ionized. This implies that any gas clean-up that occurs in the discharge should not affect the total argon pressure excessively. This calculation of current densities is only approximate, since the discharge system, in practice, has a large magnetic field applied along its axis.

5.12 Optical microscope

The surfaces of the sputtering targets are investigated, before and after prolonged sputtering, with a Vickers projection microscope. This is to determine how rough the surfaces become with ion bombardment, since this will affect the ion current density and the sputtering yield of the material. The results are shown in more detail in Chapter 6.

5.13 Electron microscope

During the course of the investigation, an electron microscope, made by Hitachi (Model HS-19), is used to look at the surfaces of some of the sputtered and evaporated films grown under various conditions (some outgassed, others not). The results for some metals are interesting and are discussed in more detail in the following chapter. Carbon replicas are made of the films by evaporation in a subsidiary vacuum system. The replica is scored with criss-cross lines using a sharp knife, and a small quantity of the carbon removed. This removal, however, is often difficult, and a technique is used, by which the sample is first immersed in liquid nitrogen and then quickly dipped in water. By this means, small pieces of the carbon replica often float away from the film and may be collected on a formvar-covered copper microscope grid. The grids used are about 3 mm in diameter and have

200 mesh lines per inch, with "windows" 90 micron square.

5.14 Computer calculations

An I.C.L. 4130 computer is used to facilitate the calculations of the partial pressures from the mass spectrometer data and consequently the concentrations of gas in the films. It is also used to calculate the theoretically postulated concentrations using the Winters and Kay model. The programmes and results are discussed in the next chapter. The programmes written for these three calculations are given APPENDIX A, D and E, respectively.

CHAPTER VI

Results and discussion of results

6.1 Introduction

The first section, 6.2, contains the mass spectrometric analysis, using the QRGA, of the residual gases present in the vacuum system, under various conditions of pumping and gas leaking. The calculation of the amounts of gas present before and after a sputtering experiment, as well as on flash evaporating the deposited film, are also presented.

Sections 6.4 - 6.6 deal with the results and discussion of the argon gas concentration measurements from different metal films prepared by sputtering and evaporation under different conditions. These sections also include the results of the optical and electron microscope studies of the target and film surfaces.

The nitrogen concentration found in the above mentioned films is similarly dealt with in sections 6.7 - 6.8.

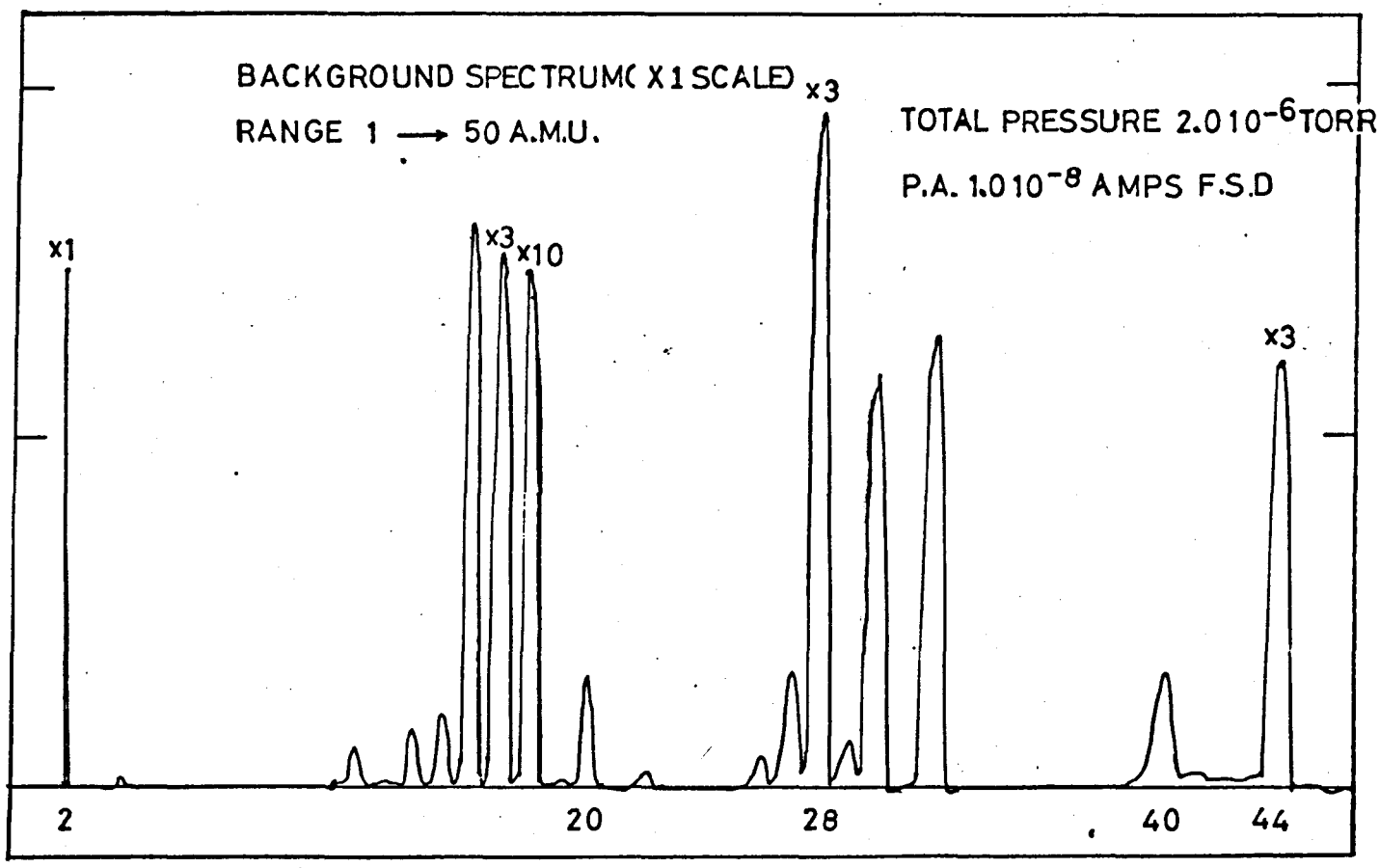

Figure 6.1

Figure 6.2

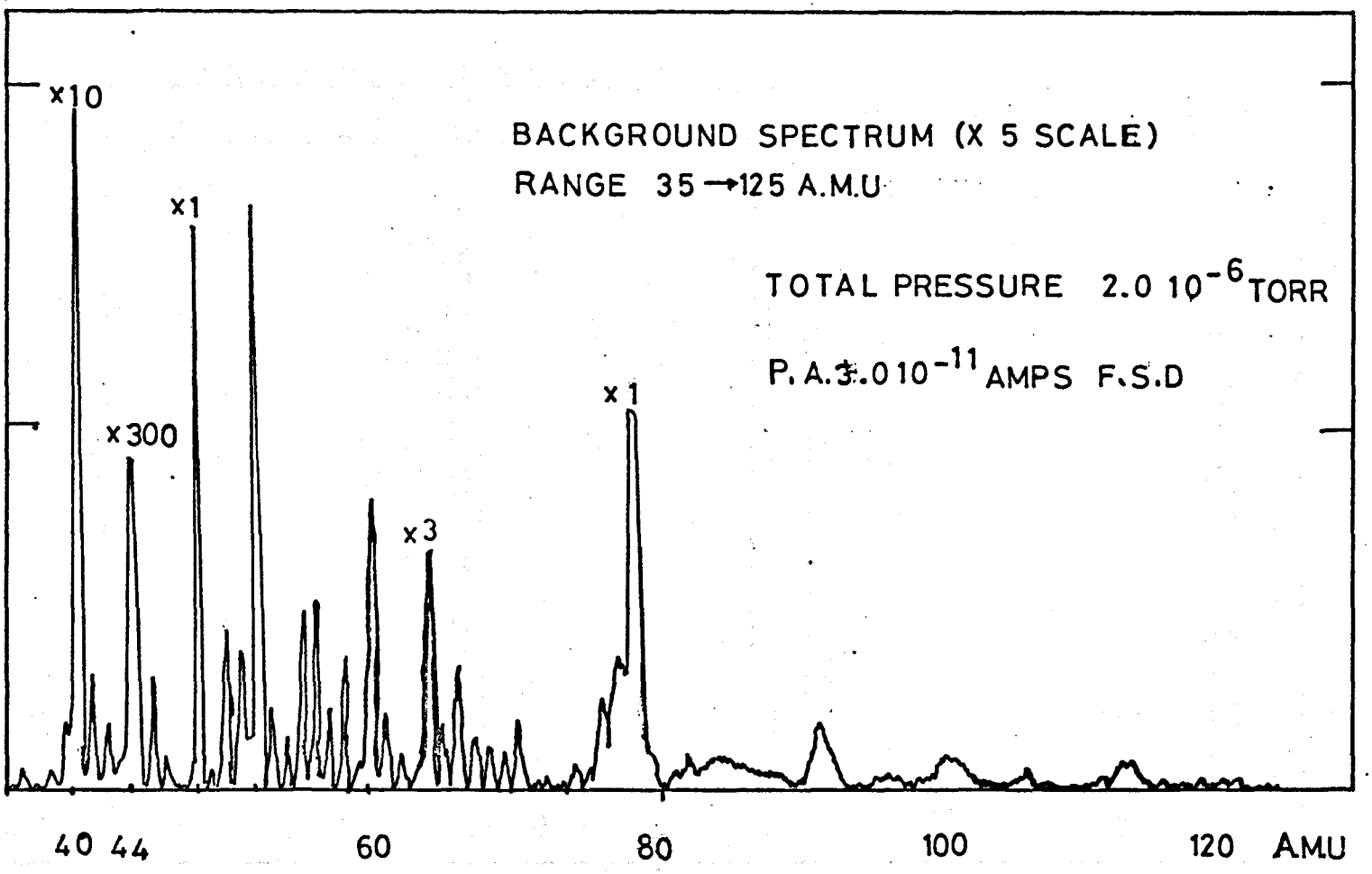
x10
x1
x300
x3
x1
BACKGROUND SPECTRUM (X 5 SCALE)
RANGE 35 → 125 A.M.U
TOTAL PRESSURE 2.0 10^-6 TORR
P.A. 3.0 10^-11 AMPS F.S.D
40
44
60
80
100
120
AMU

6.2 Mass spectrometric studies

By using the quadrupole residual gas analyser (QRGA), the residual gases present in the vacuum system could be determined. Typical spectra of the gases present in the unbaked system after ion pumping for one hour, are given in Figures 6.1 and 6.2. For the former, the spectrum range is from 0-50 a.m.u. and for the latter from 35-125 a.m.u. It should be noticed that the picoammeter (P.A.) reading is 1.0 10^{-8}amps f.s.d. for the 0-50 range and 3.0 10^{-11}amps f.s.d. for the higher range.

For a sorption roughed and ion pumped system it is unlikely that there will be any contaminating effects due to fluids, such as mercury, and silicone and hydrocarbon-based oils which are found with rotary/diffusion pumped systems. If any of these were present it should be possible to identify them by the 'fingerprint' spectra associated with each of them[248]. These 'fingerprint' spectra consist of hydrocarbon, silicone, and mercury vapour peaks found predominantly in the higher mass range, as a series of complicated peaks of various intensities. It may not, therefore, be necessary to look for these gases in an ion pump system except, possibly, to ensure that the cleaning chemicals and cutting oils, used in the fabrication of parts of the vacuum system, have been entirely removed. This supposition is vindicated, see Figure 6.2 where it is seen that the highest peak, at a.m.u. 63, although not identified, has a partial pressure of less than about 4.10^{-11} torr (assuming that it has the same sensitivity as nitrogen). All the other peaks above CO_2^+ indicate partial pressures less than 10^{-11} torr. This being so, the method chosen to calculate the partial pressures (given below) is little affected by omitting to include the gas pressure peaks appearing above a.m.u. 50. The spectra obtained by the QRGA were all

measured with the ion current signal amplified about 10^3 times by the addition of the electron multiplier stage at the collector end of the analyser head. Hence, in reality, ion currents of about 10^{-11} and 3.10^{-14} amp f.s.d. respectively, were involved in Figures 6.1 and 6.2.

There are several methods by which the 'uncorrected' partial pressures for each gas may be found from the spectra obtained. One method is to multiply each peak height, measured in amperes, by the sensitivity factor (in amps/torr) given by the manufacturers. Whilst this technique may be suitable if the ion current resulting from a given gas species is measured directly, it is not very useful when using the electron multiplier attachment, which converts the original ion current into an electron current and amplifies it by a given amount. It was possible to determine the multiplying factor at any given time by a process of measuring a gas peak height with and without the multiplier connected. It was found, however, to vary appreciably over a period of time, as the dynode surfaces became contaminated. These then required baking with the result that a new value of amplification was produced. This being so, the following method was adopted.

The sum of the partial pressure peaks is proportional to the total pressure. Hence, the 'uncorrected' partial pressure (pp) is expressed by

$$pp_{\text{uncorrected}} = \frac{\text{partial pressure peak height x total pressure}}{\text{sum of all partial pressure peaks.}}$$

The total pressure was measured either with the UHV ionization gauge or the millitorr gauge, both of which were calibrated for nitrogen. This expression is only approximate, and does not give the true partial pressures representative of the gases in the vacuum system. To obtain these, the peak

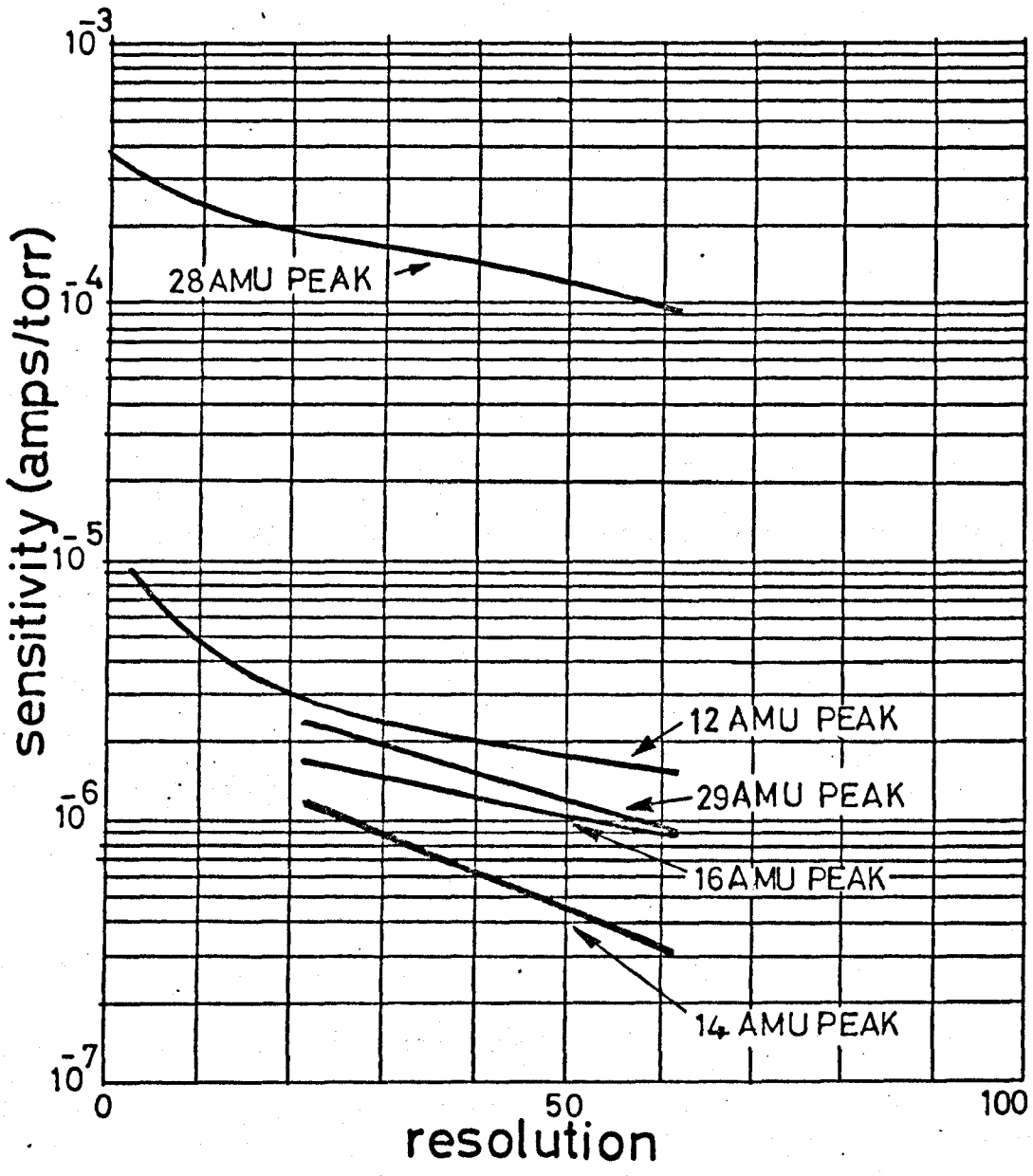
10⁻³
10⁻⁴
10⁻⁵
10⁻⁶
10⁻⁷
sensitivity (amps/torr)
28 AMU PEAK
12 AMU PEAK
29 AMU PEAK
16 AMU PEAK
14 AMU PEAK
0
50
100
resolution

Figure 6.3

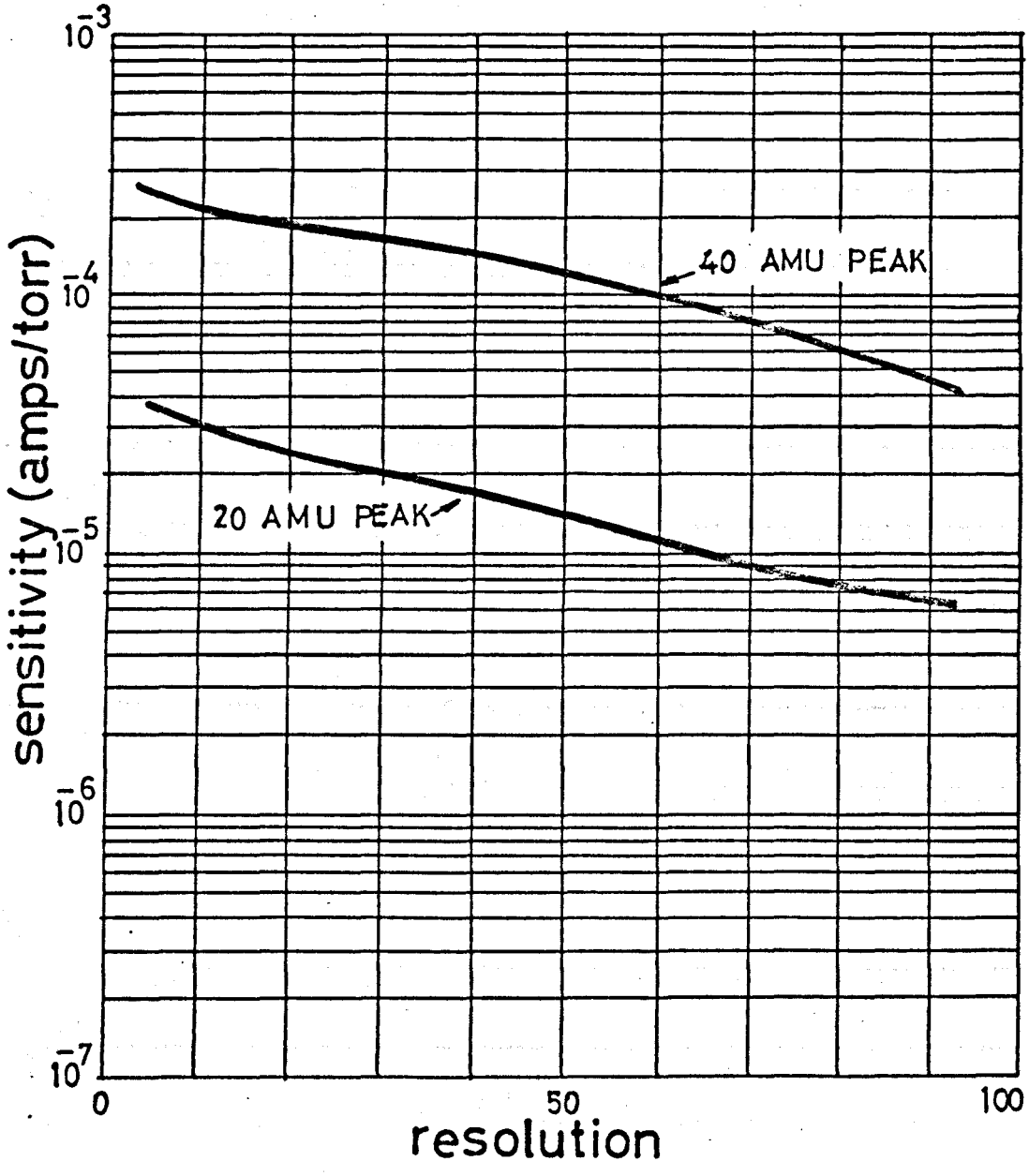
10^{-3}
10^{-4}
10^{-5}
10^{-6}
10^{-7}
sensitivity (amps/torr)
40 AMU PEAK
20 AMU PEAK
0
50
100
resolution

Figure 6.4

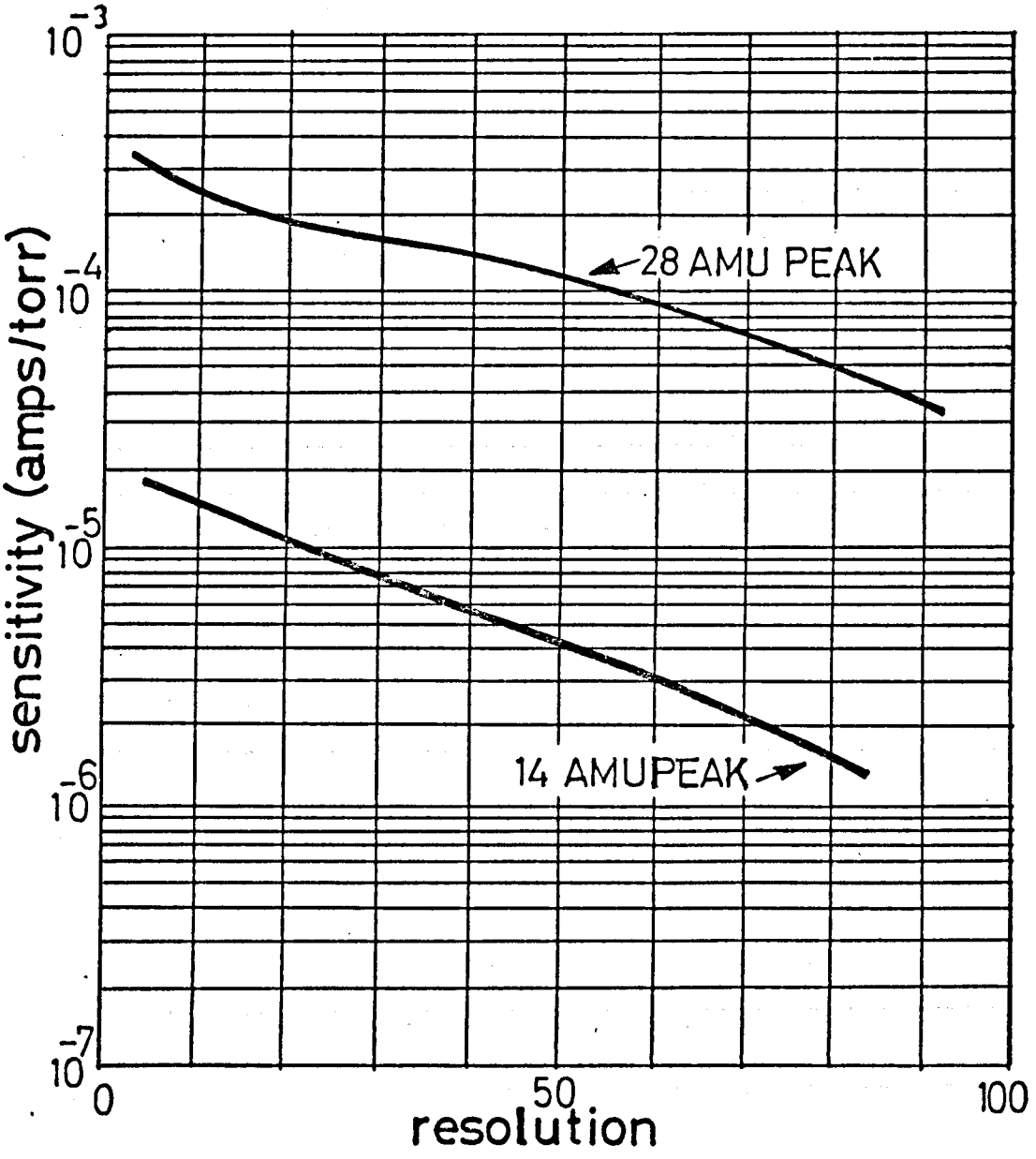
10^{-3}
10^{-4}
10^{-5}
10^{-6}
10^{-7}
sensitivity (amps/torr)
28 AMU PEAK
14 AMUPEAK
0
50
100
resolution

Figure 6.5

Sensitivities of gases at Resolution 50., (Normalised to 100 for Nitrogen).

	H_2	He	CH_4	H_2O	Ne	N_2	CO	C_2H_6	O_2	Ar	CO_2
1	0.07										
2	10.0	0.38									
4		16.7									
12			0.83				1.50				0.81
13			1.67								
14			3.75			3.47	0.415				
15			27.5								
16			34.2	0.68			0.875		4.25		3.1
17				7.5							
18				29.2							
20					66.6					11.7	
22					6.66						0.71
24								0.25			
25								1.17			
26								7.1			
27								10.8			
28						100.0	100.0	36.6			9.25
29							1.0	8.2			
30								10.0			
32									55.8		
36											
40										100.0	
44											73.0

heights must be 'corrected' by taking into account

(a) the sensitivity/resolution of the QRGA, and

(b) the ionization efficiency (expressed as a cross-section[249])

for each of the gas species appearing in the spectrum.

The partial pressure (pp) expression is then modified to:-

$$pp_{\text{corrected}} = \frac{\text{corrected pp peak heights x total pressure}}{\text{sum of all corrected pp peak heights}}$$

(a) and (b) have both been investigated by Varian, the manufacturers of the QRGA. A series of graphs were provided by them, plotting the product of sensitivity and ionizing efficiency against gas species. Examples of these are shown in Figures 6.3, 6.4 and 6.5. A further problem in the interpretation of the mass spectrum arises because of the 'cracking', in the ion source, of a proportion of the singly ionized parent molecules into singly and doubly ionized daughter components. These are also shown in Figures 6.3 to 6.5. Table 6.1 has been calculated from all the available Varian graphs, and shows the corrected sensitivities of the gases normally encountered in UHV from 0 to 50 a.m.u., together with their cracking species. (The table is normalized to the nitrogen parent molecule = 100). The Varian graphs were determined at a pressure of $1.0\ 10^{-6}$ torr. It has been assumed that Table 6.1 holds for all pressures up to about $2.0\ 10^{-4}$ torr, at which stage, the mean free path of the ions becomes comparable with the dimensions of the quadrupole structure. Since no similar graph was available for the QRGA, Figure 6.6. shows the ion current versus pressure graph for a 1 cm radius 180° magnetic deflection analyser[250]. If the reasonable assumption is made that, for pressure not too high, only the ion mean free path is involved, the graph may be modified for the quadrupole situation.

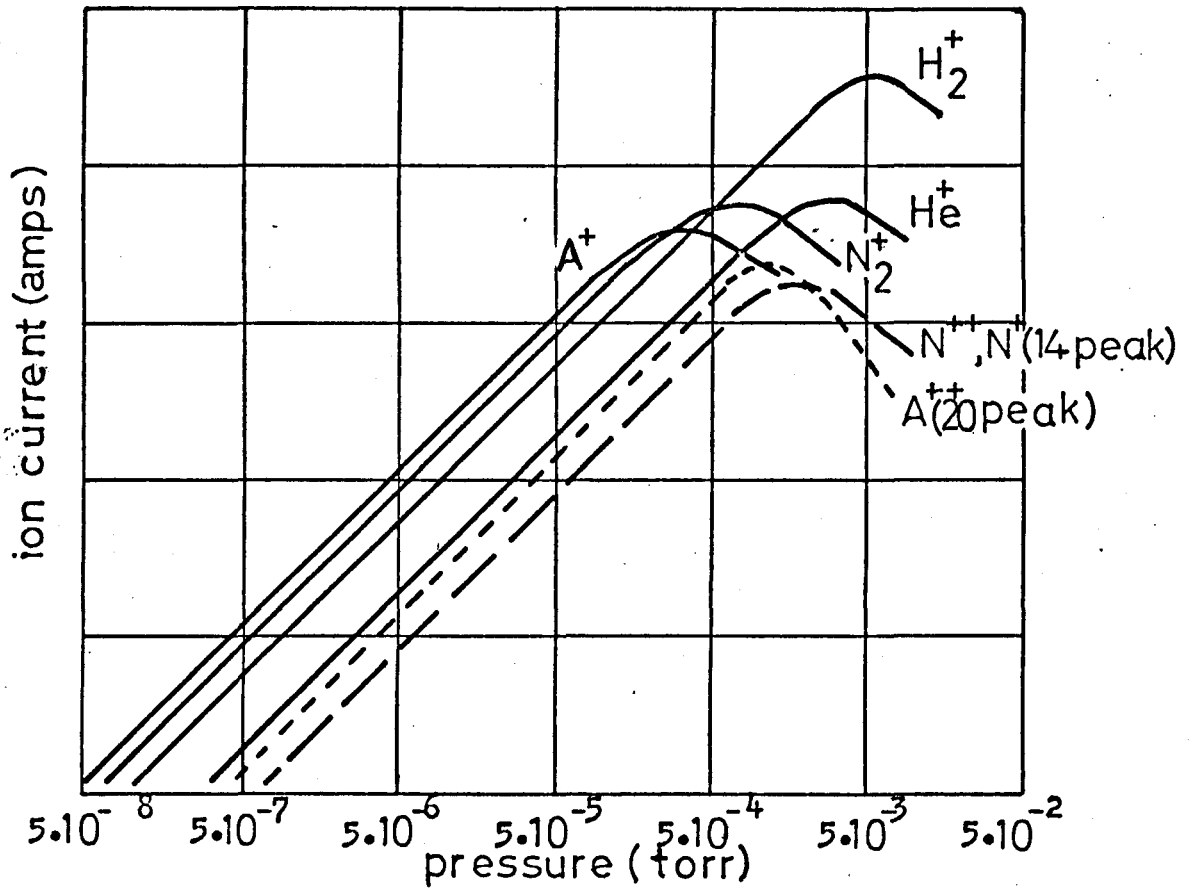

Figure 6.6 Ion current linearity with gas pressure (modified to illustrate the situation for the QRGA)

Here, the distance between ion source and collector is about 15 cm, so the pressure, in Figure 6.6, at which linearity begins to fail, is about 5 times higher than for the magnetic analyser.

The absolute partial pressures for argon, oxygen and carbon dioxide are uniquely defined by a.m.u.'s 40, 36 and 44, respectively, and no further complications arise in the calculation of the partial pressures for these gases. However, for some gases, such as nitrogen and carbon monoxide the situation is not so simple, as their parent peaks both appear at a.m.u. 28. To determine the absolute partial pressures due to these and other similarly placed gases, use must be made of their cracking patterns. For the nitrogen, carbon monoxide case, the following procedure was adopted:- First the contributions due to CO_2 and O_2, uniquely represented by a.m.u. 44 and 32 respectively, were subtracted from the lower peaks at a.m.u.'s 12, 16, 22 and 28. Simultaneous equations based on either the a.m.u. 12, 14 or 28 peaks could then be set up and solved to determine the relative contributions of CO and N_2 at a.m.u. 28. In a similar way, the best fit solution could be found, whereby the corrected contributions at each mass peak, from all the overlapping cracking patterns, combined to produce the spectrum obtained.

Since this is rather a long hand calculation, and because of the large number of these calculations that it was necessary to make, an ICL 4130 computer was utilized to facilitate the calculations. A programme in Fortran 4 was written to obtain the corrected absolute partial pressures for the commonly occurring gases between a.m.u. 0-50 and with particular reference to argon, carbon monoxide and nitrogen. The programme is given in Appendix A.

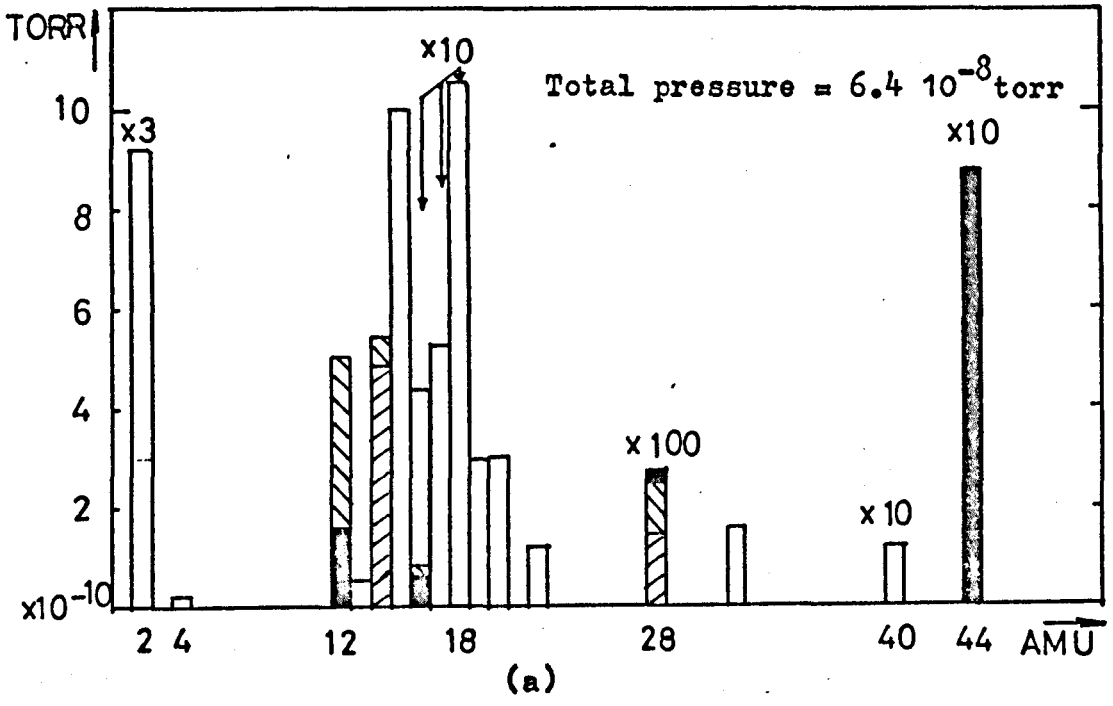

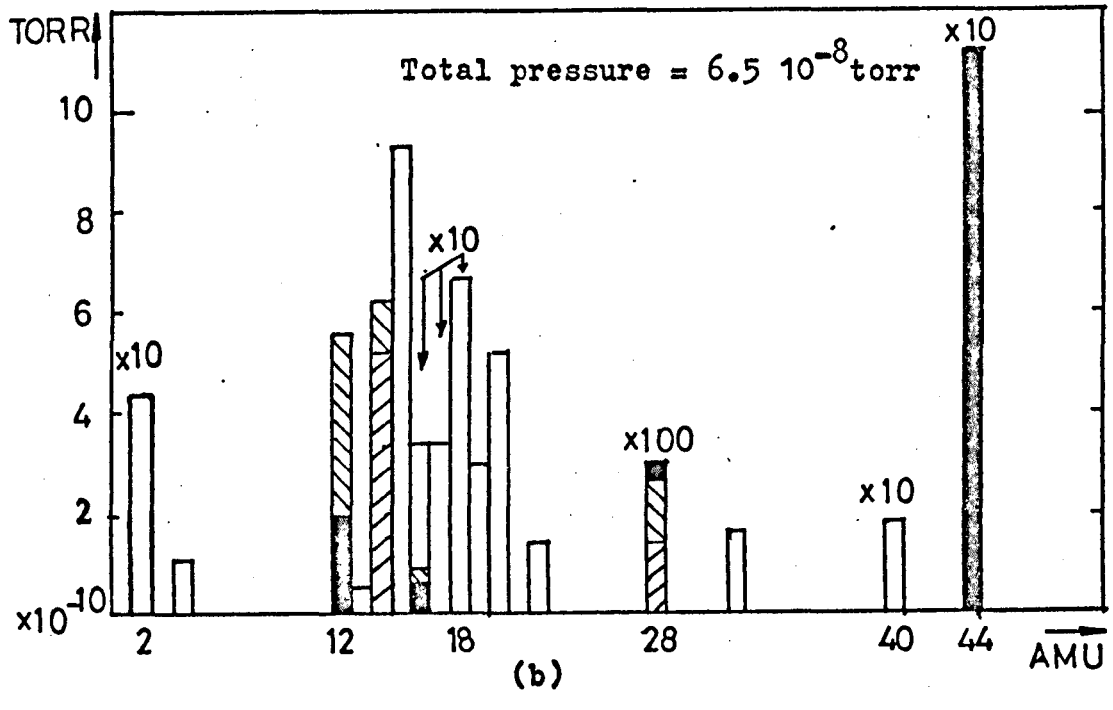

Figure 6.7 (a) With all pumps on.

(b) With only liquid nitrogen cooled sublimator.

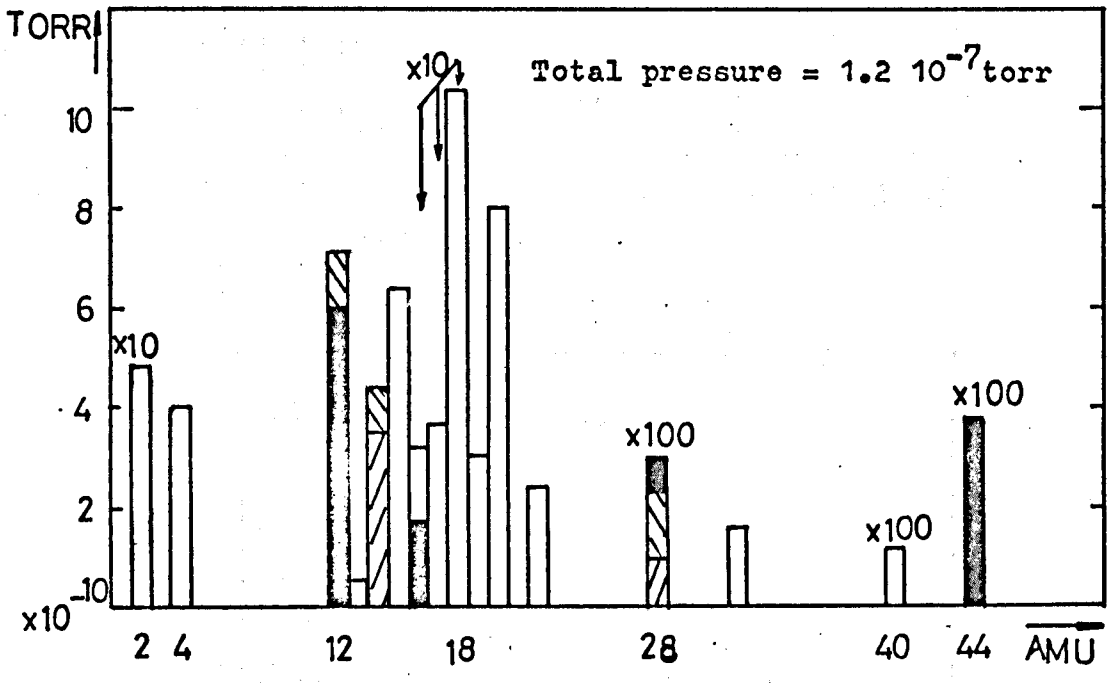

Figure 6.8 With filament and magnet on.

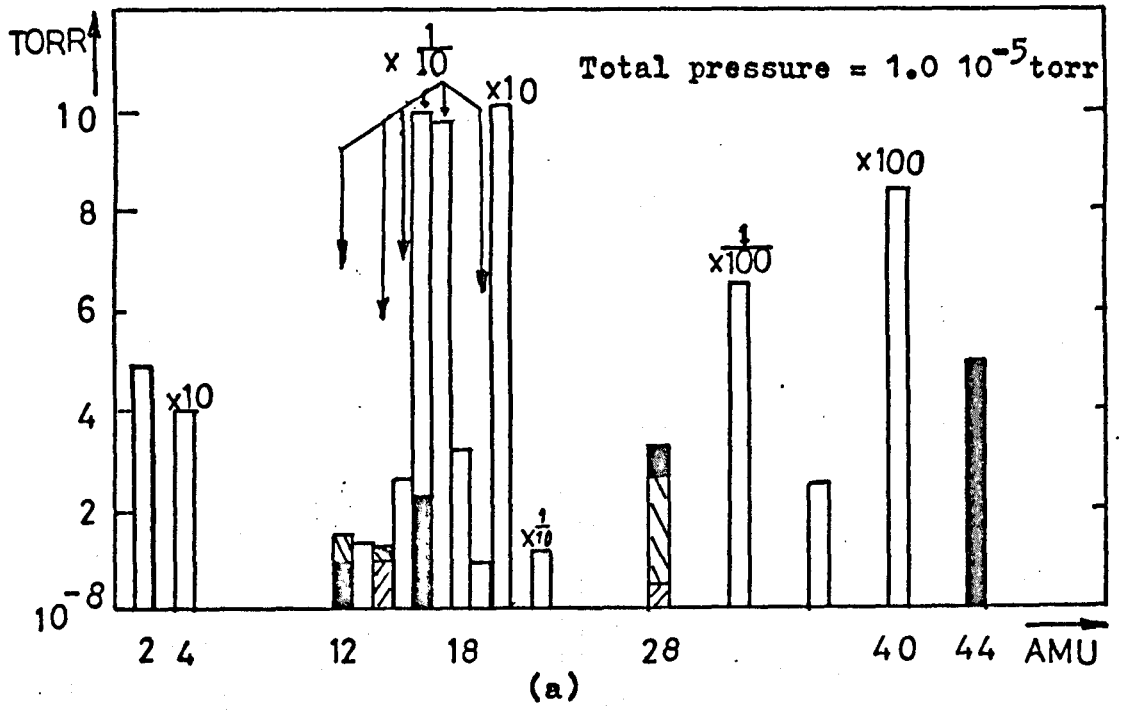

(a)

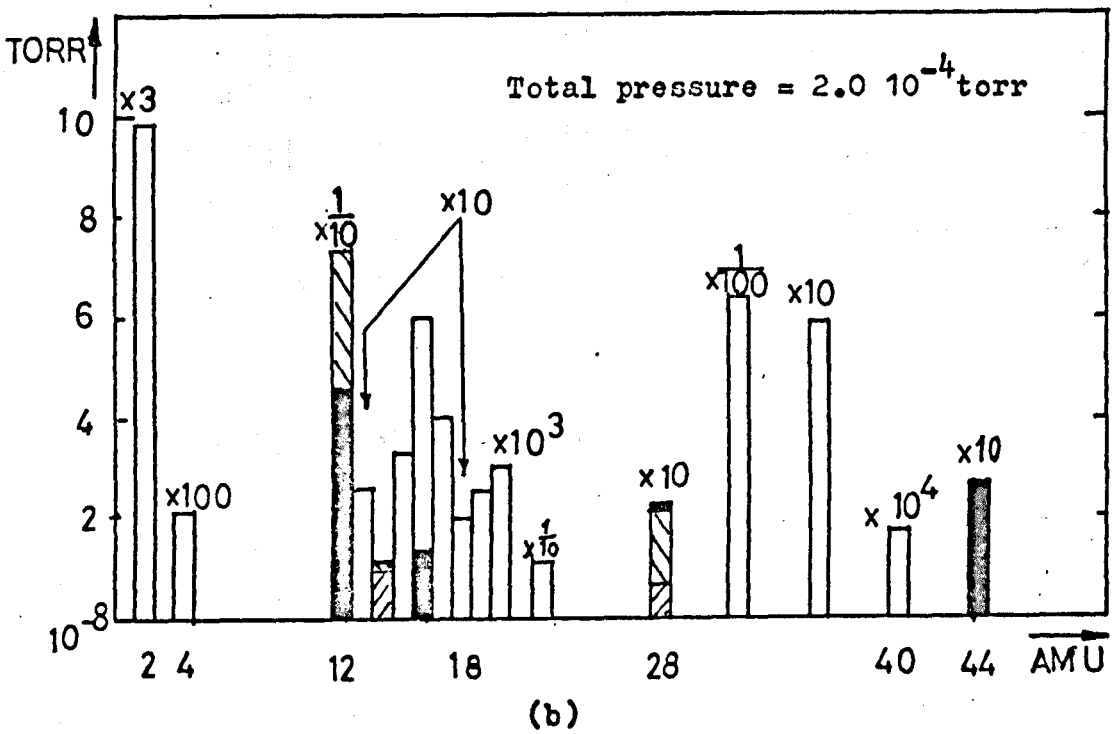

(b)

Figure 6.9 (a) Leaking argon

Figures 6.7(a) and (b) give histograms representing the typical values of the absolute corrected partial pressures in the vacuum system. The pressures are directly read from the histogram, unless multiplied by a factor indicated above the peak. Figure 6.7(a) shows the partial pressures with all pumps operating and Figure 6.7(b), with the liquid nitrogen-cooled titanium sublimator only cycling, all other pumps being isolated. It is seen that in the latter case, although the total pressure remains almost unaltered, the relative contributions due to various gases are affected. For example, the CO_2,H_2 and Ar pressures increase, whilst the water vapour peaks fall. Hydrogen is known to be relatively poorly pumped by evaporated titanium, and argon not at all[231], whereas it appears that some of the water vapour arises from the ion pumps themselves.

Figure 6.8 shows the effect on the residual gas composition when operating the thermionic cathode and magnet coils, with only the sublimator in operation. Hydrogen and carbon dioxide are seen to be evolved. The inert gases, in particular argon, continue to increase because of the non-pumping action of the sublimator for these gases.

The effect of leaking argon into the vacuum system is shown in Figures 6.9(a) and (b)for total pressures of $1.0\ 10^{-5}$ torr and $2.0\ 10^{-4}$ torr, respectively. As well as the obvious increase in argon at a.m.u. 40 and 20, peaks occur at a.m.u. 13.3, representing triply ionized argon (Ar^{3+}) and at a.m.u. 36 which is one of the isotopes of argon.
An overall increase in the other gas peaks is also evident, although apart from helium, no gas species has a pressure greater than about 0.1% that of the parent argon peak.

Some preliminary experiments were also carried out to determine

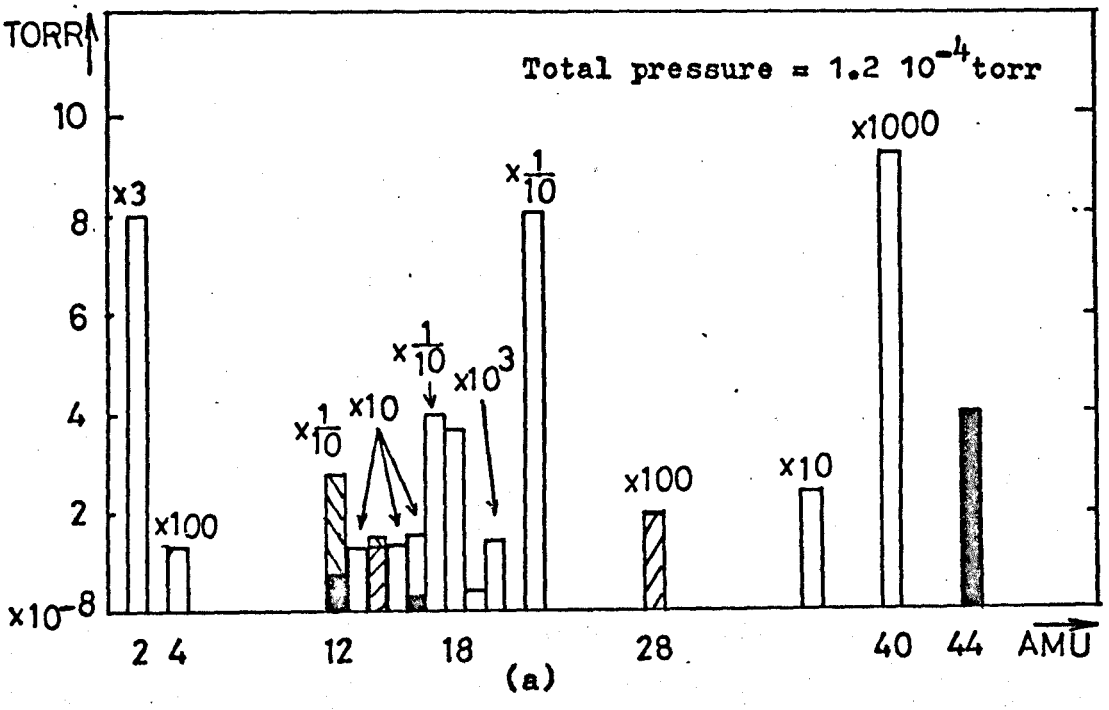

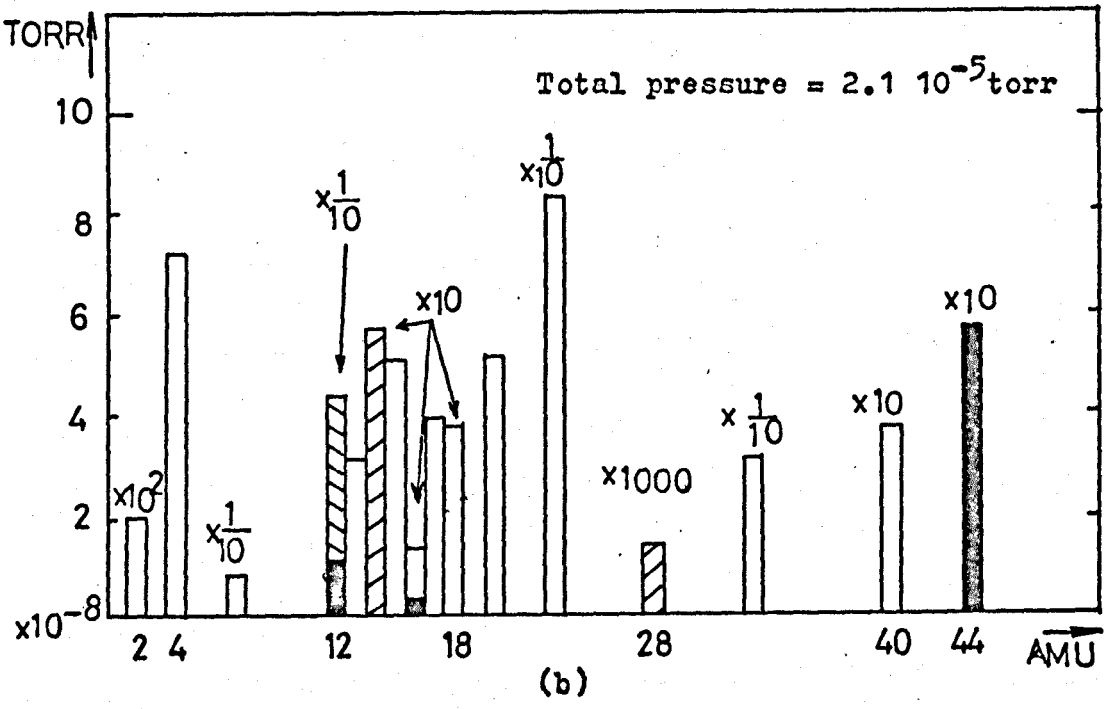

Figure 6.10 (a) Leaking argon + nitrogen (P_{N_2} = 2.0 10^{-6}torr)

(b) Leaking argon + nitrogen (P_{N_2} = 1.4 10^{-5}torr)

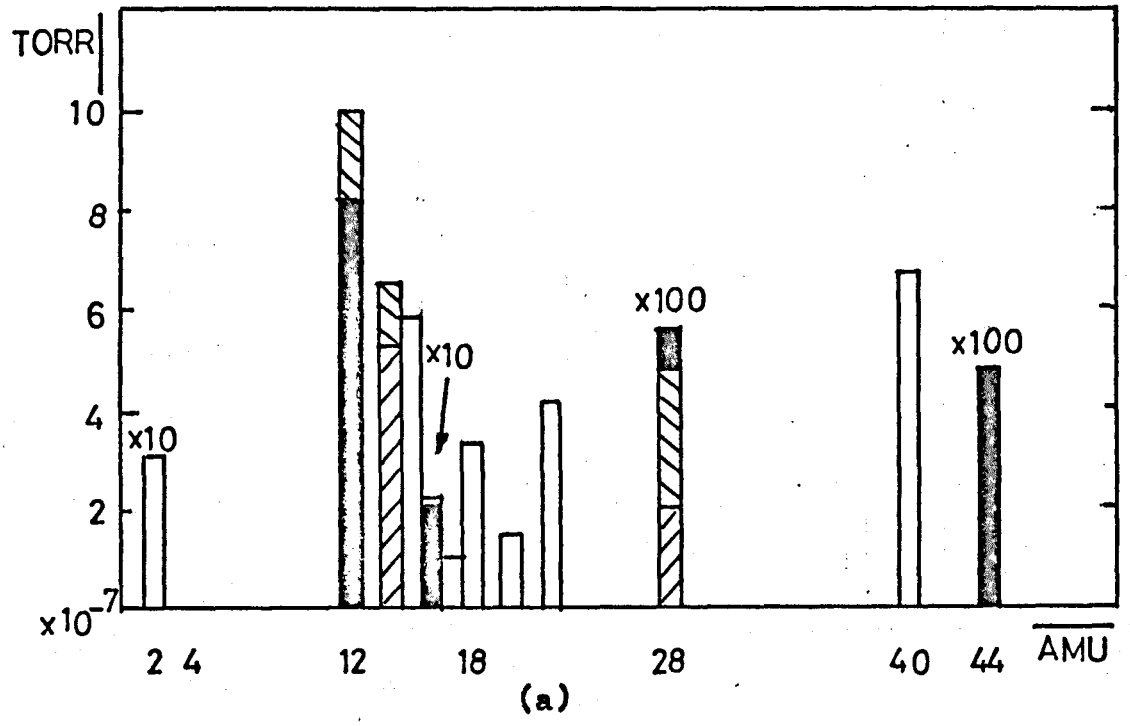

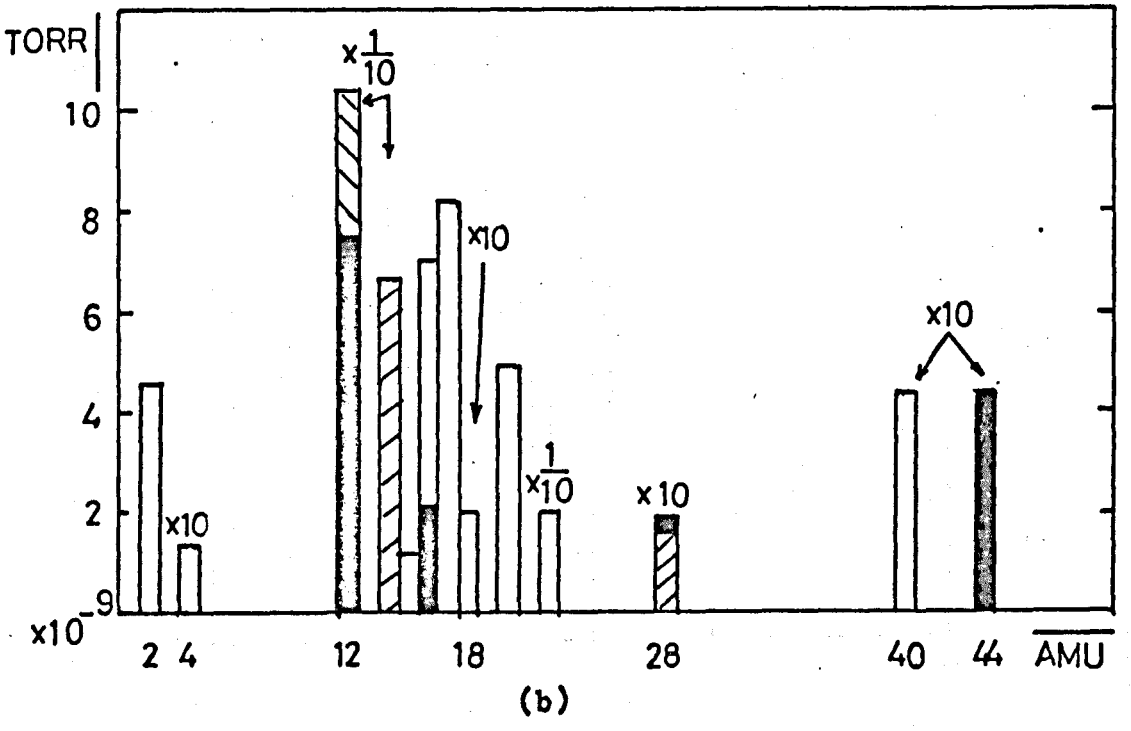

Figure 6.11 (a) Flashing substrate after 24 hours in air.

(b) Flashing substrate after 24 hours in vacuum.

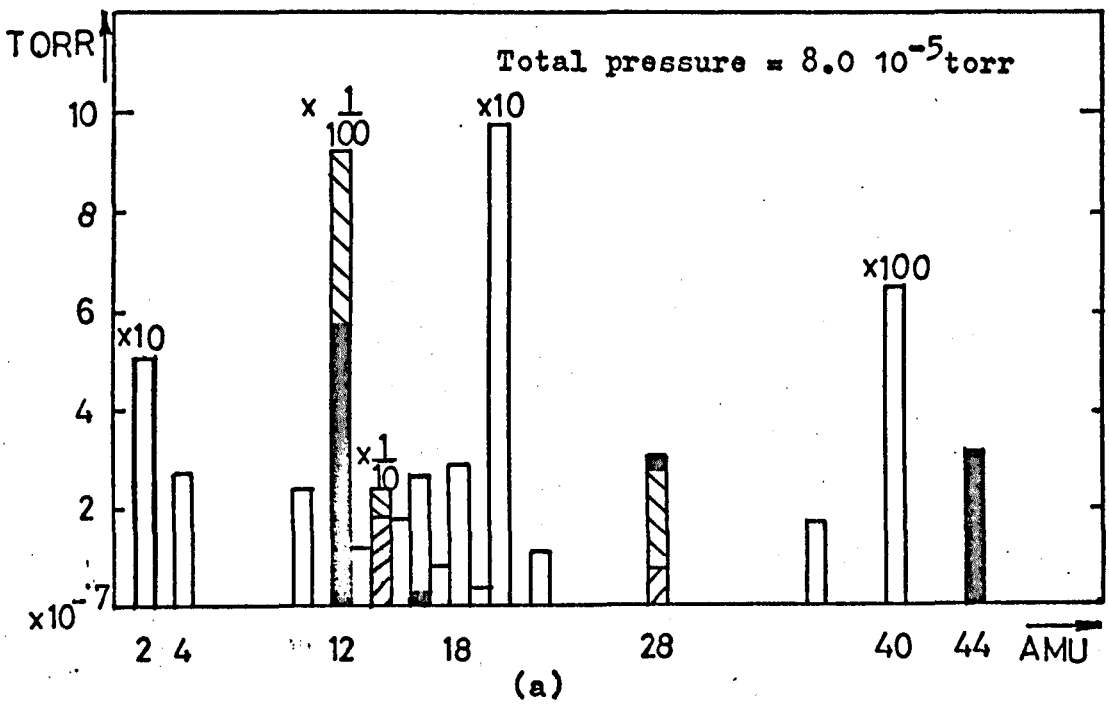

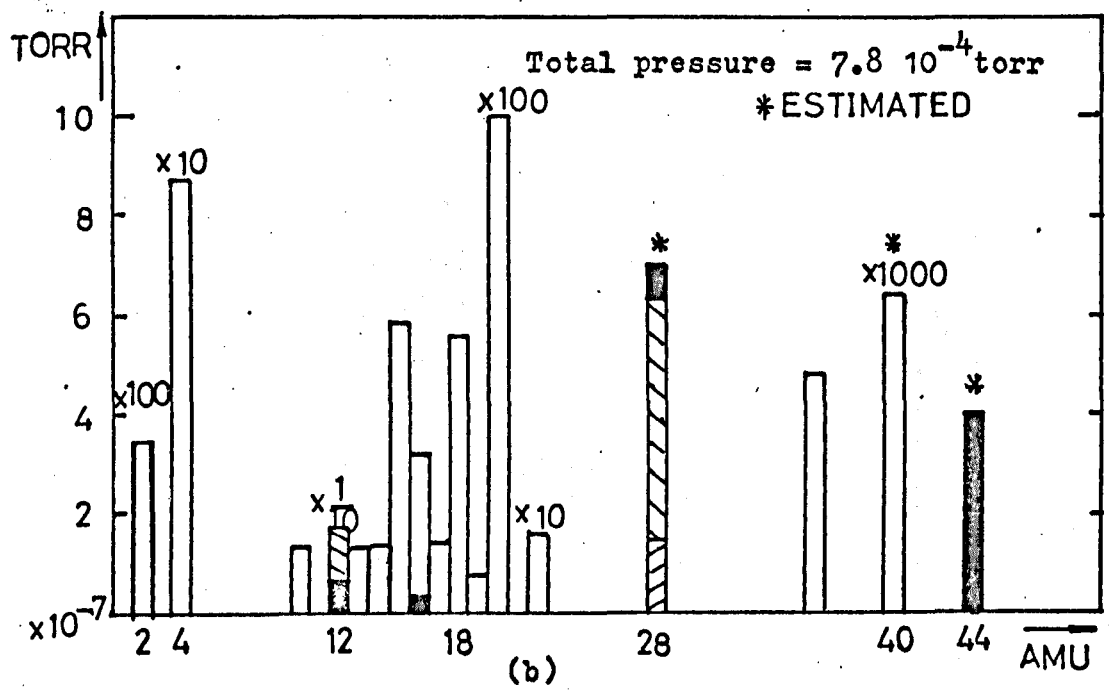

Figure 6.12 (a) After 25 mins sputtering and momentary pumpdown.

(b) After 90 mins sputtering , no pumpdown.

the effect of nitrogen partial pressure on the nitrogen content in the deposited films. To do this, the ambient pressure of nitrogen was increased by leaking nitrogen from a commercial BOC cylinder through a down-to-air inlet valve, in the roughing system, into the main chamber. Two of the nitrogen pressures used at 2.0 10^{-6} torr and 1.4 10^{-5} torr, are indicated in Figures 6.10(a) and (b). In the former an argon pressure of about 9.0 10^{-5} torr has also been added. A small amount of oxygen appears at a.m.u. 32, probably due to an oxygen impurity in the nitrogen cylinder.

The substrates were flash heated before deposition. An attempt was made to see what effect leaving a cleaned tungsten substrate in a nitrogen/air atmosphere for 24 hours prior to re-flashing would have on its gas content. This is seen in Figure 6.11(a) which indicates that a large amount of nitrogen, carbon monoxide and carbon dioxide are sorbed by the substrate, during this time. This result implies that great care must be taken in the evaluation and interpretation of the reactive gas content of the deposited films, if the substrate is exposed to atmospheric conditions after deposition, but prior to gas analysis, which was one of the experimental conditions prevalent in previous investigations[187]. Figure 6.11(b) shows the flash desorbed gases from a tungsten substrate which had been flash heated 24 hours previously and then maintained, in the intervening period, under vacuum conditions of about 10^{-7} torr (N.B. the pressure scale in (b) is 100 times smaller than in (a)).

The spectrum after different times of film deposition, in the presence of a gas discharge, is indicated in Figure 6.12(a) and (b). Ideally, the spectrum should have been obtained at the discharge pressures used. However, because of the problem of non-linearity in ion current collection

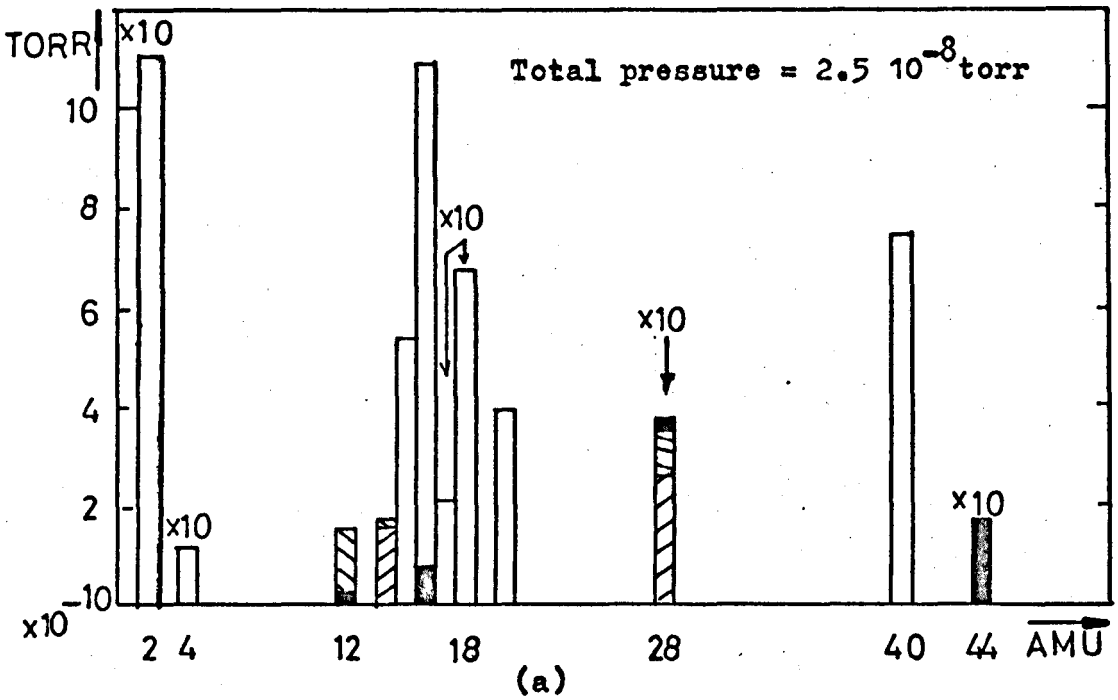

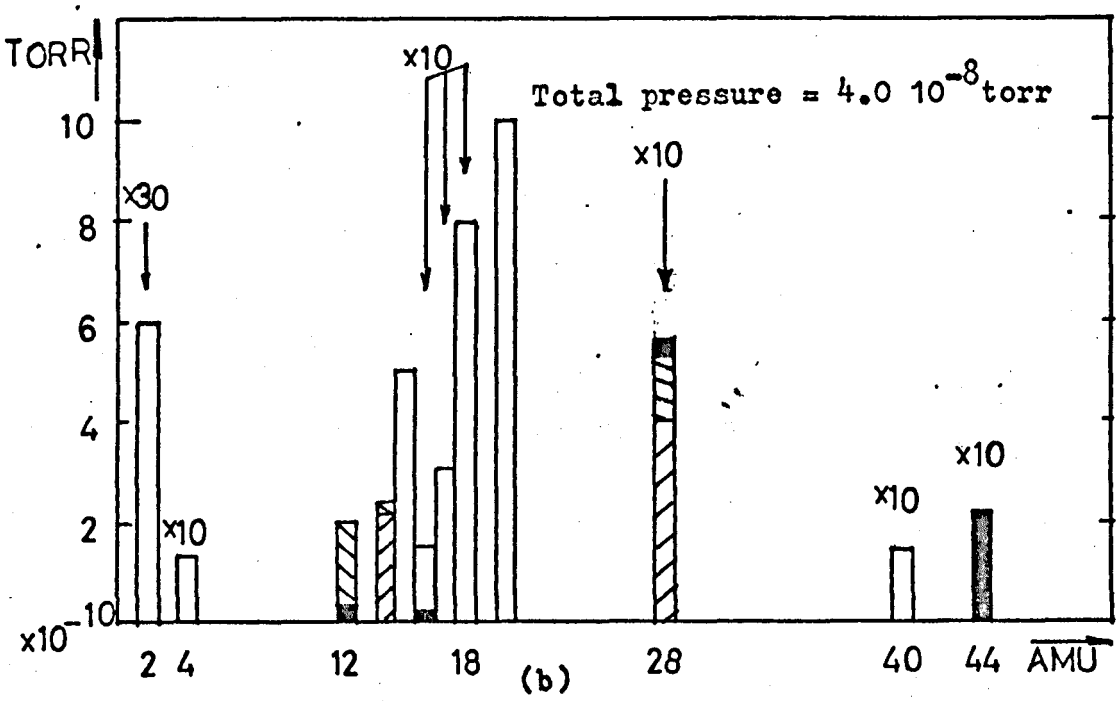

Figure 6.13 (a) After sputtering and 3hr pumpdown, subl'r on.

(b) After sputtering and 3hr pumpdown, subl'r off.

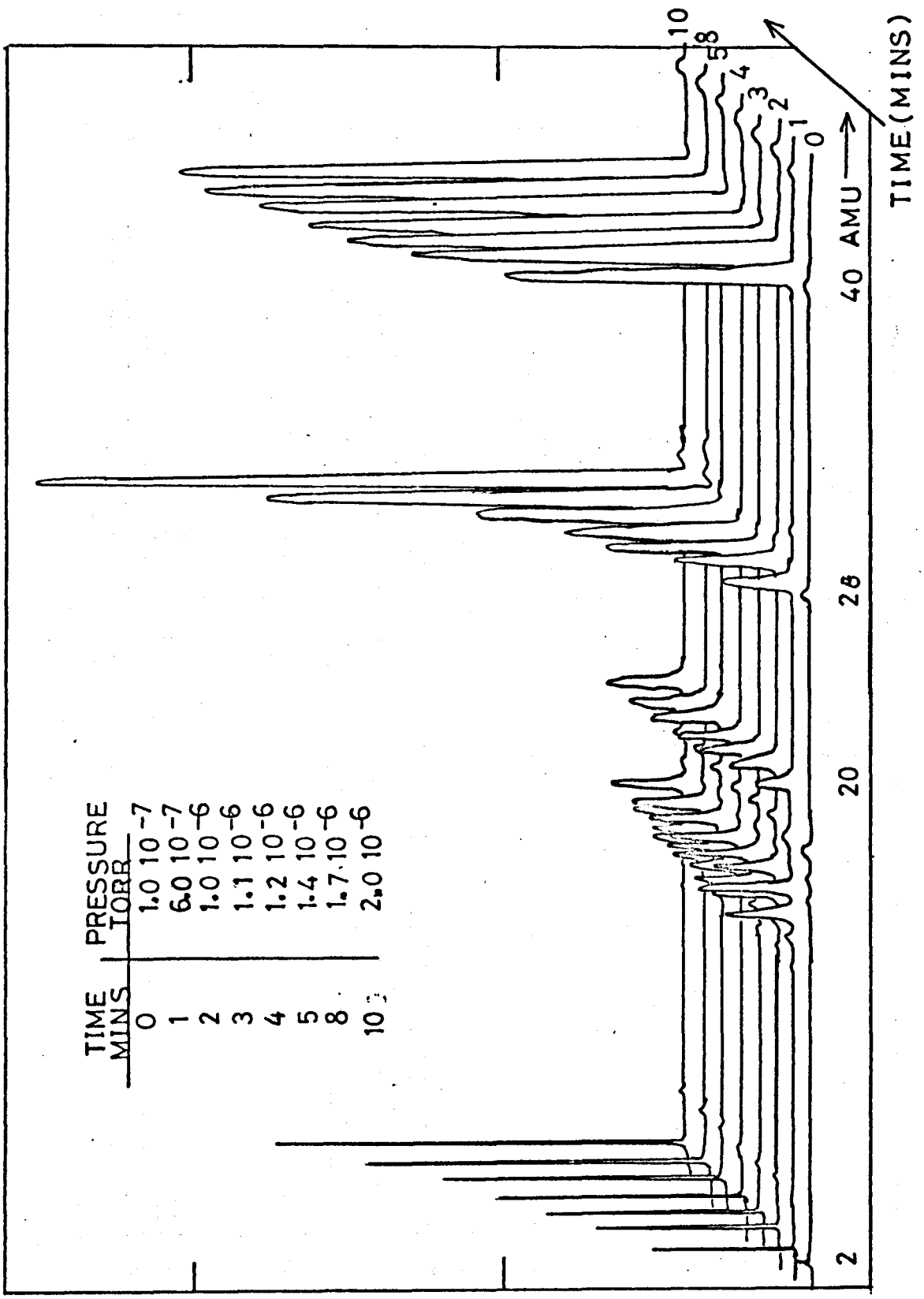

Figure 6.14 Side-arm background pressure increase with time

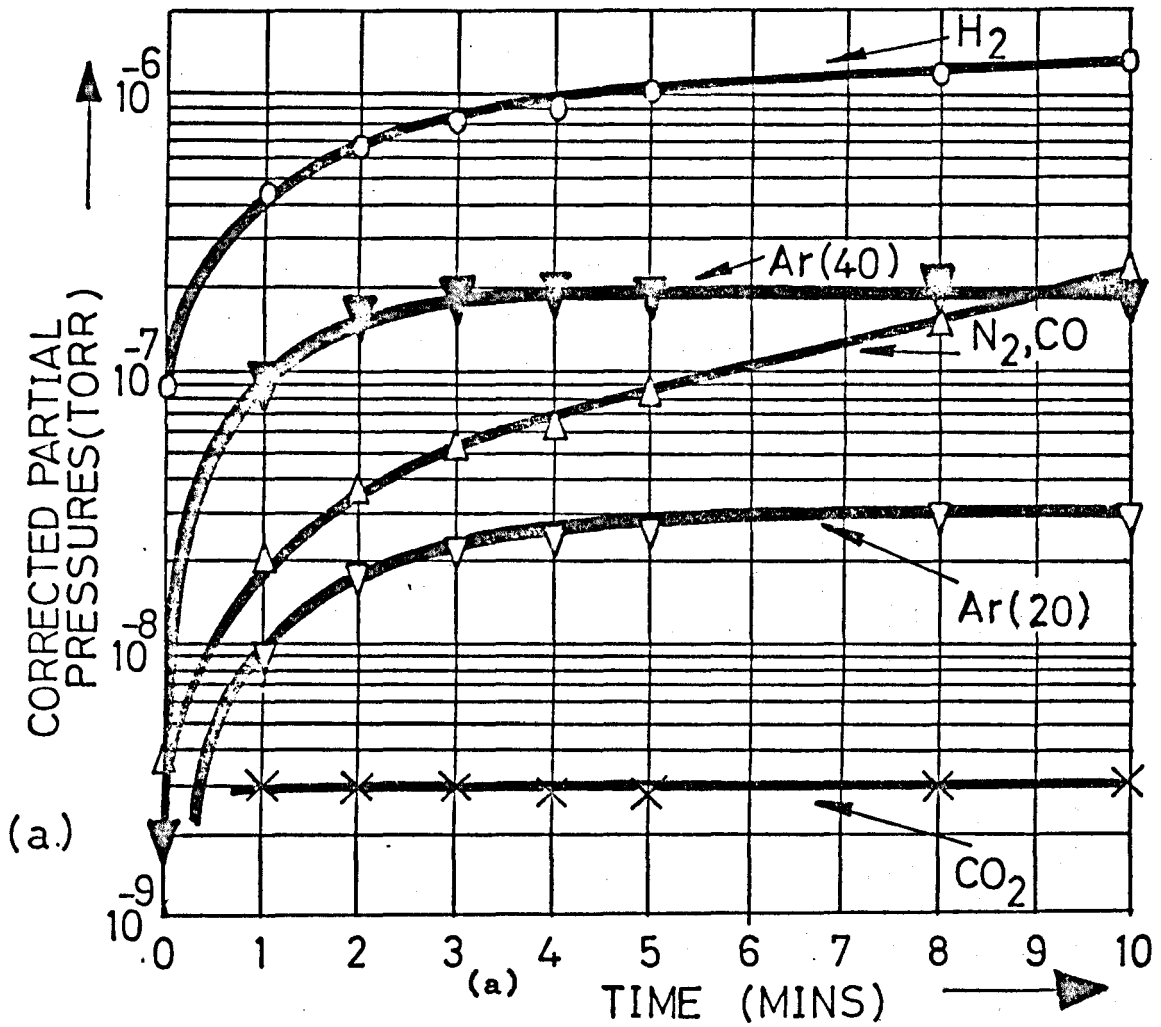

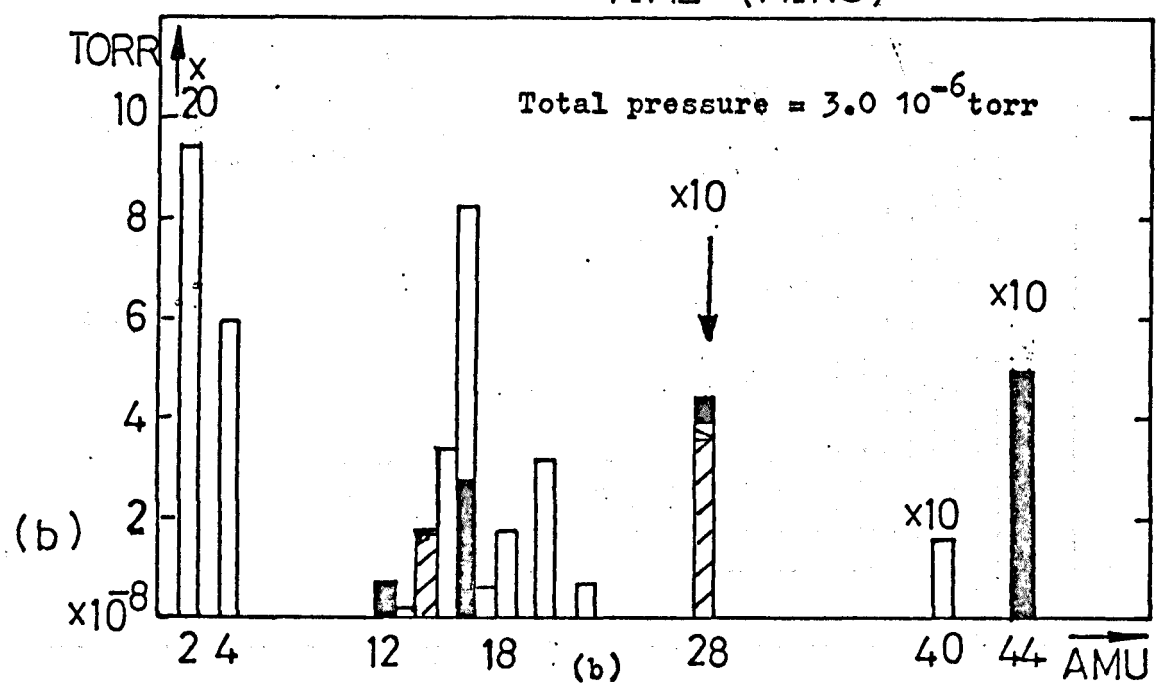

Figure 6.15 (a) Corrected partial pressures from Figure 6.14.

(b) Bkgd pressure in side-arm after 5 mins.

at pressures above 2.0 10^{-4} torr, this was impractical, and meant that if it were to be done, it was necessary to estimate the partial peaks at a.m.u. 28, 40 and 44 from their corresponding, and lower, daughter peaks. This is shown in Figure 6.12(b), for a sputtering time of 90 minutes at an argon pressure of about 6.8 10^{-4} torr. Figure 6.12(a) shows the effect of momentarily using the 110 l/s ion pump to evacuate the vacuum system to 8.0 10^{-5} torr, after 25 minutes sputtering. It was observed that in common with reports from other investigators[182,251] the partial pressure of hydrogen, in the deposition chamber, rose by a large amount when a gas discharge was initiated and maintained for even a short time. The origin of the hydrogen increase is not entirely clear, but it seems likely that the electrical discharge helps to dissociate some of the water vapour and hydrocarbons (such as methane), either present in the system or desorbed from the surroundings by the 'scrubbing' action of the plasma.

After a prolonged sputtering experiment and repumping the system for approximately 3 hours, the total pressure is reduced to a value even lower than that prior to the experiment. This is shown in Figures 6.13(a) and (b), which may be compared with Figures 6.7(a) and (b).

As pointed out in section 4.10, the quantity of gas released from the films is corrected for the residual pressure increase in the side-arm analysing system. Figure 6.14 shows the residual partial pressure increase with time, plotted on the XY recorder. The corrected partial pressures are illustrated in Figure 6.15(a). The importance of outgassing the filaments of the QRGA and pressure gauges, in the side-arm, is demonstrated by comparing Figure 6.15(b), where the filaments have not been outgassed, with the equivalent time/pressure values in Figure 6.15(a). Although there is little

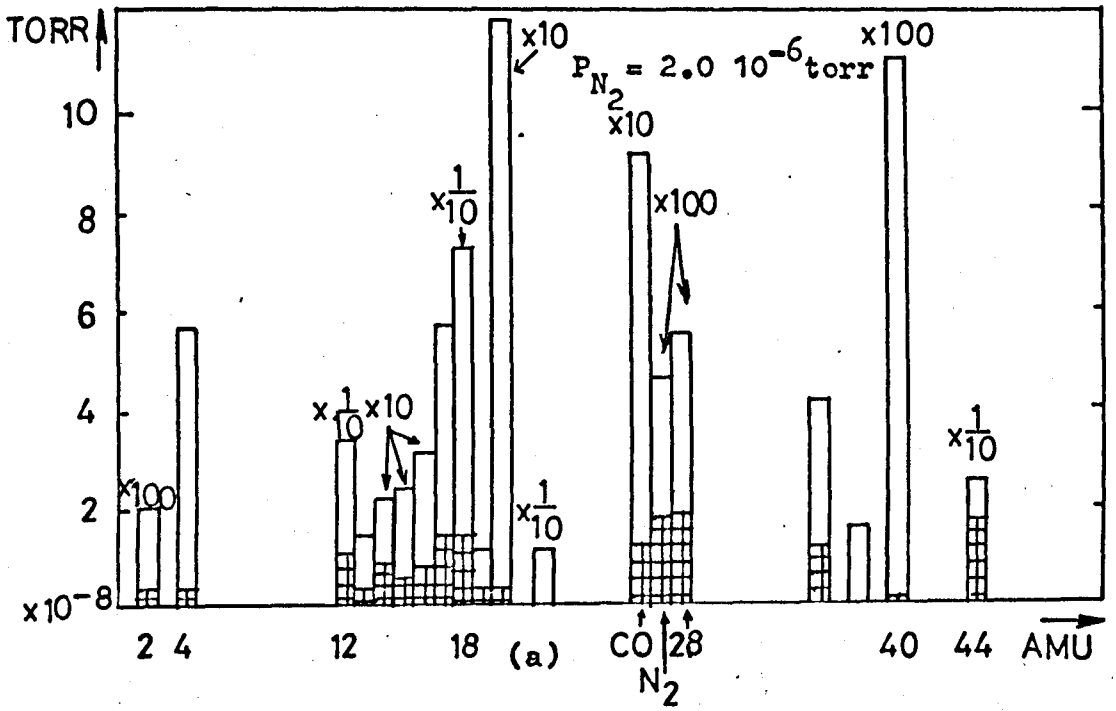

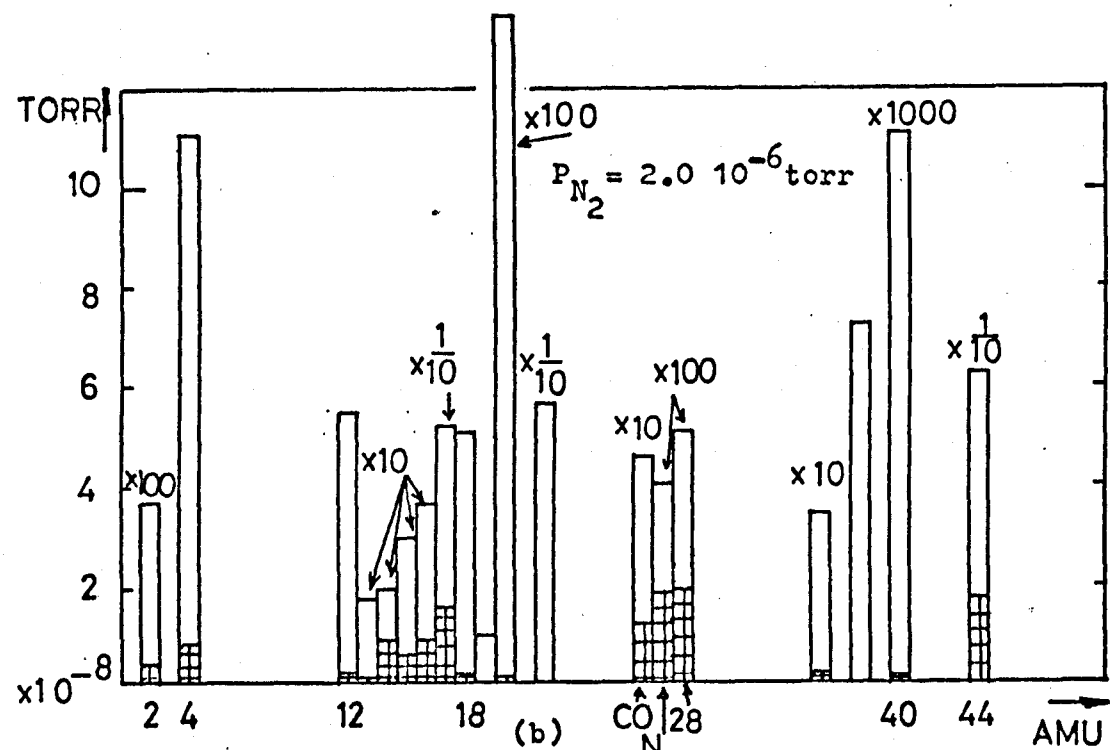

Figure 6.16 (a) Outgassing copper film on tungsten, V_b = -100 V.

(b) Outgassing copper film on tungsten, V_b = -300 V.

change in the inert gas partial pressures, there is a large change in the a.m.u. 44, 15 and 16 peak heights which arises, in part, from the evolution of methane and carbon dioxide from the filaments[231].

Two examples are given, see Figure 6.16(a) and (b) which show the spectra obtained when outgassing 1000 Å sputtered copper films on tungsten, grown with voltage biases of -100 V and -300 V respectively. The corresponding residual gas pressures have been added to the histograms, in the form of square hatching, and, for convenience, the nitrogen and carbon monoxide pressure peaks at a.m.u. 28 have been drawn adjacent to the 28 position, rather than superimposed on it.

To explain in detail the changing pattern of the mass spectra, produced under the various conditions described, would be exceedingly difficult, since it would be necessary to consider all the very large number of 'sources' and 'sinks' of gas, present in the system. Some, such as the quadrupole and pressure gauge filaments, and the property of the plasma to desorb weakly-bound molecules from surrounding surfaces, have already been mentioned. Others, such as the ion and sublimation pumps, the thermionic tungsten filament cathode, the magnetic coils, and other metal, ceramic, and glass surfaces exposed to the vacuum, all contribute, to some degree, both as 'sources' and 'sinks' under varying conditions of temperature and pressure.

Sources of error

On flash heating the films, gas can be released from (a) the film surface, and (b) the substrate, as well as from the bulk of the film itself. In some circumstances, the effects of (a) and (b) will limit the sensitivity of the gas content measurements. The effects of (b) are

minimised in the present investigation, at least when using the tungsten substrates, as was seen in Figure 6.11(b). This was one of the reasons why tungsten, in preference to glass and stainless steel, was used for most of the experiments. The effect due to (a) is unlikely to occur for argon. But it may effect the sensitivity for the measurements of the nitrogen content (and other active gases), if they are chemisorbed by the film surface prior to analysis. This, together with the background pressure in the analysing system, present during desorption, is expected to reduce the sensitivity, for nitrogen in a 1000 Å film, to about 1 part in 10^4, i.e. a gas concentration of about 10^{-2} atomic %. With thorough baking of the side-arm system after every substrate replacement, and low reactive gas pressures in the deposition chamber, the sensitivity could be improved to about 10^{-4} atomic %.

The different sputtering and evaporation sources, and the deposited films themselves, can have a strong effect on the partial pressures measured by the QRGA and can lead to an inaccurate determination of,

(a) the partial pressures present during deposition, and

(b) the gas content of the deposited films.

The first arises, especially for the reactive gas determinations, because of the possible 'gettering' effect associated with evaporating and sputtering reactive metals, such as tungsten, zirconium and titanium. The metal films so produced will condense on surrounding surfaces, as well as on the substrate. This film may sorb reactive gases from the ambient pressure in the immediate vicinity of the film. The QRGA and pressure gauge, which are placed some distance from the film, will then reflect inaccurately the gases present immediately above the growing film. The gas contents measured for the

reactive gases, and released from the films by flash evaporation may also be unrepresentative of the gases actually present in the films. In this case, the error will arise because, as pointed out in Chapter 4, the induction heating causes evaporation of the metal film as well as the release of gas from it. The metal vapour will condense on the surrounding surface, which in this case is the glass Tee section, where it may re-adsorb some of the gas just released. The same result will then follow as in (a). Although little can be done to alleviate the problem of 'gettering' associated with (a), its effect in (b) may be reduced by, (i) shortening the time of heating, so that the gas is released, but evaporation of the film does not take place, and (ii) obtaining the mass spectrum as soon as practicable after film desorption. This is usually between 30 to 60 seconds from the time of flash heating. Even so, for the outgassed zirconium and some of the titanium films, it was found that within seconds of outgassing the film, re-adsorption took place, with a noticeable reduction in the total pressure increase, measured on the millitorr gauge. The subsequent partial pressures obtained by the QRGA were then lower, and often even smaller than would have been expected from the background pressure in the analysing system itself.

A further source of error in the gas content measurement could arise if all the gas was not released from the film on flash heating. The films deposited on stainless steel and glass substrates were particularly susceptible to this sort of error and this was a further reason for the use of tungsten substrates in most of the present experiments. The results presented in the following section were all obtained for films deposited on tungsten substrates, unless otherwise stated. The stainless steel substrates were only found to be of use in the preliminary setting-up experiments, and

the results obtained using them, are only presented here for the case of sputtered nickel. The glass substrates, on the other hand, were found to be useful in the electron microscope studies because little evaporation of the film took place and also the relative ease with which the carbon replicas could be removed from them, compared with the metal substrates.

The present investigation is concerned primarily with the argon and nitrogen incorporation in the films. The former, partly because of its continual presence in the sputtering discharge, and the latter, so that Winter's suggestion (see section 3.5.3), that metals can be placed in three classes, can be investigated. However, since other gases, such as hydrogen, carbon monoxide and methane are released when the films are outgassed, see for example, Figures 6.16(a) and (b), the gas content for these gases can also presumably be found. Interpretation of the results, however, is likely to be even more difficult than for argon and nitrogen. This is because of the high reactivity of the other gases with many metals and the difficulty in maintaining constant pressure conditions for these gases, in the vacuum system during deposition.

6.3 Gas content measurements

The argon and nitrogen concentrations of seven metals have been investigated, and will be presented in two sections. The first for the argon and the second for the nitrogen concentrations. The metals investigated were:-

aluminium, copper, nickel, titanium, tungsten, zirconium and gold.

Sputtered films, and evaporated films for most of the metals, were made at the same time, so that comparisons between the gas contents could be made.

For the nitrogen incorporation, WINTERS et al[212] have suggested that metals can be divided into three classes or groups, namely:-

Class 1 - metals which chemisorb molecular nitrogen and form nitrides.

Class 2 - metals which do not chemisorb molecular nitrogen but form nitrides.

Class 3 - metals which neither chemisorb molecular nitrogen nor form nitrides.

The metals investigated were chosen so that at least one was in each class, i.e. tungsten, titanium and zirconium are in class 1, nickel, copper and aluminium are in class 2, and gold falls into class 3.

To try to understand the influence of parameters such as sticking coefficients, sputtering yields, atomic radii, etc., on the adsorption, and hence the incorporation of gas in the growing films, the experimental results were compared with the theoretical model proposed by WINTERS et al[205]. This model was chosen in preference to that of MAISSEL and SCHAIBLE[185] because the latter was not as versatile as the former. For example, the sputtering yields of adsorbed gases are not generally known, but in WINTERS' model this problem can partially be overcome by treating the sputtering yield of the gas as a constant fraction of that of the metal. Furthermore, Maissel's model does not consider the different sorption processes that can take place at the film surface, such as chemisorption, impact activated sorption, etc., but rather lumps then all together under a single sticking factor. On the other hand, Winters' model includes sticking probabilities for each process (although in only a few cases, are exact values known for them). It also simplifies the problem of choosing the correct sticking probability, which arises through an inexact knowledge of the surface coverage of the various gas species at the film surface.

A computer programme, in Fortran 4, was written, on the basis of Winters' model, so that the concentrations of argon and nitrogen in the metal films when subjected to ion bombardment, could be calculated. The programme was run on an ICL 4130 computer.

The programme was designed to plot out graphically the gas concentrations, calculated in atomic %, as a function of ion energy (i.e. voltage bias) in eV.

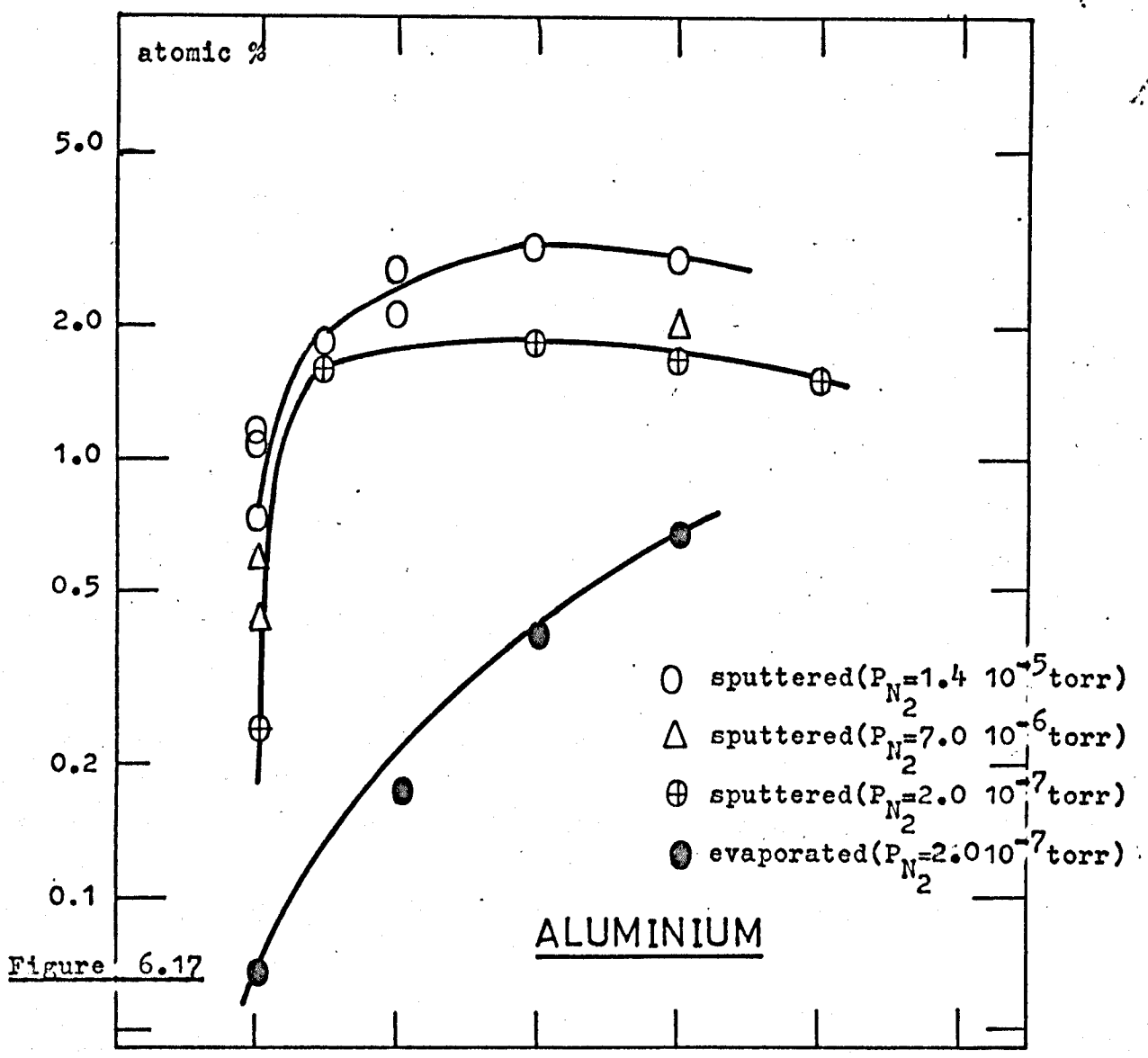

Figure 6.17

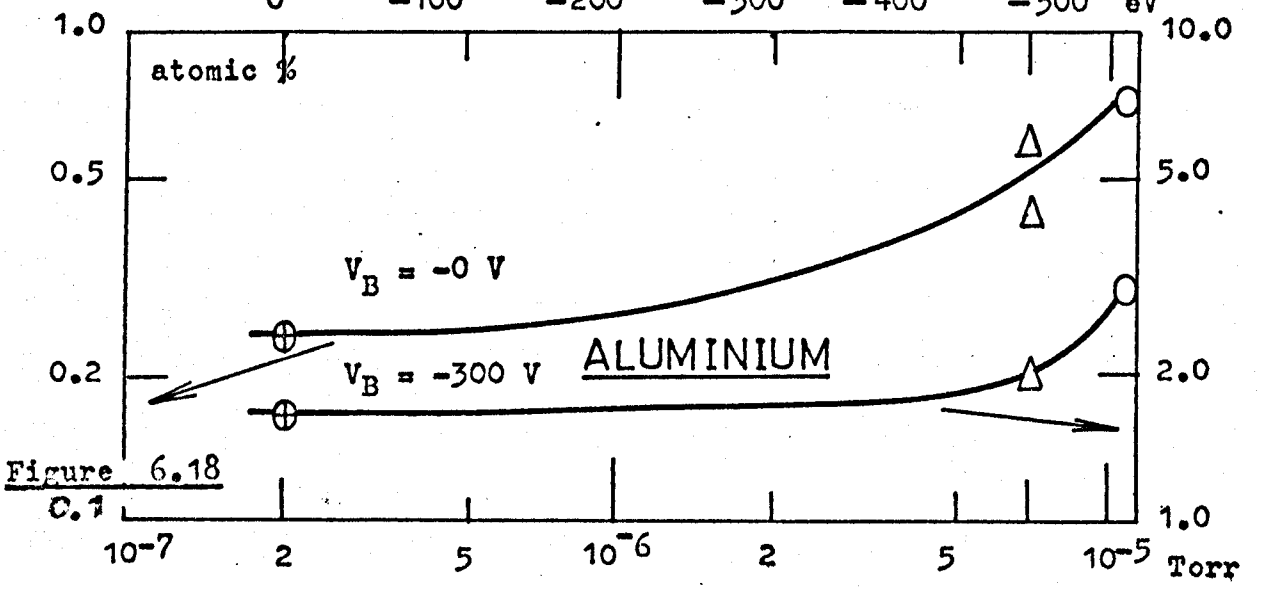

Figure 6.18

6.4 Inert gas incorporation

Results

1. Aluminium

Although, chemisorption has not been observed for argon, and the amount of physical adsorption of argon on metal films, at room temperature, would be very small[61], large amounts of argon have nevertheless been found in the sputtered films, even in the unbiased mode, i.e. with zero bias (ZB) applied to the film. In addition, the sputtered films have more argon trapped in them than the equivalent evaporated films, even when deposited in the presence of a gas discharge. This is seen, for example, in Figure 6.17. for aluminium films. The amount of argon trapped in ZB aluminium films is about an order of magnitude less than that in the equivalent sputtered films.

As the amount of ion bombardment on the film increases, i.e. by applying a bias voltage, the argon concentration increases in the evaporated films, reaching a concentration of $\sim$ 1 atomic % at -400 V and, apparently, converging towards the values for the sputtered films. The concentrations in the sputtered films increase more slowly after -100V and, at biases of about - 400 V, actually begin to fall slightly. Several curves are seen for the sputtered films, which were all prepared at the same argon pressure of $6.8\ 10^{-4}$torr, but with different amounts of nitrogen present, the pressures of which are indicated on the Figure. It can be seen, from Figure 6.18, that more argon is trapped in films which are grown in the presence of higher nitrogen pressures, even when voltage bias is applied.

2. Copper

Increasing the argon pressure causes a decrease in argon concentra-

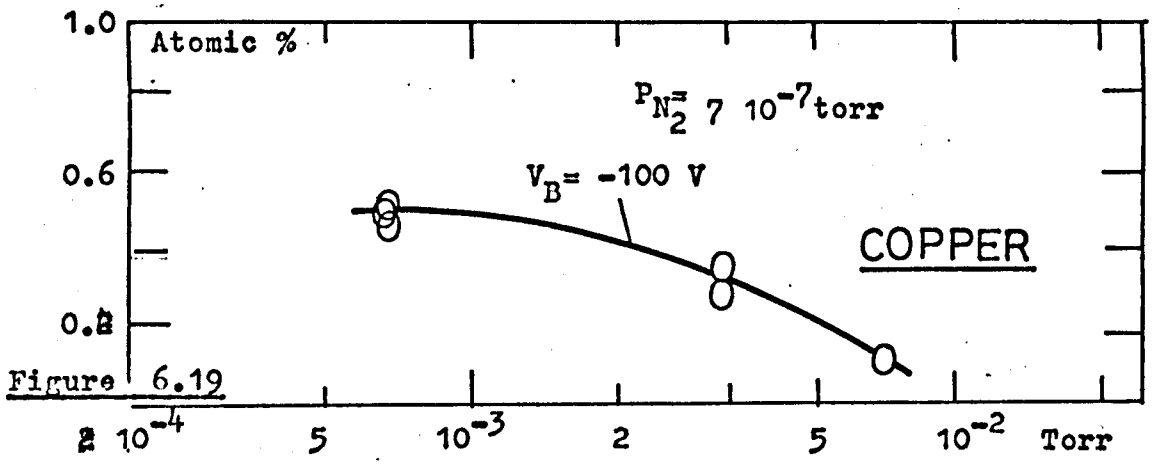

Figure 6.19

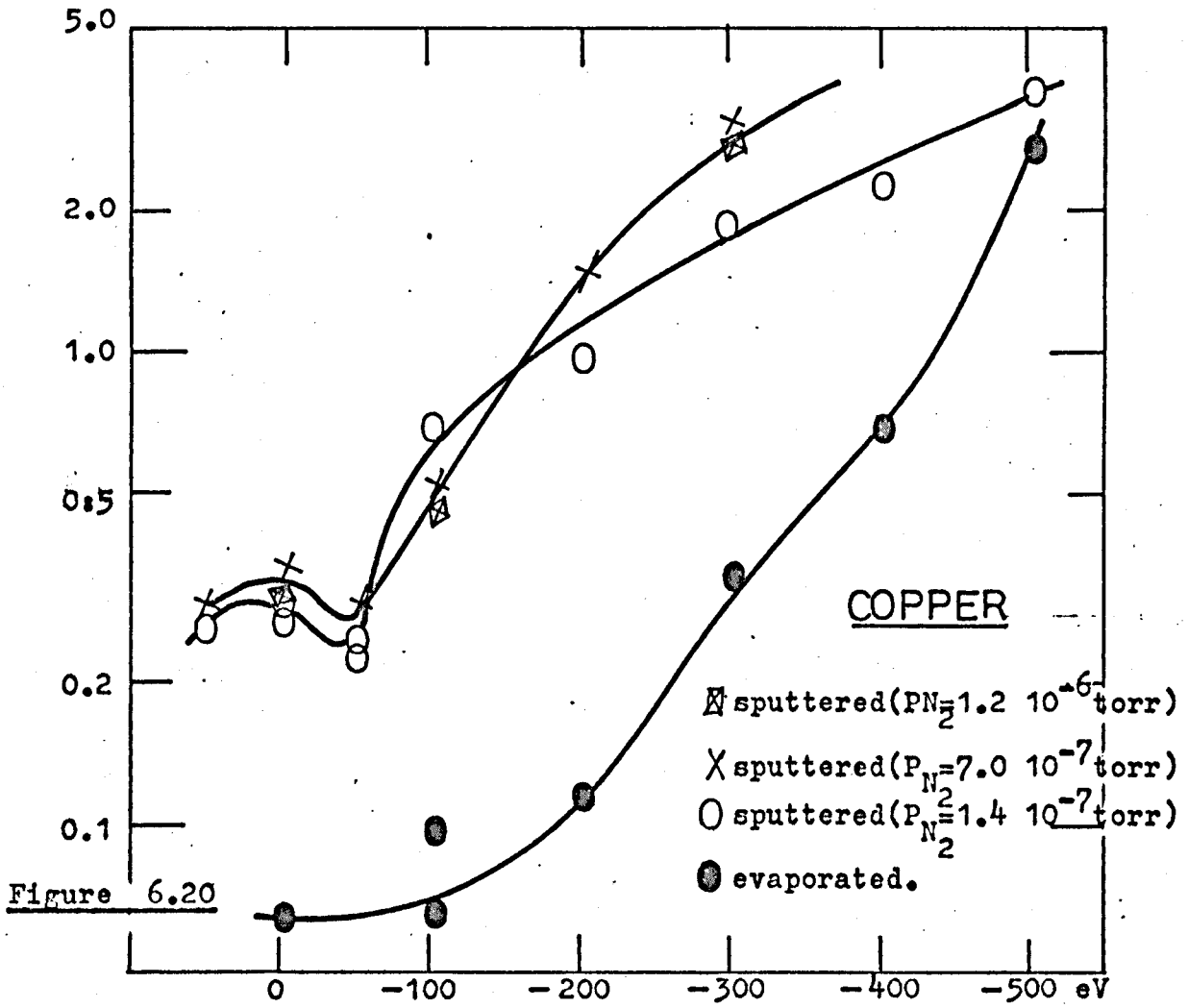

Figure 6.20

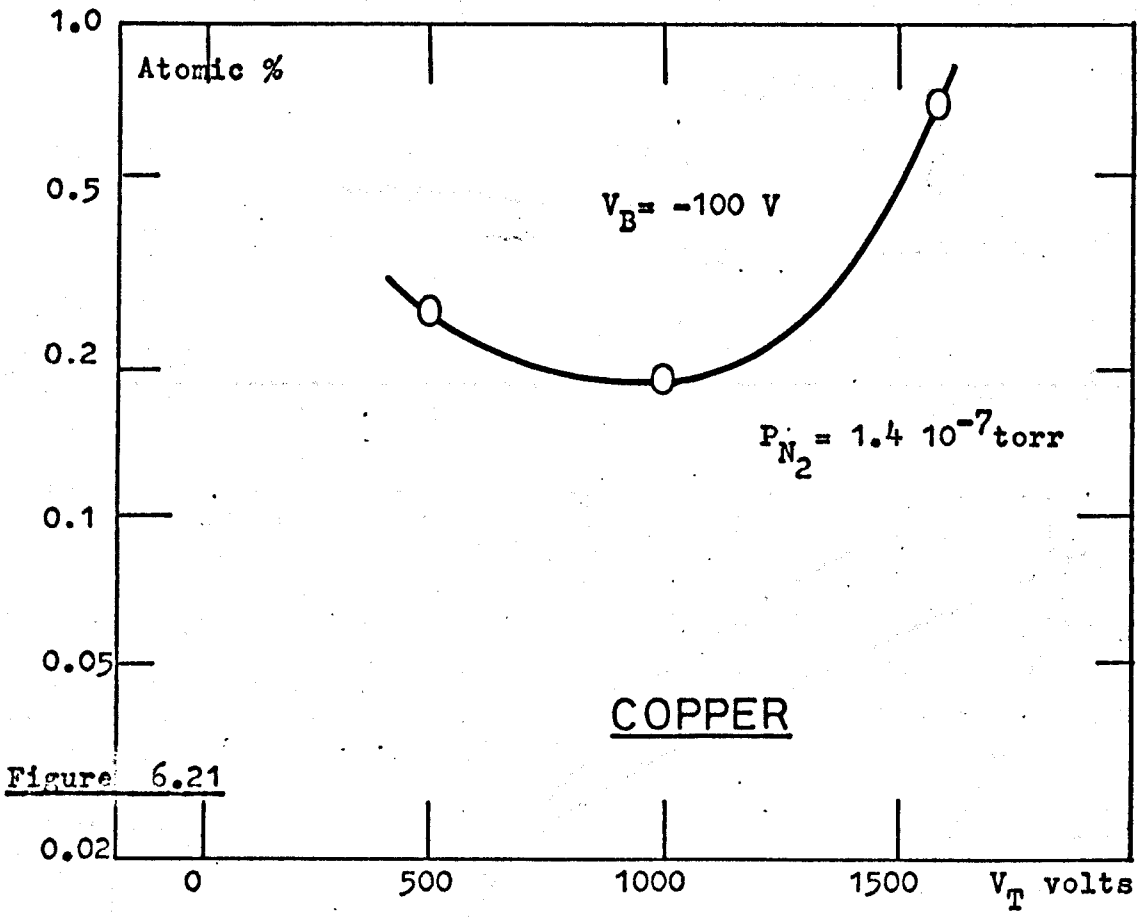

Figure 6.21

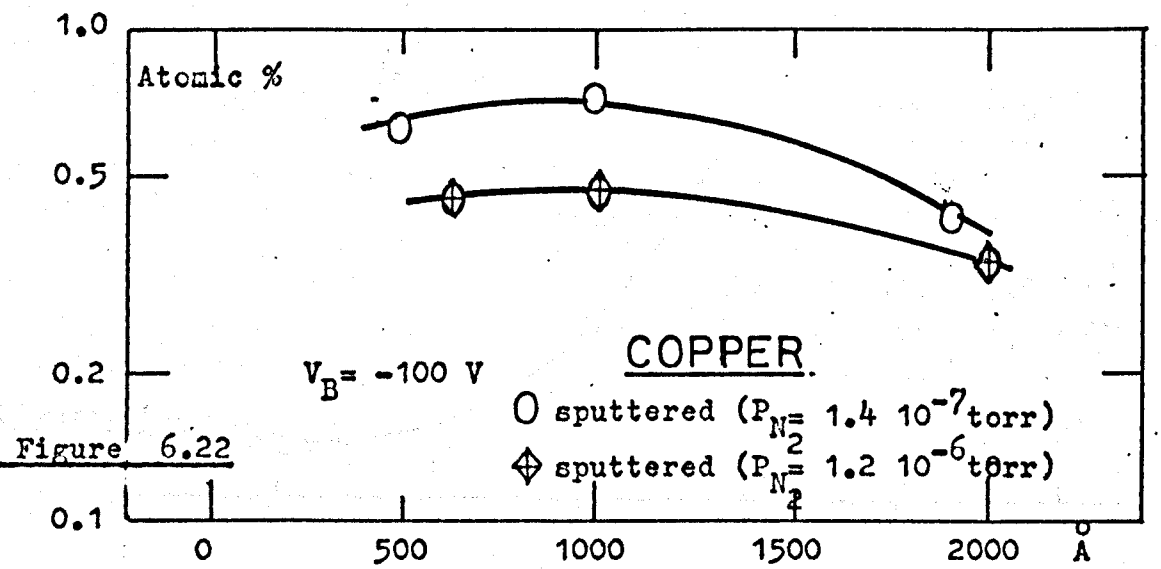

Figure 6.22

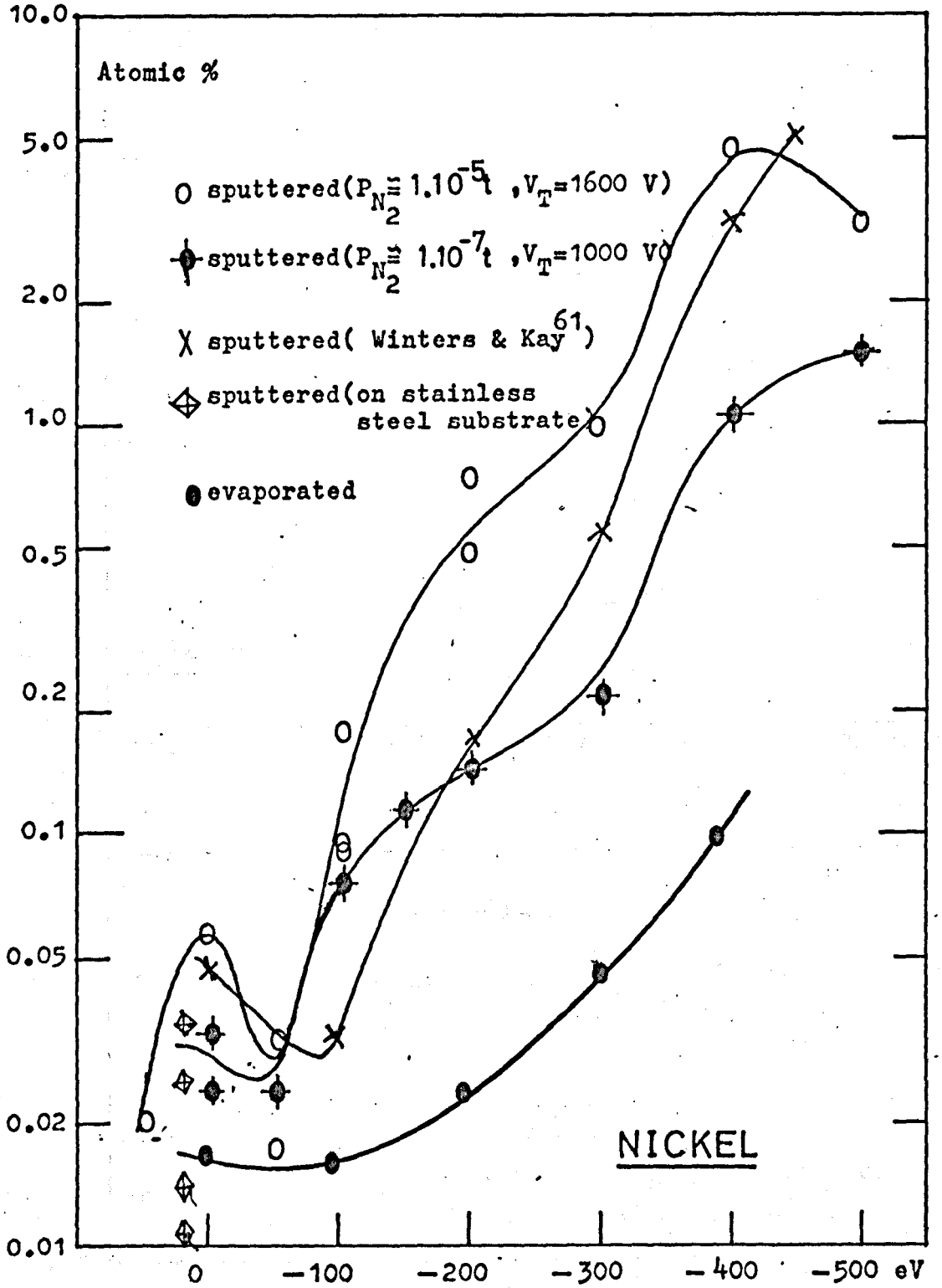
10.0
Atomic %
5.0
2.0
1.0
0.5
0.2
0.1
0.05
0.02
0.01
O sputtered($P_{N_2} \cong 1.10^{-5}$ t , V_T=1600 V)
sputtered($P_{N_2} \cong 1.10^{-7}$ t , V_T=1000 V)
X sputtered(Winters & Kay[61])
sputtered(on stainless steel substrate)
evaporated
NICKEL
0
−100
−200
−300
−400
−500 eV

Figure 6.23

tion in otherwise identical sputtered films, as seen in Figure 6.19.

The same effect on argon concentration is observed for copper as aluminium, for sputtered and evaporated films with increasing voltage bias, as is shown in Figure 6.20. At zero bias, the concentration in the evaporated films is about 6.0 10^{-2} atomic %, which is about an order of magnitude less than for the sputtered films. In addition, for the sputtered films, a decrease in concentration is observed at small negative and positive bias voltages. The argon concentration increases for both types of film with increasing bias voltage, with the values for the evaporated films approaching the sputtered ones at -500 V. The sputtered films do not exhibit a maximum concentration, but a continual increase is observed up to -500 V (the maximum voltage bias applied). Again, the films sputtered at higher pressures of nitrogen have higher, although only slightly higher, argon concentrations than their counterparts, deposited at lower nitrogen pressures.

The effect on concentration of varying the target voltage is illustrated by Figure 6.21, which suggests that target voltage can have a pronounced effect on the amount of argon trapped in the film.

One of the consequences of Winters' model, is that the composition of each atomic layer of the sputtered film should be the same as the preceding one[205]. This is roughly what is observed in Figure 6.22, which shows the change in concentration with thickness of the sputtered films.

3. Nickel

The variation of argon concentration with voltage bias for sputtered nickel films has been investigated by WINTERS and KAY[60] and their results are shown in Figure 6.23, for comparison with those of the present work.

The concentration for the ZB evaporated films is found to be less

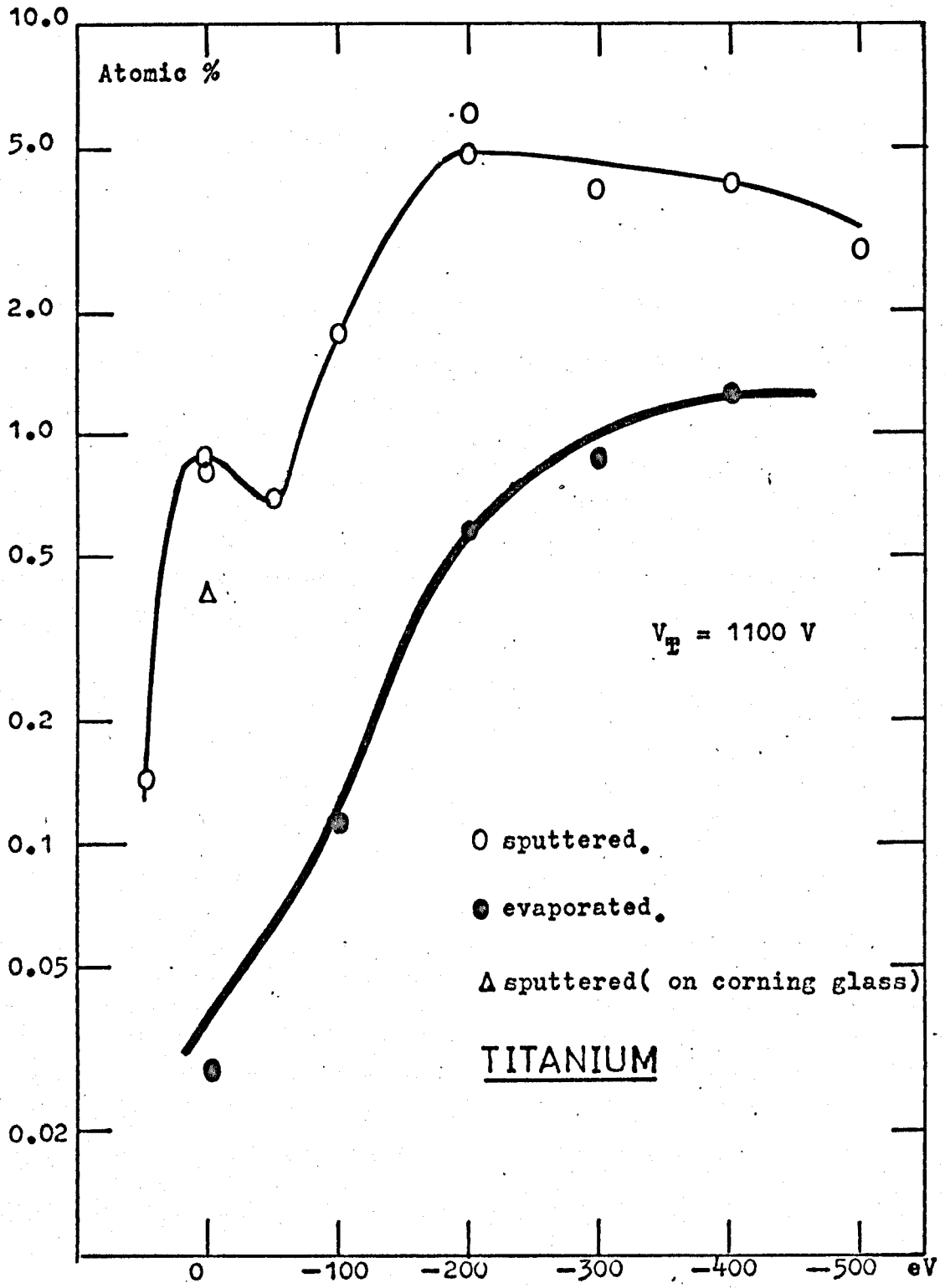
10.0
Atomic %
5.0
2.0
1.0
0.5
0.2
0.1
0.05
0.02
O
O
O
Δ
V_T = 1100 V
O sputtered.
● evaporated.
Δ sputtered(on corning glass)
TITANIUM
0
−100
−200
−300
−400
−500
eV

Figure 6.24

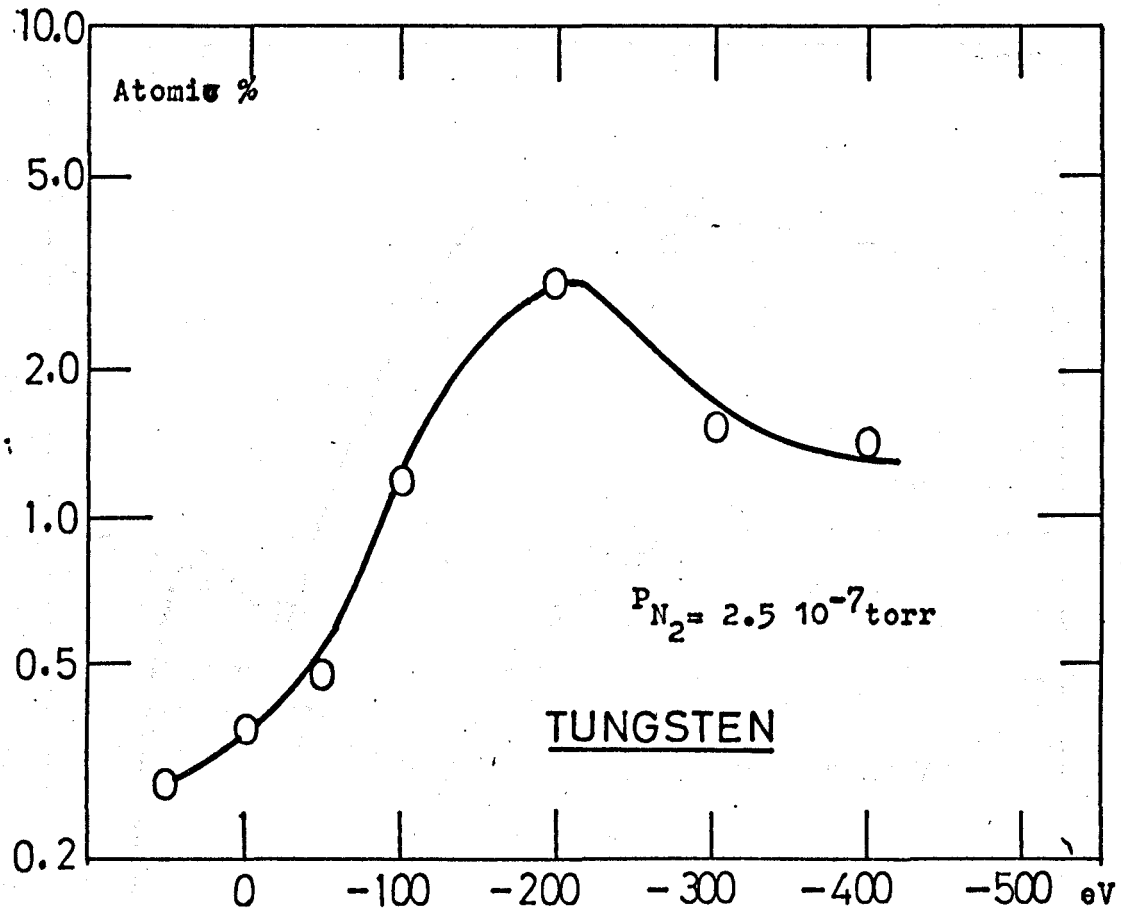

Figure 6.25

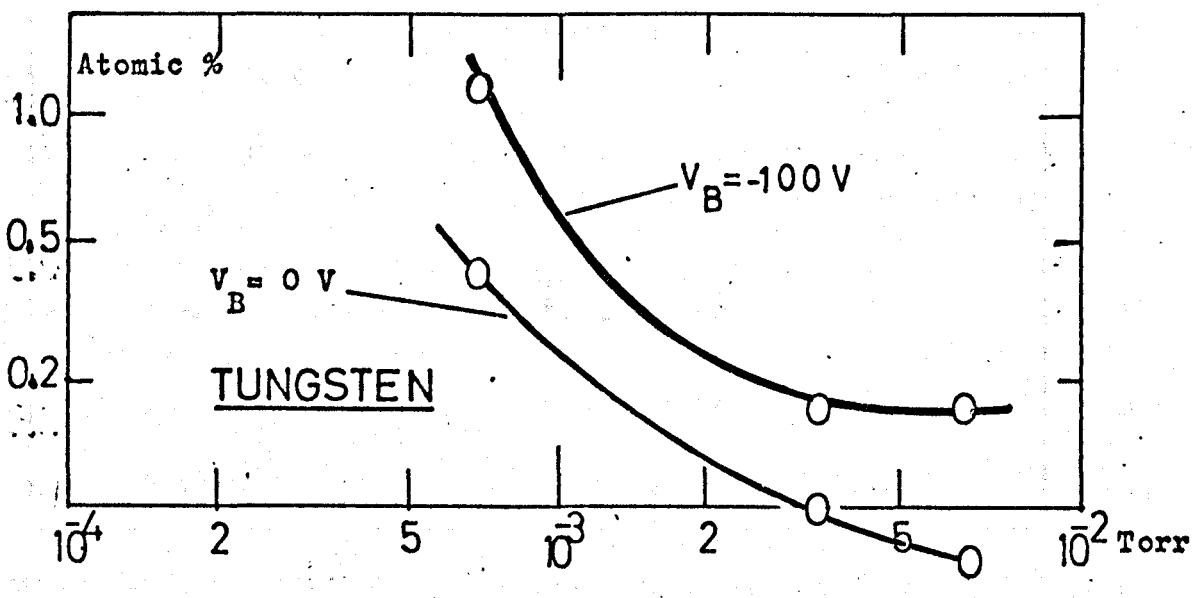

Figure 6.26

than 2.10^{-2} atomic % and is not very different from the values obtained for the sputtered films with bias voltages of ±50 V. The concentration for ZB sputtered films is about 2 - 3 times higher. With applied target voltages of -1600 V and -1000 V and nitrogen partial pressures of $\sim 5. 10^{-6}$ torr and $\sim 5.10^{-8}$ torr respectively, a difference in concentration amounting to a factor of 3, is found at bias voltages above -200 V. Both curves indicate a lessening in the concentration increase at about -500 V bias, although, it is noticeably more pronounced in the -1600 V case. There is reasonable agreement with the results of Winters and Kay, even though their films were grown in a diode sputtering arrangement, with target voltages of -3000V and at argon pressures of around $7.0\ 10^{-2}$ torr.

4. Titanium

The curve for the sputtered films exhibits a maximum in concentration of about 5 atomic % at -200 V bias and a slight decrease thereafter, see Figure 6.24. In addition, a minimum appears at -50 V, although it is not very different from the concentration at ZB, of about $9.0\ 10^{-1}$ atomic %. There is a large fall in concentration when electron bombardment of the film takes place, by the application of a positive voltage bias. The corresponding curve for films evaporated from a titanium/molybdenum alloy filament, shows a rapid rise in concentration, with increasingly negative voltage bias, and approaches, within a factor of 2-3, the value for the sputtered films at -500 V. One additional plotted point is evident from the Figure, which is for titanium sputtered on corning glass at ZB.

5. Tungsten

Figure 6.25 indicates that a maximum concentration of about 4 atomic % was obtained at -200 V voltage bias, with a decrease to $\sim$ 1.5 atomic %

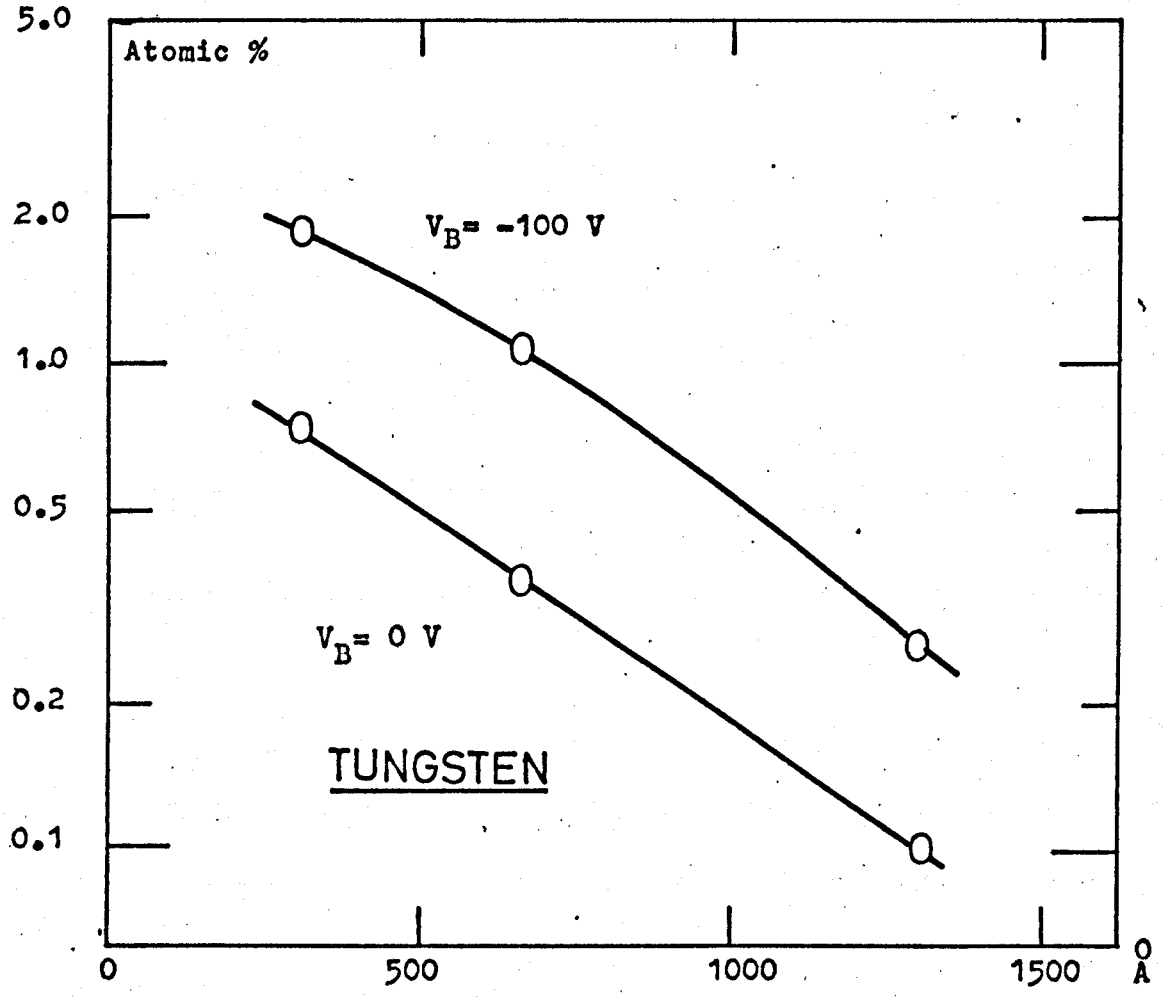

Figure 6.27

at -400 V. No minimum was found at -50 V, and the concentration at ZB was about 4.0 10^{-1} atomic %. Attempts to resistively evaporate tungsten were unsuccessful, and so no comparison could be made with the sputtered films.

As seen in Figure 6.26, increasing the argon pressure resulted in a decrease in argon concentration (for the same film thicknesses), although there appeared to be little change at the higher pressures. Figure 6.27 shows there to be a large decrease in concentration, by almost an order of magnitude, for the thickest tungsten films deposited when compared with the thinnest ones. This occurs for both the -100 V biased and the ZB films, and is in contrast with the results obtained for copper and gold films shown in Figures 6.22 and 6.30, respectively. This observation for tungsten may be due to the fact that, of all the metals, tungsten has one of the lowest sputtering yields (and hence deposition rates), whereas, gold and copper have some of the highest, and so will require a shorter deposition time to produce the same film thickness.

In contrast with the present results, LEE et al[187] found much higher values of argon concentration in ZB tungsten films, deposited by triode sputtering. For example, about 12 atomic % at a pressure of 2.10^{-3} torr, with a fall to about $\sim$ 2 atomic % at 8 10^{-3} torr. There was, in addition, some indication, from their results, that there was an equally, if not more dramatic fall in concentration below 2 10^{-3} torr. Unfortunately it proved impossible to determine the actual values from their curves, and therefore, any interpretation of their results, at low pressures, must be treated with caution.

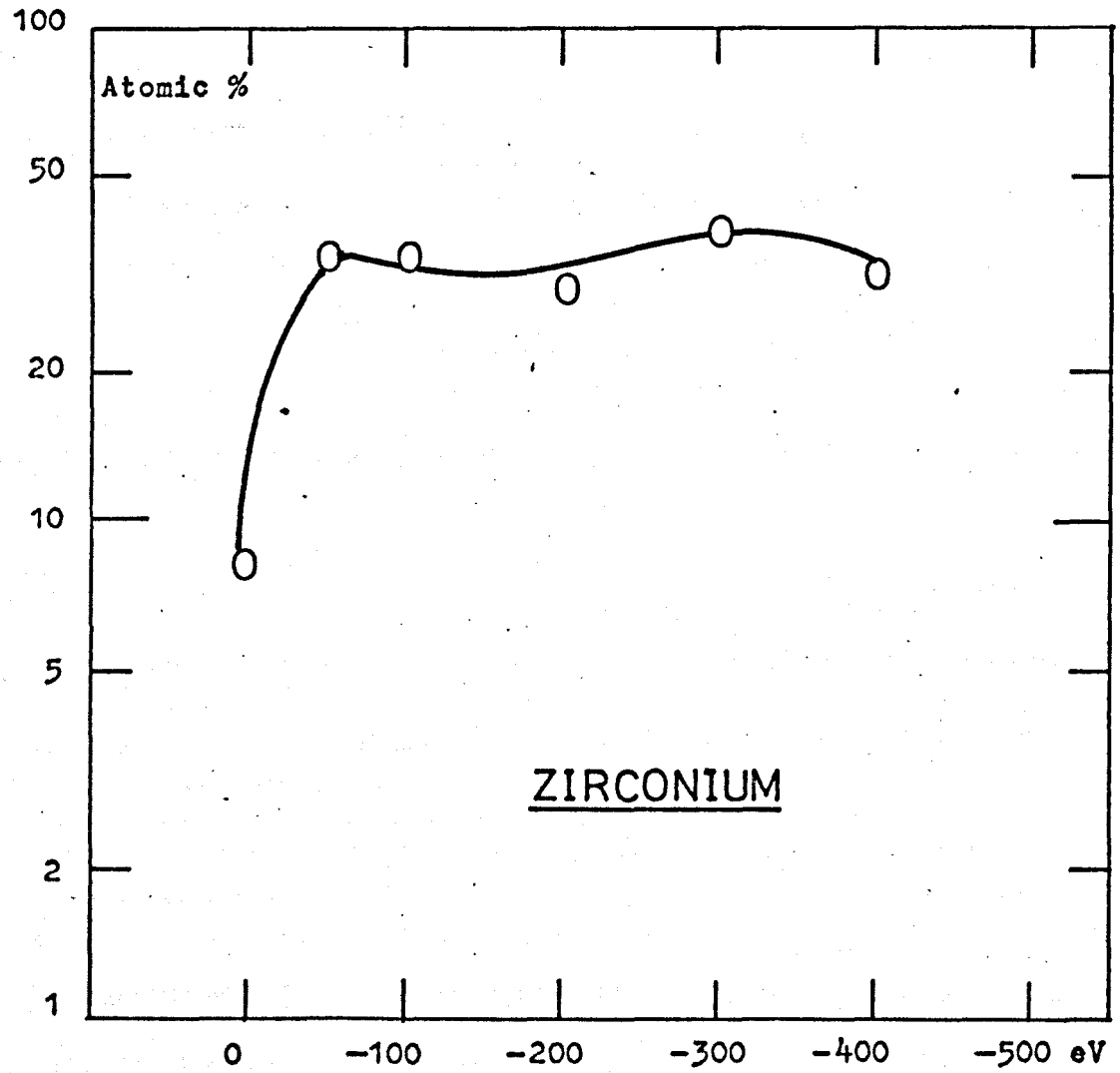

Figure 6.28

6. Zirconium

High values of argon concentration were calculated for the sputtered zirconium films, as shown in Figure 6.28, and are evident for all values of voltage bias, from -50 V to -400 V. Even at ZB, the concentration was about 8 atomic %, rising to ∿ 35 atomic % at -300 V. Above -50 V, the voltage bias appeared to have little effect on the concentration, which remained at around 30 atomic %, although there is some indication of a decrease at the highest biases. The results for zirconium, however, must be treated with a certain amount of caution, since although the amount of argon trapped was undoubtedly high, great difficulty was encountered in correctly reading the total pressure, which fell rapidly in the first ∿ 30 secs following the flashing of the films, and more slowly thereafter. This pressure drop was presumably related to regettering by the flash evaporated film and/or the zirconium film itself. For this reason, the results obtained may possibly be high by as much as 100%, and any discussion concerning the results for the zirconium films will only be able to take place on a qualitative basis.

7. Gold

A large difference in concentration, of about two orders of magnitude, is found between the evaporated and sputtered films grown at zero bias voltage, on tungsten substrates. This is shown in Figure 6.29. Increasing the bias voltage leads to a rapid increase in the argon concentration for the evaporated films, and a more steady increase for the sputtered films. At a voltage bias of about -500 V, both types of film have argon concentrations closely approaching each other, at about ∿ 5 atomic %. No minimum is observed for either type of film at -50 V bias, in contrast

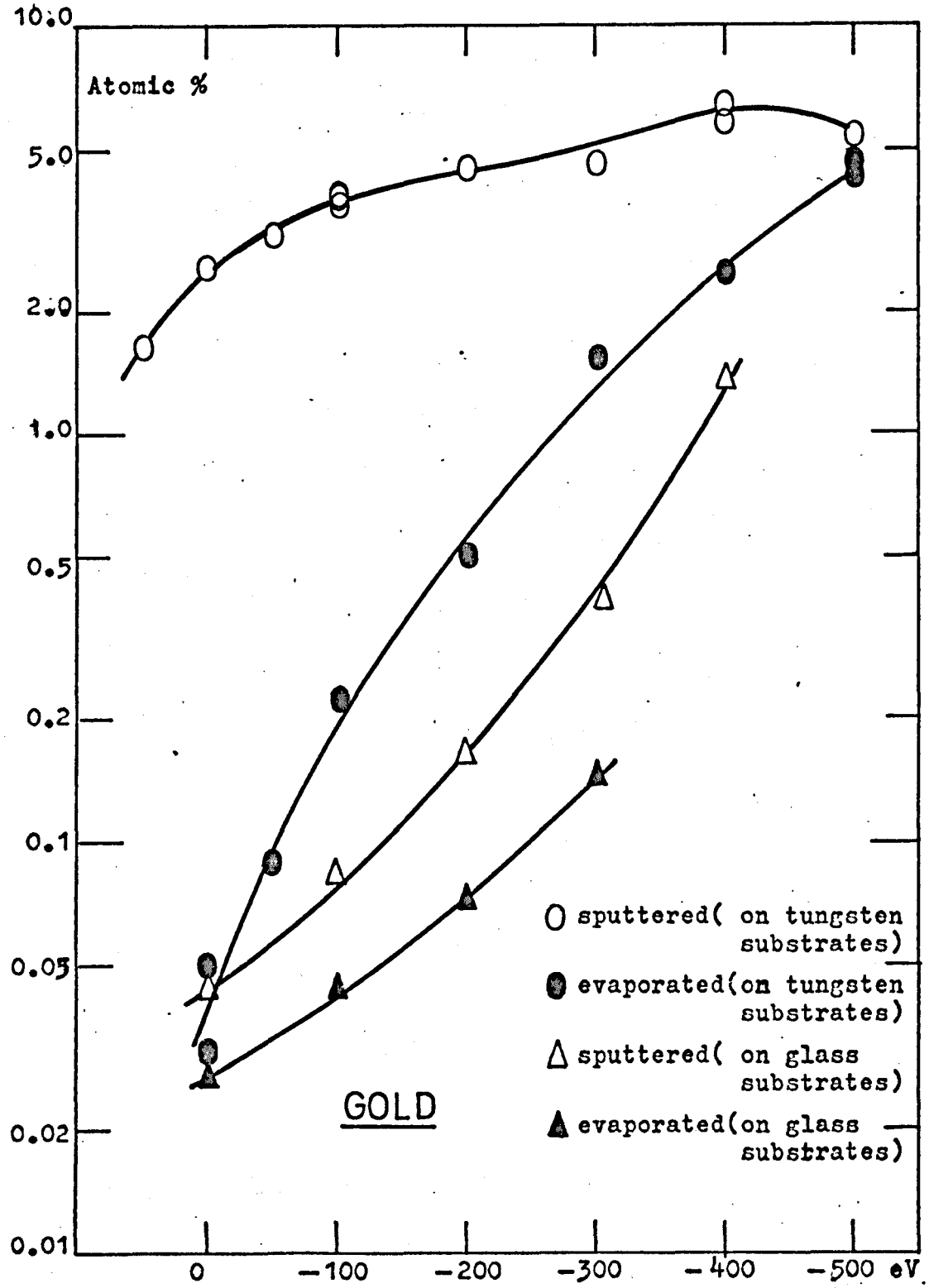
10.0
Atomic %
5.0
2.0
1.0
0.5
0.2
0.1
0.05
0.02
0.01
0
−100
−200
−300
−400
−500 eV
O sputtered(on tungsten substrates)
evaporated(on tungsten substrates)
Δ sputtered(on glass substrates)
evaporated(on glass substrates)
GOLD

Figure 6.29

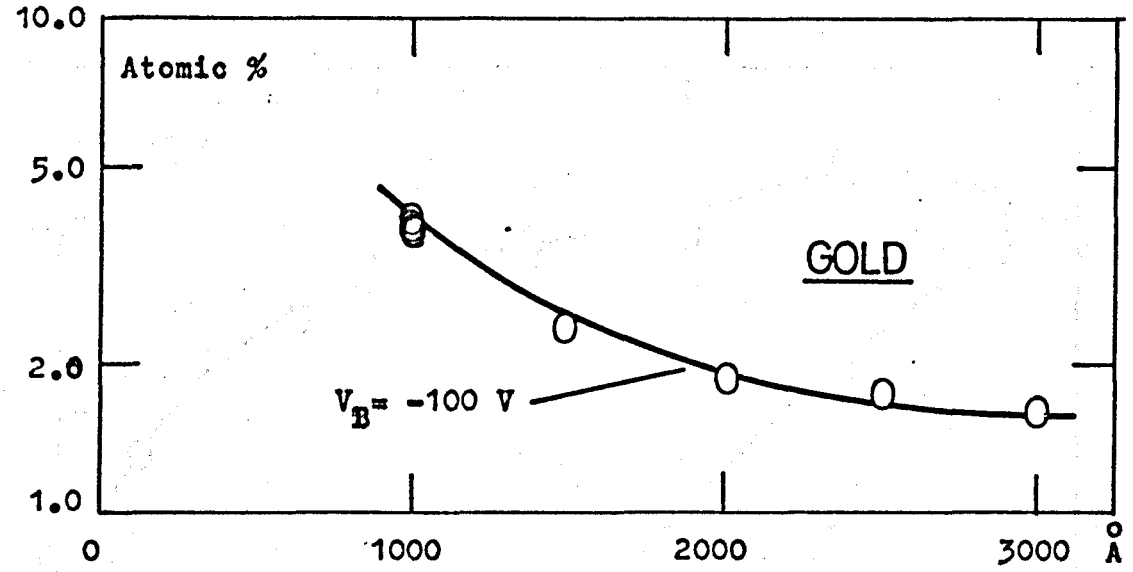
10.0
Atomic %
5.0
GOLD
2.0
V_B= -100 V
1.0
0
1000
2000
3000
Å

Figure 6.30

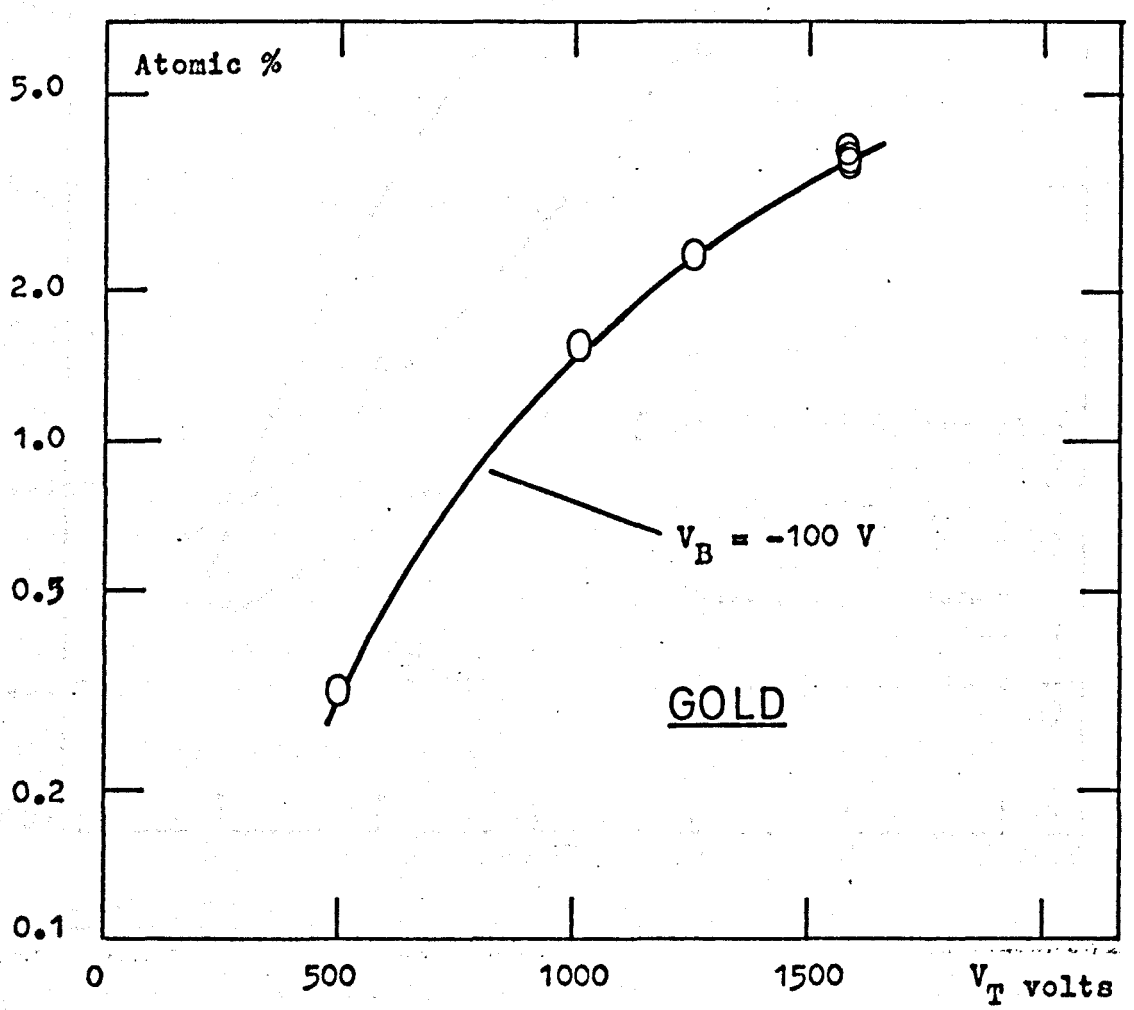
Atomic %
5.0
2.0
1.0
V_B = -100 V
0.5
GOLD
0.2
0.1
0
500
1000
1500
V_T volts

with the results for copper and nickel. For gold films deposited on glass substrates, and shown in Figure 6.29 a somewhat different result is observed. Both ZB sputtered and ZB evaporated films are found to have small argon concentrations of $\sim 3.\ 10^{-2} - 5\ 10^{-2}$ atomic %. The rise in concentration with increasing voltage bias, although rapid, did not approach the values, even for the films evaporated on tungsten. Nevertheless, in all cases, more argon was trapped in the gold films sputtered on glass than in their evaporated counterparts. The low values of concentration obtained for argon, released from the films deposited on glass, may have been partly due to the difficulty in the heating and hence, outgassing, of the films. Film temperatures around the melting point of the glass ($\sim 450^{\circ}$ C) could not be sustained for any length of time, because of the danger of the glass substrates fracturing. The glass substrates were often completely deformed after heating. Even so, the metal films were still visible on them and apparently little or no evaporation had taken place.

Figure 6.30 shows the effect on the argon concentration of increasing the thickness of the gold films. The thickness is seen to have little effect, at least above about 1500 Å.

On the other hand, increasing the target voltage has a pronounced effect on the concentration, see Figure 6.31. The argon concentration is found to increase by almost an order of magnitude when the target voltage changes from -500 V to -1600 V.

6.5 Discussion

6.5.1 Argon incorporation at zero bias (ZB)

Comparison between the sputtered and evaporated films grown in an unbiased mode, i.e. when the substrate is at earth potential, indicates that

the sputtered films will, in general, contain more argon than the evaporated ones. The gas must first be sorbed at the surface of the film before it can be trapped. This is unlikely to occur, either (a) through chemisorption, since this has not been observed in the case of the noble gases, or (b) through physisorption, at least not at the temperatures, between room temperature and 100° C, normally encountered in gas discharge systems.

To examine the effect of physical adsorption alone, on the argon content of the films, each of the metals, with the exception of tungsten and zirconium, was evaporated under conditions of gas pressure, temperature, deposition rate, etc., similar to those of the sputtered films, but with no discharge present. In all cases, the argon concentration in the evaporated films was too small to be detected. Even with the analysing system well baked, which improved the sensitivity of detection to about 10^{-3} atomic % for a 1000Å film, the amount of argon trapped in the films was not detectable. It can, therefore, be stated with some degree of confidence, that physical adsorption plays little or no part in the trapping of argon in the deposited films. This being so, other mechanisms must be invoked to explain the presence of argon in the films, deposited in the presence of a gas discharge.

It is well known[11] that there is a definite probability that inert gas ions, with sufficient kinetic energy, (of $\gtrsim$ 100 eV) can become trapped in a surface. The same should also hold true for energetic neutral gas atoms, since the approaching ions themselves are often neutralized, by an Auger process[10] on approaching a metal surface. In addition to a sticking probability, characterising the energetic ion and neutral/metal surface

interaction, there is also a significant probability that they will be reflected from the surface, often with a substantial fraction of their original energy[85]. In the unbiased mode, however, there should be few ions available in the vicinity of the growing film with energies anywhere near that necessary for trapping. This is not the case at the surface of the target. Here, a large flux of ions with energies approaching the target voltage ($\sim$ 1000 to 1600 V) are bombarding the target, Some will be trapped at the target surface, where they can later be sputtered as argon atoms. These sputtered atoms can possess energies ranging from $\sim$ eV up to many tens of eV[252]. Others, and probably the more significant fraction, are Auger neutralized at the target surface and reflected, with appreciable energy, in the general direction of the growing film. Both these processes yield a flux of argon atoms in the vicinity of the film, with energies high enough for sorption to take place, and may, in part, account for the high argon content in sputtered films, measured at zero bias voltage. They will not, however, account for the discrepancy in the argon concentration, found in the evaporated films grown with and without the presence of the discharge. Here, no voltage is applied to the target and hence no high energy sputtered and reflected ions and neutrals are created at the target.

LEE[187], when comparing the gas concentration found in tungsten films, grown in triode and diode sputtering arrangements, has proposed other mechanisms whereby argon may be sorbed at the surface of ZB films. He suggested that the sorbed argon arises from the large population of low energy ions in the supplementary discharge column, which is maintained by the thermionic cathode, in a triode system. For the low discharge pressures used ($\sim 6.10^{-4}$ torr), an anode voltage of about +90 V is required, to draw an electron current of about 1 ampere, through the confined discharge column.

Depending on the exact position of the substrate in this column, ions in the vicinity of the substrate should have energies at least in the order of tens of volts, and probably around 30 to 60 eV. Exactly how these low energy ions contribute to the gas incorporation, is not known, but two mechanisms can be considered. The first, suggests that whilst most ions undergo Auger neutralization near the surface[10], some may still remain ionized, or, at least, be in an excited state when they collide with the surface. For this reason, they may have a longer residence time on the surface of the film, because of their higher activation energy for re-emission, than neutralized argon atoms of equivalent kinetic energy. The flux of metal atoms which is continuously arriving at the same time may cause a proportion of the gas to be buried and trapped in the film. The second mechanism arises because, although the sticking probability for argon ions, of energies up to 60 eV, is low, their large population makes it possible for at least some of them to be trapped. Furthermore, if the low energy argon flux impinges on previously sorbed gas atoms, in a 'knock-on' process, there is a possibility that this will further increase the trapping probability for those gas atoms. These processes, whilst suggested to explain the gas concentrations found in the evaporated ZB films, may equally well occur for the sputtered films. However, their effect, in most cases, is likely to be overshadowed by the larger effect produced by the reflected and sputtered gas atoms, arising at the target. Nevertheless, in almost every case where a positive voltage bias (+50 V) was applied to the sputtered films, a reduction in the gas content resulted. This indicated that, to some extent, there was a real possibility that the processes suggested by Lee were taking place. It must be pointed out though, that the application of a positive bias can also cause re-emission of gas through substrate heating and/or desorption,

induced by electron bombardment[252] However, with temperatures less than 100°C (at a water-cooled substrate) and low energy electron bombardment (∿ 50 eV), little gas desorption should take place by these mechanisms.

An estimate of the energy possessed by the neutrals, reflected from a metal surface, has been given in section 2.4.1. When the ion scattering was characterised by two atom binary collisions, it was found that, for argon ions of 1600 eV energy incident on a nickel surface, the reflected neutrals should possess an energy amounting to as much as 20% that of the incident ions. Furthermore, using as an example KORNELSEN'S[198] result of 0.4 for the reflection coefficient of argon ions, (in his case, incident on a tungsten filament) a qualitative estimate can be made of the number of energetic neutrals reflected from the target. In the present experiments, an ion current of about 0.8 mA cm^{-2}, measured at the target, (this was not corrected for secondary electron emission, and so may be high by about 10%[9]) gives a value of 5.10^{15} ions cm^{-2} sec^{-1} impinging at the target, which in turn, yields about 1.25 10^{15} energetic reflected neutrals cm^{-2} sec^{-1}. It is difficult to determine the number of these which will actually reach the growing film. Assuming that they all did, then for tungsten, with a deposition rate typically about 5.10^{14} metal atoms cm^{-2} sec^{-1} and using a sticking probability of about 0.1, a concentration of about ∿ 2 atomic % should be obtained at zero bias. This value is higher than is generally observed. In practice, the reflection coefficient, surface coverage, energy distribution, number of reflected neutrals and deposition rate, will be different for different target voltages, ion/target masses, target materials and angles of incidence. Although the angle of incidence is nominally normal to the target surface, the state of the surface after prolonged sputtering makes this impossible.

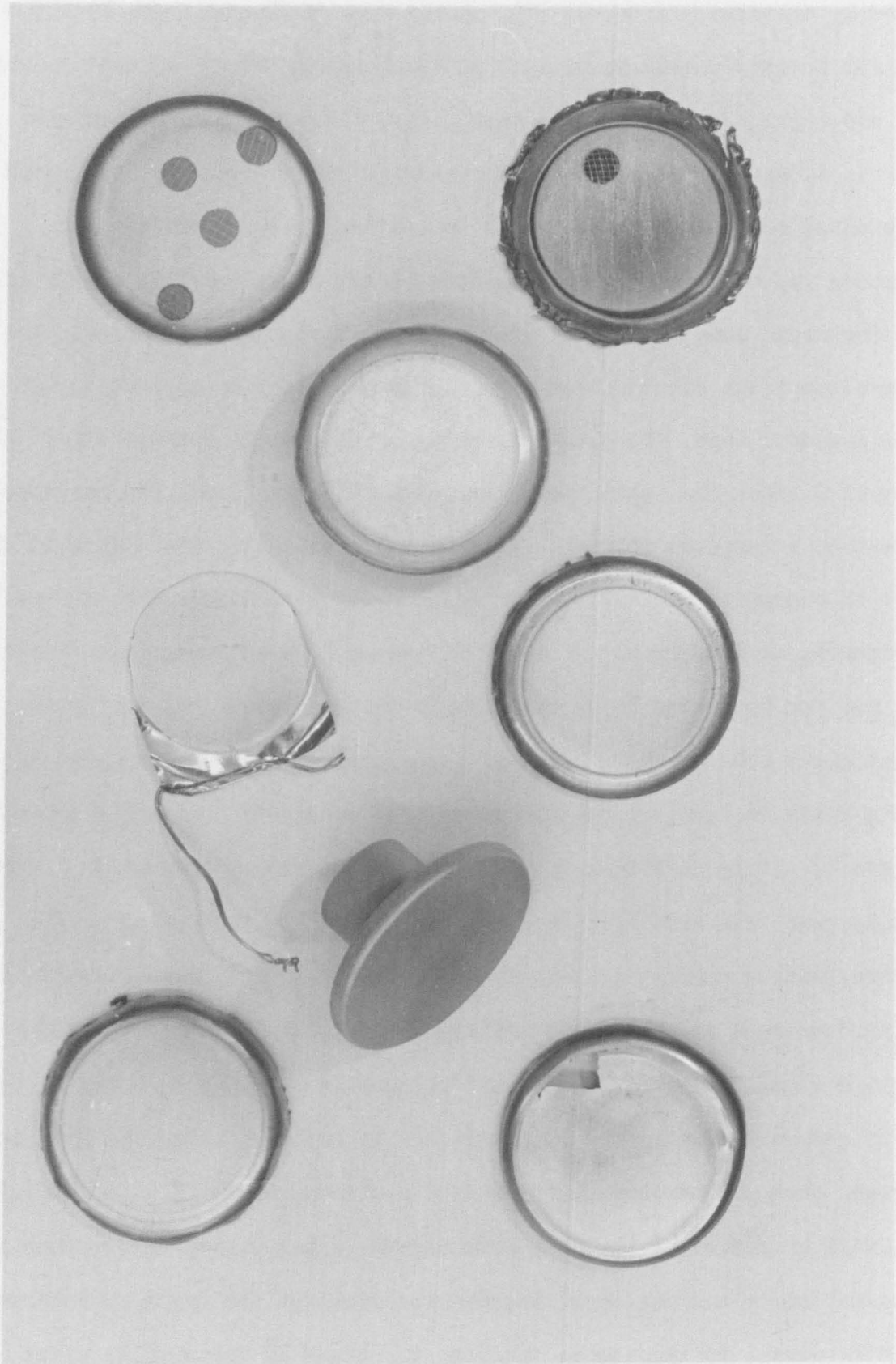

Figure 6.32

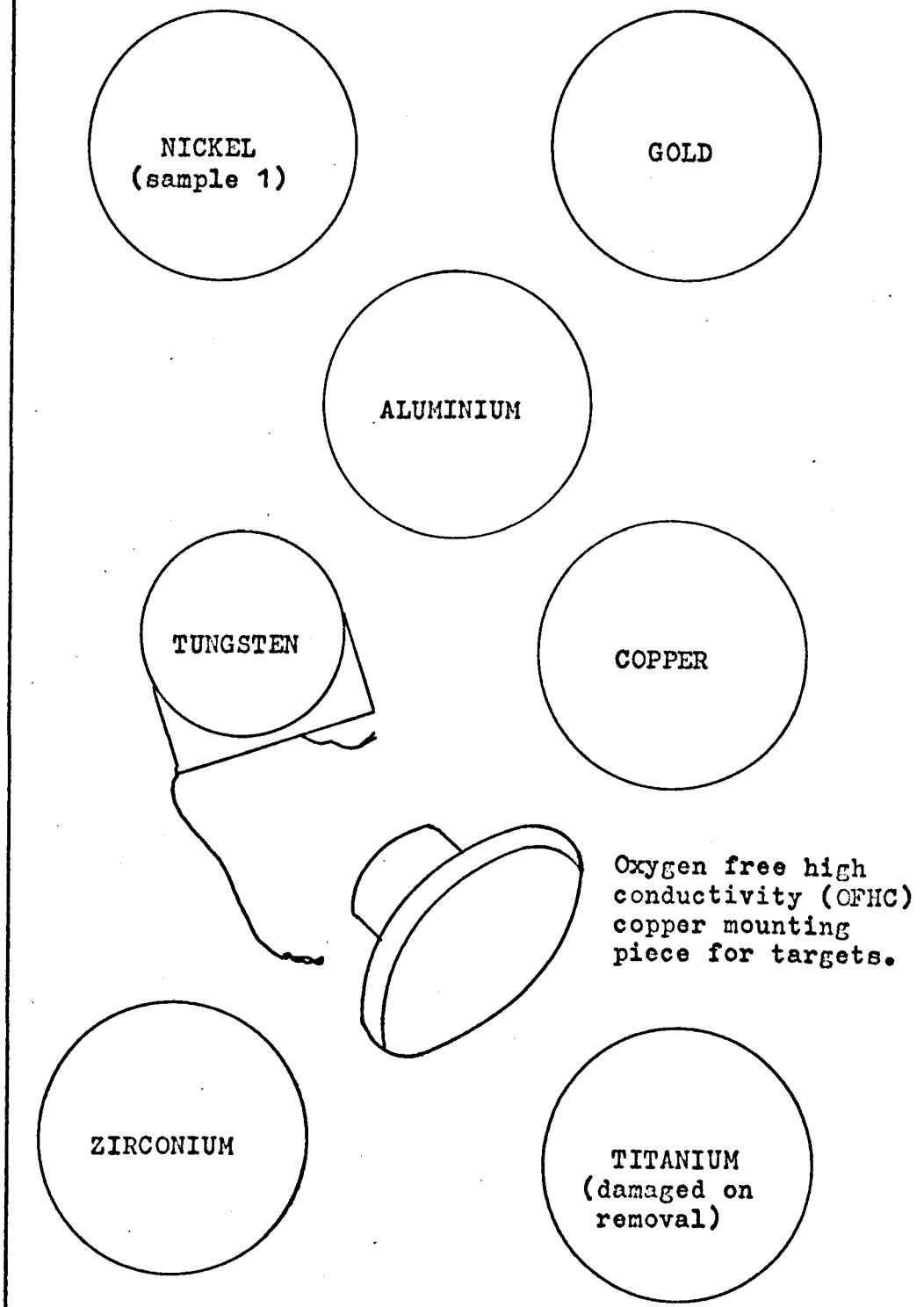

Figure 6.32 Sputtering targets.

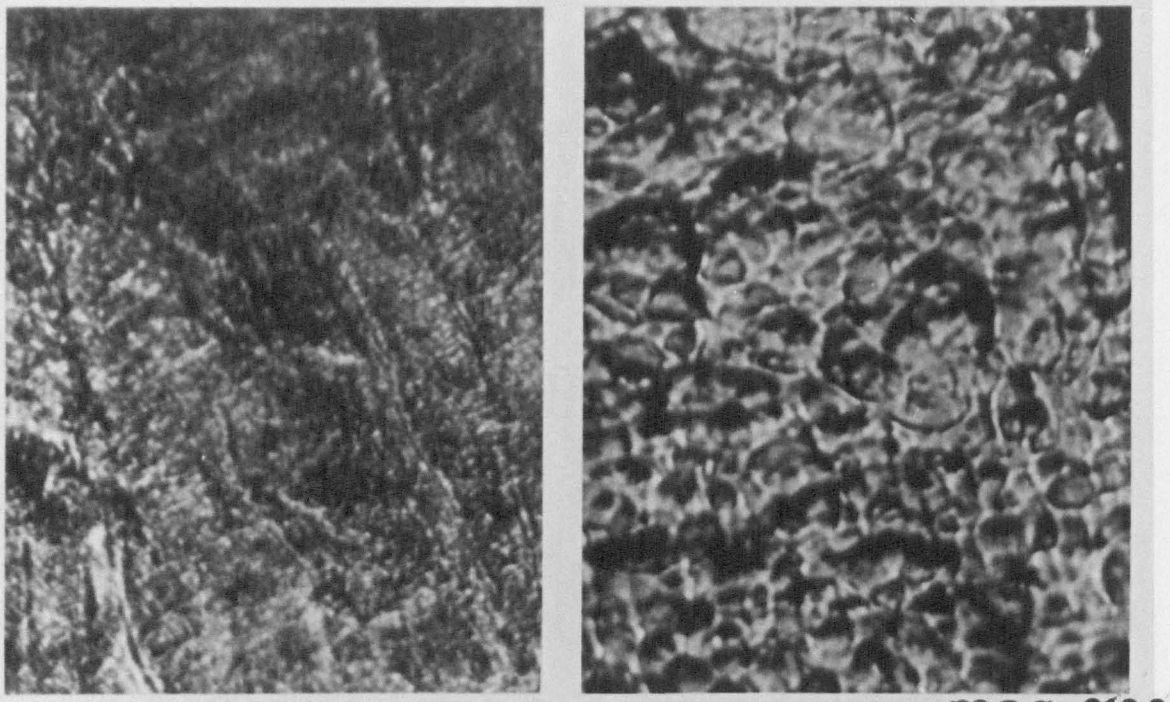

a)↕ COPPER b)↕ mag x2100

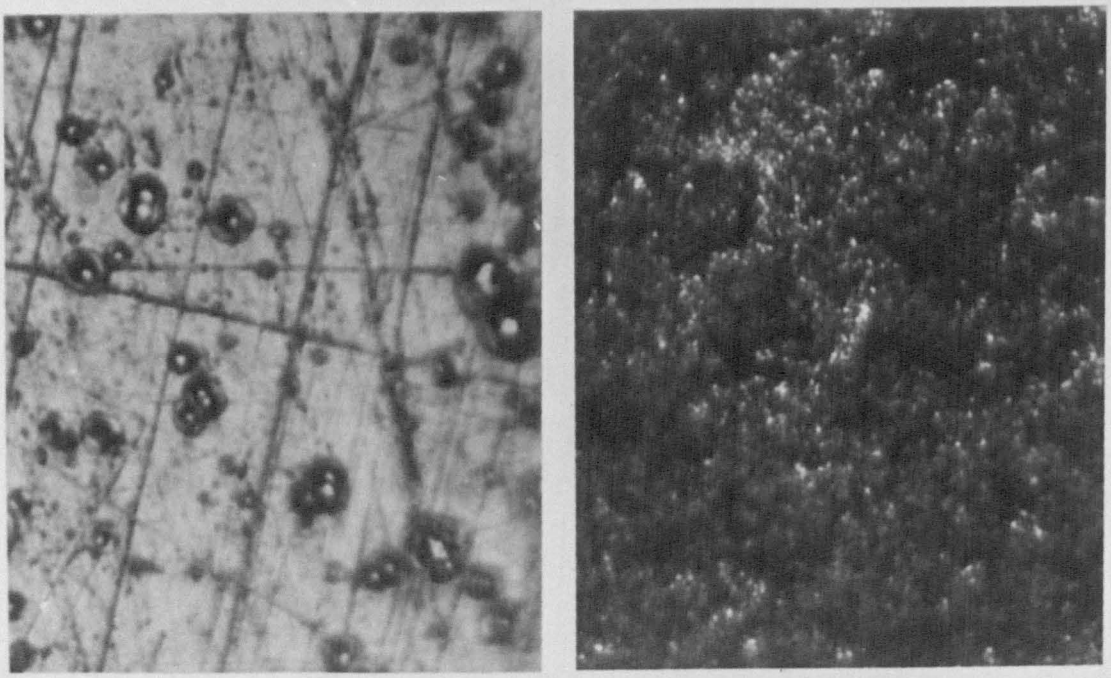

ALUMINIUM

figure 6.33
Target surface a)before & b)after sputtering

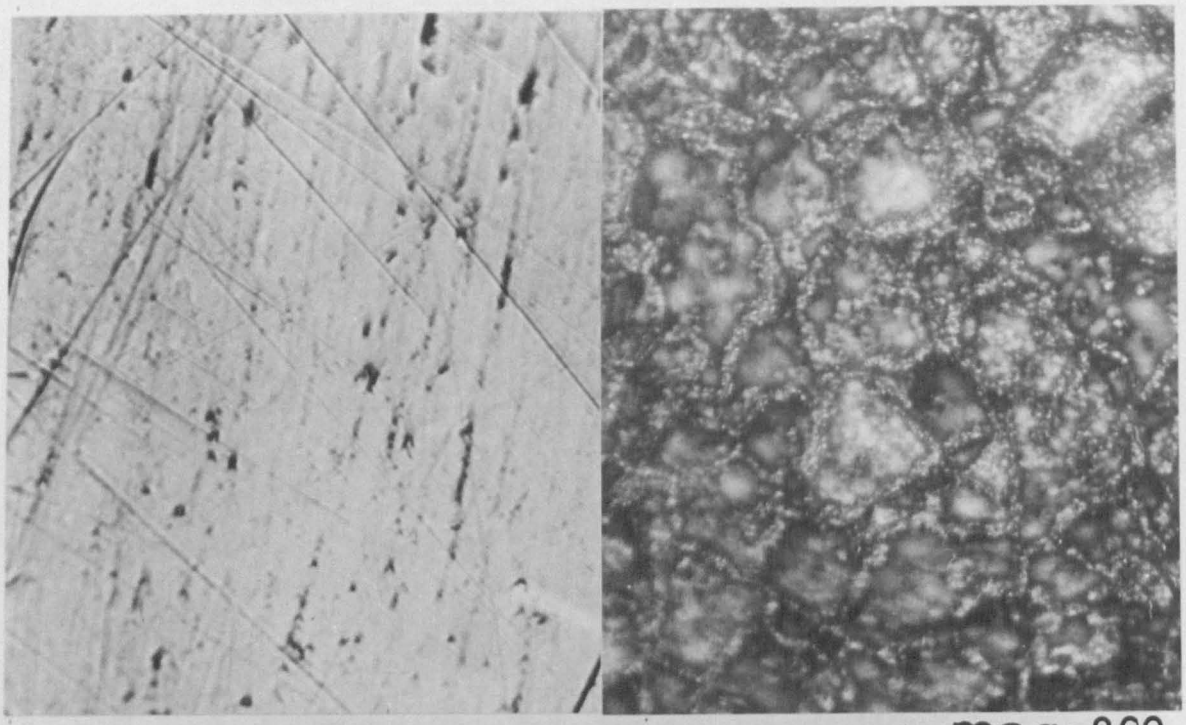

figure 6.34
Target surface a) before & b) after sputtering

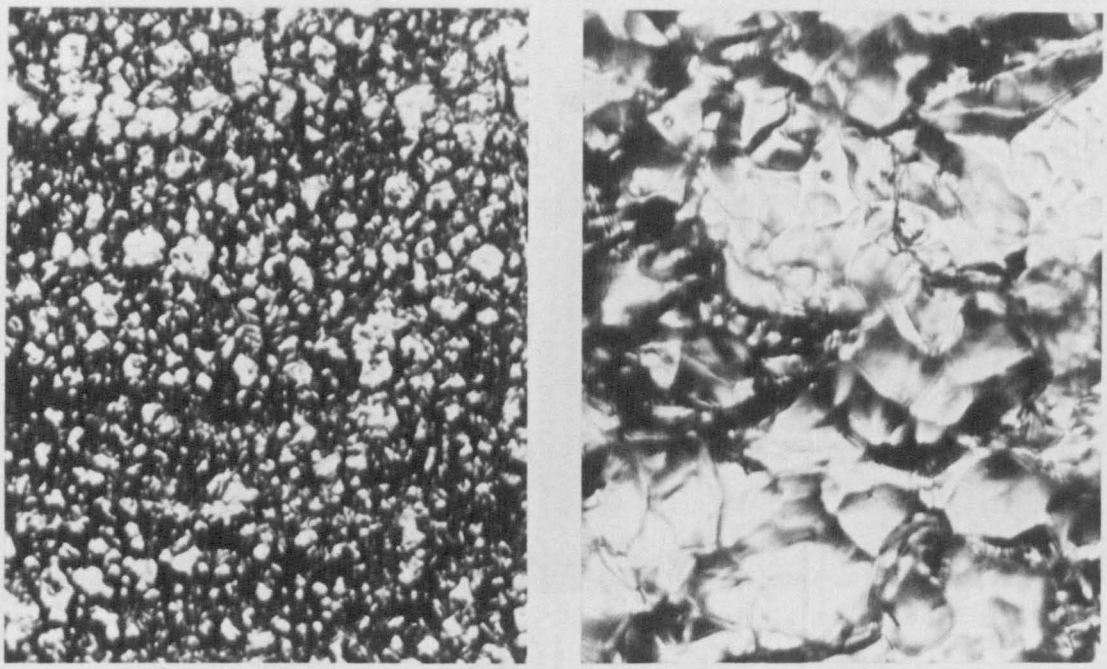

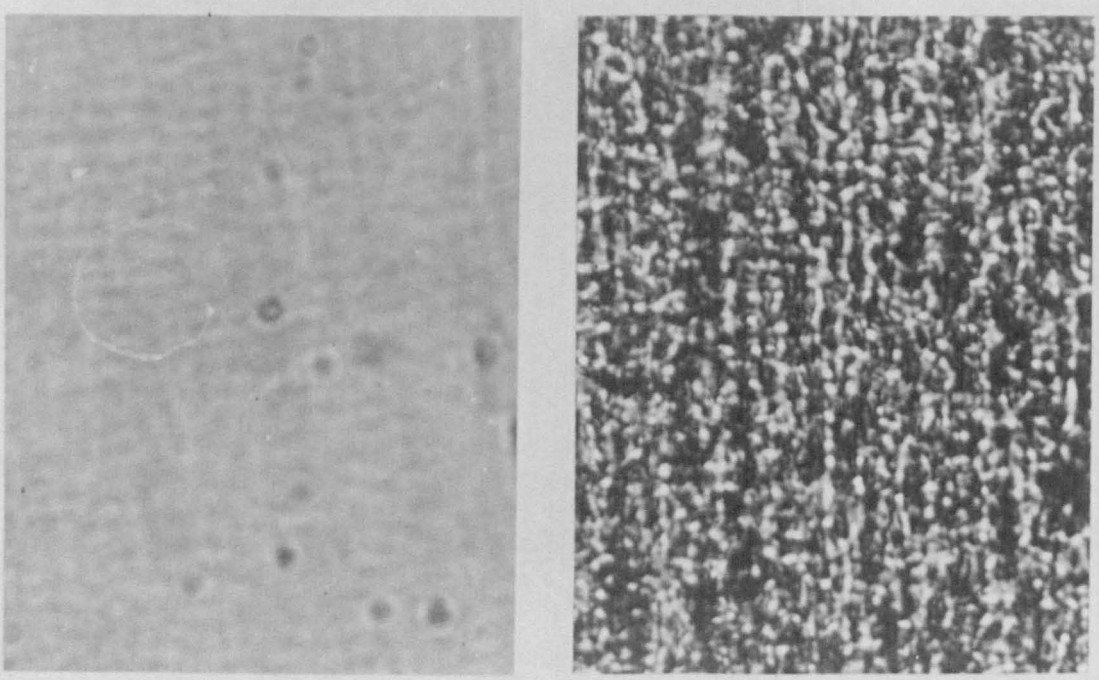

figure 6.35
Target surface a) before & b) after sputtering

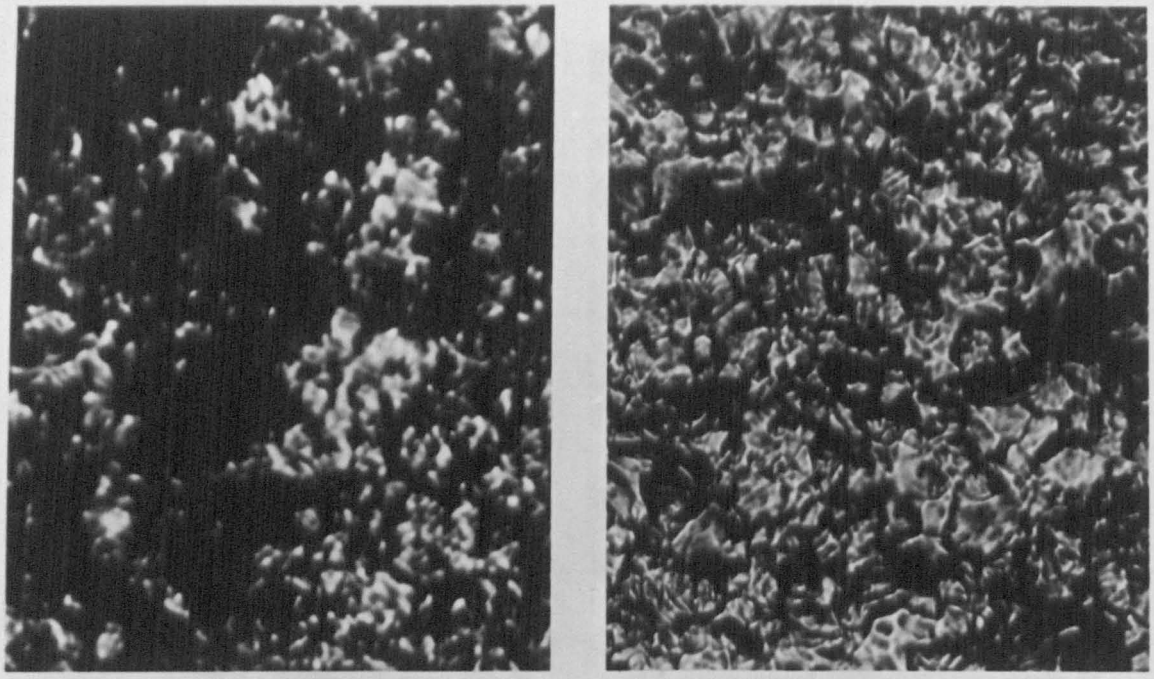

a)↕ ZIRCONIUM b)↕

mag x2100

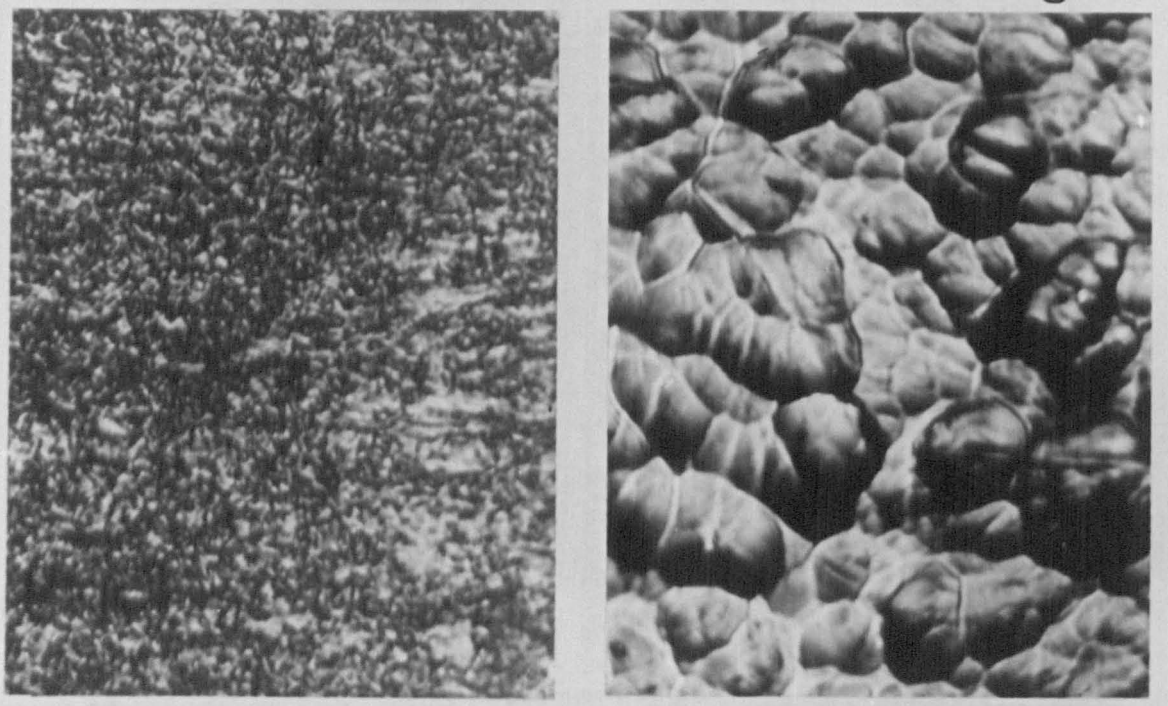

TITANIUM

figure 6.36

Target surface a) before & b) after sputtering

The target surfaces, see Figure 6.32, were examined using a Vickers microscope, and are shown in Figures 6.33-6.36. A magnification of x1500 was used in all cases, except where indicated.

The state of the target surface before sputtering is also shown for purposes of comparison. It can be seen that the surfaces were significantly rougher after prolonged sputtering. This roughness should have a strong effect both on the measurement of the ion current density, because the real surface area will be larger than the geometrical area, and on the angle of incidence and 'reflection' that the ion and reflected neutral trajectories make with the surface. Under these circumstances, only a proportion of the neutrals will find themselves actually at the surface of the growing film. As a rough estimate, assuming uniform reflection of the ions through a hemisphere (it is well known that the distribution of material sputtered from a polycrystalline target follows a roughly cosine distribution[7]) and with target to substrate distance of 6 cm, this yields $\sim 10^{13}$ neutrals cm^{-2} sec^{-1} at the substrate, leading to concentrations of $\sim 10^{-1}$ atomic %. This calculation, however, is rather too pessimistic and a value somewhat higher would be expected in practice.

A summary of the average argon concentrations found in the zero bias films are given below:-

Atomic % Concentration

Al	Cu	Au	Ni	Ti	W	Zr
		SPUTTERED				
2.10^{-1}	4.10^{-1}	2	5.10^{-1}	9.10^{-1}	4.10^{-1}	8
		EVAPORATED				
6.10^{-2}	6.10^{-2}	6.10^{-2}	$<2.10^{-2}$	4.10^{-2}	-	-

For the sputtered films, it is interesting to note that gold, which gives, on the basis of binary collisions, one of the highest values for the energy and hence sticking probability of the reflected argon neutrals, as well as having the highest atomic weight and density, has also the largest amount of argon incorporated at ZB. Whereas, aluminium, which has the lowest atomic weight and density and a small sputtering yield, contains the lowest concentration of argon at ZB. It is difficult to find reasons for the very high concentrations found in zirconium films at ZB, although these results must be treated with some caution because of (a) the extremely reactive nature of this metal with active gases,

and

(b) because of the previously mentioned inaccuracy in the concentration measurements, see section 6.4.6.

With increasing pressure, the mean free path of the reflected noble atoms will decrease, and it would be expected that through collisions, their energies would begin to approach thermal values, with correspondingly small sticking probabilities at the film surface. The result is that the argon concentration in ZB films should decrease with increasing pressure. This was observed experimentally, for example, in Figure 6.26 as well as for films grown at -100 V bias as seen in Figures 6.19. This leads to the slightly surprising conclusion that, other things being equal, purer films can be obtained by working at higher, rather than lower, argon pressures (at least within the pressure limits used here).

Increasing the target voltage should increase the energies of the reflected neutrals. However, this will be at the expense of their numbers, which will decrease with increasing voltage, because their sticking

probability at the target surface will increase at higher bombarding energies (up to a limit of ∿ 0.6 above a few keV's, from Kornelsen). The final gas content will then depend on which effect is predominant, for a given target voltage, as seen in Figure 6.21.

6.5.2. Argon incorporation with voltage bias.

If a film, deposited by sputtering or evaporation, in a triode sputtering system, is given a negative voltage bias relative to the plasma, a positive ion sheath is formed around it. This ion sheath is exactly the same in nature as the Langmuir dark space, which is found around the sputtering target, and which was described in chapter 2. The entire bias voltage is dropped between its outer edge and the film surface. Ions from the plasma, arriving at the edge of the sheath, will be accelerated across it. These will hit the growing film with an amount of energy related to the bias voltage. Provided that the argon pressure is low enough, no collisions will take place within the Langmuir dark space, and the ions will possess the full bias volt energy. As with the target, there will be a probability, related to the incident ion energy, that the ions will be sorbed at the film surface. However, in contrast with the target, these ions may be buried and trapped in the film by the continuous flux of metal atoms arriving at the same time, from the evaporating or sputtering source, at the surface. Thus the large increase in the argon concentration, with increasing voltage bias, can be related to the burying of energetic argon ions, of increasing energy, in the film. This effect will be apparent for both the evaporated and the sputtered films, as seen for all the metals investigated, and, for example, in Figures 6.20 and 6.23. This explanation is, more or less, that invoked to explain the 'gas clean-up phenomenon',

observed for noble gases on metal surfaces, maintained at negative potentials and in the presence of a gas discharge.

At the same time, re-emission of gas and metal atoms can take place by resputtering, and re-evaporation processes, brought about by the flux of energetic bombarding ions and enhanced through diffusion, knock-on collisions and reflection mechanisms. The net amount of trapping will depend on all these factors, although more on some than others, depending on the exact circumstances in which the films are deposited.

It was postulated (see chapter 2) that a sputtering yield could be associated with the gas, as with the solid target. It was further suggested that the magnitude of this quantity might be used as a means of determining which of two theoretically proposed processes was taking place:- gas release through a specifically gas sputtering mechanism, or gas release through a target sputtering and erosion mechanism, or both. This is quantitatively discussed, albeit tentatively, on the basis of the Winters model, in the following section. The sputtered films have, in all cases, larger amounts of incorporated argon than the evaporated ones. This may be explained, at least in part, by including the additional processes taking place at the sputtering target, which were described in the previous section. In addition, the differences in energies, with which the sputtered and evaporated metal atoms are known to arrive at the substrate [252], and their respective binding energies on forming the film, may go some way towards explaining the differences found.

A tentative study was made, of some of the sputtered and evaporated films, using an electron microscope,

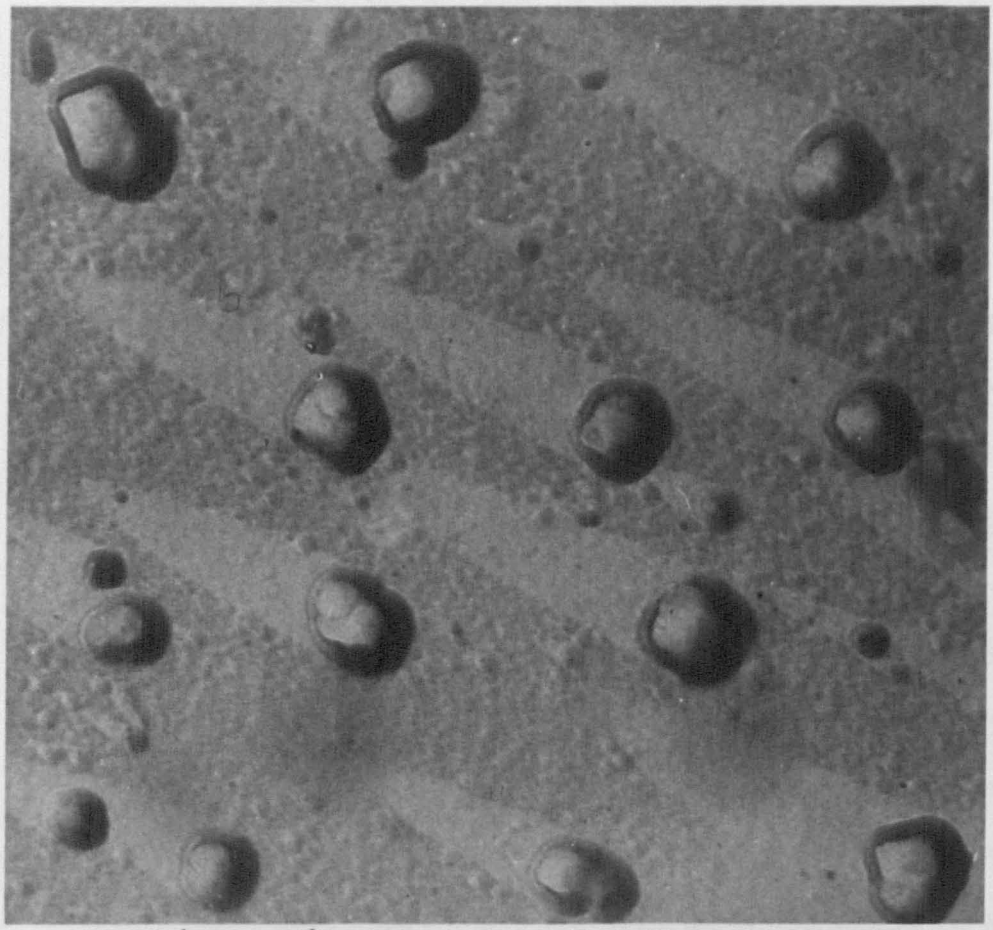

shadowed mag x72,000
not shadowed mag x72,000

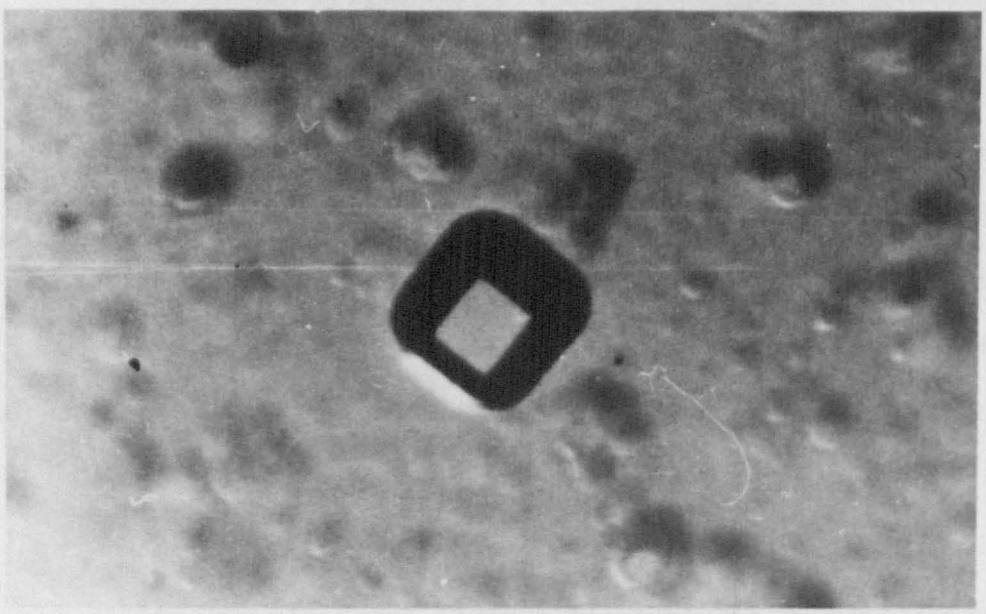

figure 6.37 Sputtered and outgassed nickel on glass

in an effort to explain on the basis of surface structure the discrepancy found in argon content between these two types of film.

It is well known[254] that sputtered atoms impinge on the substrate with energies much higher than do evaporated atoms and, by so doing, may effect the surface of the growing film. For example, BOVEY showed[252] that the crystallite size of sputtered gold films was larger than for evaporated films. If the evaporated films were rougher than their sputtered counterparts, it might be more difficult for the argon to be sorbed. At the same time, it might be easier for any argon that was sorbed, to be released, either by the effect of the ion bombardment (since the sputtering yield is higher for larger angles of incidence[5]) or by trapped gas arriving, by some diffusion process, at inhomogeneities in the film. In fact, on studying the films' surfaces, with the electron microscope, it was difficult to discern much structural difference between the two types of film. This may have been partly due to the presence of the gas discharge during both types of deposition. However, when the films were outgassed prior to examination, (these were deposited on corning glass and so little or no evaporation of the film took place whilst being outgassed) some interesting differences in structure were observed, for some of the metals.

For sputtered and outgassed nickel, Figures 6.37(a) and (b) show that some sort of 'crystallites', were present on the surface of the film. No such 'crystallites' were seen for either the non-outgassed sputtered samples or the evaporated nickel films, although the underlying 'texture' of the films was similar in all cases, to that seen in the background of Figure 6.37(a). The 'crystallites', which appear to be of cubic shape (in plan) were from 500 to 1000 Å across and less than about 100 Å high

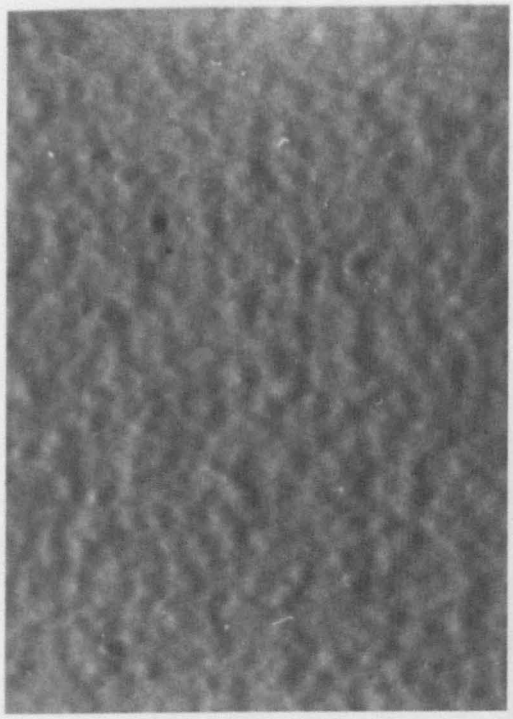

mag 50,000x
SPUTTERED
& NOT OUTGASSED

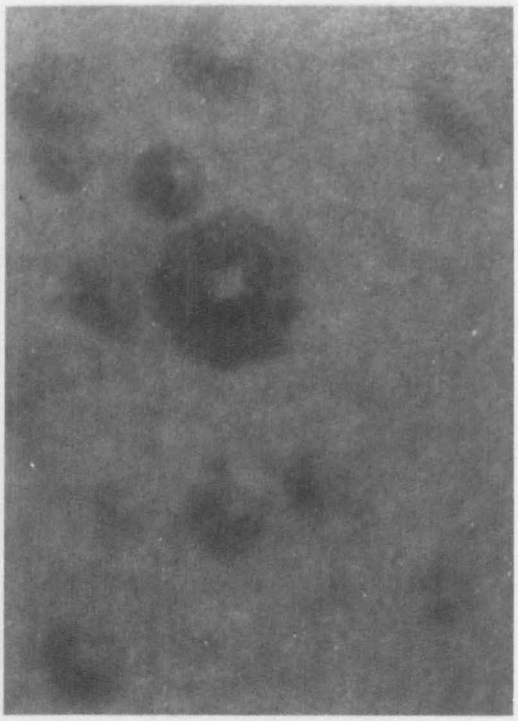

mag 80,000x
SPUTTERED
& OUTGASSED

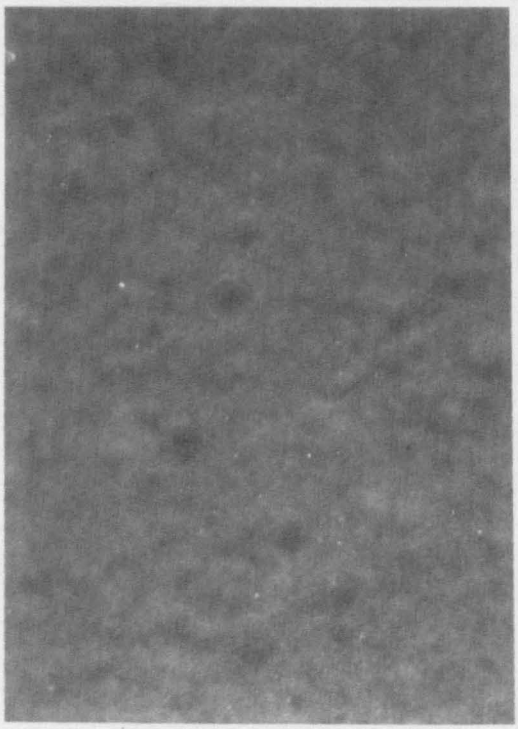

mag 64,000x
EVAPORATED
& NOT OUTGASSED

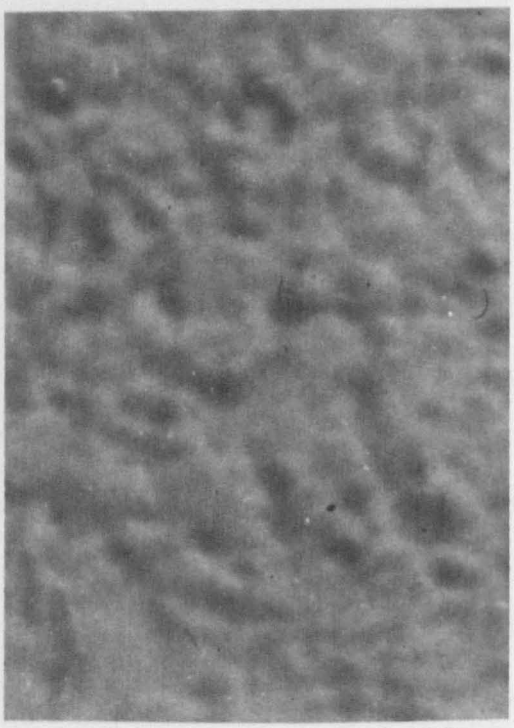

mag 72,000x
EVAPORATED
& OUTGASSED

FIGURE 6.38 GOLD ON GLASS

(determined from a shadowing experiment). The surface profile appeared to be similar to that shown below:-

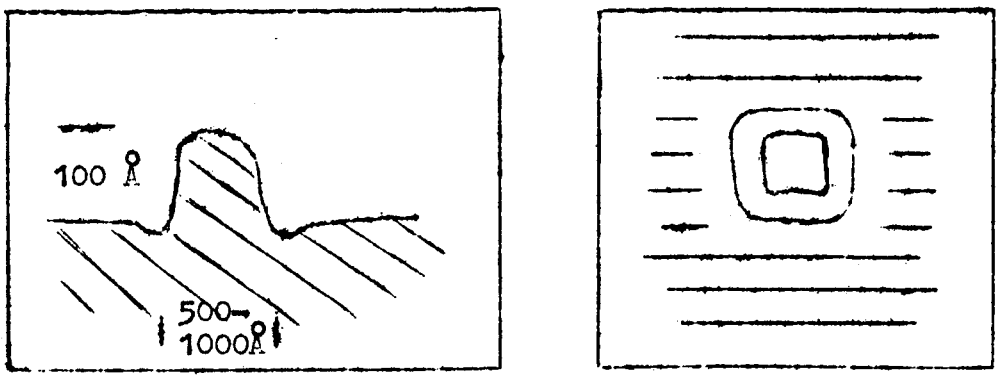

Section Plan

They were also fairly evenly distributed across the surface with a number density of about $2. 10^{+8} cm^{-2}$. There was a similar, although not nearly so prominent, indication of 'crystallites' for sputtered and outgassed gold films, although again, no sign of them for the evaporated and non-outgassed films, as shown in Figures 6.38(a)-(d). The origins of these crystallites, if they are crystals, is not known at present. For the other metals examined; titanium, zirconium and tungsten, little or no discernible structure, or difference in structure, was found for any of the films, either outgassed or otherwise.

Since, no differences in structure were seen between the pre-outgassed sputtered and evaporated films, and a study of the outgassed sputtered films lay somewhat outside of the immediate 'terms of reference' of the present investigation, no further work was carried out on the origin and growth of these crystallites.

However , the growth of these crystallites must depend to some extent on the deposition processes involved , and it would

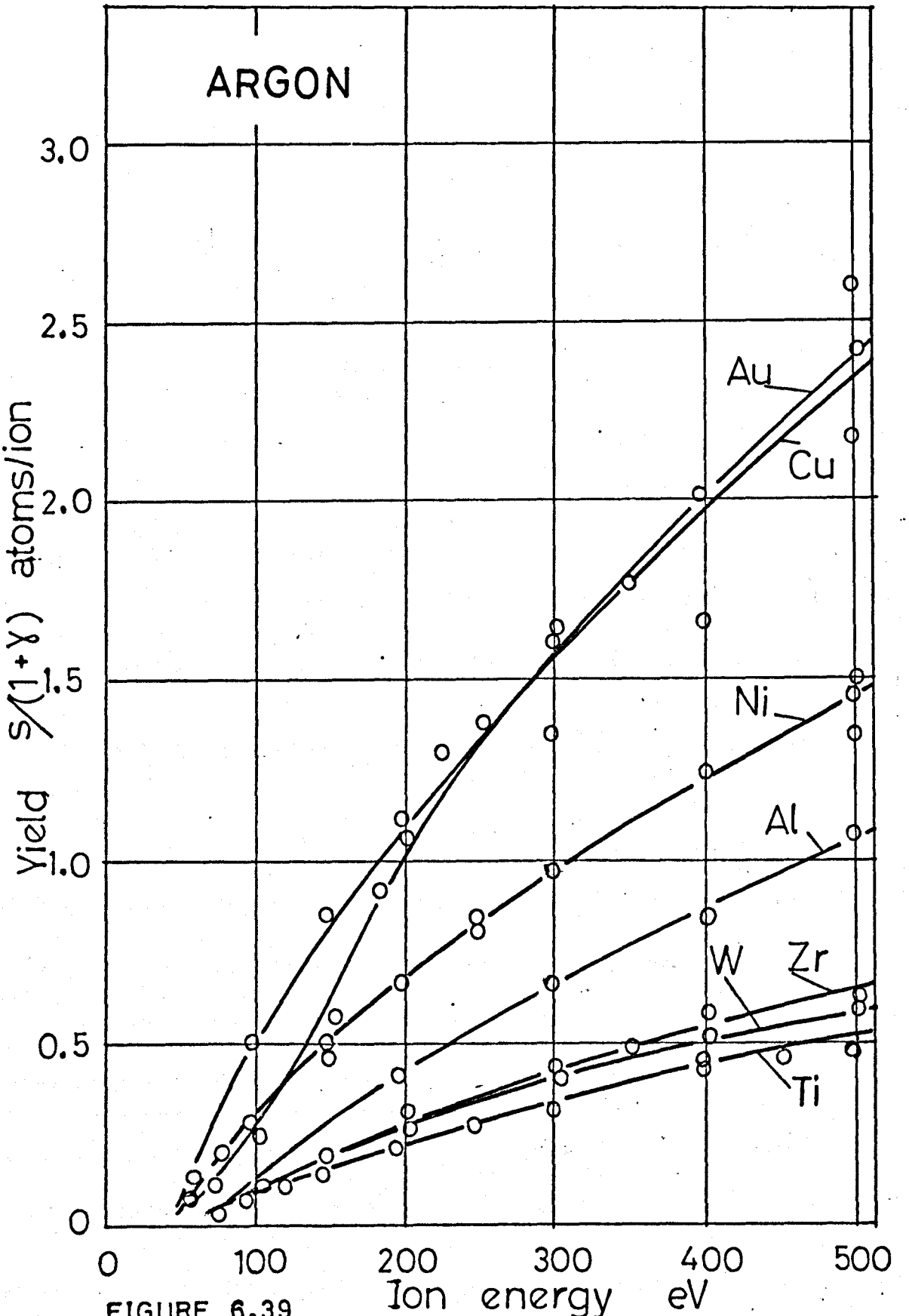
ARGON
3.0
2.5
2.0
1.5
1.0
0.5
0
Yield S/(1+γ) atoms/ion
Au
Cu
Ni
Al
W
Zr
Ti
0
100
200
300
400
500
Ion energy eV

FIGURE 6.39

appear to be an interesting and possibly fruitful line of research to follow up at a later date. This is at present being actively considered.

It can be seen, see Figures 6.17 and 6.24, that, as the voltage bias increases, the difference in concentrations is steadily diminished, and that in some cases, for example Figure 6.29, for gold, and Figure 6.20, for copper, the gas concentrations at -500 V bias are almost the same.

It is interesting to note that both these metals have high sputtering yields, compared with the other metals studied. At the higher voltage biases, the argon concentrations, in some of the sputtered metals, actually begin to decrease, as seen in Figure 6.25. The reason for this is not entirely clear, although, the higher bombarding energies may cause argon to be precipitated (by diffusion, surface damage or some gas sputtering mechanism) nearer the surface of the film, where it may be more easily sputtered. However, it might be thought that this effect would be equally noticeable in the evaporated films, which, in fact, was not so.

6.5.3 Bias sputtering - on the basis of Winters' model

A computer programme was written, in Fortran 4, based on Winters' model, described in chapter 3, to see how it compared with the experimentally determined results of argon concentration in the thin films. The model contains no adjustable parameters as such, but depends on a knowledge of measured quantities, such as the sizes of the atoms, the ion current density to the substrate and target, the sticking coefficients for the various sorbing processes, and the sputtering yields for the various atom species. The sputtering yields for the metals at low bombarding energies were obtained from those of WEHNER[219], seen in Figure 6.39.

Argon in Material	Ion Energy (eV	λ^4 Ar *	$\frac{a_1}{\times \pi^{-1} 10^{16} cm^{-2}}$	a_2	α_2 atoms ion^{-1}	N_1 cm^{-2} sec^{-1}	N_2 cm^{-2} sec^{-1}	depn rate $\mathring{A} min^{-1}$	ℓ $gm\ cm^{-3}$	Atomic wt
	0	0.0			0.0	1.80				
	100	0.05			0.05	11.85				
	200	0.10			0.20	19.30				
TITANIUM	300	0.25	2.13	2.097	0.35	21.43	5.9	66	4.54	47.90
	400	0.38			0.45	29.90				
	500	0.51			0.50	34.30				
	1100				0.85					
	0	0.0			0.0	1.80				
	100	0.05			0.05	11.85				
	200	0.10			0.30	19.30				
TUNGSTEN	300	0.25	2.13	1.88	0.40	21.43	5.36	52	19.3	183.86
	400	0.38			0.50	29.90				
	500	0.51			0.60	34.30				
	1600									
	0	0.0			0.0	1.80				
	100	0.05			0.10	11.85				
	200	0.10			0.30	19.30				
ZIRCONIUM	300	0.25	2.13	2.526	0.40	21.43	4.0	77	6.35	91.22
	400	0.38			0.60	29.90				
	500	0.51			0.65	34.30				
	1600				1.20					
REFERENCES		77	218	218	219,9a					

* for Ar^+ in nickel.

Table 6.2

Argon in Material	Ion Energy (eV)	λ^4 Ar *	a_1 / $\pi^{-1}10^{16}$ cm^{-2}	a_2	α_2 atoms ion^{-1}	N_1 cm^{-2} sec^{-1}	N_2 cm^{-2} sec^{-1}	depn rate Å min^{-1}	ℓ gm cm^{-3}	Atomic wt
	0	0			0.0	1.80				
	.100	0.05			0.13	11.85				
	200	0.10			0.43	19.30				
ALUMINIUM	300	0.25	2.13	2.05	0.75	21.43	7.4	74	2.70	26.98
	400	0.38			0.93	29.90				
	500	0.51			1.08	34.30				
	1600									
	0	0.0			0.0	1.80				
	100	0.05			0.50	11.85				
	200	0.10			1.10	19.30				
COPPER	300	0.25	2.13	1.633	1.55	21.43	16.5	118	8.96	63.54
	400	0.38			2.00	29.90				
	500	0.51			2.30	34.30				
	1600				4.0					
	0	0.0			0.0	1.80				
	100	0.05			0.25	11.85				
	200	0.10			1.10	19.30				
GOLD	300	0.25	2.13	2.08	1.60	21.43	12.7	125	19.34	197.0
	400	0.38			2.00	29.90				
	500	0.51			2.40	34.30				
	1600				5.0					
	0	0.0			0.0	1.80				
	100	0.05			0.30	11.85				
	200	0.10			0.70	19.30				
NICKEL	300	0.25	2.13	1.563	1.00	21.43	10.8	72	8.91	58.71
	400	0.38			1.25	29.90				
	500	0.51			1.50	34.30				
	1000				2.1					
	1600				2.5					

continued

A summary of the data used, obtained from a variety of sources, is given in Table 6.2.

The gas sputtering yields for argon are known for only a very few metals and only at one or two ion energies[11]. For this reason, instead of using one particular 'guessed' value, it was decided to treat the sputtering yield of argon, α_1, as a fixed ratio to that of the metal, α_2, i.e.

$$\alpha_1/\alpha_2 = n. \quad \text{where} \quad n = 1 \text{ to } 20.$$

The effect of varying α_1 is achieved, in the programme, by using a 'DO' loop so that twenty different curves are derived in the computer calculations. The two equations used are those derived in section 3.5.3: equations (14) and (5):-

$$K_1 = \lambda_1 N_1 - \alpha_1 n_i \; a_1 K_1/(a_1 K_1 + a_2 K_2)$$

and $$K_2 = \lambda_2 N_2 - \alpha_2 n_i \; a_2 K_2/(a_1 K_1 + a_2 K_2) \qquad (14)$$

and the concentration is given by :

$$C_{1/2} = \frac{K_1}{K_1+K_2} \times 100 \text{ atomic \%.} \qquad (5)$$

It is difficult for the computer to handle equations (14) in this form. Therefore by rearrangement, and using the following substitutions;

$$N_1 = \lambda_1 R_1, \quad N_2 = \lambda_2 R_2 \quad \text{and} \quad X = \alpha_2 a_2/\alpha_1 a_1$$

two equations can be obtained in terms of K_1 and K_2 only and are given by :-

$$(X-1)K_1^2 - ((2X-1)R_1 - (X-1)n_i\alpha_1 + \frac{a_2}{a_1}R_2)K_1 + R_1(XR_1 + \frac{a_2}{a_1}(R_2 - \alpha_2 n_i)) = 0 \quad (1)$$

and

$$K_2 = R_2/(1 + X(R_1/K_1 - 1) \quad (2)$$

Equation (1) is a quadratic equation in K_1 of the form $AK_1^2 + BK_1 + C=0$, and can be solved by the standard solution:-

$$K_1 = \frac{-B \pm (B^2 - 4AC)^{\frac{1}{2}}}{2A}$$

where $A = (X - 1)$

$$B = -((2X - 1)R_1 - (X - 1)n_i\alpha_1 + \frac{a_2}{a_1}R_2)$$

$$C = R_1(XR_1 + \frac{a_2}{a_1}(R_2 - \alpha_2 n_i))$$

Some of the symbols have been changed to make the calculations acceptable in Fortran 4. The corresponding symbols are listed below:

LM4 = λ^4_{Argon}, the sticking probability for argon ions on metal.

K1 = K_1, the number of incorporated argon atoms cm^{-2} sec^{-1}.

K2 = K_2, the number of incorporated metal atoms cm^{-2} sec^{-1}.

R1 = R_1, the number of impinging argon ions cm^{-2} sec^{-1} sorbed.

R2 = R_2, the number of impinging metal atoms cm^{-2} sec^{-1} sorbed.

A1 = a_1, the cross-sectional area of an argon atom.

A2 = a_2, the cross-sectional area of the metal atom.

NA = n_i, the number of impinging argon ions cm^{-2} sec^{-1}.

AP1 = α_1, the sputtering yield of argon.

AP2 = α_2, the sputtering yield of the metal.

CA1 = $C_{1/2}$, the concentration of argon atoms in the metal films.

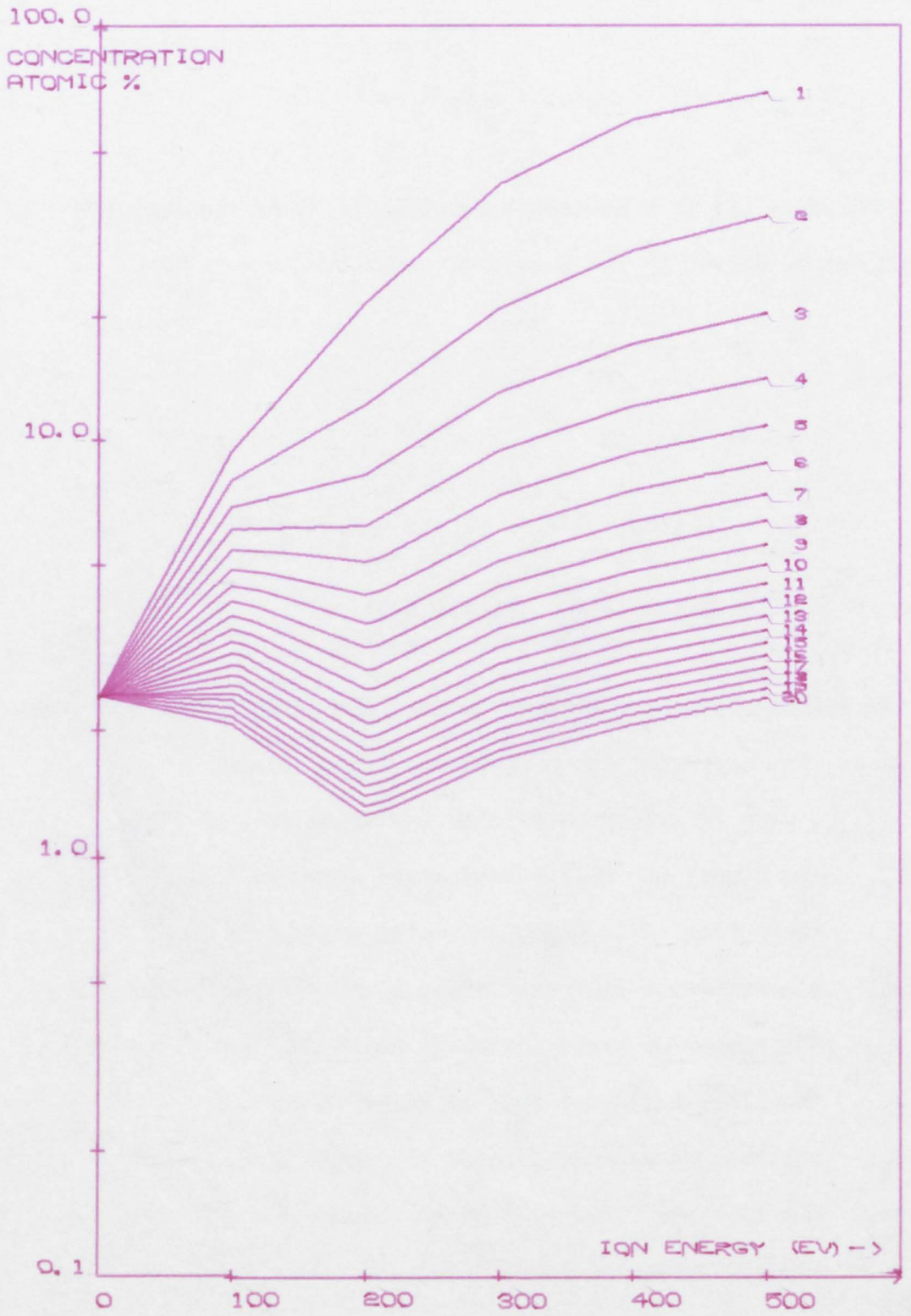

FIGURE 6.40. ARGON CONCENTRATION IN ALUMINIUM WITH VARIATION IN ION ENERGY.

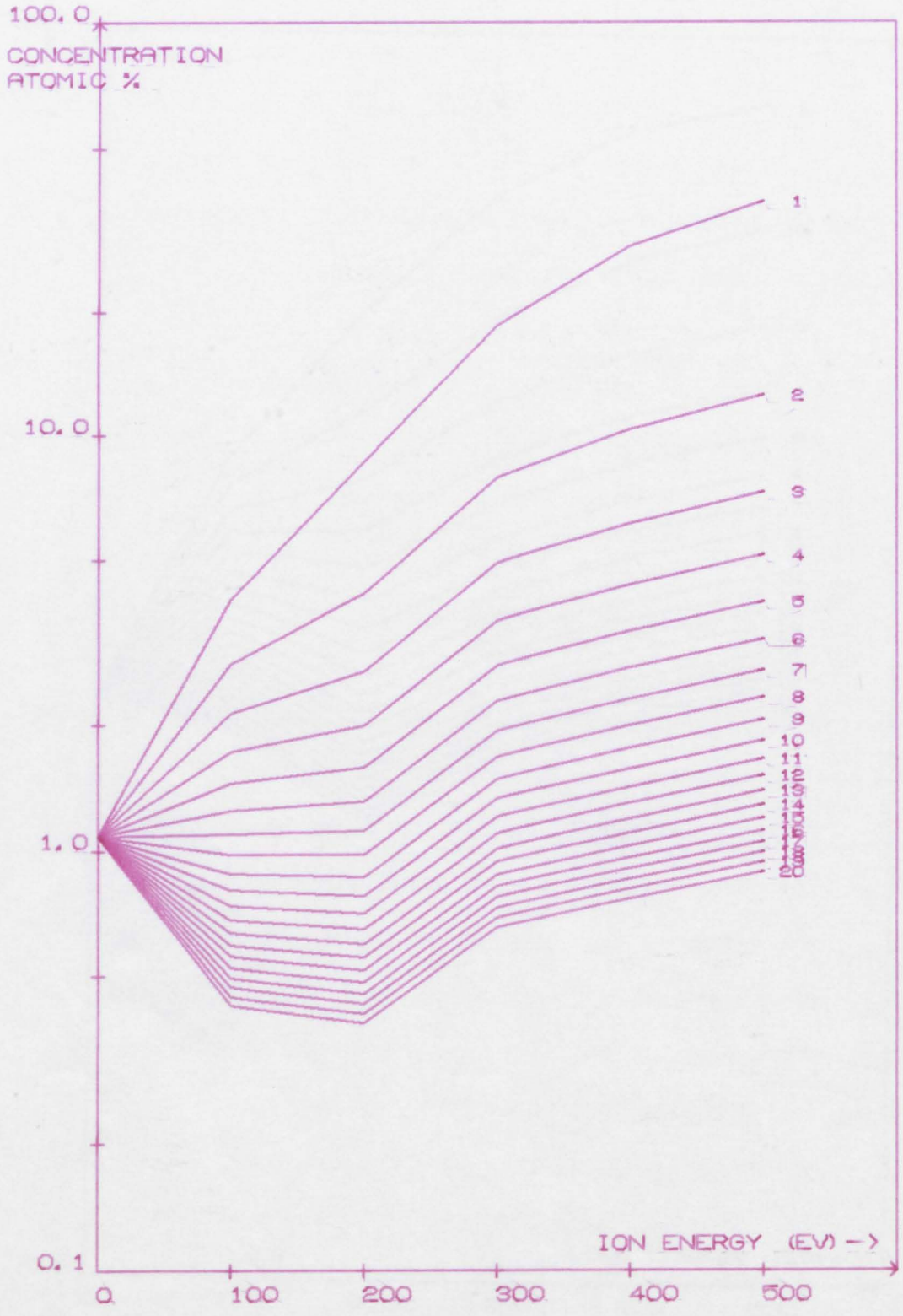

FIGURE 6.41. ARGON CONCENTRATION IN COPPER WITH VARIATION IN ION ENERGY.

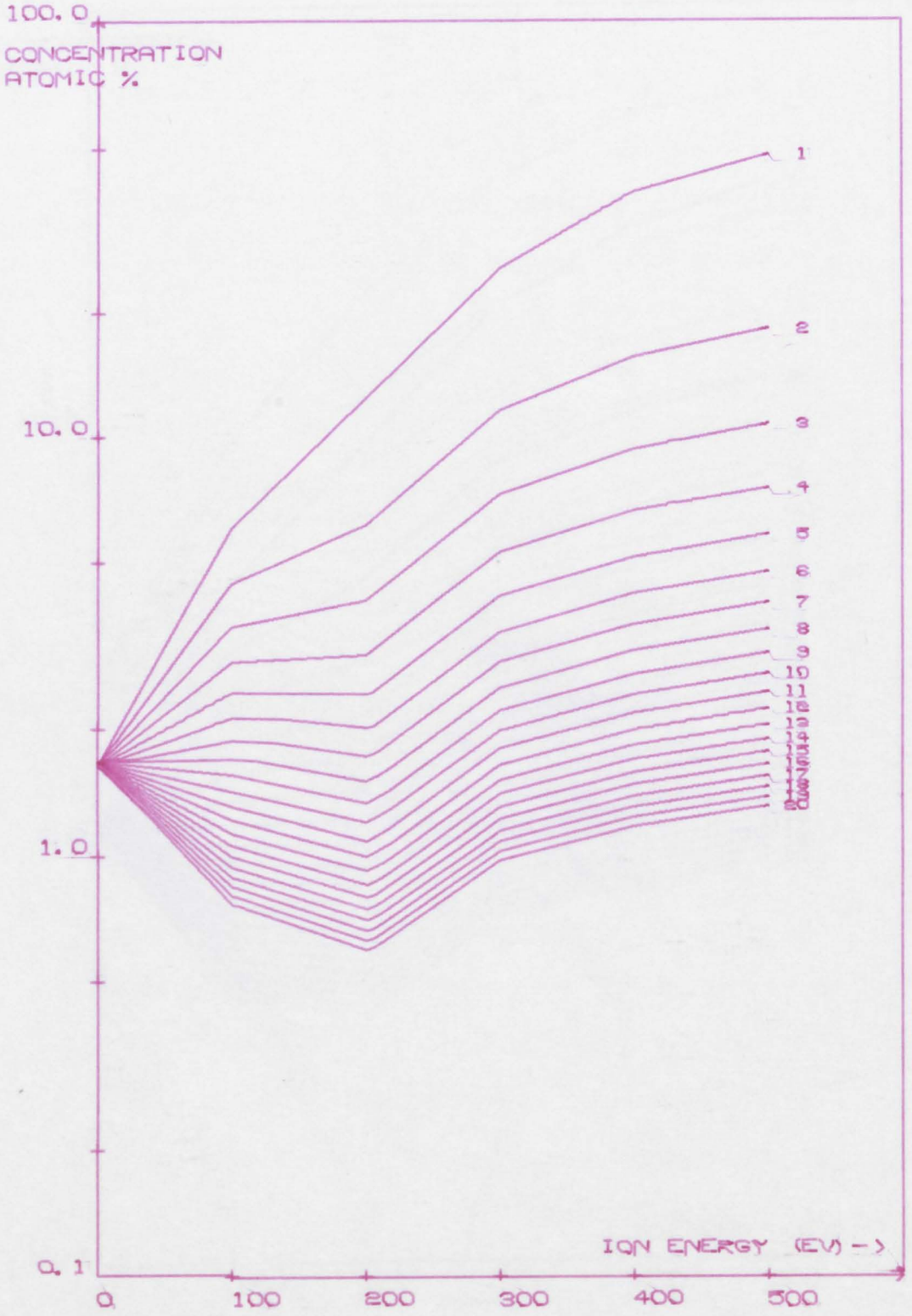

FIGURE 6.42. ARGON CONCENTRATION IN NICKEL WITH VARIATION IN ION ENERGY.

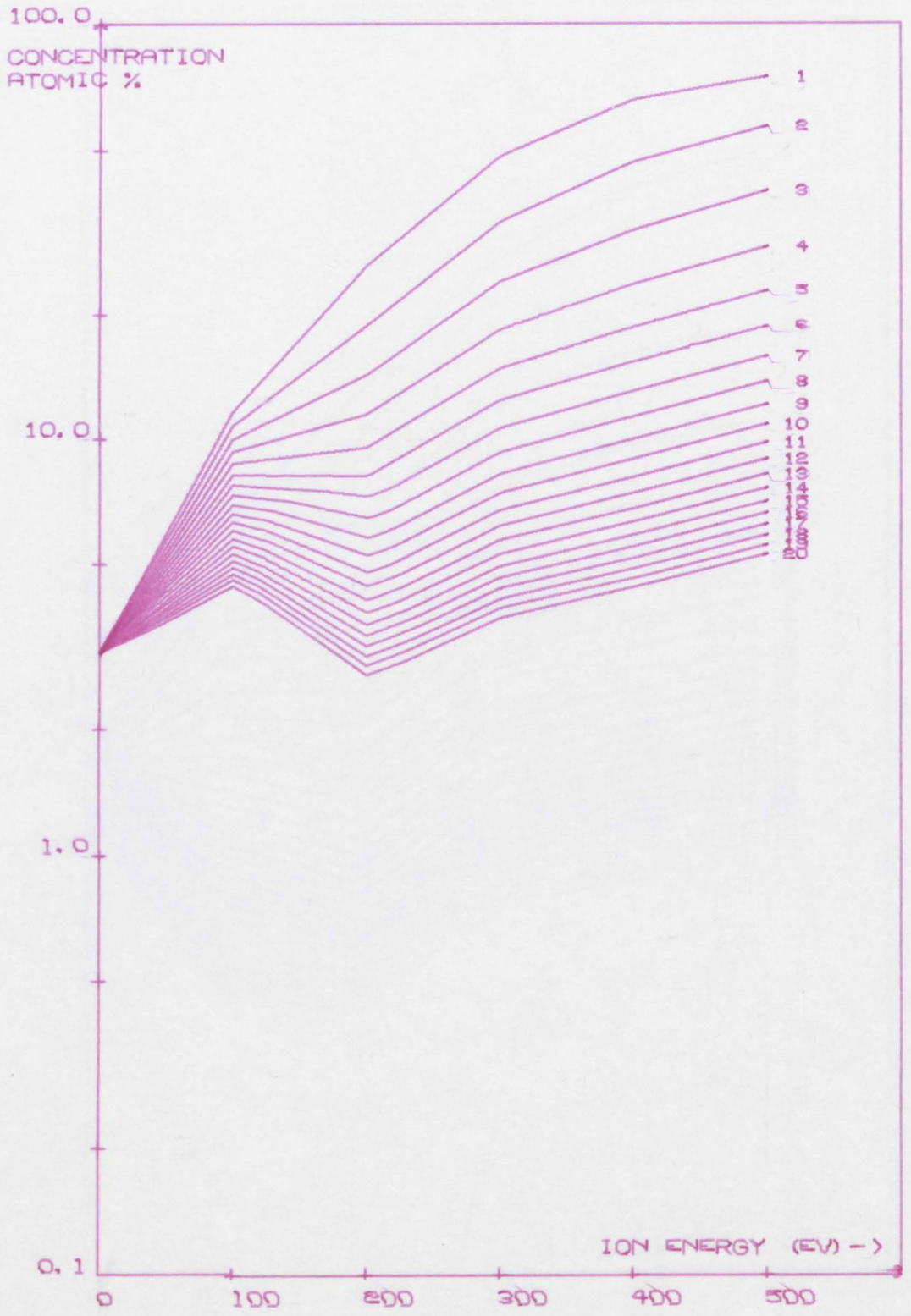

FIGURE 6.43. ARGON CONCENTRATION IN TITANIUM WITH VARIATION IN ION ENERGY.

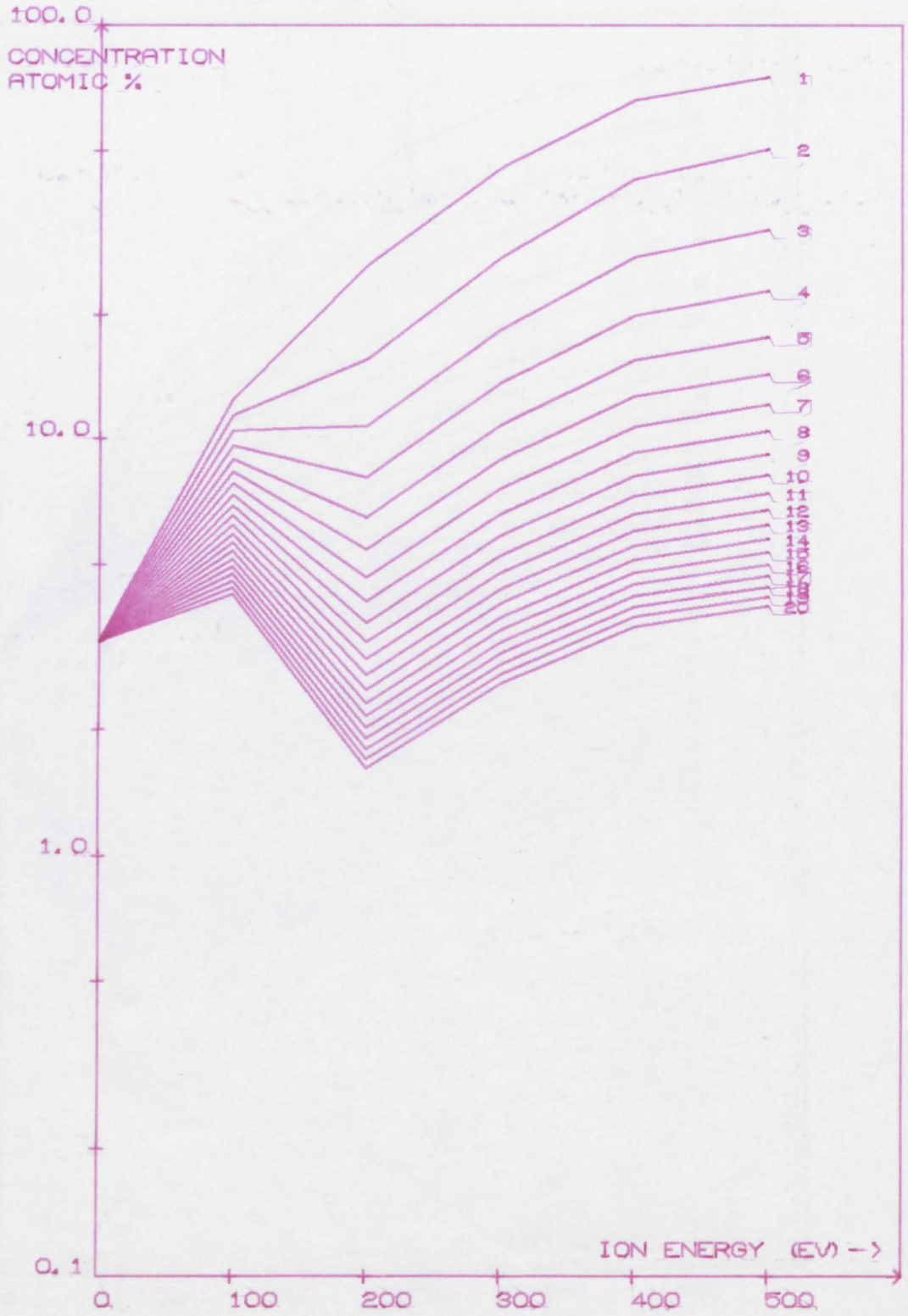

FIGURE 6.44 ARGON CONCENTRATION IN TUNGSTEN WITH VARIATION IN ION ENERGY.

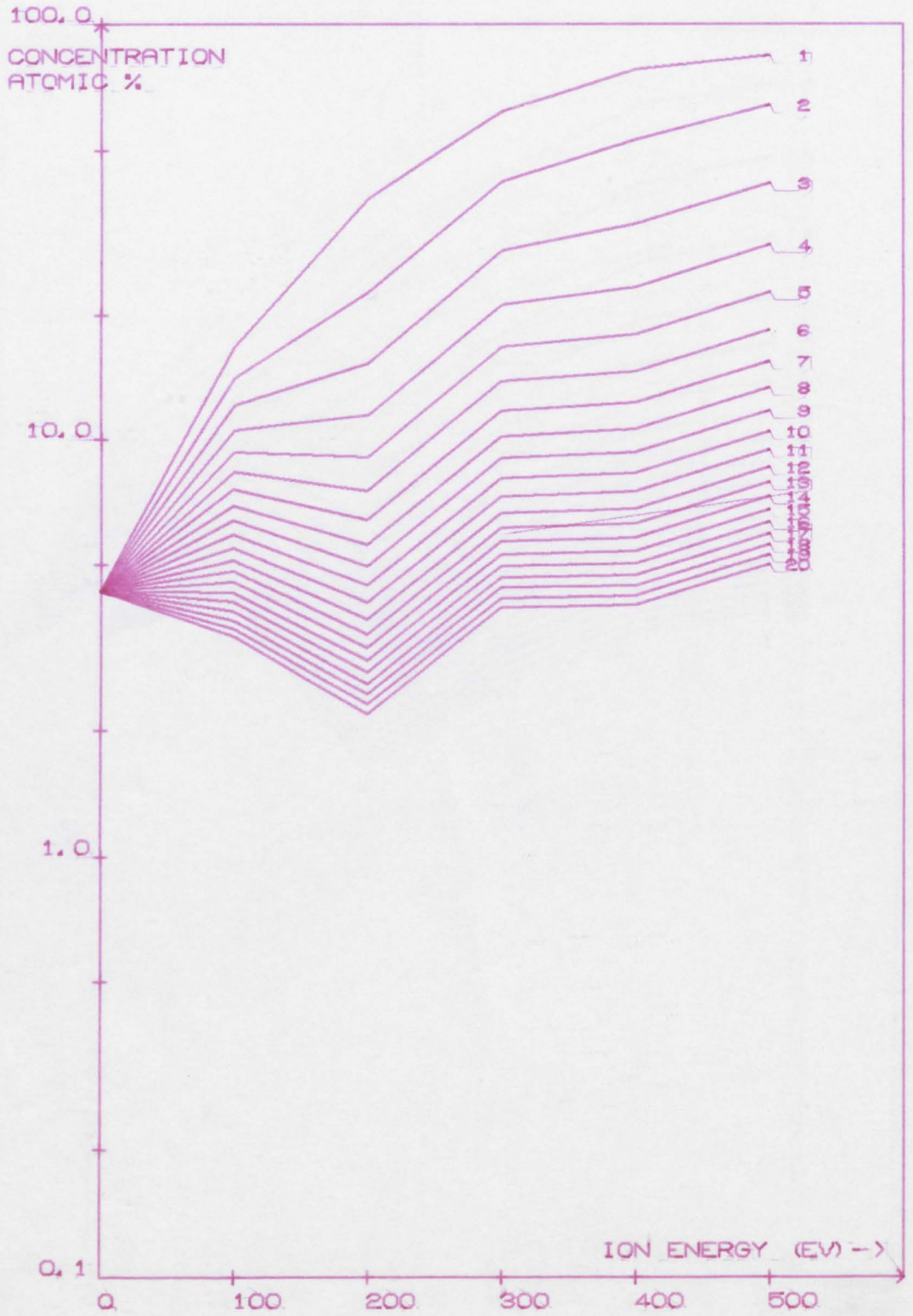

FIGURE 6.45. ARGON CONCENTRATION IN ZIRCONIUM WITH VARIATION IN ION ENERGY.

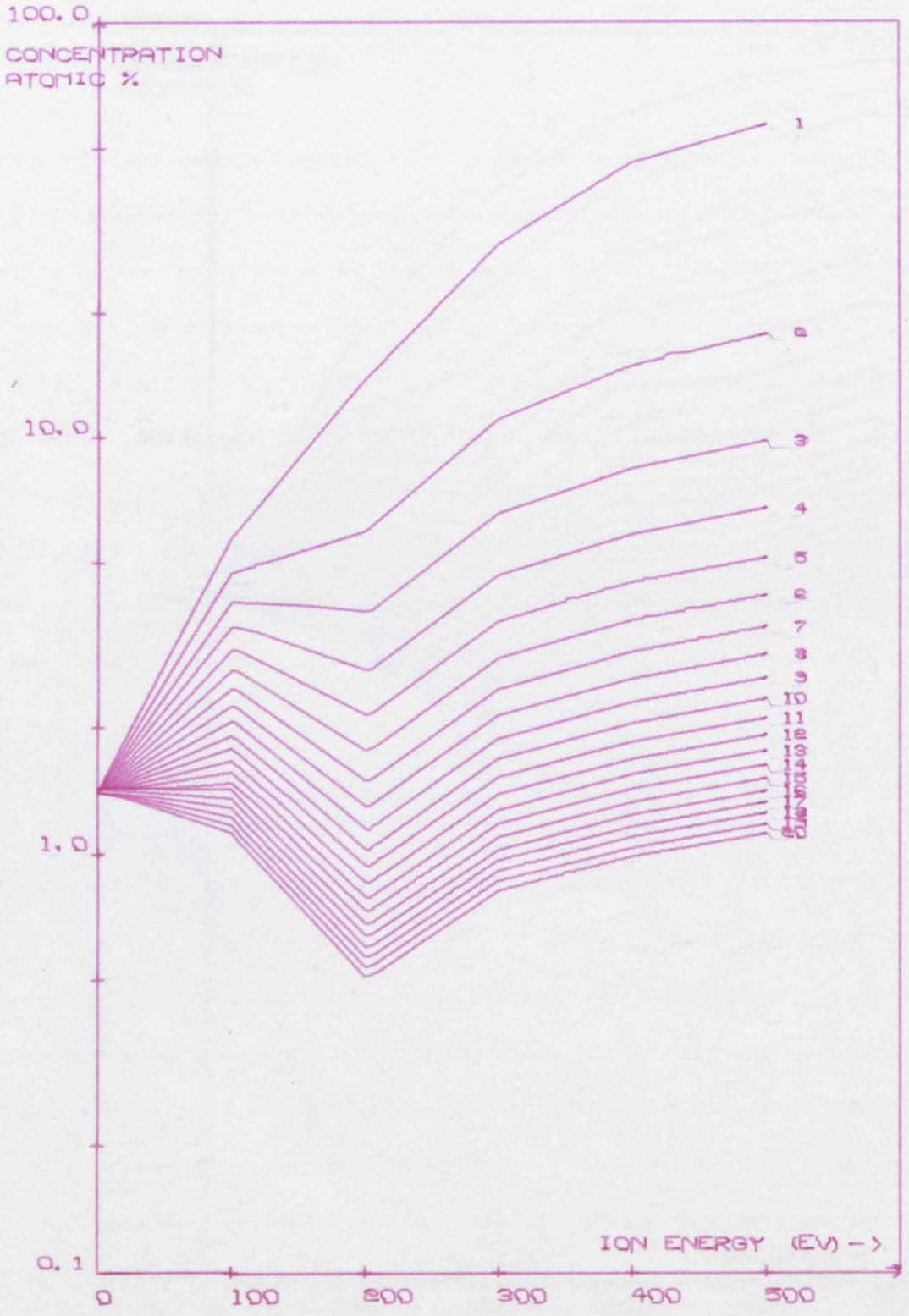

FIGURE 6.46

ARGON CONCENTRATION IN GOLD WITH VARIATION IN ION ENERGY.

The programme is given in APPENDIX E

Figures 6.40 - 6.46 show the results obtained, using the data in Table 6.2 and calculated by the computer, for the sputtered metal films.

Discussion

Although Winters' model makes no distinction between the different methods of deposition, it would appear, when comparing the experimentally determined concentrations for the evaporated films with those predicted from the model, that very little agreement can be found between them. It must be presumed from this, and from the earlier discussions, that Winters' model does not hold for evaporated films, with or without voltage bias. This may be, because re-evaporation of argon (see page 63, equation (8)) is a more important process for evaporated films than for sputtered ones. But without more exact information on the activation energies for desorption of the gas atoms from the surface and the surface coverage, etc., no real comparison can be made.

Comparing the computer results with those experimentally determined for sputtered films, shows better, although not in most cases remarkably good, agreement. This is not really surprising because many of the parameters used in the calculation are only estimates and 'guesses', as the true values are not known. Nonetheless, as expected, the curves indicate that an overall increase does take place in the concentration of argon trapped in all the metal films with increasing voltage bias. The effect of varying the sputtering yield value of the gas, compared with that of the metal, gives a set of 20 curves for each metal. It is seen that with most metals, for $\alpha_1 > 10\ \alpha_2$, there is relatively little change in argon concentration, at least at the higher bombarding energies. The concentrations calculated for ZB films are somewhat arbitrary, since very little is known about the actual

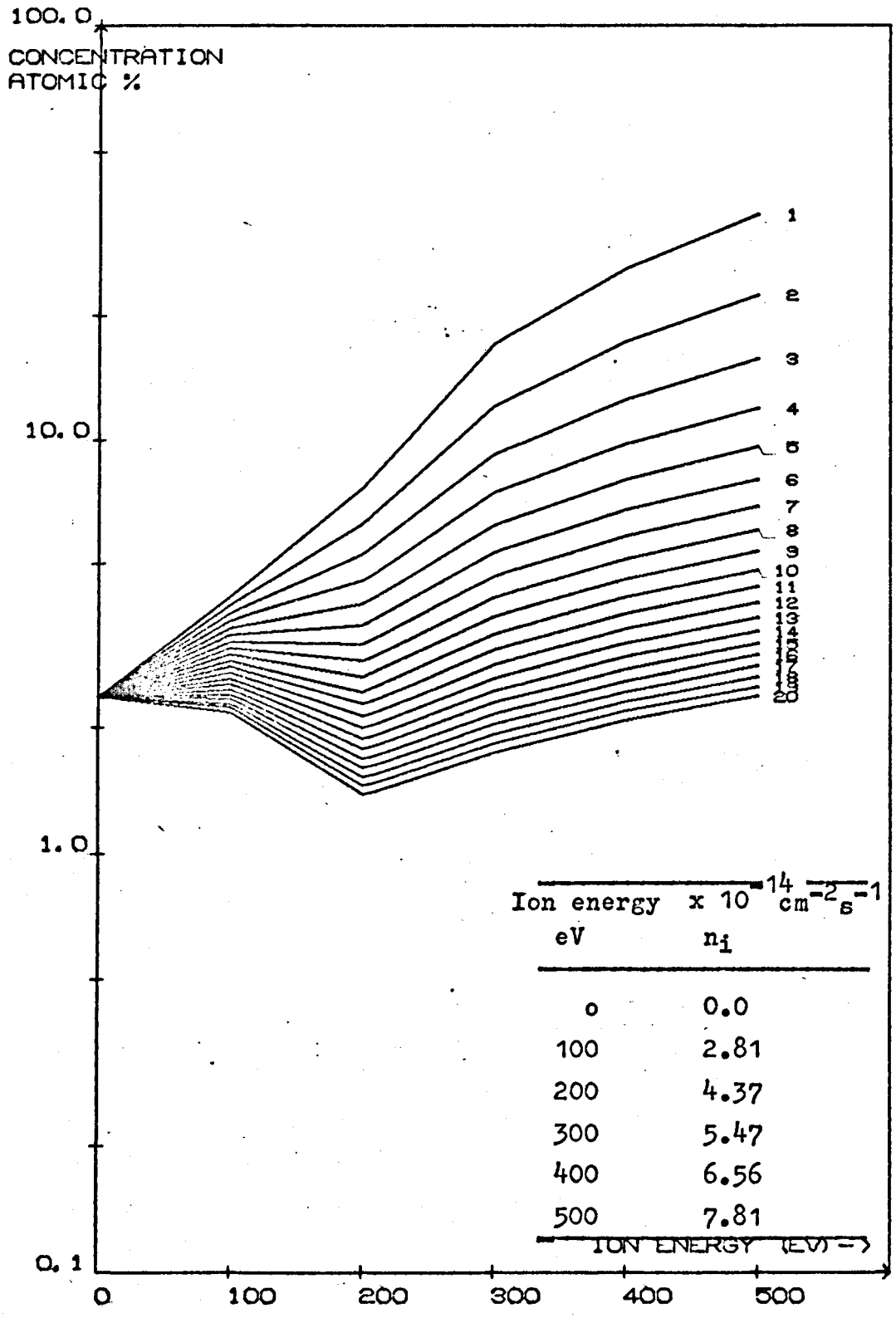

Ion energy eV	x 10^{14} $cm^{-2}s^{-1}$ n_i
0	0.0
100	2.81
200	4.37
300	5.47
400	6.56
500	7.81

FIGURE 6.47. ARGON CONCENTRATION IN ALUMINIUM WITH VARIATION IN ION ENERGY.

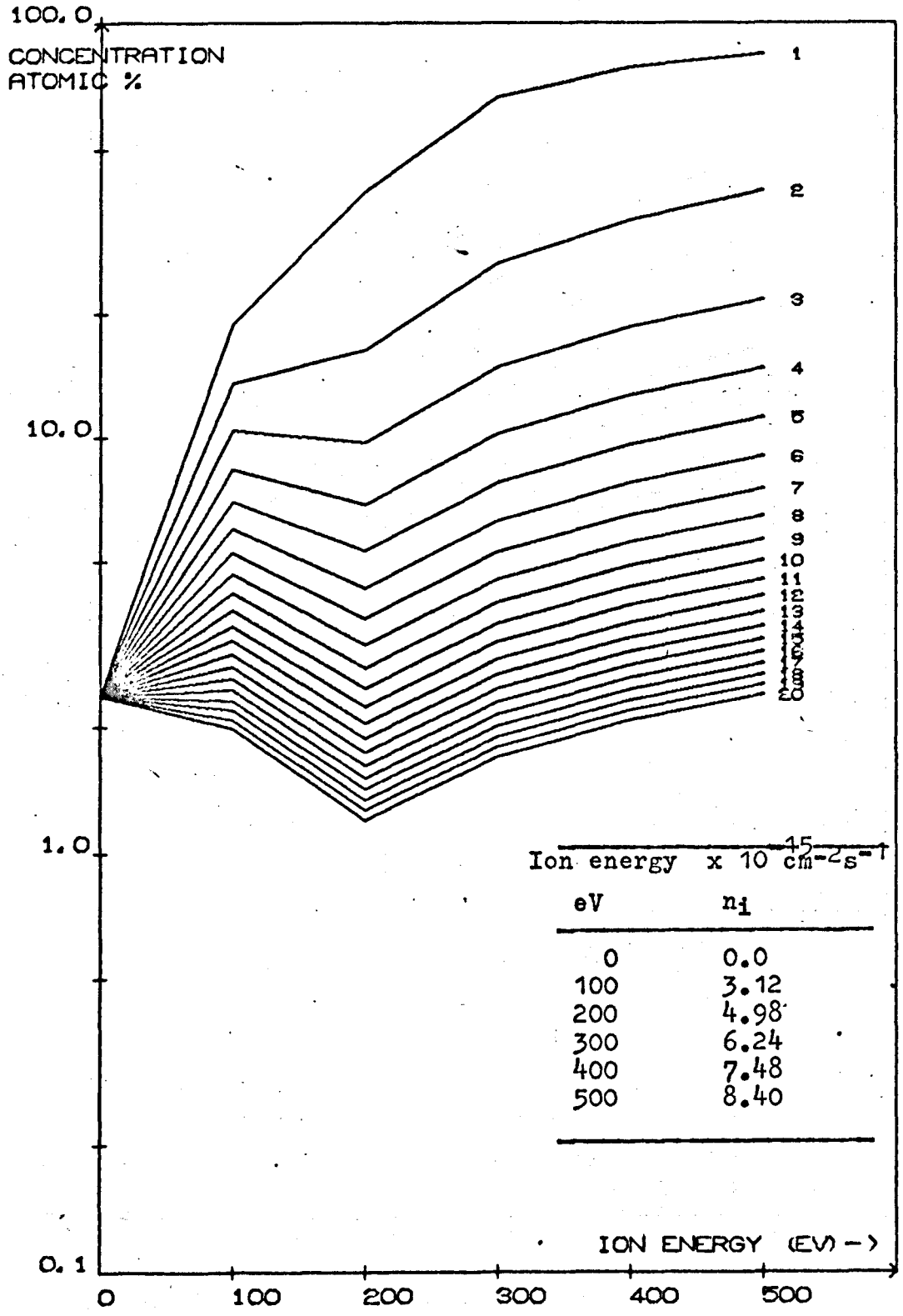

Ion energy eV	n_i x 10^{15} $cm^{-2}s^{-1}$
0	0.0
100	3.12
200	4.98
300	6.24
400	7.48
500	8.40

FIGURE 6.48. ARGON CONCENTRATION IN ALUMINIUM WITH VARIATION IN ION ENERGY.

number of argon atoms which arrive at the growing film with energies sufficient to be incorporated. For simplicity, a value of $N_1 = 1.8\ 10^{14}$ atoms cm^{-2} sec^{-1} arriving at the film ZB was used for all the metals, with a sticking probability of 0.1. The value N_1 was obtained by multiplying the number of reflected neutrals by a probability, of 0.4^{255}, that they will actually arrive at the surface of the growing film. By comparing, where possible, the experimentally determined concentrations in Figures 6.17-6.31 with the computer curves, and assuming that the sputtering yield of the metal film is the same as that of the metal target (using Wehner's data in Figure 6.39), the sputtering yield for the argon gas can be read off from the curves. This is given as the product of the multiplication factor (shown to the right of each curve) and the metal sputtering yield for that particular ion energy. The results for this determination are summarised in Table 6.5.

For some metals, the model predicts that the argon concentration at low negative bias voltages should be less than in the ZB films, as for example, in Figure 6.40 and 6.41 for copper and nickel, respectively. To some extent, this is observed experimentally, although only up to $\sim$ - 100 V bias, and then only by small amounts. For gold, no minimum in concentration is found, even though one would have been expected on the basis of the model.

Uncertainty in the bias current density measurement, and hence the rate of ion bombardment of the growing film, was investigated by changing the value of n_i in the computer programme. Examples of the resulting changes in concentrations can be seen, for aluminium, in Figures 6.47 and 6.48. Changing the value of n_i by a factor of ten appears to have little effect

Argon sputtering yields derived from the theoretically and experimentally determined graphs of argon concentration.

Material \ Ion Energy (eV)	Gas sputtering yield (Atoms/Ions)				
	100	200	300	400	500
Aluminium	∿2	∿3-5	∿10-13	∿16	-
Copper	∿6,9	∿7,9	∿ 8,11	∿13	∿13
Gold	∿0.5	∿3.0	∿6.5	∿ 8	∿12
Nickel	-	∿11,15	∿19	∿8	∿13
Titanium	∿2	∿2	∿6	∿9	∿15
Tungsten	-	∿3.3	∿12	∿17	-
Zirconium	-	∿0.6	∿0.8	∿2	-

Table 6.3.

on concentration at high biases, whereas it can have a more significant effect at the lower bias range.

The assumptions on which the model is based, described in section 3.5.3, do not allow diffusion or knock-on collision processes to take place. However, at voltage biases $\sim$ -500 V, it is likely[10] that a fraction of the argon ions, arriving at the surface of some of the metals, will travel further into the film than the top layer, thus violating some of the assumptions and invalidating the model. This may explain why, at high voltage biases, the argon concentrations are actually found to decrease for some metals. This argument is further reinforced by the large values of gas sputtering yields, determined from the experimental and theoretical curves and summarised in Table 6.3. Here, the sputtering yields at voltage biases above about -300 V may be as high as $\sim$ 16 atoms/ion for some of the metals, and as low as $\sim$ 5 atoms/ion for others. The large values of gas sputtering yields imply that a specifically 'gas sputtering mechanism' was in operation, rather than a 'target sputtering' process, where the erosion of the target surface exposes and releases buried gas atoms. For the latter process, gas sputtering yields would be expected of about the same value as those of the metal, from which the gas was released, i.e. $\sim$ 1-4 atoms/ion. For the former mechanism, where an incident ion causes the release of trapped gas but does not supply enough energy per particle to sputter the solid, the possibility of obtaining large values of gas sputtering yield is to be expected, as seen in Table 3.4. On the other hand, for some metals, such as gold and zirconium, at least for the lower region of ion energy, the release of gas through a target sputtering mechanism may be predominant. This is indicated by the low values of gas sputtering

yield, which are only larger than the equivalent target sputtering yield by a factor of $\sim$ 2-3.

It must be concluded then, that there is a strong probability that some form of 'gas sputtering' mechanism is causing the release of the trapped argon at the higher voltage biases, whilst a 'target sputtering mechanism' is more likely to be responsible at lower ion energies. Moreover, for the medium range of ion energies used,

it is likely that, to some extent, both mechanisms are in operation at the same time.

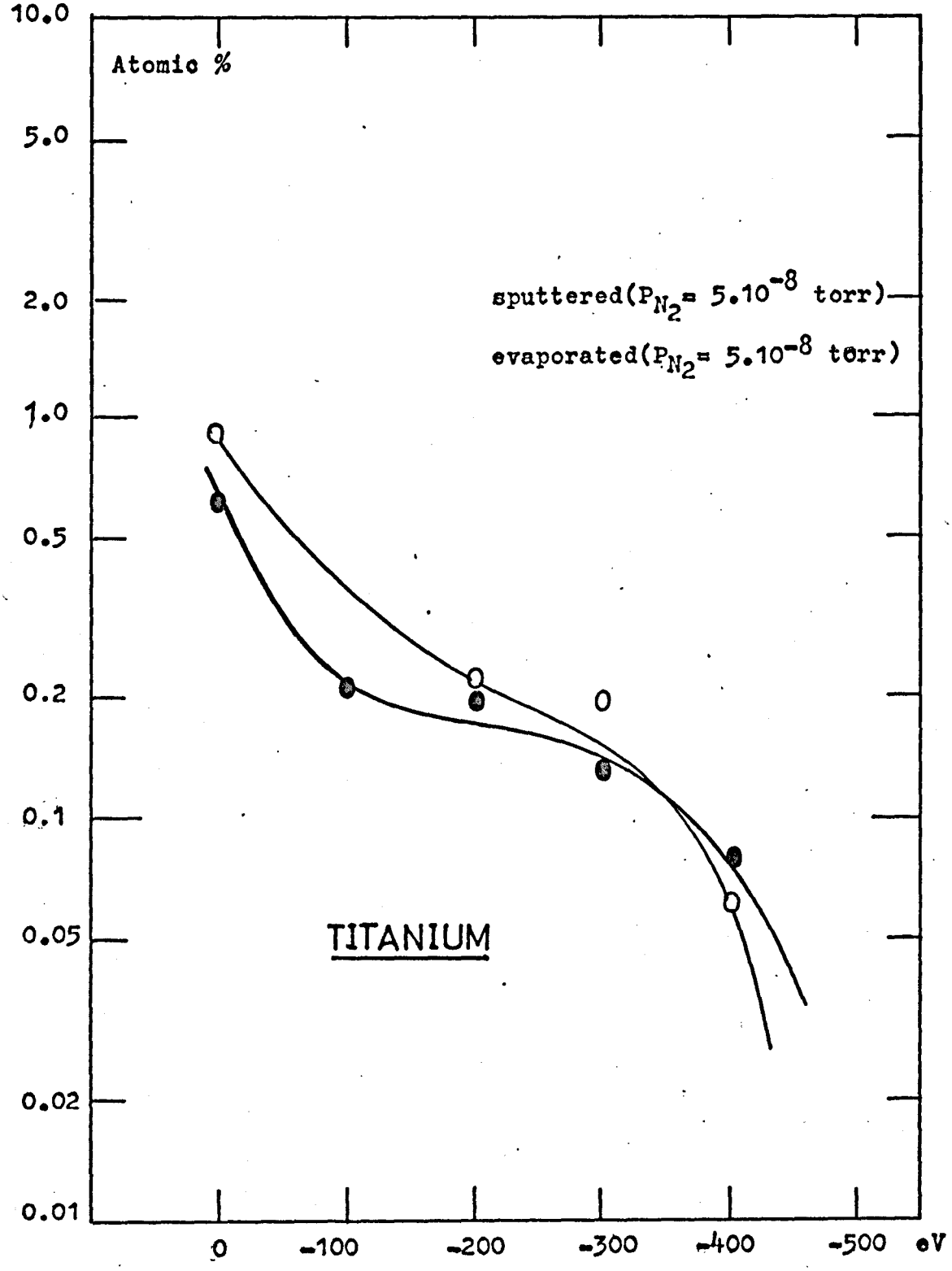
10.0
Atomic %
5.0
2.0
1.0
0.5
0.2
0.1
0.05
0.02
0.01
sputtered(P_{N_2}= 5.10^{-8} torr)
evaporated(P_{N_2}= 5.10^{-8} torr)
TITANIUM
0
-100
-200
-300
-400
-500
eV

Figure 6.49

6.6 Nitrogen gas incorporation

Results

The results are grouped together under the headings; class 1, 2 and 3 on the basis of Winters' definition, given in section 6.3.1. The nitrogen concentrations presented below were obtained, in most cases, from the same films for which the argon concentrations were determined.

Class 1

1. Titanium

The nitrogen concentrations measured in sputtered and evaporated titanium films are shown in Figure 6.49. These were deposited in the presence of a nitrogen pressure of $\sim 5.\ 10^{-8}$ torr and at an argon pressure of $6.8\ 10^{-4}$ torr. It is clearly seen that an increase in voltage bias produces a decrease in nitrogen concentration, reaching a value of about 10^{-1} atomic % at -400 V from about 1 atomic % at ZB. The curves for both types of film are closely similar, which suggests that for this metal, the method of deposition is not such an important parameter, as it is for argon trapping (see Figure 6.24).

The small number of points, evident in Figure 6.49, is indicative of the difficulty in outgassing the films without regettering the active gases. Many more films were deposited, but, on heating, too much evaporation took place and the nitrogen was pumped away very quickly, making any measurement impossible. It cannot even be certain, that the results, presented in Figure 6.49, were not susceptible to this effect, and consequently may be under-representing the true situation.

2. Tungsten

Again, and in accordance with Winters' model, the nitrogen

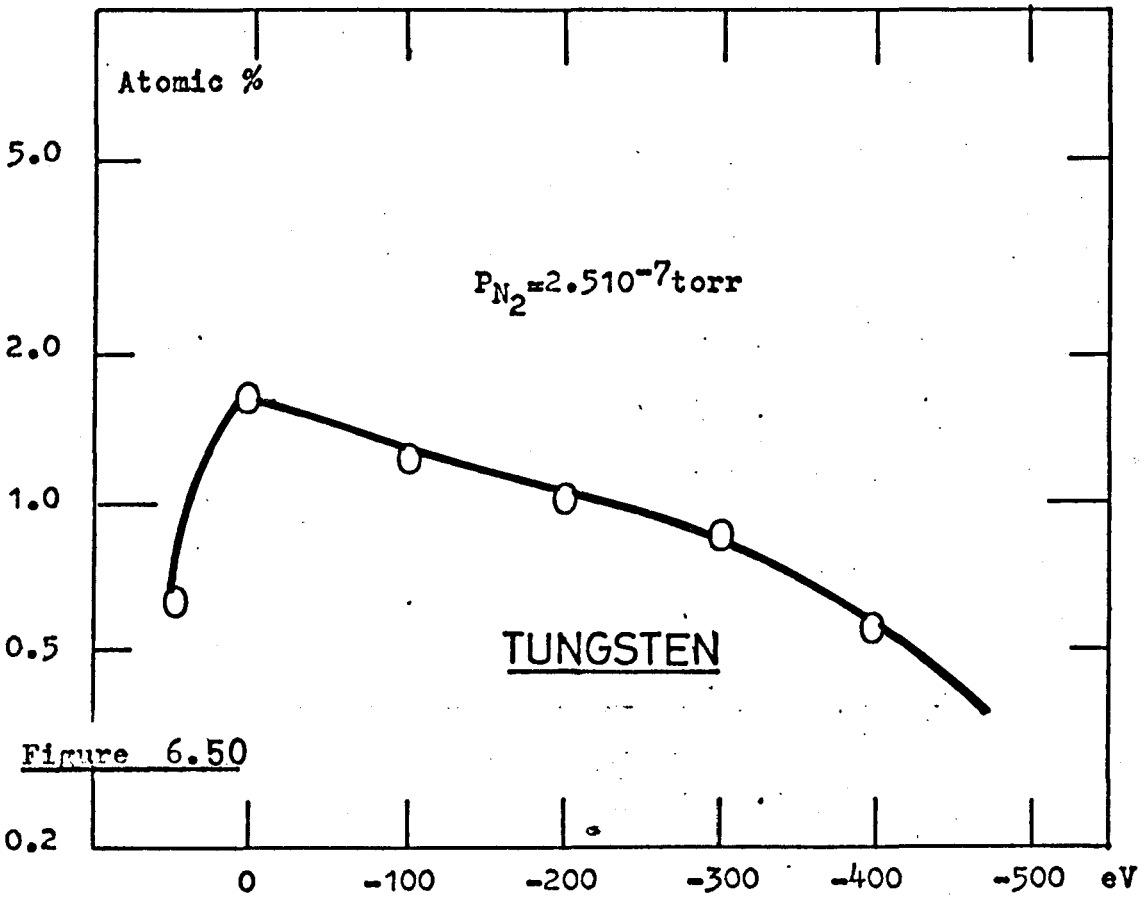

Figure 6.50

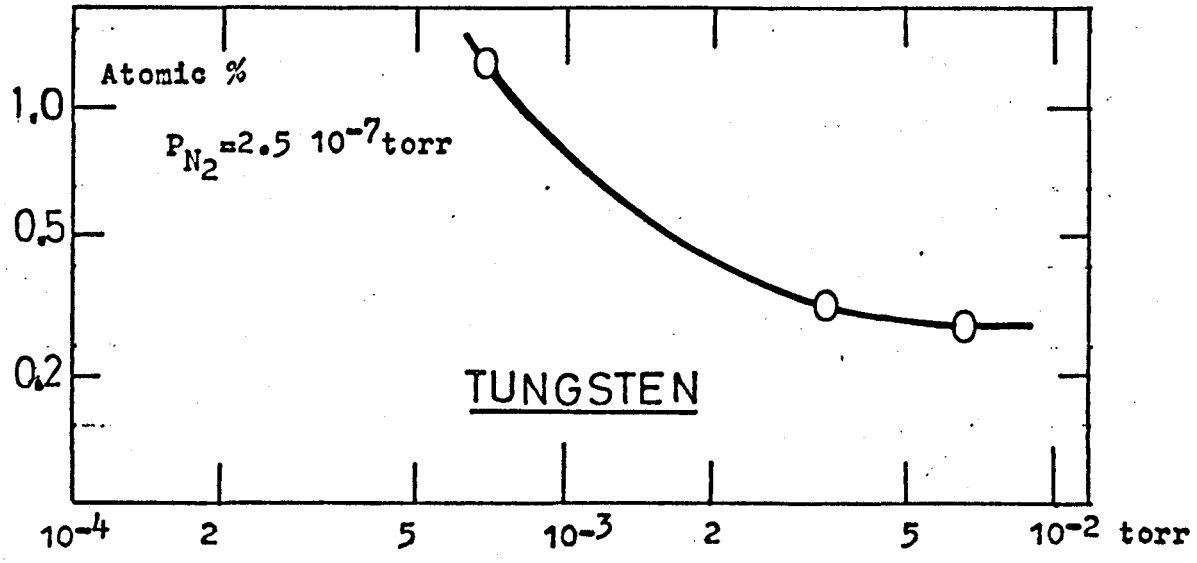

Figure 6.51

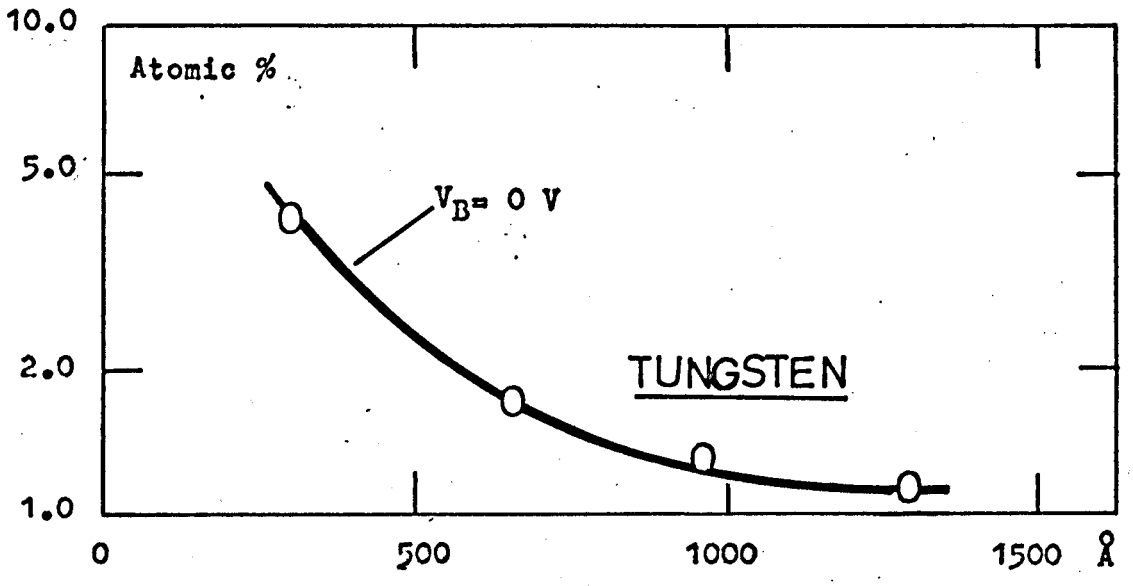

Figure 6.52

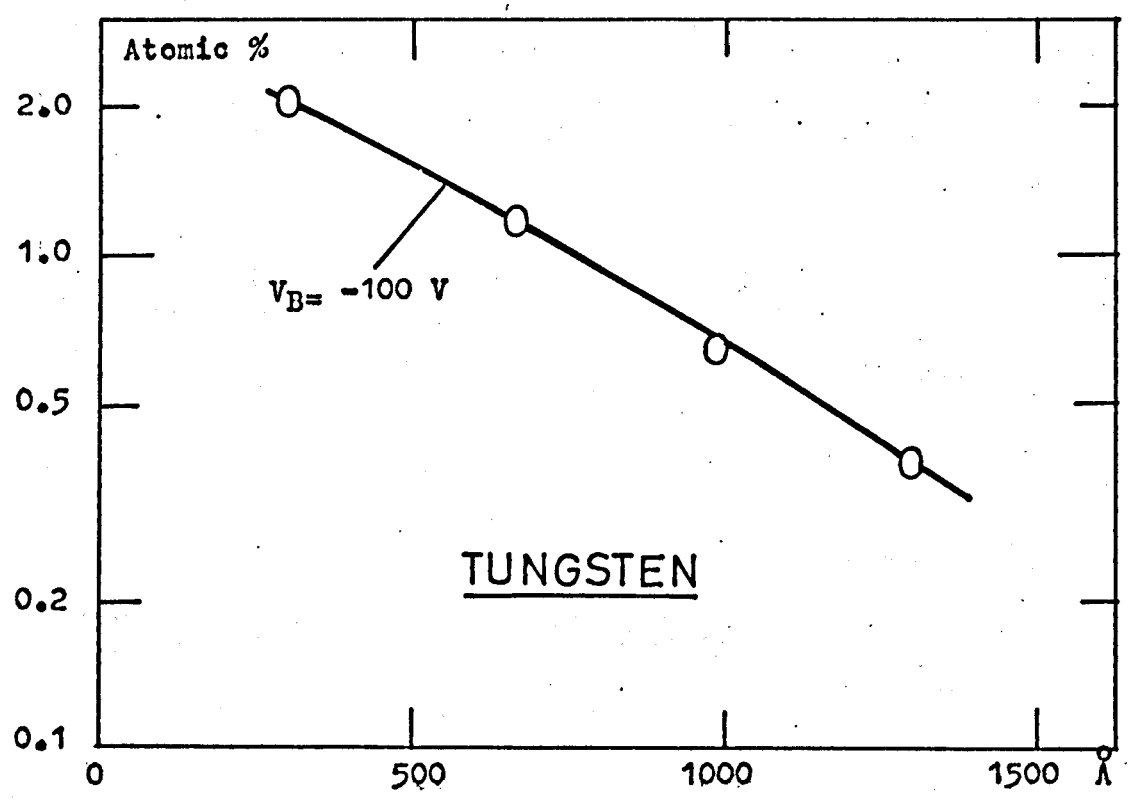

Figure 6.53

concentration decreases with increasing bias. This is shown in Figure 6.50. In this case, the ZB films contained about 2 atomic % and the concentration fell to about 5. 10^{-1} atomic % at -400 V. Since no evaporated tungsten films were deposited, no comparison could be made to see whether the nitrogen concentration was affected by the method of deposition. However, the titanium results, suggest that for a metal which chemisorbs nitrogen, the nitrogen gas content should be relatively unaffected by the deposition method.

It is interesting to note that, for positive bias voltages (+50 V), the concentration also fell, to about 6.10^{-1} atomic %, indicating that low energy electron bombardment may be helpful in precipitating nitrogen to the surface. As with the argon measurements, increasing the sputtering pressure causes a decrease in the concentration, as shown in Figure 6.51. This would be expected, from the same reasoning as was used for argon. Figures 6.52 and 6.53 show the variation of concentration with thickness, when deposition takes place in the presence of 0 and -100 V bias, respectively. In the former, the concentrations are relatively unchanged above thicknesses of about 600 Å and lie between 1 and 2 atomic %. For the latter, at -100 V bias, a steady decline in concentration throughout the thickness range, is observed.

3. Zirconium

Attempts at evaporating zirconium were unsuccessful, and so no evaporated zirconium samples were made. Moreover, it proved impossible to measure the nitrogen gas content from the sputtered films. This was because this gas was strongly regettered on heating the films, and the regettering took place with such rapidity that the mass spectra obtained

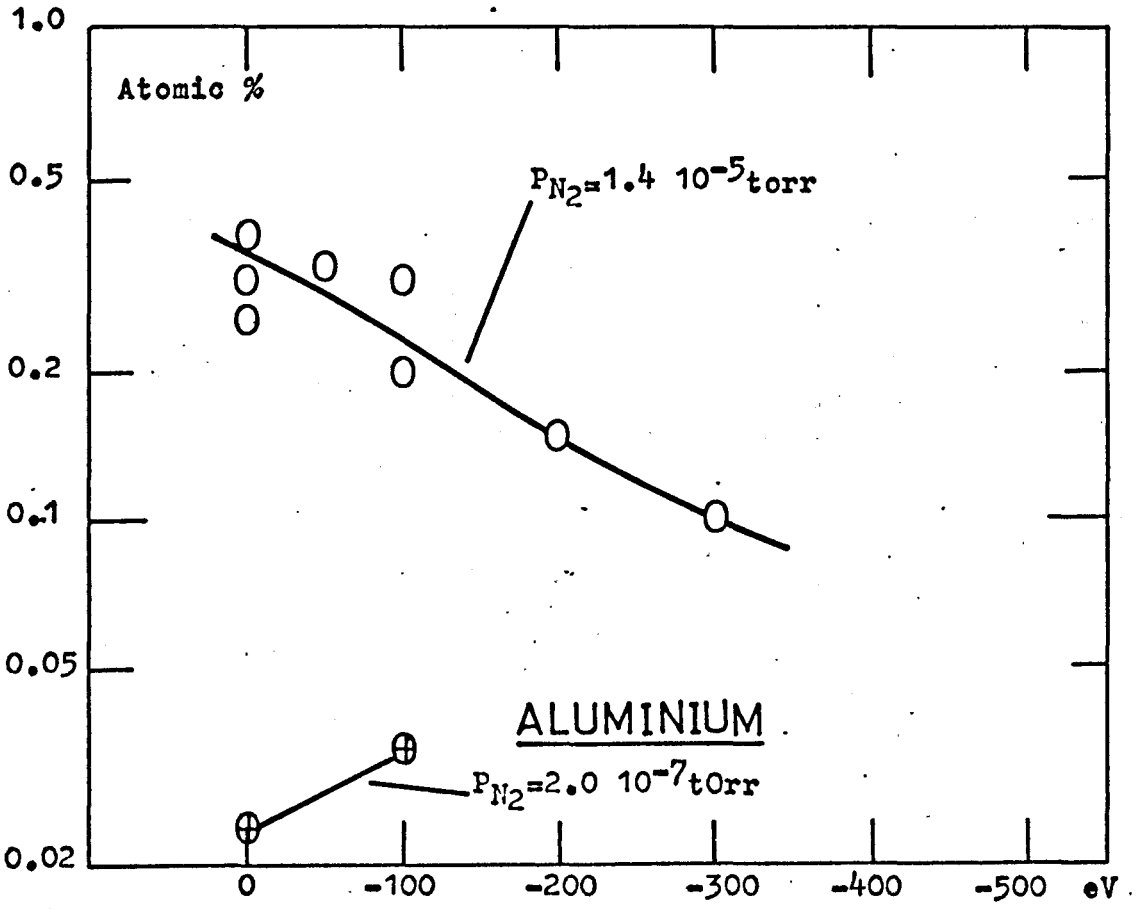
1.0
Atomic %
0.5
P_{N_2}=1.4 10^{-5}torr
0.2
0.1
0.05
ALUMINIUM
P_{N_2}=2.0 10^{-7}torr
0.02
0
-100
-200
-300
-400
-500
eV

Figure 6.54

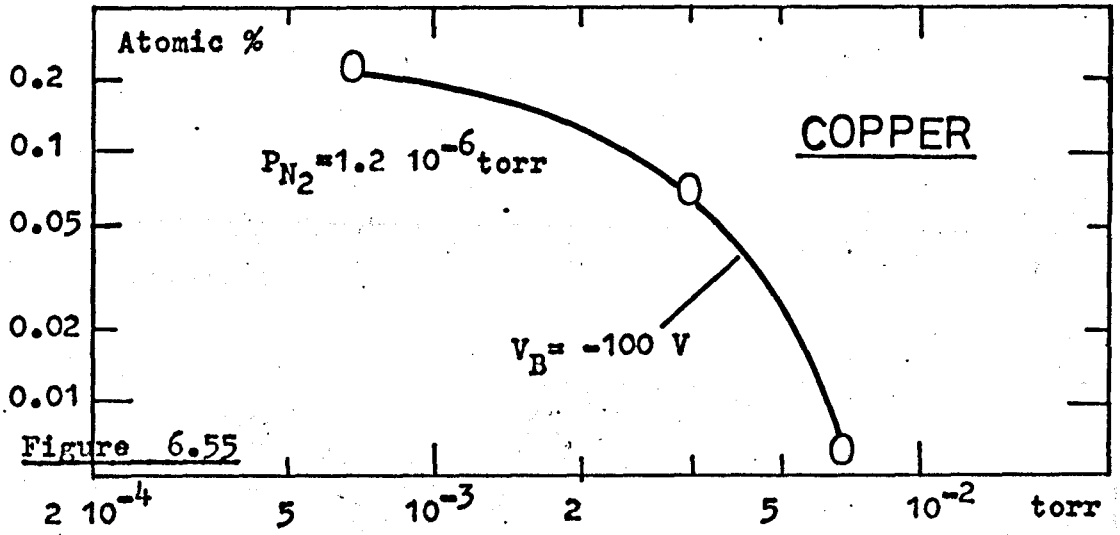

Figure 6.55

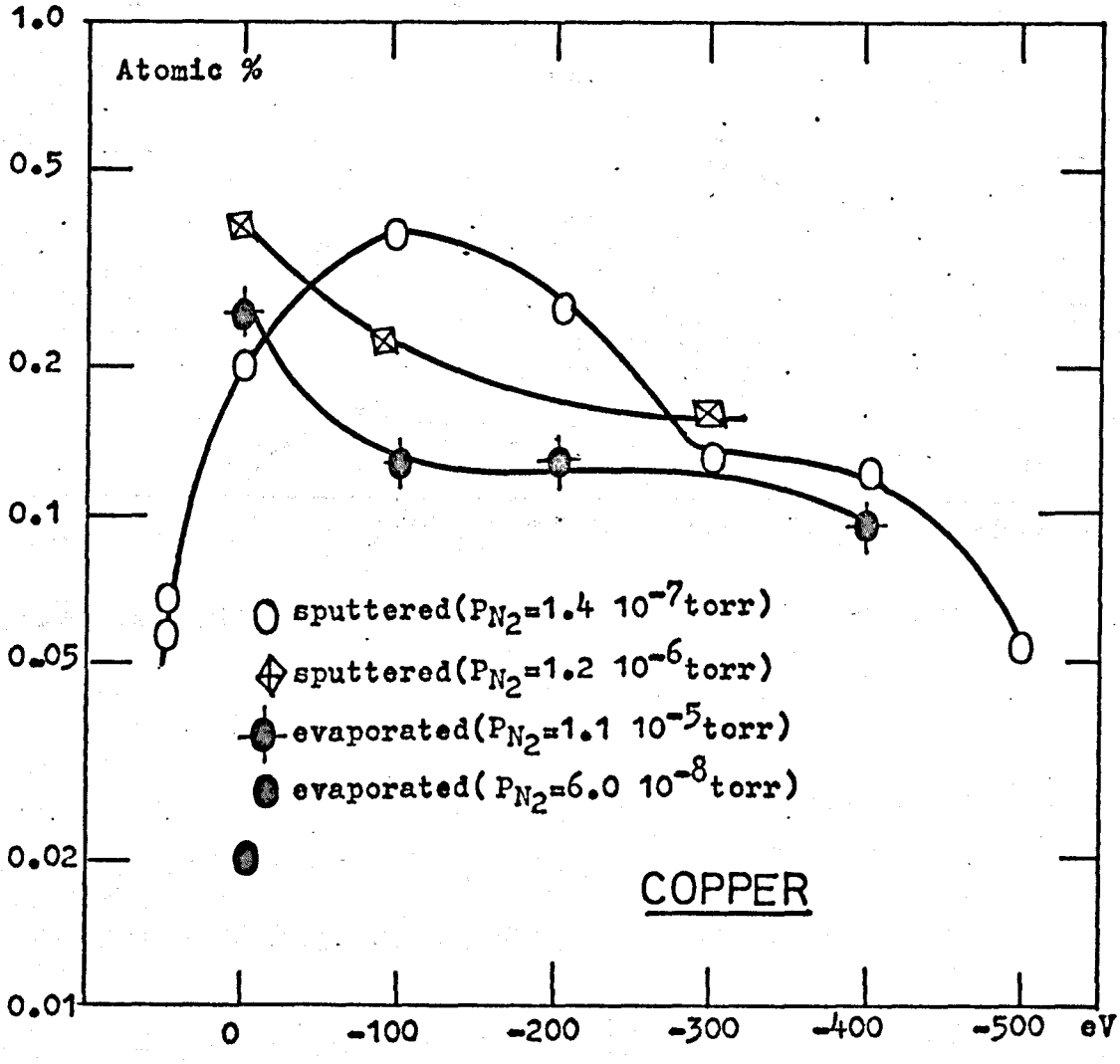

Figure 6.56

did not give any indication of the nitrogen released from the films. For these reasons no results were obtainable for the nitrogen content of these films.

Class 2

4. Aluminium

Figure 6.54 shows the nitrogen concentration with voltage bias for two values of nitrogen pressure:- $1.4\ 10^{-5}$ torr and $2.\ 10^{-7}$ torr. For the former, a noticeable decrease in concentration is observed with increasing voltage bias. The concentration fell by a factor of about 3 when the bias changed from 0 to -300 V. For the latter, and lower nitrogen pressure range, there is a tentative indication that the concentration increased with bias voltage. For the lower pressure range, the concentration for the ZB films is an order of magnitude less than for the ZB films sputtered at the higher pressure.

5. Copper

Figure 6.55 shows that the nitrogen concentration decreased markedly with increasing argon pressure, in a fashion similar to that for argon (compare with Figure 6.19), although more steeply, decreasing from $\sim 2\ 10^{-1}$ atomic % at $6.8\ 10^{-4}$torr to $6.\ 10^{-2}$ atomic % at $6.8\ 10^{-3}$torr. Several curves are shown in Figure 6.56. These show the variation in nitrogen concentration with bias voltage, for both evaporated and sputtered films, deposited at different partial pressures of nitrogen. It is seen that the concentration can increase or decrease, depending on the relative amount of nitrogen present during deposition. At a nitrogen pressure of $1.4\ 10^{-7}$ torr, the concentration increases sharply to a value of about 4.10^{-1} atomic % at -100 V, and decreases thereafter to about

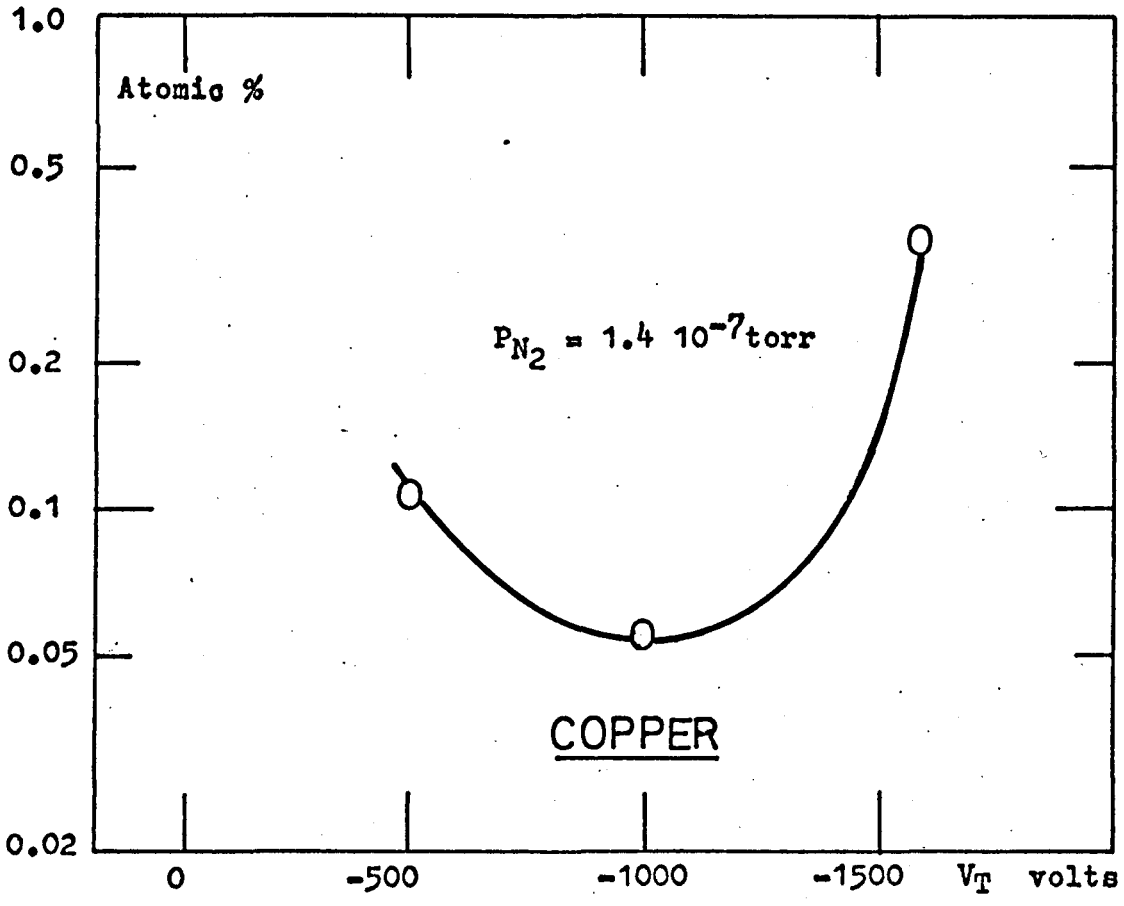

Figure 6.57

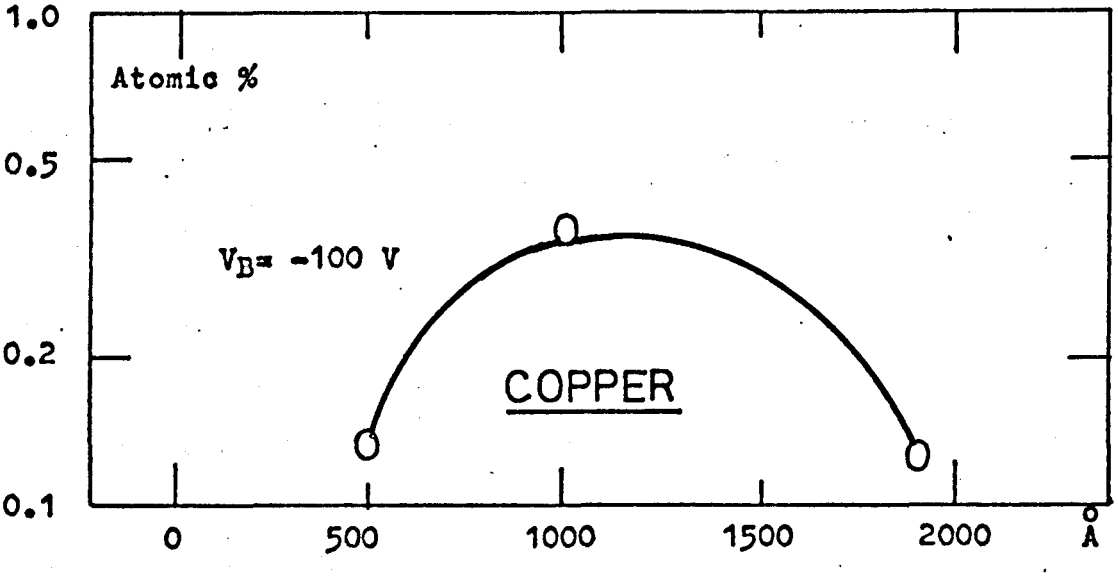

Figure 6.58

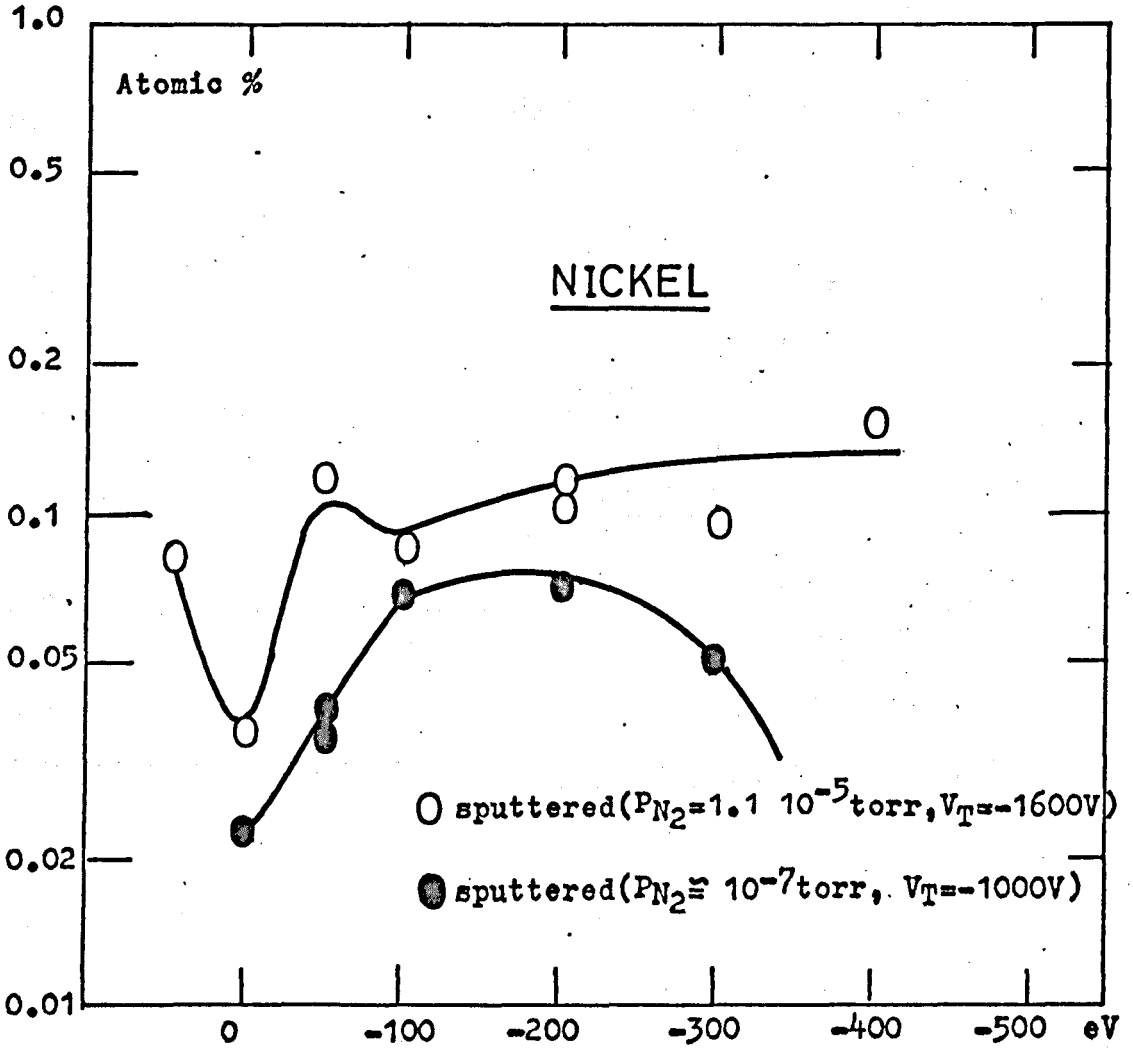
1.0
Atomic %
0.5
NICKEL
0.2
0.1
0.05
0.02
0.01
O sputtered(P_{N_2}=1.1 10^{-5}torr, V_T=-1600V)
sputtered(P_{N_2}= 10^{-7}torr, V_T=-1000V)
0
-100
-200
-300
-400
-500
eV

Figure 6.59

5 10^{-2} atomic % at -500 V bias. For the 1.2 10^{-6} torr films, the concentration decreases throughout the bias voltage range. At 1.1 10^{-5} torr, the concentrations in the evaporated films also decrease with increasing bias, from a value of 2.10^{-1} atomic % at ZB to $\sim 10^{-1}$ atomic % at -400 V. Figures 6.57 and 6.58 indicate the effect of target voltage and film thickness, respectively, on the nitrogen concentration. A minimum concentration of about 5.10^{-2} atomic % occurs at a target voltage of -1000 V, whereas the concentration passes through a maximum of 4.10^{-1} atomic % at a film thickness of 1000 Å.

6. Nickel

Figure 6.59 shows the nitrogen concentration in films of sputtered nickel with variation in bias voltage. For both curves there is an increase in concentration up to a bias voltage of about -200 V. In one, using a target voltage of -1600 V and at a nitrogen pressure of 1.1 10^{-5} torr, the curve continues upwards and reaches a concentration of about 1.5 10^{-1} atomic % at -400 V. The other, at a target voltage of -1000 V and a pressure of 10^{-7} torr begins to decrease after -200 V voltage bias. The evaporated films all gave nitrogen concentrations less than 10^{-2} atomic %.

Class 3

7. Gold.

Gold is the only metal investigated which lies in class 3; i.e. it does not chemisorb molecular nitrogen nor does it form a nitride. Figure 6.60 shows that for gold, deposited on tungsten substrates, there is an increase [256] in nitrogen concentration with bias voltage, up to about -300 V, and a decrease thereafter. For the gold films sputtered on glass, the nitrogen concentrations show only a slight tendency to

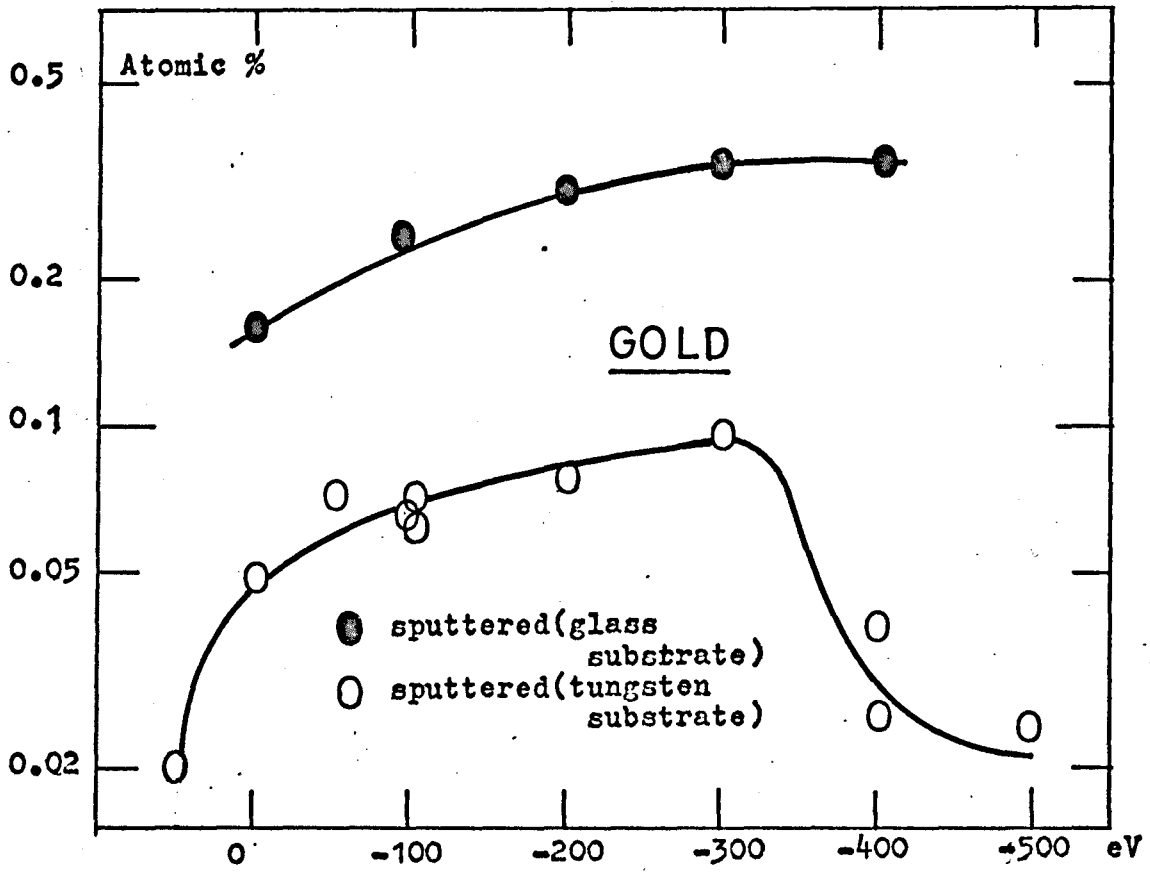

Figure 6.60

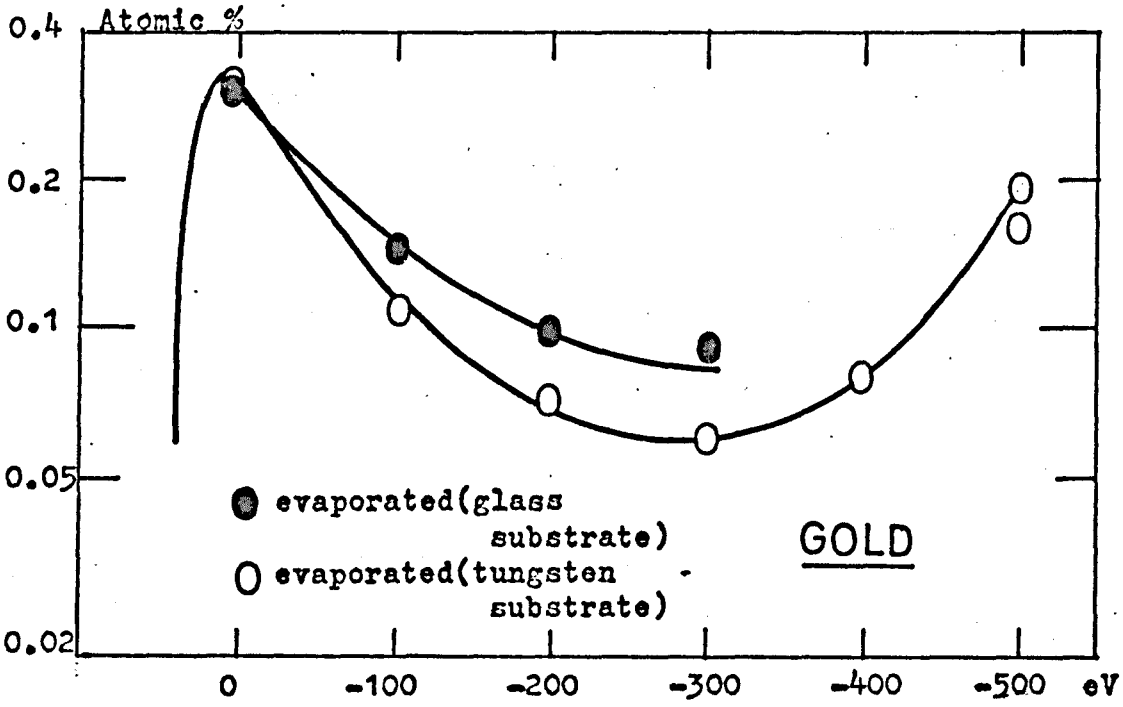

Figure 6.61

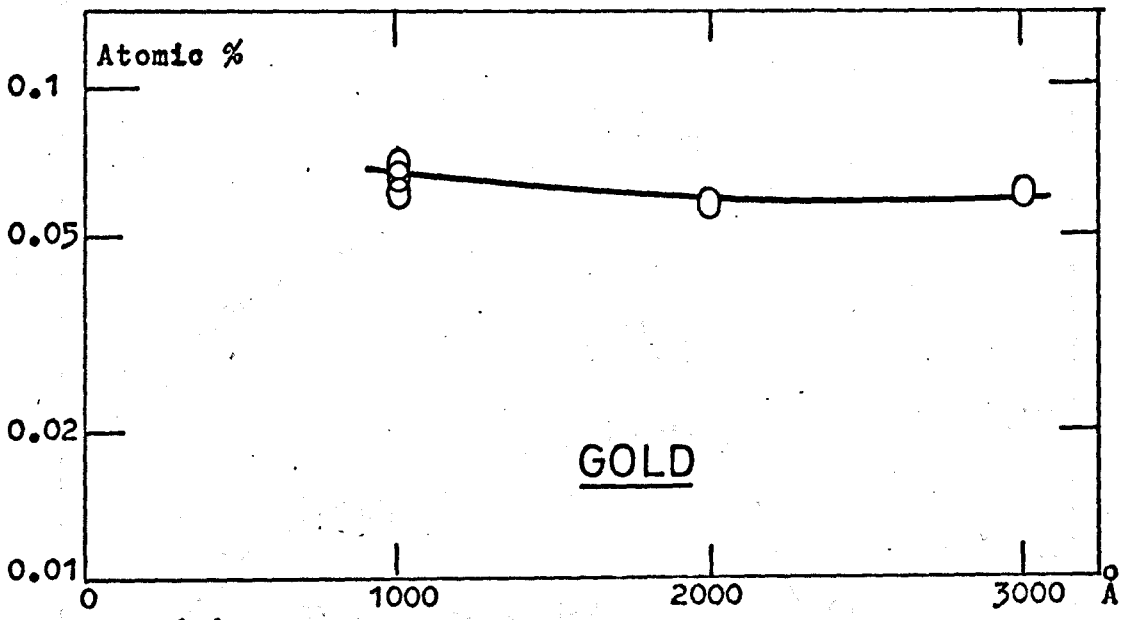

Figure 6.62

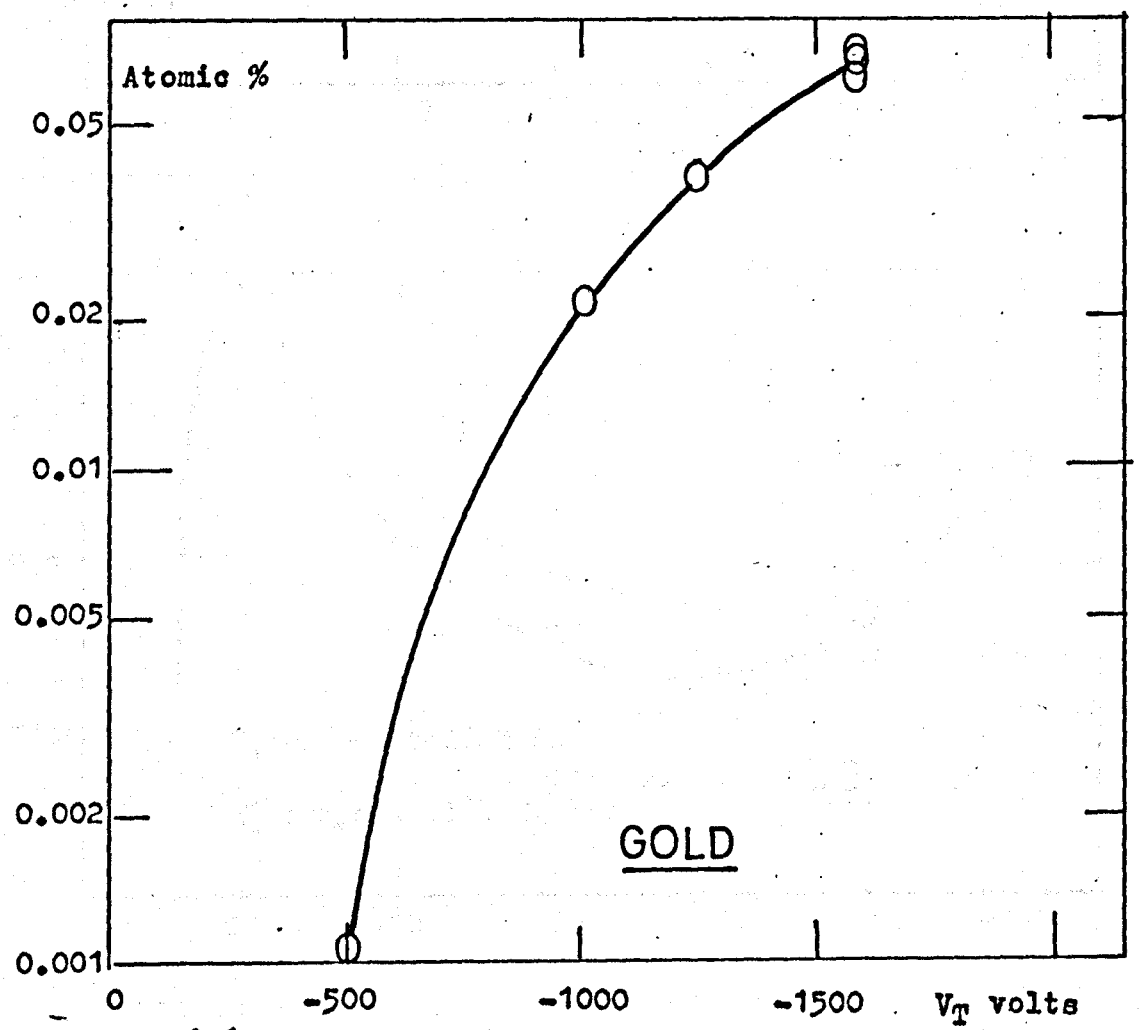

Figure 6.63

decrease at high bias voltages. With low energy electron bombardment, i.e. +50 V bias, the nitrogen gas content falls to about 2. 10^{-2} atomic %. The effect of bias appears to be quite different for the evaporated films, as Figure 6.61 shows. Here, increasing the negative bias voltage, up to -300 V, causes a decrease in nitrogen concentration, and an increase thereafter, to about 2.10^{-1} atomic % at -500 V. Increasing the thickness of the sputtered films appears to have little effect on the nitrogen concentration, as seen in Figure 6.62. On the other hand, an increase in target voltage produces a very large change in nitrogen concentration, from $\sim 10^{-3}$ atomic % at a target voltage of -500 V to about $\sim 6\ 10^{-2}$ atomic % at -1600 V, as shown in Figure 6.63.

6.7 Discussion

6.7.1 Nitrogen incorporation in biased and zero-biased films

As with any gas incorporation process, the reactive gases must be sorbed at or near the film surface, before permanent incorporation can take place. For nitrogen, the incorporation is much more complicated than for argon. This is because of the many different ways by which the prior sorption of nitrogen can take place on the metal film surface.

Clean surfaces of reactive metals, such as tungsten, titanium, and zirconium, can chemisorb approximately a monolayer of nitrogen, when exposed to some partial pressure of molecular nitrogen. Other metals, such as nickel, copper and aluminium, will not chemisorb molecular nitrogen, although they are known to form compounds with nitrogen, such as copper nitride and aluminium nitride in chemical reactions. Gold, on the other hand, does not chemisorb molecular nitrogen nor has it been known to combine with nitrogen to form a chemical compound. Nevertheless, for

all the metals investigated, including the ones which do not appear to chemically sorb nitrogen, various amounts of nitrogen are seen to be incorporated in the films, as seen for example, in Figures 6.49 and 6.30. It is necessary, then, to discuss the various ways, apart from normal chemisorption, by which nitrogen can be incorporated in the films. It is known, for example,[207] that whilst some surfaces may or may not sorb molecular nitrogen, they all usually contain sites which can be populated by atomic nitrogen. Therefore, the problem can be reduced to postulating mechanisms by which atomic nitrogen can be created during film deposition.

In addition, energetic (> 100 eV) molecular nitrogen ions and neutrals, as well as the atomic species, can be trapped, both at reactive and non-reactive surfaces, by a mechanism similar to that invoked earlier for argon.

Nitrogen atoms can be produced at a surface if low energy (> 9 eV) nitrogen molecules and molecules ions, impinging on it, dissociate. Decomposition of gases, such as ammonia (NH_3), nitrous oxide (NO) and N_2, through collisional processes occurring in the gas discharge, may also result in a flux of atomic nitrogen arriving at the surface of the growing film. Moreover, bombardment of physically adsorbed nitrogen molecules at the surface, by electrons created in the discharge, may also play a small part in creating atomic nitrogen, although this last mechanism is unlikely to occur, to any great extent, because the inefficiency of the energy exchange process[253] and the temperatures normally encountered in sputtering experiments. Dissociation chemisorption has been shown to occur for the molecular species only if the binding energy, E_a, of the atom to the surface, is greater than half the molecular dissociation energy

of the molecule[212], i.e. an exothermic reaction. For nitrogen, this means that $E_a > 4.9$ eV. This leaves the endothermic sites, i.e. where $E_a < 4.9$ eV and the activated exothermic sites on the film to be filled by atomic nitrogen, created by one of the previously mentioned 'impact activated' processes.

Nitrogen incorporation at the surface of a growing film can therefore be related to three sorption processes:-

At zero bias;-

(1) The chemisorption of molecular nitrogen, and

(2) The 'chemisorption' of atomic nitrogen, created by one or more of the impact activated processes[212].

In addition, with voltage bias applied to the film:-

(3) the trapping of energetic (> 100 eV) molecular and atomic, ions and neutrals.

For a sputtering experiment, the third process may also take place at zero bias voltage, through reflection at the target, etc., in a manner similar to that for argon.

The electron-impact ionization cross-section[257] and the dissociation cross-section for N_2[203] have been shown to be similar both in magnitude and shape, see following Table:

Ionization cross-section[203] X 10^{16} cm^2	Electron energy (eV)	Dissociation cross-section, X 10^{16} cm^2	
		TATE et al.[257]	WINTERS[203]
0.23	50	0.72	1.8
0.27	100	1.90	2.1
2.58	200	1.79	1.75
2.14	300	1.40	1.45
1.69	500	1.00	0.73
0.94	1000	0.56	-

In addition, from probe measurements in the field-free plasma region of the discharge, see chapter 5 and [60], it has been shown that the ratio of ions and excited atoms to neutral molecules is less than 10^{-3}. At zero bias, only sorption process (2) is likely to occur for metals which do not chemisorb molecular nitrogen. As indicated above, there is only likely to be one atom or ion created for every 1000 neutral molecules present. Consequently, for N_2 pressures less than about 10^{-5} torr the amount of nitrogen incorporated in these films at ZB is likely to be small.

Metals which do chemisorb molecular nitrogen, such as tungsten and titanium, are likely to have much more nitrogen incorporated in them than Class 2 and 3 materials, for the following reason :
On a pre-existing Class 1 surface the molecular sticking probability decreases, from a typical value of 0.3 to zero, as the surface becomes saturated. However, for a growing film, a continuously fresh and unsaturated surface is being presented to the molecular nitrogen and,

Nitrogen concentrations in ZB films at various nitrogen pressures P_{N_2}

Class 1

P_{N_2} (Torr)	Concentration in atomic %			
	Titanium		Tungsten	
	SP	E	SP	E
5.10^{-8}	1	8.10^{-1}	1.8	-

Class 2

P_{N_2} (Torr)	Concentration in atomic %					
	Aluminium		Copper		Nickel	
	SP	E	SP	E	SP	E
2.10^{-7}	2.10^{-2}	$<10^{-3}$				
$1.4.10^{-7}$			2.10^{-1}	-	2.10^{-2}	10^{-3}
$1.2\ 10^{-6}$			4.10^{-1}	-		
$1.4.10^{-5}$	$3\text{-}4.10^{-1}$	-				
$1.0.10^{-5}$			-	3.10^{-1}	4.10^{-2}	-

Class 3

P_{N_2} (Torr)	Concentration in atomic %		
	Gold		Substrate
	SP	E	
5.10^{-8}	5.10^{-2}	3.10^{-1}	Tungsten
5.10^{-8}	$1.8.10^{-1}$	3.10^{-1}	Glass

SP = Sputtered E = Evaporated.

Table 6.4

in this way, a high nitrogen sticking probability is maintained throughout the growth of the film. Moreover, the surface coverage can be further increased by the processes occuring for Class 2 materials, involving atomic adsorption.

For a ZB sputtered tungsten film, deposited at a rate of about 10^{15} atoms cm^{-2} sec^{-1} in a nitrogen atmosphere of 10^{-7} torr, a rough estimate, on the basis of chemisorption alone, yields a concentration of about 2 atomic %. This calculation is apparently independent of the deposition method and a similar value would be expected for evaporated films deposited under the same conditions of pressure, deposition rate and temperature. This supposition is supported by the results shown in Figure 6.49, for evaporated and sputtered titanium films grown at ZB. Table 6.4 summarises the average concentrations found in ZB films for the seven metals investigated.

In general, the class 1 metals, even when grown at $P_{N_2} \sim 10^{-7}$ torr, do indeed contain larger concentrations of nitrogen than the other two classes, in spite of the fact that some of these are deposited in the presence of nitrogen pressures as high as $\sim 10^{-5}$ torr. Gold (class 3) is found to contain more nitrogen, at ZB, than nickel and aluminium (class 2). The reason for this is not clear, since it would be expected that for class 2 surfaces, any nitrogen that was sorbed might form nitride patches, where molecular nitrogen could then be chemisorbed, thus enhancing the nitrogen concentration. This would not occur for gold, which does not form a nitride at any nitrogen pressure. However, the effect of reflected neutrals is expected to be different for gold and aluminium (and the other metals) and may account for some of the differences found. Moreover, this

effect would also lead to different concentrations, for class 2 and 3 surfaces, between sputtered and evaporated films. This is experimentally observed, as for example in Figure 6.56 for copper, although it does not account for the large amount of nitrogen found in the evaporated gold films.

With voltage bias applied, the film is being continuously bombarded with a flux of gas ions, most of which will be argon, but a fraction of which will be N_2^+. These may be incorporated in the film by a process similar to that for argon ions. For the class 1 surfaces, Winters' model predicts that the nitrogen concentration should decrease with increasing bias. This is because the chemisorbed gas is preferentially re-sputtered with respect to the metal. Figure 6.49 for titanium and Figure 6.50 for tungsten tend to bear out this prediction. On the other hand, for class 2 and 3 metals, the nitrogen content should tend to increase with increasing bias. This is because, in this case, the incorporation is primarily due to molecular (and atomic) ions of nitrogen embedding themselves in the surface. This is borne out, to some degree, by the experimental results for gold and nickel, shown in Figures 6.60 and 6.59, respectively. Copper and aluminium also exhibit similar increases in concentration, but only at low ambient pressures of nitrogen. At higher pressures, they begin to act more like class 1 materials as their surfaces become partially nitrided and the concentrations fall with increasing bias, as seen in Figures 6.56 and 6.54.

6.7.2 Nitrogen incorporation - on the basis of Winters' model

Winters' model was used to calculate the nitrogen concentration, when applying voltage bias to the sputtered films. A programme similar in form to the one for argon was used, except that this time the various

different sorbing processes at the surface were taken into account. This was achieved by changing $R_1 = \lambda_1 N_1 + 1.8.10^{14} \times 0.1$ to:-

$$R_1 = \lambda_1(1+0.4\lambda_1)7.7.10^{20} \times P_{N_2} + \lambda_2 F(P_N) + \lambda_3 N_N + \frac{\lambda_4 P_{N_2} x n_i}{6.8.10^{-4}} + \frac{1.8.10^{14} x P_{N_2} x 0.1}{6.8.10^{-4}}$$

The first term results from the chemisorption processes taking place at the film and target. The second term results from atomic nitrogen being formed in the discharge or nitrogen sputtered from the target as atoms. The third term relates to adsorption due to molecular dissociation upon impact with the surface. The fourth term describes the adsorption due to the impact of energetic nitrogen with the surface and the fifth term arises from the ions reflected towards the film from the target. A wide measure of disagreement exists between various authors on the value of sticking probability of nitrogen on various metal surfaces. Figure 2.11 shows, for example, its values on tungsten. For this reason a value of 0.3 was used for the chemisorption sticking factor for molecular nitrogen, λ_1, on tungsten, titanium and zirconium films. This figure was chosen as a reasonable and typical sticking probability for all these metals, although, for example, initial values as high as $\sim$0.5 have been reported[257], on titanium at room temperature. It was difficult to determine values for the second term due to an inexact knowledge of the numbers of nitrogen atoms being formed in the discharge ($F(P_N)$) and their relationship to the ambient nitrogen pressure. For this reason the second term (and for similar reasons, the third term) were left out of the calculation. These omissions were unlikely seriously to affect the concentrations derived for class 1 and 3 materials. This was not true for the class 2 metals, since these do not chemisorb molecular nitrogen but do form nitrides (or nitride patches on the surface). The values of

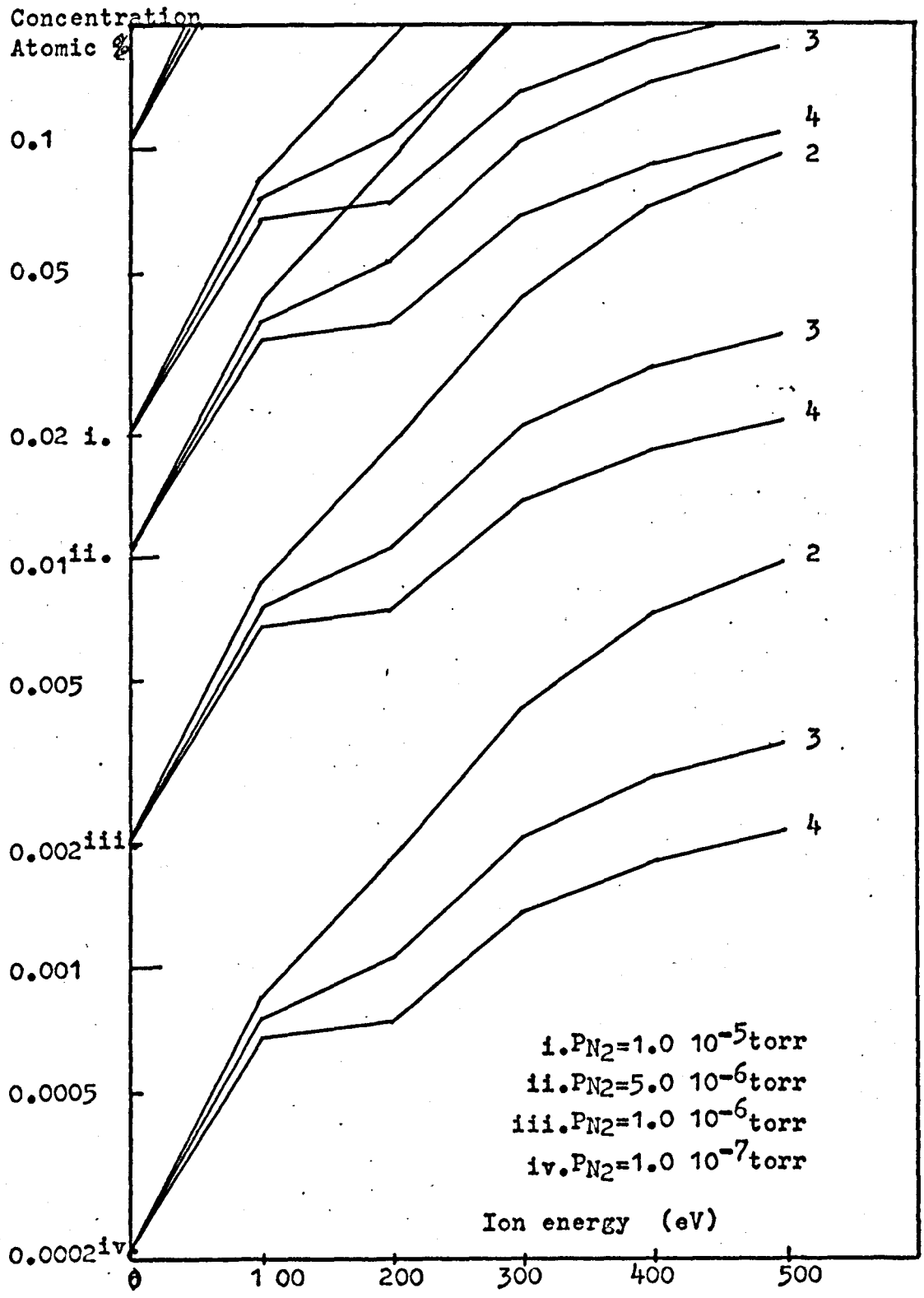

Figure 6.70 . Nitrogen concentration in Gold with variation in ion energy.

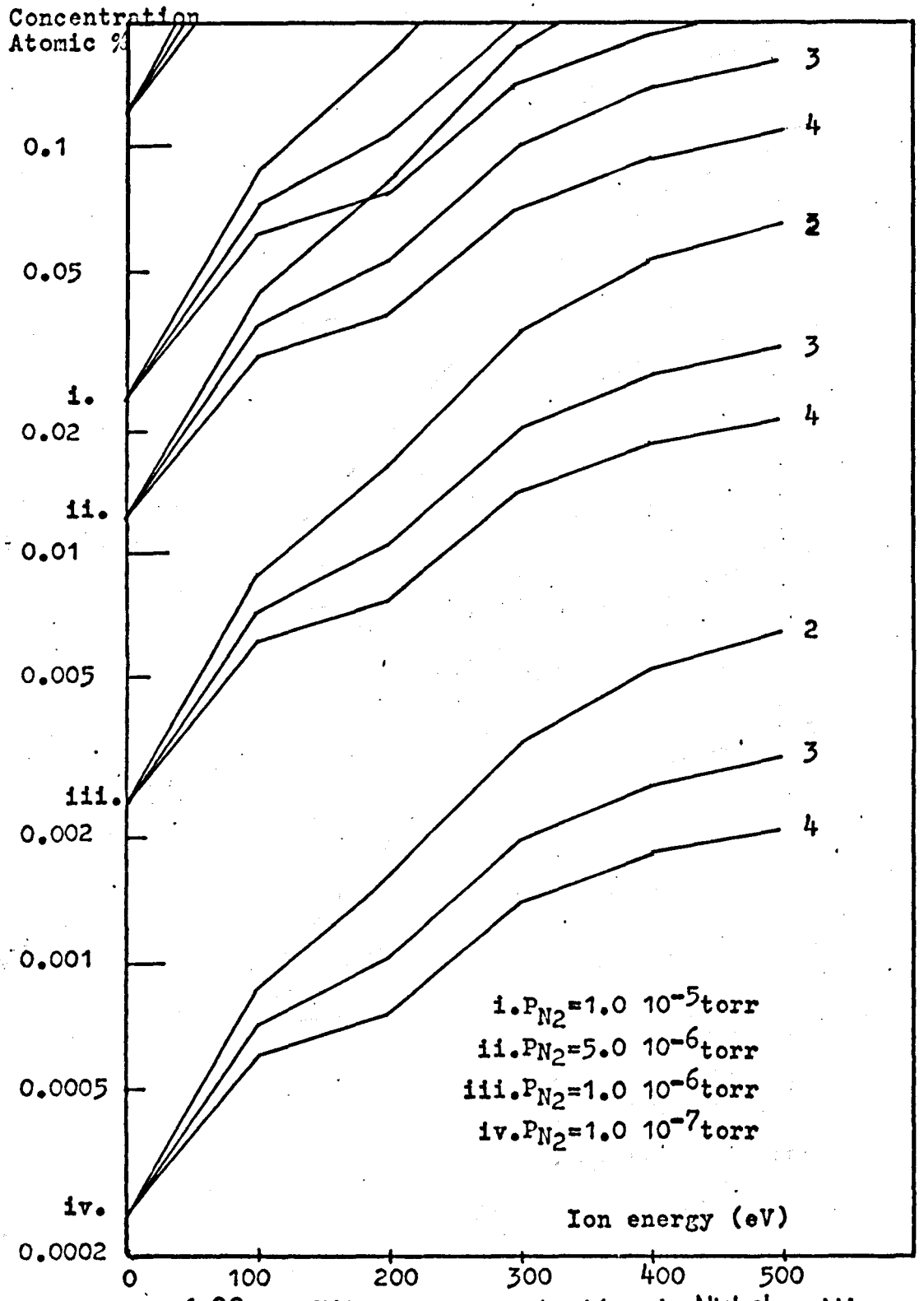

Figure 6.69 . Nitrogen concentration in Nickel with variation in ion energy.

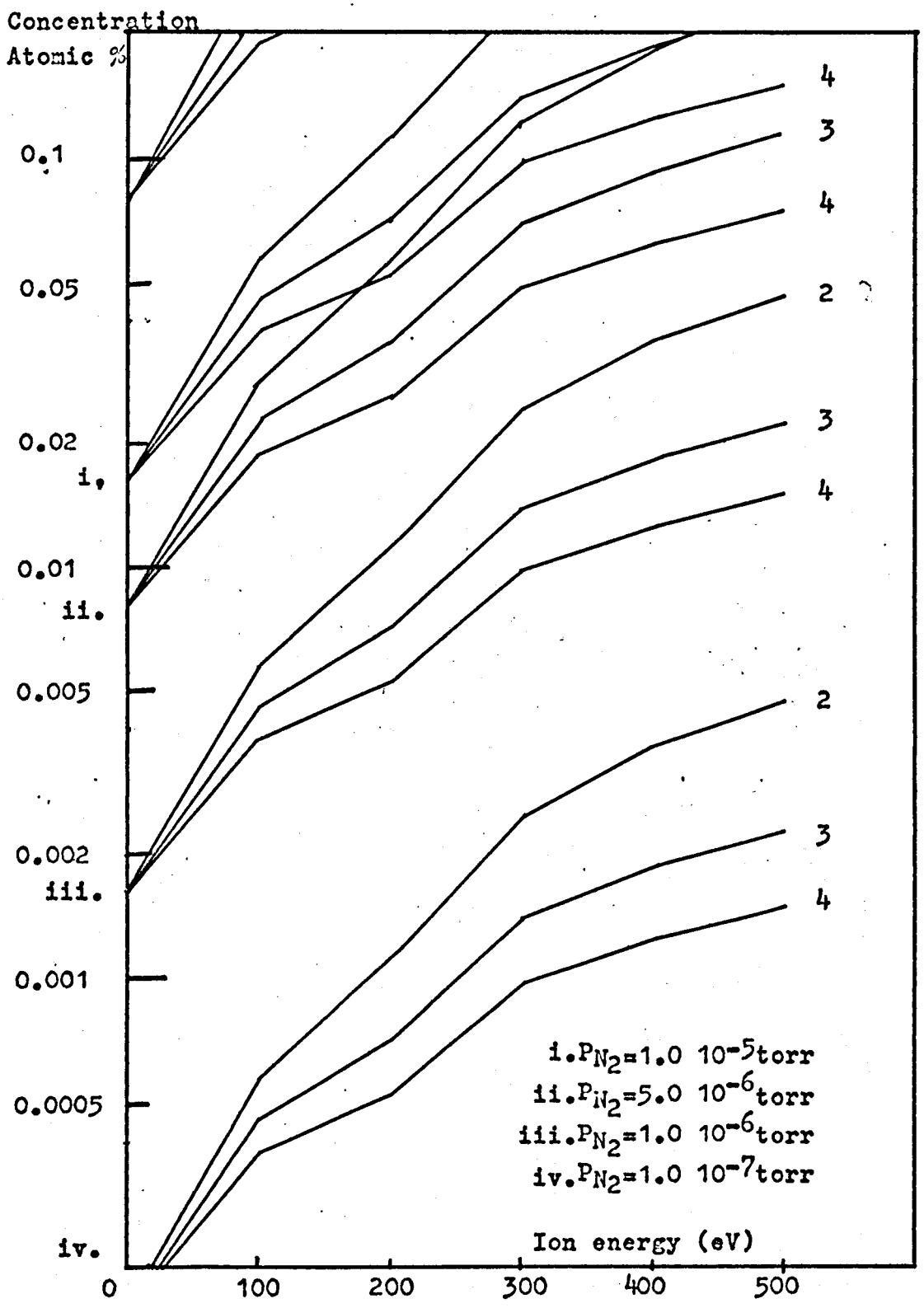

Figure 6.68. Nitrogen concentration in Copper with variation in ion energy.

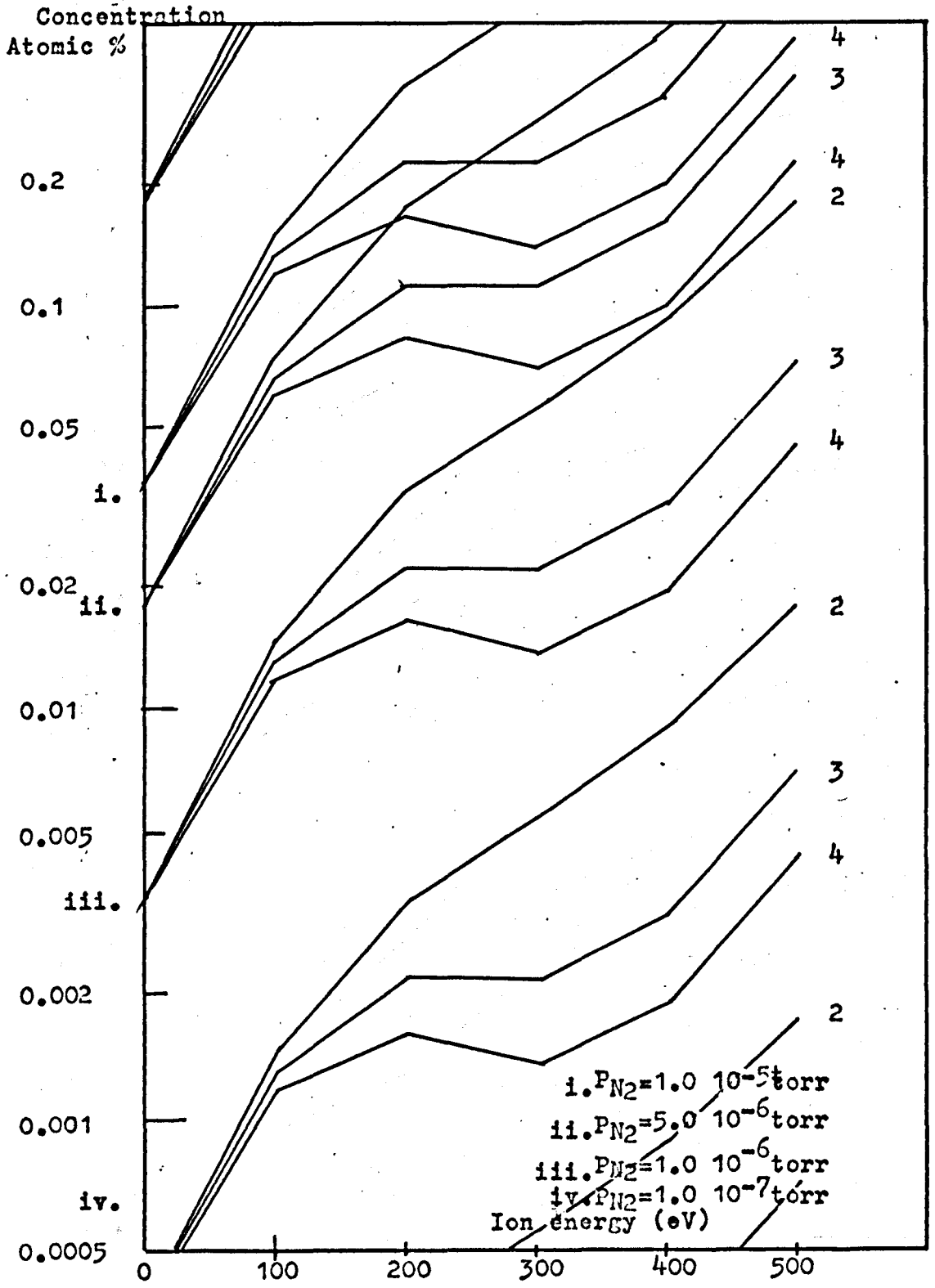

Figure 6.67. Nitrogen concentration in Aluminium with variation in ion energy.

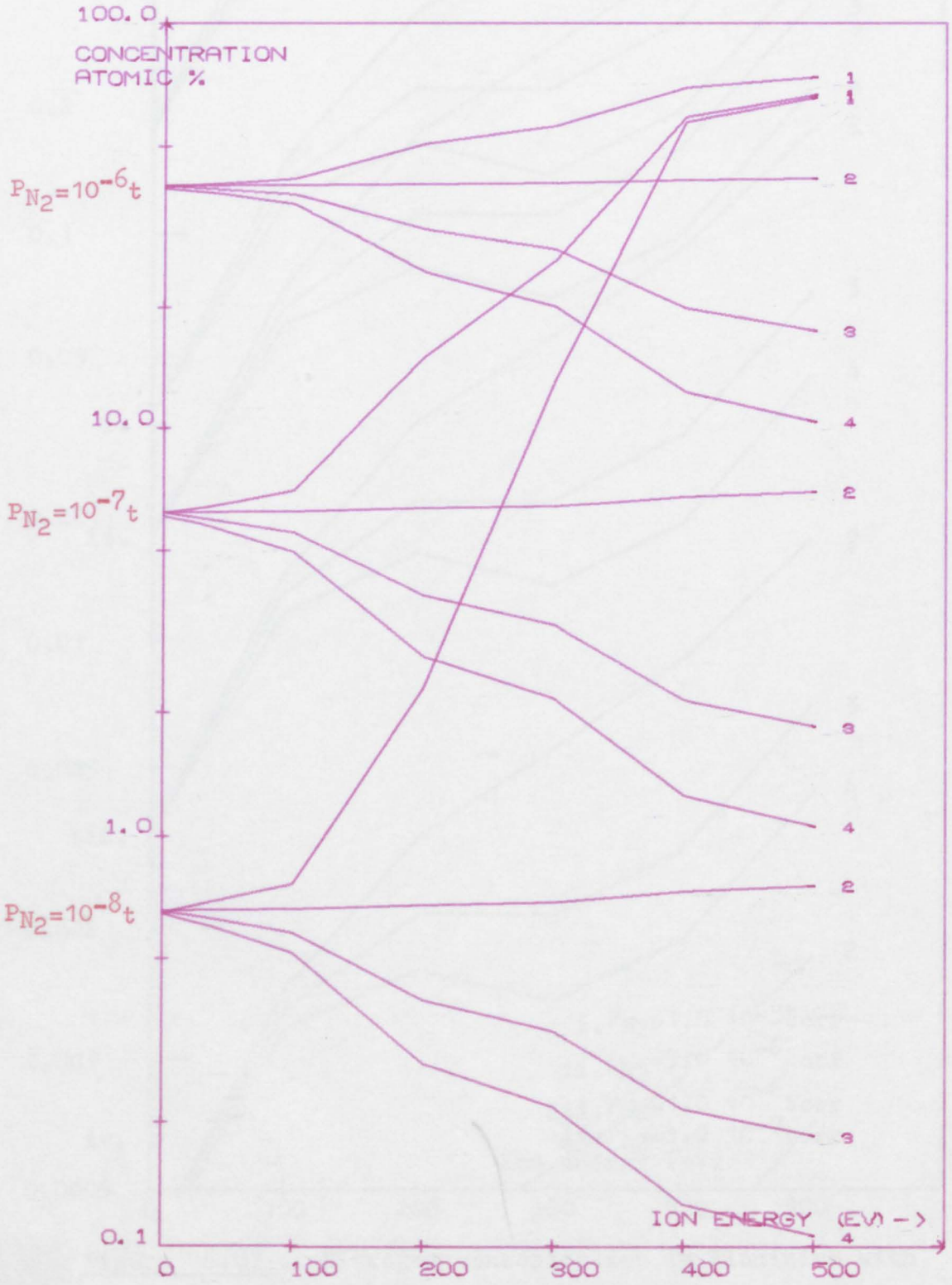

FIGURE 6.66. NITROGEN CONCENTRATION IN ZIRCONIUM WITH VARIATION IN ION ENERGY.

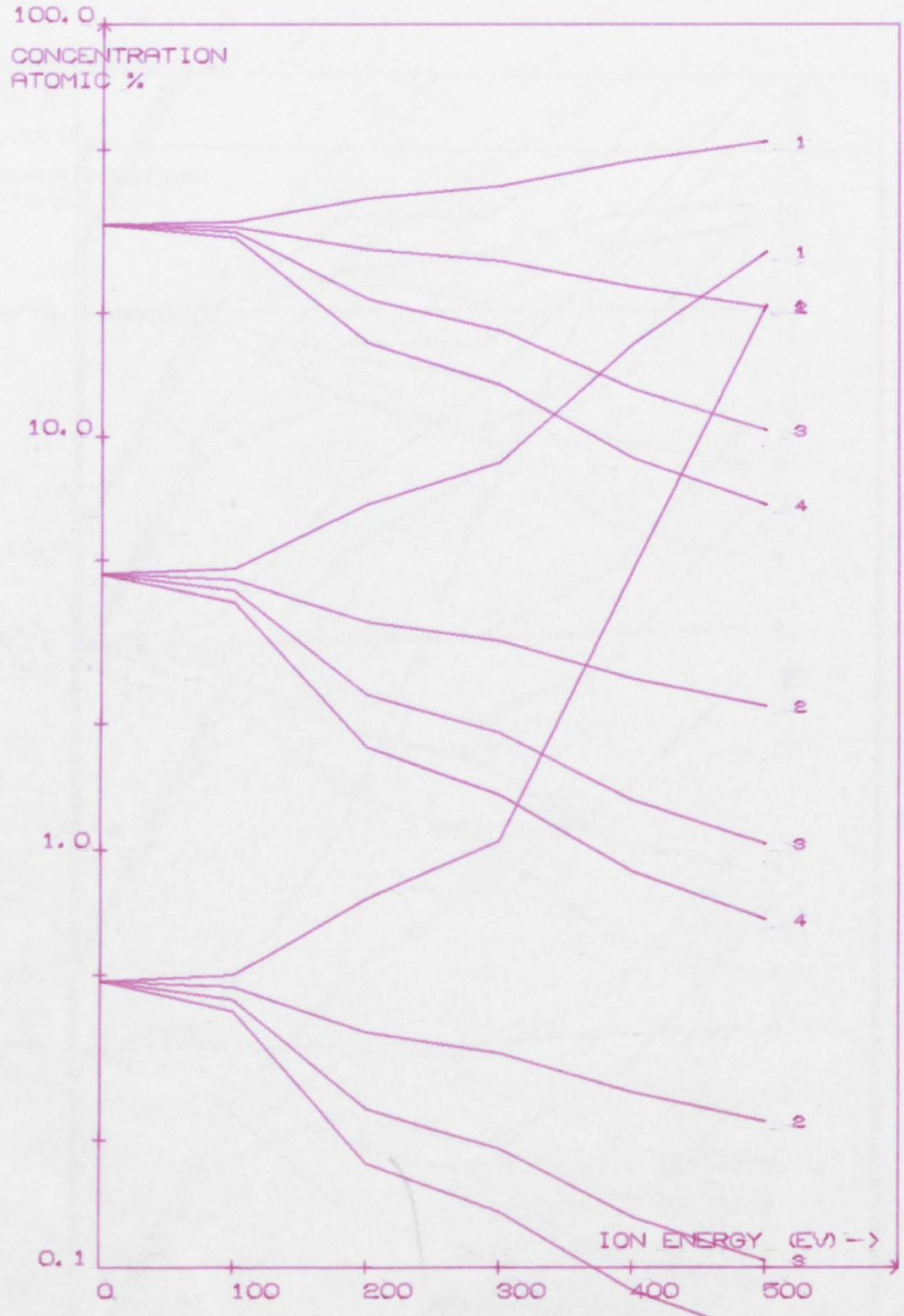

FIGURE 6.65 . NITROGEN CONCENTRATION IN TUNGSTEN WITH VARIATION IN ION ENERGY.

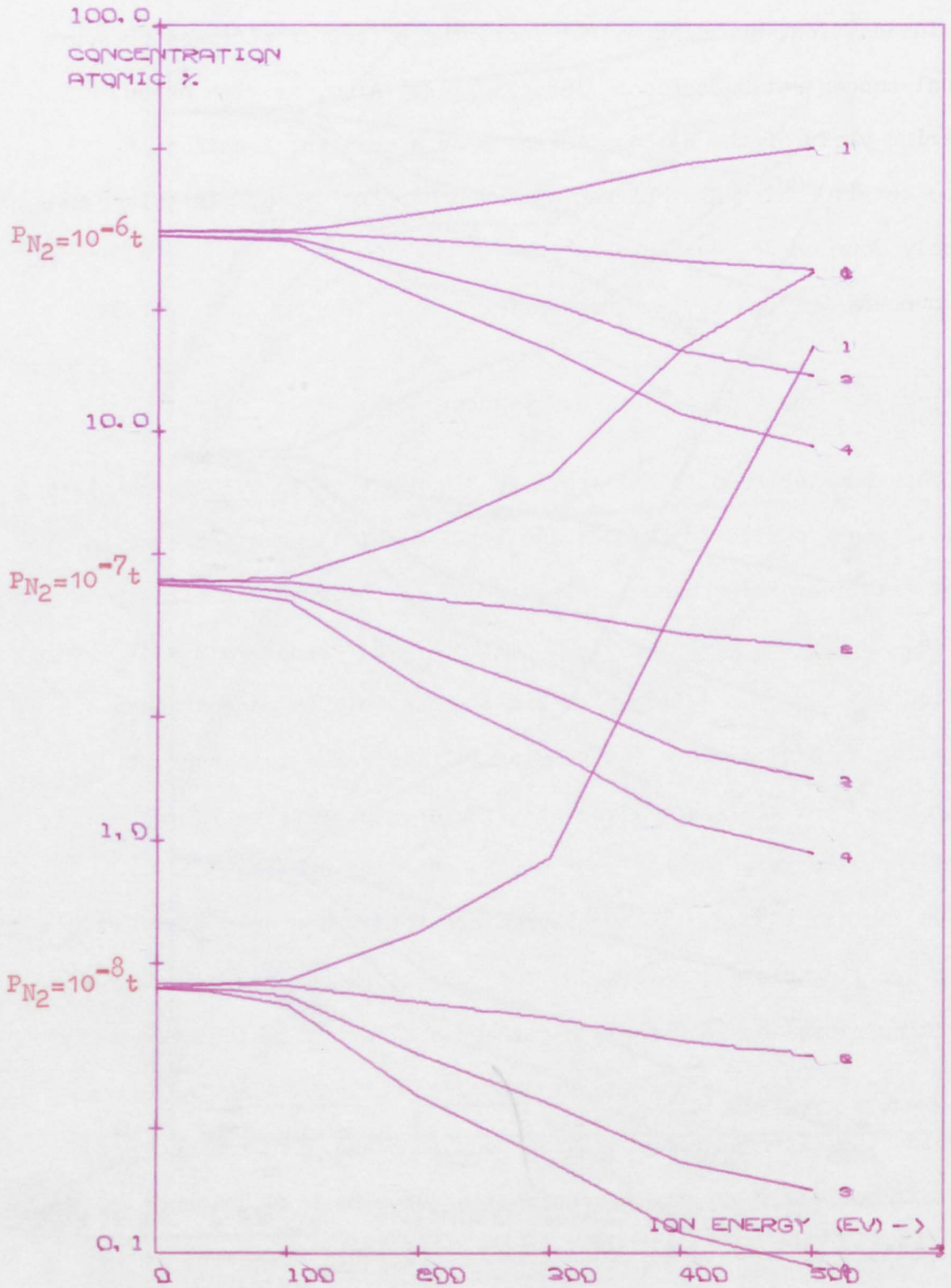

FIGURE 6.64. NITROGEN CONCENTRATION IN TITANIUM WITH VARIATION IN ION ENERGY.

λ_4 for energetic N_2^+ are taken to be the same as those for equivalent Ar^+ ions[205].

In addition, by using a 'DO' loop, the effect of nitrogen pressure on the final concentration could be investigated. Also, as with argon, the sputtering yield of the gas was taken to be a constant fraction of that of the metal. This was achieved with another 'DO' loop. In this case, however, only four curves were generated:-

numbers 1, 2, 3 and 4 representing

$$\frac{\alpha_1}{\alpha_2} = 0.5,\ 1.0,\ 1.5 \text{ and } 2.0 \text{ respectively.}$$

The computer results are shown in Figures 6.64 to 6.70. For class 1 materials, with gas sputtering yields > α_T, the model shows a decrease in gas content with increasing bias. This, indeed is observed for titanium and tungsten, in Figures 6.49 and 6.50, although the actual values of concentration are low by a factor of about 3 - 5. This is understandable when the gettering action above the growing film is taken into account. This gettering effect will reduce the actual nitrogen pressure in the vicinity of the film to a value less than the measured one (P_{N_2}).

On the other hand, the model predicts that where chemisorption does not occur, i.e. class 3 materials, the concentration should increase with increasing bias, thus acting in a fashion similar to that found earlier for argon. This is seen for gold in Figure 6.70. Figure 6.60 indicates that for gold, the nitrogen concentration does increase with ion energy. However, it is not clear why the concentration curve has gas contents an order of magnitude or more higher than those predicted. Moreover, it is difficult to find an explanation for the fact that the gas concentrations

for the evaporated films fall with increasing bias voltage and why there is such a large discrepancy between the values obtained for gold, deposited on tungsten and glass substrates, respectively.

The computer curves for the class 2 materials all show the nitrogen content increasing with ion energy. This is understandable, because by failing to include terms 2 and 3 in the R_1 equation, the class 2 materials are treated exactly as if they were class 3 materials. However, the nitriding properties of the class 2 metals are likely to have an effect on the concentrations found in these films. The concentrations in the class 2 films of aluminium, copper and nickel, will then behave like class 3 or class 1 materials or like a mixture of the two, depending on the ambient nitrogen pressure that they are grown in. Thus, in aluminium for example, it can be seen in Figure 6.54, that at low nitrogen pressures, $\sim 10^{-7}$ torr, the concentration increases with bias, whilst for nitrogen pressures a factor of 100 greater, the concentration decreases with bias.

Although, the results for the nitrogen incorporation, determined by the model, are necessarily speculative because of the uncertainty in the values of the parameters used, such as the number of nitrogen atoms reaching the film and the sticking probabilities for the various sorbing processes, it can be seen that the sputtering yield for the gas is also an important quantity in the incorporation process. If the yield is small compared with that of the metal, e.g. $\alpha_1 = 0.5\ \alpha_2$ the concentrations should increase with bias voltage for all metals, including those in class 1. This is at variance with the experimental results for tungsten and titanium. WINTERS[208] has measured the sputtering yield of chemisorbed nitrogen on tungsten and found it to be about twice that of tungsten. Furthermore, it

seems unlikely that, for most metal/gas combinations, the sorbed gas that would be exposed, when the target surface was eroded under ion bombardment, would have larger binding energies to the metal than exist between the metal atoms themselves. It follows then, that the sputtering yields for nitrogen are at least equal to those of the metal and thus is in agreement with the experimental results. In accordance with this reasoning, the experimentally derived titanium curve, shown in Figure 6.49, together with Figure 6.64, indicates a sputtering yield for nitrogen of about twice that of titanium. However, the quantitative agreement for the class 2 and 3 materials is not good and it is difficult to draw any conclusions as to the gas sputtering yields for these materials.

CHAPTER VII

Summary, conclusion and suggestions for further work.

This thesis necessarily shows only a small part of the large amount of work actually carried out by the author in setting up this new research group and in building the experimental apparatus from scratch.

The argon and nitrogen gas concentrations in thin films of seven metals have been measured. The metals were deposited by sputtering and evaporation techniques onto tungsten and glass substrates in a stainless steel ultra high vacuum system. The evaporation took place with and without a gas discharge present. The concentrations were measured as a function of bombarding ion energy (voltage bias), target voltages, gas pressure and film thickness. The partial pressures of the gases were deduced from the mass spectra, obtained using a Varian quadrupole residual gas analyser (QRGA). The vacuum conditions were such that the background pressure during deposition was, in most cases, better than 10^{-7} torr.

The technique used for outgassing the films has been shown to be effective, and with care and good vacuum baking techniques the sensitivity of the measuring method is better than 10^{-3} atomic % for a 1000 Å film. Calculation shows that the expected error in the concentration measurements has a value of about ± 25%, although the concentrations are more likely to have higher, rather than lower values, providing regettering of the gases does not take place. With improved techniques the expected error can be reduced to less than ± 10%.

Measurements for the argon, show a wide variation in concentration between the sputtered and evaporated deposits, even when grown at zero bias

(ZB). This can partly be attributed to the additional process of ion neutralization and reflection which takes place at the target of the sputtered samples but not at that of the evaporated ones. It was shown that, for argon, physical adsorption played little or no part in the incorporation process for either type of film. Increasing the bombarding ion energy, led, in all cases, to an overall increase in argon concentrations in the sputtered and evaporated films. This can be related to the gas clean-up mechanism by which energetic ions embed themselves in the film, where they become trapped by the continual flux of metal atoms arriving at the surface. For some metals a small decrease in concentration was observed at the highest biases applied of $\sim$ - 500 eV. The results have been compared with a model proposed by WINTERS et al[205] and are generally in accord with it. For a more rigorous comparison however, it would be necessary to have much more detailed knowledge of the values of the various parameters used in this model, since, at present, they are only tentatively known. With this in mind, sputtering yields for argon at various energies were deduced, based on the best fit between the theoretical and the experimental results. High sputtering yields for argon from various metals were indicated at the high voltage biases. and this suggests that a gas sputtering mechanism is in action. At lower ion energies, between 100 - 200 eV, the indications are that a target sputtering process is more likely to predominate as the means of gas release. This gives gas sputtering yields correspondingly lower and of the same order as those of the target material.

Differences in surface structure were looked for, using an electron microscope, to try to explain the discrepancy in inert gas content found between sputtered and evaporated films. No differences were observed for the

pre-outgassed films. For the outgassed sputtered samples, small 'crystallites' were observed on the surface. However, as yet, no reason has been found to explain the presence of these 'crystallites'.

Measuring the concentration at various argon pressures led to the slightly surprising conclusion that, within the pressure limits used here of 6.10^{-4} - 6.10^{-3} torr, working at higher pressures leads to purer films, i.e. lower argon concentrations.

For nitrogen incorporation, the seven metals investigated fit reasonably well into the three classes suggested by Winters. For class 1 metals titanium and tungsten, the incorporation is primarily by the chemisorption of molecular nitrogen and the concentration decreases with ion energy, as predicted by the Winters' model. The sputtering yields deduced for chemisorbed nitrogen of about twice those of titanium are in reasonable agreement with Winters' measurement on tungsten[208]. The incorporation in class 2 materials aluminium, copper and nickel, at low nitrogen pressures, is primarily by chemisorption of atomic nitrogen at endothermic and activated exothermic sites on the film surface. At higher nitrogen pressures the gas which is sorbed may form a partially nitrided surface which, in turn, may chemisorb molecular nitrogen. The concentration has been shown, then, to increase or decrease depending on the nitrogen pressure.

The primary incorporation mechanism for gold, a class 3 metal, is by energetic molecules and molecular ions, which physically embed themselves and become trapped in the film lattice. In accordance with Winters' model, the concentration increases with ion energy. However, to relate more clearly Winters' model to the experimental results, more detailed information must be known of; the state of the film surface during ion

bombardment; the actual number of reflected particles at the target arriving at the film surface and the sticking probabilities for the various different sorbing processes taking place at the growing films.

Many investigators have shown that applying a voltage bias during film growth often leads to an improvement in the film properties, for example, a reduction in the resistivity to a value more nearly approaching that of the bulk. They have related the improved properties to a reduction in the impurity concentration, brought about by the preferential resputtering of the impurity atoms, compared with the metal atoms. However, the results from the present work show that this generalisation is not necessarily true in every case and that in some situations, for example nitrogen in gold, bias sputtering actually leads to an increase rather than a decrease in the impurity content.

In order to expand the present investigation, several facilities should be added to the apparatus. By the addition of RF sputtering equipment the gas incorporation in sputtered dielectric films may be studied. Using a focussed pulse laser, rather than an induction heater, as a means of outgassing the films, many different depositions may be made on a single substrate. Furthermore, a pulsed laser, together with a long persistence screen oscilloscope, coupled to the QRGA, might help to reduce the difficulty, due to the regettering effect, in measuring the gas content in reactive metals.

A useful extension to the present work would be to measure a specific property of the film, such as its resistivity, during growth and to try and relate changes in it to the gas content, obtained under various conditions of voltage bias, target voltage, etc.

Also, the addition of specific amounts of various pure gases, such as oxygen, hydrogen, nitrogen, to the deposition chamber and the investigation of the gas content in sputtered and evaporated films, of different metals, as a function of these partial pressures, might also lead to a fuller understanding of the sorbing processes that occur for different gas/metal combinations.

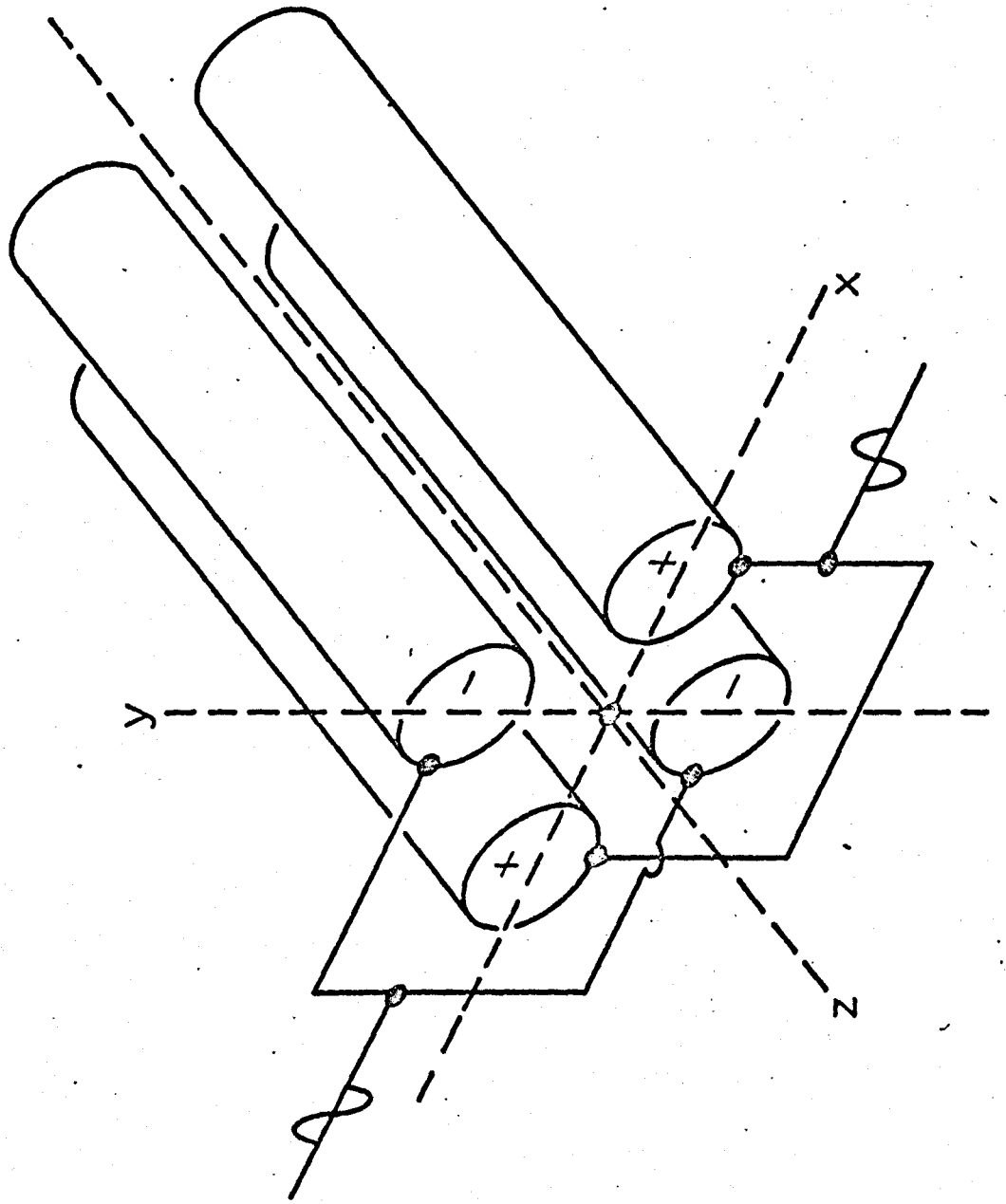

FIGURE A1. Geometry of the quadrupole mass filter.

APPENDIX A.

(1) The quadrupole residual gas analyser.

The quadrupole analyser was first described, in 1953, by PAUL and STEINWEDEL[259]. It is an electrostatic device and requires no magnetic field for its operation. Ideally, the analyser is composed of four long hyperbolic cylinders in a square array. The inside radius of the array being equal to the smallest radius of curvature of the hyberbolae. However, in practice, circular cross-section cylinders well approximate the hyperbolic array. Figure A.1. shows schematically the geometry of the quadrupole mass filter. As seen, opposite pairs of rods are connected electrically and both D.C. and A.C. potentials applied to them. The D.C. potentials, U, are opposite in sign and the A.C. potentials, V, are 180^{o} out of phase. An ion source is positioned at one end of the array of rods, and lying along the z axis. The ions are analysed as they travel along the array axis, and the resulting signal collected at the other end.

The potential at any point in the quadrupole is given by;

$$\Phi = (U + V \cos \omega t) \left(\frac{x^2 - y^2}{r_o^2}\right)$$

where r_o is half the separation between opposite rods. It can be seen that when $x = y = 0$, i.e. along the z axis, the potential Φ is zero, and in the two planes xz and yz, given by $y = 0$, $x = 0$ respectively, the electric fields are given by:

$$E_x = \frac{-\partial \Phi}{\partial x} = -2(U + V.\cos.\omega t) \frac{x}{r_o 2}$$

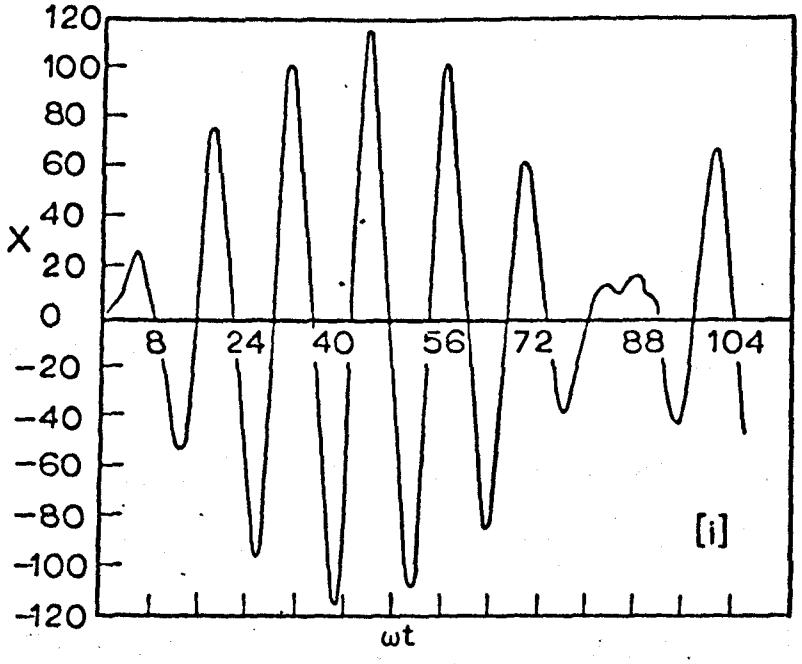

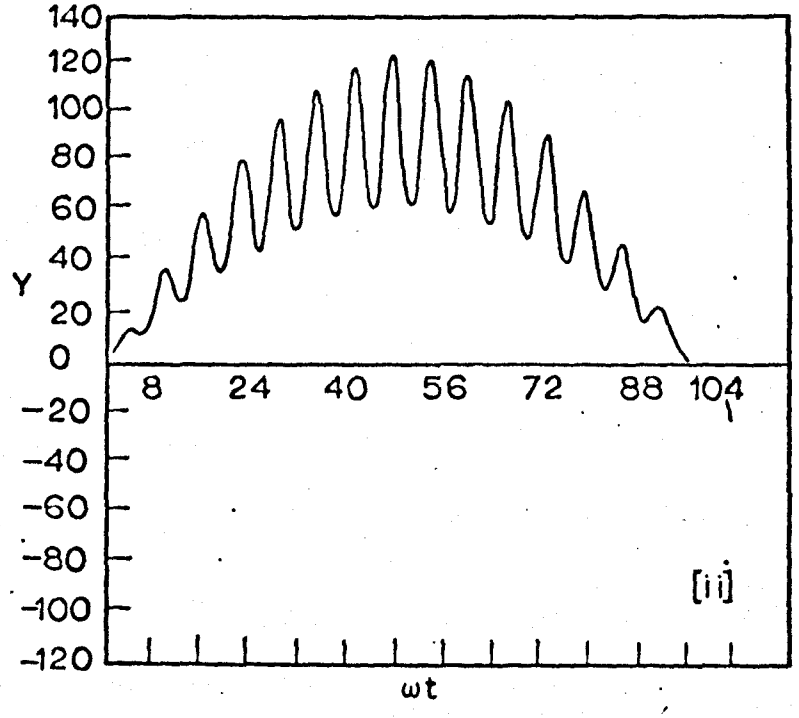

FIGURE A.2 Ion trajectories in
[i] the x-z plane
[ii] the y-z plane
for a = 0·231 and q = 0·7038

$$E_y = \frac{-\partial\phi}{\partial y} = -2(U + V.\cos.\omega t)\frac{y}{r_o^2}$$

$$E_z = \frac{-\partial\phi}{\partial z} = 0$$

A positively charged particle in the array will experience forces on it given by:

$$F_x = M\ddot{x} = eE_x = \frac{-2ex}{r_o^2}(U + V.\cos.\omega t)$$

$$F_y = M\ddot{y} = eE_y = \frac{-2ey}{r_o^2}(U + V.\cos.\omega t)$$

$$F_z = 0.$$

Using the substitutions:

$$t = 2S,\ a = \frac{8eU}{Mr_o^2\omega^2} \text{ and } q = \frac{4eV}{Mr_o^2\omega^2},$$

the equations are simplified to the so-called Mathieu equations:-

$$\frac{d^2x}{dS^2} - (a + 2q.\cos 2S).x = 0$$

and

$$\frac{d^2y}{dS^2} - (a + 2q.\cos 2S).y = 0.$$

These generally can only be solved approximately, and only for a certain range of a and q. The approximate solutions for the ion trajectories are given in Figure A.2 for the two basic situations; along the xz planes and yz planes, when assuming that U = 200 volts and V = 1000 volts

In the xz plane.

Positive ions are strongly focussed by the positive D.C. potential alone, whilst the ion trajectory oscillates, about the z axis, at half the RF

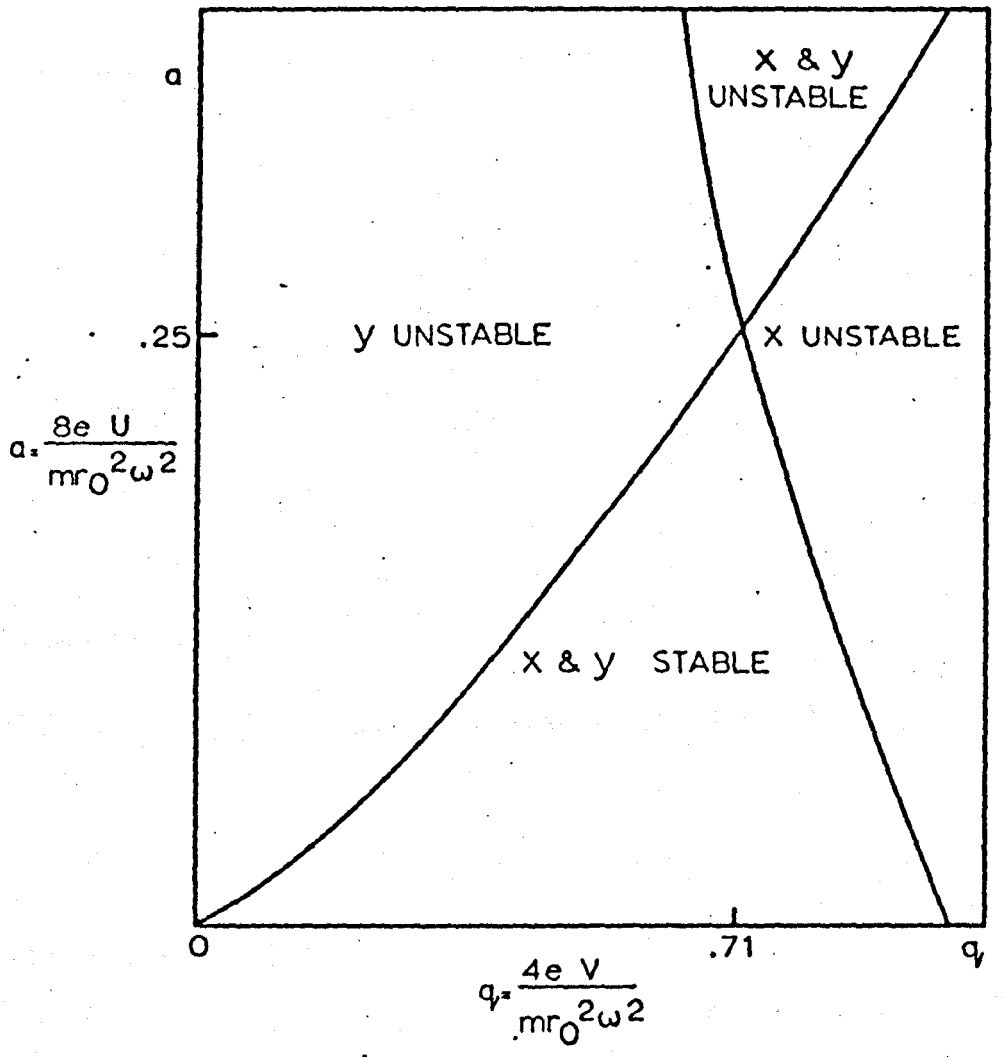

FIGURE A.3 Stability diagram showing the values of a and q_y for which stable ion trajectories are possible.

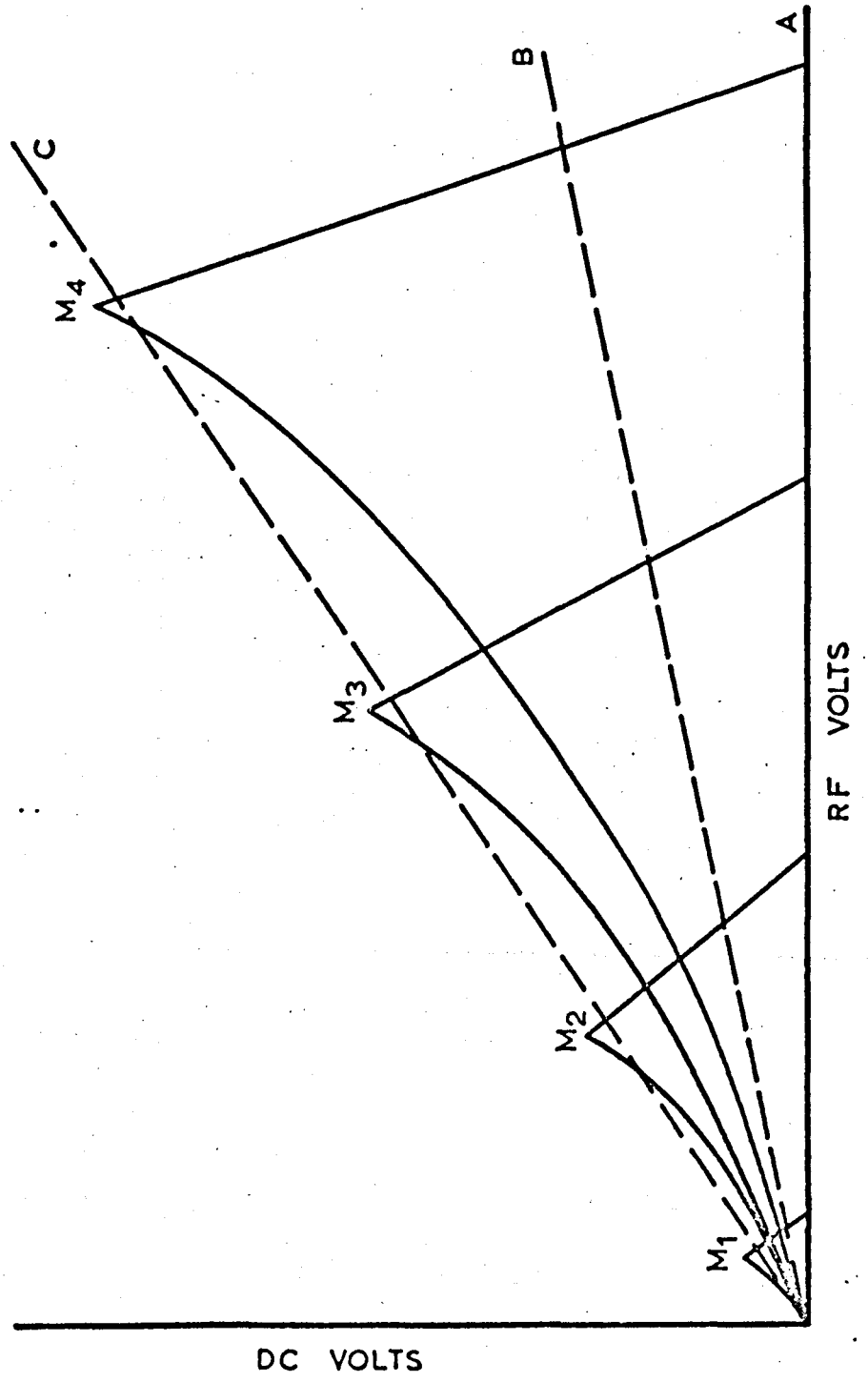

FIGURE A.4 Stability diagrams for four masses $M_1 < M_2 < M_3 < M_4$

frequency, due to the RF field. At their oscillating extremities, the ions are reflected by coincidence with the positive cycle of the RF potential on opposite rods.

In the yz plane

The ions are defocussed by the negative D.C. potential, but net focussing arises because of the effect of the larger R.F. voltage. The frequency of oscillation is, in this case, equal to the R.F. frequency, and the final ion trajectory lies unsymmetrically to one side of the z axis. The net focussing effect lies in the fact that the ion is closer to the rod when it is positive, than when it is negative, so that, at the reflection point nearest the rod, the acceleration towards the z axis is always greater than away from it.

This will, however, only occur if the voltages and ion masses are well chosen. For example, if the ion mass is such that the RF field fails to balance the D.C. potential in the yz plane, or alternatively if the oscillations in the xz plane, due to the R.F. field, are too large, the ion will not pass through the array but will be collected at one of the rods.

Figure A.3. shows a stability diagram for which a and q have their lowest range of values. So long as an ion has (a, q) values lying in the stable region of this diagram, it will move in a stable trajectory, through the filter, to the collector. If it's (a, q) value lies outside the 'triangle' of stability, it's trajectory is unstable, in at least one plane, and, providing the filter is long enough, the ion will be collected at one of the rods. For constant values of r_o, e, and ω, a range of M/e can be scanned by varying the potentials U and V. Figure A.4 shows, as an example, the stability 'triangles' for four masses where $M_1 < M_2 < M_3 < M_4$. It can be seen

that the ion mass varies linearly with V and the 'triangle' area varies linearly with mass. Thus, a linearly varying mass spectrum is obtained by sweeping the D.C. and R.F. voltages simultaneously, whilst keeping their ratio, U/V, constant. The width of the mass peaks and their separation, i.e. their 'resolution' depends on the ratio U/V. If U = 0, so that U/V = 0, no peaks are resolved and ions of all masses pass along the filter on stable trajectories to the collector. This corresponds to line A and is used for total pressure measurement. For low ratios of U/V, such as, line B, on the figure, mass separation is achieved but the peak width is rather wide. The optimum separation, and hence resolution, occurs when U/V ~ 0.16, corresponding to line C in Figure A.4.

In practice, the stability diagram only has a 100% stability in the body of the 'triangle' with the probability of stability decreasing at it's top and edges. This arises because of the effects of fringing fields at entry and exit apertures, radial and axial ion velocities, analyser length etc. To ensure that the scanning line passes through a region of 100% stability (and hence transmission), this must be at the expense of optimising the mass separation and mass width, i.e. the resolution. Thus resolution is traded off against sensitivity and vice versa.

(2) Calculation of partial pressures.

A computer programme, in Fortran 4, was written to facilitate the calculations of the partial pressures obtained from the mass spectra, and as described in chapter 6. To make the programme acceptable in Fortram 4, some of the symbols have been changed. The corresponding symbols are given below:

PPCO = pp_{co}, the absolute corrected partial pressure of carbon monoxide in torr.

PPN2 = $pp._{N_2}$, the absolute corrected partial pressure of nitrogen in torr.

PP2 = pp_2, the absolute, corrected partial pressure of hydrogen in torr.

PP28 = pp_{28}, the absolute, corrected partial pressure of a.m.u.28 in torr.

PP40 = pp_{40}, the absolute, corrected partial pressure of argon in torr.

The programme

```
    REAL N2
    DIMENSION NB(20),A(20),AMU(50)
   1SM(20),P2(20),P28(20),P40(20),PCO(20,3),PN2(20,3)TPT(20),NPT(20)
888 READ(7,100) DATE, T1,T2,NEXP
100 FORMAT(3A5,I5)
    WRITE(2,110)  DATE,T1,T2
110 FORMAT(1H1//10X,2A5,4X,2HON,A5/10X,21(1H*))
    READ(7,101)(NB(I),I=1,18)
101 FORMAT(18I4)
    DO 999 III=1,NEXP
    READ(7,102) (A(I),I=1,18)
102 FORMAT(8F10.2)
    READ(7,103) TP,NP
103 FORMAT(F10.2,I10)
    TPT(III)=TP
    NPT(III)=NP
    DO 1 I =1,44
```

```
    1 AMU(I)=0
      DO 2 I=1,18
    2 AMU(NB(I))=A(I)
      AMU(2)=AMU(2)*10.5
      AMU(4)=AMU(4)*16.5
      AMU(44)=AMU(44)*0.73
      SUM=0.
      DO 3 I=1,18
    3 SUM=SUM+AMU(NB(I))
      PP2=AMU(2)*TP/SUM *10.**NP
      PP40=AMU(40)*TP/SUM*10.**NP
      PP28=AMU(28)*TP/SUM*10.**NP
      SM(III)=SUM
      P2(III)=PP2
      P28(III)=PP28
      P40(III)=PP40
      WRITE(2,104) (NB(I),I=1,18),(A(I),I=1,18),SUM,PP2,PP40,PP28,TP,NP,
     1      III
  104 FORMAT(////6X,18I7//6X,18F7,1///17X,3HSUM,17X,3HPP2,16X,4HPP40,
     1           16X,4HPP28,12X,8HTOT/PRES, 9X,5HPOWER/F20.3,
     2          3E20.11,F20.3,I12,I10)
      NAMU=12
      NN=1
      CO5=1.29
      CO=66.6*AMU(NAMU)-1.7/1.5*AMU(44)-21/1.5*AMU(16)*0.357
    4 N2=AMU(28)-12.6/100.*AMU(44)-CO
      CON2=CO+N2
      PPCO=CO*TP/SUM *10.**NP
      PCO(III,NN)=PPCO.  PPN2=N2*TP/SUM*10.**NP.  PN2(III,NN)=PPN2.
      WRITE(2,105)NAMU,CO,N2,CON2,PPCO,PPN2
  105 FORMAT(//10X,8HFOR AMU(,I2,1H)/10X,11(1H*)//18X,2HCO,18X,2HN2,
     1           15X,5HCO+N2,16X,4HPPCO,16X,4HPPN2/5E20.11)
      NAMU=14
      NN=NN+1
      CO=3.47/3.0*(AMU(28)-0.126*AMU(44)-25.6*AMU(14)+CO5*AMU(16)*0.36)
```

```
      CO5=0.0
      IF(NN.LT.4) GOTO 4
  999 CONTINUE
      WRITE(2,110) DATE,T1,T2
      WRITE(2,108)
  108 FORMAT(//7H NUMBER,7X,3HSUM,15X,3HPP2,14X,4HPP28,14X,4HPPCO,14X,
     1        4HPPN2,14X,4HPP40,15H TOTAL PRESSURE,5X,5HPOWER)
      DO 444 I=1,NEXP
      WRITE(2,106) I,SM(I),P2(I),P28(I),PCO(I,1),PN2(I,1),P40(I),
     1             TPT(I),NPT(I)
  106 FORMAT(/I7,F10.2,5E18.2,F15.2,I10)
      DO 44 J=2,3
   44 WRITE(2,107) J,PCO(I,J),PN2(I,J)
  107 FORMAT(45X,3H(14,I1,1H),3X,2E18.2)
  444 CONTINUE
      GO TO 888
      STOP
      END
```

APPENDIX B

Calculation of sheath thickness.

Sheath thickness around target is given by

$$d^2 = \frac{4\epsilon_o}{9j} \left[\frac{2q}{m}\right]^{\frac{1}{2}} V^{3/2}$$

V is target voltage in volts = Typical values -1600

j is current density due to ions in Am^{-2} = +10

m is the mass of ion in Kg = $6.7\ 10^{-26}$ (for argon)

q is the charge on a singly ionized ion in C. = $1.6\ 10^{-19}$

ϵ_o is permitivity of free space in Fm^{-1} = $8.85\ 10^{-12}$

Therefore

$$d^2 = \frac{4x8.85x10^{-12}}{9x10} x \left[\frac{2x1.6x10^{-19}}{6.7x10^{-26}}\right]^{\frac{1}{2}} x\ 1600^{3/2}$$

$$d^2 = 51.2\ 10^{-6}$$

$$d = 7.2\ 10^{-3} \text{ metres}$$

i.e. $d \simeq 7$ mm.

APPENDIX C.

Filament calculations.

For a temperature of 2600°C. (i.e. white light emission)

$$i/_d{}^{3/2} = 1632 \text{ Amps cm}^{-3/2}$$

where i is the current required, d is the filament diameter,

For a diameter d of 0.075 cm:-

$$d^{3/2} = 20.54\ 10^{-3} \text{ cm}^{-3/2}$$

$$\therefore i = 1632 \times 20.54 \times 10^{-3} \text{ Amps}$$

$$i = 33.6 \text{ Amps}$$

(From tables 3 and 4, page 149-150, Bachman Experimental Physics.)

Life of filament at 2600°C diameter 0.075 cm

equals 0.231 x 4890 hours

= 1130 hours approx.

APPENDIX D

To calculate gas concentrations in metal films

To make the programme acceptable in Fortran 4, some of the symbols have been changed. The corresponding symbols are listed below:-

PP and NPW = pp_i, the partial pressure of gas i where pp_i is in the form $PP.10^{-NPW}$ torr.

BP and NBW = bp_i, the background partial pressure of gas i where bp_i is in the form $BP.10^{-NBW}$ torr.

AA = A_s, the area of the film in cm^2.

TH = T_s, the thickness of Å of film.

CM = $C_{i/m}$, the concentration of gas, i, in metal, in atomic % and is defined as $\frac{N_g^i}{N_g^i+N_m} \times 100$ (in chapter 4).

GG = is the coefficient obtained for N_g^i/N_m after substituting for V, ℓ_m, and M_n, in equations (5) and (6), page 105, chapter 4.

Material	Aluminium	Copper	Gold	Nickel	Titanium	Tungsten	Zirconium
GG	3.06	2.17	3.20	2.02	2.23	2.91	4.30

THE PROGRAMME

```
DIMENSION TITLE(6),PP(5),NPW(5),BP(5),CC(5),NBW(5)
INTEGER TH,EXPNO,YY
READ(7,99) NOS
```

```
 99 FORMAT(8I10)
    DO333 JJ=1,NOS
    READ(7,100) (TITLE(I),I=1,6),AA,GG,NBP
100 FORMAT   (6A5,2F5.2,I5)
    WRITE(2,101) (TITLE(I),I=1,6),AA,GG
101 FORMAT(1H1///10X,6A5,10X,2F5.2 ,/10X,30(1H*)///33X,2HP2,12X,3HP28,
   1             10X,5HP12N2,
   2              10X,5HP14N2,12X,3HP40,7X,8HTOTPRESS,3X,9HTHICKNESS
   3             6X,4HXO/G//)
    DO 13 NN=1,NBP
    READ(7,102) (BP(I),I=1,5),TP,NEXP
    READ(7,99) (NBW(I),I=1,5),NTW
    DO 12 I=1,5
    BI=BP(I)
    NB=NBW(I)*(-1)
 12 BP(I)=BT*10.**NB
    NB=NTW*(-1)
    TP=TP*10.**NB
102 FORMAT(6F10.2,2I10)
    WRITE(2,103) (BP(I),I=1,5),TP
103 FORMAT(//18X,2HBP,6E15.6/)
    DO 14  J=1,NEXP
    READ(7,102) (PP(I),I=1,5)TP,TH,YY
    READ(7,99) (NPW(I),I=1,5),NTW,EXPNO
    DO11 I=1,5
    PT=PP(I)
    NB=NPW(I)*(-1)
 11 PP(I)=PT*10.**NB
    NB=NTW*(-1)
    TP=TP*10.**NB
    WRITE(2,104) EXPNO,(PP(I),I=1,5)TP,TH,YY
104 FORMAT(/13X,4HPPNO,I3,6E15.6,2I10/)
    DO 51 I=1,5
    CC(I)=0.
    BT=BP(I)
```

```
      PT=PP(I)
      PBT=PT-BT*YY
      IF (PT.LT.0.OR.BT.LT.0.OR.PBT.LT.0) GO TO 51
      CC(I)=PBT*GG*10.**7/TH/AA
      CM    =100*CC(I)/(100+CC(I))
      CC(I)=CM
   51 CONTINUE
   14 WRITE(2,105) (CC(I),I=1,5)
  105 FORMAT(/16X,4HCONC,5E15,3,/16X,82(1H*)//)
   13 CONTINUE
  333 CONTINUE
      STOP
```

APPENDIX E

THE PROGRAMME

```
      REAL LM4,NA,K1,K2,NB
      DIMENSION CX(10,30),NAME(3)
      READ (7,100 ) NN
100   FORMAT ( 8I10)
      CALL ORIGIN(300,0)
      DO 99 I=1,NN
      READ ( 7,102) NAME, B2
102   FORMAT(2A4,A2,F10.2)
      WRITE (2,103 ) I, NAME
103   FORMAT(///I5,5X,9HARGON IN,2A4,A2,/5X,30(1H*) //6X,10HION ENERGY,
     13X,5HLAMDA, 2X,6HALPHA1, 2X, 6HALPHA2,6X, 2HA1,6X, 2HA2, 6X,2HR2
     26X, 2HNI, 2(8X,2HK1,8X,2HK2,7X,3HCA1)//)
      CALL ORIGIN(300,0)
      CALL WAY(0,4)
      III=0
      CALL MOVE(0,- 540)
      WRITE (9,200) III
200   FORMAT (I1)
      CALL MOVE(0, - 500)
      DO 250 III=1,6
      LL=III*100
      KK=LL*1.6+0.5
      CALL DRAW(KK     , -500)
      IF (III.EQ.6) GO TO 252
      CALL CENCH (1)
      CALL MOVE(KK     ,-540)
      WRITE(9,202) LL
202   FORMAT(13)
250   CALL MOVE(KK     ,-500)
252   CALL CENCH(9)
      CALL MOVE(-110,-500)
      YY=0.1
      WRITE(9,201) YY
```

```
201 FORMAT(F5.1)
    CALL MOVE(0,-500)
    IS=-(1.0-ALOG10(2.0))*500.0+0.5
    IT=-(1.0-ALOG10(5.0))*500.0+0.5
    DO 260 III=1,3
    CALL DRAW(0,IS)
    CALL CENCH(1)
    CALL DRAW(0,IT)
    CALL CENCH(1)
    IS=IS+500.0
    IT=IT+500.0
    CALL DRAW(0,III* 500-500)
    CALL CENCH(1)
    CALL MOVE(-110,III*500-500)
    YY=YY*10
    WRITE (9,201) YY
260 CALL MOVE (0,III*500-500)
    CALL CENCH(10)
    CALL DRAW(160*6,1000)
    CALL DRAW(160*6,-500)
    CALL MOVE(-110,950)
    WRITE(9,304)
304 FORMAT(13HCONCENTRATION)
    CALL MOVE(1110,920)
    WRITE(9,305)
305 FORMAT(9HATOMIC %)
    CALL MOVE(600,-480)
    WRITE (9,303)
303 FORMAT (17HION ENERGY (EV)->)
    CALL MOVE(-110,-610)
    WRITE(9,301)
301 FORMAT(45HFIGURE      .     ARGON CONCENTRATION IN)
    CALL MOVE(160,-640)
    WRITE(9,302) NAME
302 FORMAT(2A4,A2, 30H WITH VARIATION IN ION ENERGY.)
```

```
      DO 88 J=1,6
      EV=(J-1)*100
      READ (7,101) NB,LM4,AP1,AP2,A1,A2
  101 FORMAT (8F10.3)
      NA=NB*10.**14
      R2=B2*10.**14
      R1=LM4*NA  + 1.81*10**14*0.1
      DO 77 JJ=2,21
                  AP1=AP2*1.0(JJ-1)
      IF(AP2.GT.0.) GO TO 32
      X=A2/A1
      GOTO 37
   32 X=AP2*A2/(AP1*A1)
   37 A=X-1
      II=0
      B=((2.*X-1.)*R1-(X-1.)*NA*AP1+(A2*R2)/A1
      C=R1*(X*R1+A2/A1*(R2-AP2*NA))
      BB=B**2-4.*A*C
      IF(BB.LT.0.) GO TO 77
      K1=(-B+SQRT(B**2-4.*A*C))/(2.*A)
      K2=R2/(1+X*(R1/K1-1))
      CA1=K1/(K1+K2)
   34 II=II+1
      K1=K1/(10.**15)
      K2=K2/(10.**15)
      IF(II.EQ.1) CK2=K2
      CA1=CA1*10.**2
      GO TO (33,35),II
   33 WRITE(2,104) EV,AP1,A1,B2,K1,CA1
  104 FORMAT(6X,F10.1,2F16.3,E16.3,E18.3,E20.3)
      K1=(-B-SQRT(B**2-4.*A*C))/(2.*A)
      K2=R2/(1+X*(R1/K1-1))
      CA1=k1/(K1+K2)
      GO TO 34
   35 WRITE(2,105) K2
```

```
105 FORMAT(1H+,102X,E20.3)
106 FORMAT(80X,I10)
    WRITE(2,107) LM4,AP2,A2,NB,CK2,K1,CA1
107 FORMAT(8X,3F16.3,E16.3,3E20.3)
    CX(J,JJ) = ALOG10(CA1)
 77 CONTINUE
 88 CONTINUE
    CALL WAY(0.3)
    DO 261 JJ=2,21
    JJM=JJ-1
    IY=CX(1,JJ)*500+0.5
    CALL MOVE (0,IY)
    DO 262 J=2,6
    IY =CX(J,JJ)* 500+0.5
    IX=(J-1)*160
262 CALL DRAW(IX,IY)
    CALL MOVE(IX+5,IY-10)
261 WRITE(9,202) JJM
    CALL MOVE (0,2000)
 99 CONTINUE
    STOP
    END
```

REVIEWS

A number of reviews have been published under the general heading of sputtering or, as some prefer to call it, impact evaporation.

The very earliest work from 1952-1930 has been reviewed by FRUTH[1] in which he lists 113 references on this subject, and by GLOCKER and LIND[2] up to 1939.

More recent research performed in the last twenty years, and which is described in Chapter 3, has been extensively reviewed by:- MASSEY and BURHOP (1956)[3]; GUNTHERSCHULTZE(1953)[4]; WEHNER (1956)[5]; HOLLAND (1956)[6]; KAY (1962)[7]; BERISCH (1964)[8*]; MAISSEL (1966)[9]; and MAISSEL (1968)[9a]; KAMINSKY,as a chapter in his book on "Impact phenomena on metal surfaces" published in 1965[10]. Finally CARTER and COLLIGON in 1968 have presented, in some detail, a review of sputtering as well as ion trapping and gas release mechanisms in their book entitled "Ion bombardment of solids"[11].

REFERENCES

1. FRUTH, H.F., Physica, 2, 280, 1939.
2. GLOCKER, G. and LIND, S.C., 'Electrochemistry of gases and other dielectrics', John Wiley and Sons, 1939.
3. MASSEY, H.S.W. and BURHOP, E.H.S., "Electronic and Ionic Impact phenomena', O.U.P., N.Y., 1952.
4. GUNTHERSCHULTZE, A., Vacuum, 3, 360, 1953.
5. WEHNER, G.K., Advances in Electronic and Electron Physics, 7, 239, 1955.
6. HOLLAND, L., 'Vacuum deposition of thin films', Chapter 14, Chapman Hall, London, 1956.
7. KAY, E., Advances in Electronic and Electron Physics, 14, 245, 1962.
8. BERISCH, R., Exabt Naturwissen (translation into English privately obtained), 35, 295, 1964.
9. MAISSEL, L.I., Physics of thin films, 4, 61, 1966.

9a. MAISSEL, L.I., IBM Technical Report TR, 22-672, (latter incorporated into 'Handbook of thin film Technology', McGraw Hill, 1970)

10. KAMINSKY, M., 'Atomic and ionic impact phenomena on metal surfaces', Springer Verlag, 1965.
11. CARTER, G. and COLLIGON, J.S., 'Ion bombardment of solids', Chapter 7, Heinmann, London, 1968.

12. BLECHSCHMIDT, T.E., Ann Physik, 81, 999, 1926.
13. POHL, R. and PRINGSHEIM, P., Ver dtsch Phys Ges, 14, 546, 1922.
14. WEHNER, G.K., J. Appl. Phys, 26, 1056, 1955.
15. DAVIDSE, P.D., Trans 3rd Int. Vac. Congress, Stuttgart, 1965.

16. McCALDIN, J.O., Nucl Inst. and methods, 38, 153, 1965.

17. WEHNER, G.K., METRA, C.E., and ROSENBERG, D.C., Planetry Science, 11, 855, 1963.

18. HALL, L.D., Rev. Sci. Inst., 29, 367, 1958.

19. VAN ATTA, C.M., 'Vacuum Science and Engineering', McGraw Hill (N.Y.) 1965.

20. CARTER, G. and COLLIGON, J.S., 'Ion bombardment of solids', Heinmann (London), Chapter 9, 423, 1968.

21. GROVE, W., Trans. Roy. Soc. (London), 142, 87, 1852.

22. PLUCKER, J., Pogg Ann, 103, 88, 1858.

23. WRIGHT, J., Am. J. Science (3rd Series), 13, 49, 1887.

24. VON HIPPEL, A., Ann Physik, 81, 1043, 1926.

25. GUNTHERSCHULTZE, and TOLLMEIN, W., Z. Physik, 119, 685, 1942.

26. GUNTHERSCHULTZE, A. and MEYER, K., Z. Physik, 62, 607, 1931.

27. GUNTHERSCHULTZE, A. and MEYER, K., Z. Physik, 71, 271, 1931.

28. PENNING, F.M., and MOUBIS, J.H3A., Koninki Ned Akad Wetenschap Proc., 43, 41, 1940.

29. DITCHBURN, R.W., Proc. Roy. Soc., A141, 169, 1933.

30. WOOD, R.W., Phil Mag., 30, 300, 1915.

31. KNUDSEN, M., Ann Physik, 50, 472, 1916.

32. INGERSOLL, E.R., and HANAWALT, J.D., Phys. Rev., 34, 972, 1929.

32a. INGERSOLL, E.R. and SORDAHL, L.O., Phys. Rev., 32, 649, 1928.

33. VON HIPPEL, A. et al., Ann Physik, 86, 1006, 1928.

34. BLODGETT, K.B., and VANDERSLICE, T.A., J. Appl. Phys., 31, 6, 1960.

35. COBINE, J.D., 'Gaseous conductors', Dover (N.Y.), 1958.

36. PENNING, F.M., 'Electrical discharges in Gases', Macmillan, N.Y. 1957.

37. MAISSEL, L.I., 'Handbook of thin film technology' Ed. Glang, R. et al, McGraw Hill, Chapter 6, 1970.

38. WEHNER, G.K., Advances in Electronic and Electron Physics, 7, 244, 1955.

39. DAVIS, W.D. and VANDESLICE, T.A., Phys Rev., 131, 219, 1963.

40. KAY, E., Advances in Electronic and Electron Physics, 14, 245, 1962.

41. BLEVIS, E., Report from R.D. Mathis, February, 1964.

42. LANGMUIR, I. and TONKS, L. Phys Rev., 34, 896, 1929

43. WEIJSENFELD, C.H., Phillips Research Reports, Supplement 2, 1966.

44. FRANCIS, A., Handbuch der Physik (Editors Flugge) Springer (Berlin) 22, 53, 1956.

45. GILL, W.D. and KAY, E., Rev. Sci. Inst., 36, 277, 1965.

46. KAY, E., J. Appl. Phys., 34, 760, 1963.

47. SEEMAN, J., 'Ion implanted films', (private communication).

49. WEHNER, G.K., Bull. Amer. Phys Soc. Series II, 4, 111, 1959.

50. KOEDAM, M, Phillips Research Reports, 16, 101, 1961.

51. HOLLAND, L. and SIDDALL, G., Vacuum, 3, 245, 1953.

52. STRONG, J., Phys Rev., 43, 498, 1933.

53. STRONG, J. et al., 'Modern Physical Laboratory practice', Blackie (London), 1944.

54. DAMIANOVICH, H. et al., Proc. 8th American Science Congress (Phys & Chem. Series), 7, 137, 1940.

55. BOOMER, E.H., Proc. Roy. Soc., A109, 198, 1935.

56. WALLER, J.G., Nature, 186, 429, 1960.

57. KAY, E., Adv. in Electronic and Electron Physics, 14, 305, 1962.

58. UVAROV, E.B. et al., 'A Dictionary of Science', Penguin, 59, 1964.

59. MANDELCORN, L., Chem. Rev., 59, 827, 1959.

60. WINTER, H.F., and KAY, E., J. Appl. Phys., 38, 3928, 1967.

61. KAY, E., J. Vac. Sci. and Technol., 7, 317, 1970.

62. KORNELSON , E.V., Canadian J. of Phys., 42, 364, 1964.

63. HAGSTRUM, H.D., Phys. Rev., 104, 317, 1956.

64. BLODGETT, K.B., and VANDERSLICE, T.A., J. Appl. Phys., 31, 1017, 1960.

65. CARMICHAEL, J.H., and TRENDELBOURG, F.A., J. Appl. Phys., 29, 1570. 1958.

66. CARMICHAEL, J.H. and WATERS, P.M., J. Appl. Phys., 33, 1470, 1962.

67. NORTON, F.J., 1961 Vac. Symp. Trans., 8, 1962.

68. ROBINSON, N.W. 'Physical Principles of UHV systems and equipment' Chapman Hall (London) Chapter 7, 1968.

69. LeCLAIRE, A.D. and ROWE, A.H., A.E.R.E. Rpt. M/R, 14A, 1957.

70. HAYWARD, D.O. and TRAPNELL, B., 'Chemisorption', Butterworths (London) 1964.

71. EHRLICH,G., J. Chem. Phys., 31, 1111, 1959.

72. HOBSON, J.P., Brit. J. Appl. Phys., 14, 544, 1963.

73. BECKER, J., Solid State Physics, Academic Press (N.Y.) 7, 379, 1958.

74. LEE, D. et al., Trans. 1961 Vac. Symposium, AVS, 153, 1962.

75. LEWIN, G., 'Fundamentals of Vacuum Science and Technology', McGraw Hill (N.Y.), 4, 1965.

76. WINTERS, H.F., J. Chem. Phys., 4, 2766, 1964.

77. KAY, E. and WINTERS, H.F., Trans 3rd Int. Vac. Congress, 2, 351, 1966.

78. GLANG, R. and MAISSEL, L.I., 'Handbook of thin film technology' McGraw Hill (London), 1970.

79. KAMINSKY, M., Atomic and Ionic impact phenomena on metal surfaces, Springe Verlag, 1965.

80. HAGSTRUM, H.D., Phys. Rev., 96, 336, 1954.

81. FLUIT, J.M., KISTEMAKER, J. and SNOEK, C., Physica, 30, 870, 1964.

82. ARIFOV, U.A., et al, Bull Acad. Sci. U.S.S.R. Phys. Series, 26, 1450, 1963.

83. BRADLEY, R.C., Phys. Rev., 93, 719, 1954.

84. BRUNEE, C., Zeit t, Physik, 147, 161, 1957.

85. SMITH, D.P., J. Appl. Phys., 38, 340, 1967.

86. HINES, R.L., Phys Rev., 120, 1626, 1960.

87. NELSON, R.S., and THOMPSON, M.W., Phil. Mag., 8, 1677, 1963.

88. KORNELSEN, E.V., 1961, 8th Nat. Vac. Symp. AVS Pergammon Press, 281, 1962.

89. KORNELSEN, E.V. and SINHA, M.K., Appl. Phys. Lett., 9, 112, 1966.

90. KORNELSEN, E.V., Canad. J. of Phys., 42, 364, 1964.

91. CARMICHAEL, J.H. and KNOLL, J.S., 1958 Vac. Symp. trans., 18, 1959.

92. CARMICHAEL, J.H. and TRENDELBOURG, F.A., J. Appl. Phys., 29, 1570, 1958.

93. JAMES, L.H., and CARTER, G., Brit. J. Appl. Phys., 13, 3, 1962.

94. KUCHAI, S.A. and RODIN, A.M., Soviet J. At. Energy (English translation) 4, 277, 1958.

95. CARTER, G., COLLIGON, J.S., and LECK, J.H., Proc. Phys. Soc. (London) 79, 299, 1962.

96. WOLSKY, S.P., 1963 Vac. Symp. trans. AVS, 309, 1964.

97. JAMES, L.H. and CARTER, G., 1962 Vac. Symp. trans. AVS, 502, 1963.

98. JAMES, L.H. and CARTER, G., Brit. J. Appl. Phys., 14, 147, 1963.

99. BILLINGTON, O.S., CRAWFORD, J.H., 'Radiation damage in solids', Princeton.U., 1961.

100. THOMPSON, M.W. and NELSON, R.S., Phil. Mag., 7, 2015, 1962.

101. HAGSTRUM, H.D., Phys Rev., 96, 336, 1954.

102. KAMINSKY, M., 'Atomic and Ionic impact phenomena on metal surfaces' Springer-Verlag (N.Y.) Chapter 12, 263, 1965.

103. KINGDON, K.H. and LANGMUIR, I., Phys Rev., 21, 380, 1923.

105. BRADLEY, R.C., J. Appl. Phys., 30, 1, 1959.

106. HONIG R.G., J. Appl. Phys., 29, 549, 1958.

107. WEHNER, G.K., Phys. Rev., 103, 35, 1957.

108, WEHNER, G.K., Phys. Rev., 93, 633, 1954.

109. WEHNER, G.K., Phys. Rev., 112, 1120, 1958.

110. LAEGRID, N., WEHNER, G.K. and MECKEL, B., J. Apll. Phys, 30, 374, 1959.

111. WEHNER, G.K., J. Appl. Phys, 30, 1762, 1959,

112. LAEGRID, N. and WEHNER, G.K., J. Appl. Phys., 32, 365, 1961.

113. ROSENBERG, D. and WEHNER, G.K., J. Appl. Phys., 33, 1842, 1962.

114. ANDERSON, G.S. and WEHNER, G.K., J. Appl. Phys., 31, 2305, 1960.

115. ANDERSON, G.S., J. Appl. Phys., 34, 659, 1963.

116. ANDERSON, G.S. and WEHNER, G.K., Surface STience, 2, 367, 1964.

117. ANDERSON, G.S., J. Appl. Phys., 36, 1558, 1965.

118. ANDERSON, G.S., J. Appl. Phys, 37, 2983, 1966.

119. ANDERSON, G.S., J. Appl. Phys., 37, 3455, 1966.

120. EDGECOMBE, J., ROSNER, L.G. and ANDERSON, G.S., J. Appl. Phys., 35, 2198, 1964.

121. KOEDAM, M., Phillips Research Reports, 16, 101, 1961.

122. WEIJSENFELD,G.H., Phillips Research Reports, Supplement 2, 1967.

123. SEEMAN, J.M., Trans 8th Annual conf. on vacuum metallurgy, 1965.

124. MULY, E.C. and ARONSON, A.J., Extended Abstract AVS symposium, 145,1969.

125. NEUGEBAUER, C.A. and EKVALL, R.A., J. Appl. Phys., 35, 547, 1964.

126. THEUERER, H.C. and HAUSER, J.J., J. Appl. Phys. 35, 554, 1964.

127. BERGHAUS, B. and BURKHARDT, W., U.S. Patent 2,305,758 Dec. 1942.

128. WEHNER, G.K., U.S. Patent 3,021,271, Feb. 1962.

129. GLANG, R., HOLMWOOD, R.A. and FUROJUS, P.C., Trans 3rd Int. Vac. Congress, 1965.

130. FLUR, B.L., Proc. Int. magn. conf., 2, 4-1, 1965.

131. WINTERS, H.F., IBM Research Report RJ.898, 1971

132. FRERICH, R., J. Appl. Phys., 33, 1898, 1962.

133. HAY, R.H., Canadian J. of Research, A16, 191, 1938.

134. SPIVAK, G.V. et al., DOKL Acad. Nauk SSR, 104, 579, 1955

135. DUGDALE, R.A. and FORD, S. P., Brit. Ceramic Soc. Trans. 65, 165, 1966.

136. HINES, R.C. and WALLOR, R., J. Appl. Phys., 32, 202, 1961.

137. SCHWARTZ, N., 10th Nat. Vac. Symp., 325, 1963

138. ANDERSON, G.S., MAYER, W.N. and WEHNER, G.K., J. Appl. Phys., 33 2991, 1962.

139. DAVIDSE, P.D. and MAISSEL, L.I., 3rd Int. Vacuum Congress, Stuttgart, 1965.

140. BUSH, V. and SMITH, G.C., J. Am. Inst. of Electr. Engrs., 41, 627, 1922.

141 THOMSON, J.J., 'Rays of positive electricity', Longmans Green (N.Y.) 1921.

142. CROOKES, W., Proc. Roy. Soc. (London), 50, 88, 1891.

143. STARK, J., Zeit Elektronchem, 14, 752, 1908.

144. TOWNES, C.H., Phys. Rev., 65, 319, 1944.

145. SEELINGER, R. and SOMMERMEYER, K., Z. Physik, 93, 692, 1935.

146. ROCKWOOD, G.H., Trans. Am. Inst. Elect. Engrs, 60, 901, 1941.

147. NELSON, R.S., Phil Mag., 11, 291, 1965.

148. KINGDON, K.H. and LANGMUIR, I., Phys. Rev., 22, 148, 1923.

149. LAMAR, E.S. and COMPTON, Science, 80, 54, 1934.

150. KEYWELL, F., Phys. Rev., 91, 1611, 1955.

151. HARRISON, D.E., J. Chem. Phys., 32, 1336, 1960.

152. MOORE, W.W., Am. Scientist, 48, 109, 1960.

153. ROL, P.K., et al., Proc. 3rd Conf. Ioniz. Phenomena in gases UPPSALA 257, 1959.

154. SILSBEE, R.H., J. Appl. Phys, 28, 1246, 1957.

155. NELSON, R.S., Phil Mag., 8, 693, 1963.

156. NELSON, R.S. and THOMPSON, M.W., Phys. Lett., 2, 124, 1962.

157. ALLEN, F.G. et al, J. Appl. Phys., 30, 1563, 1959.

158. MIGNOLET, J.C.P., Rev. trav. chim., 74, 685, 1955.

159. HAGSTRUM, H.D., Phys. Rev., 104, 1516, 1956.

160. CHANG, C.C. and GERMER, C.H., Surface SCience, 8, 115, 1967.

161. RIVIERE, J.G., Bull. Phys Soc., 85, 1969.

162. ROBERTS and VANDERSLICE, 'Ultra High Vacuum and its applications' Prentice Hall (N.J.), 1964.

163. BEDAIR, S.M. and SMITH, H.P. jr., J. Appl. Phys., 40, 4776, 1969.

164. LEVINE, L.P. et al, J. Appl. Phys., 38, 331, 1967.

165. FARNSWORTH, H.E. et al., J. Appl. Phys, 29, 1150, 1958.

166. FARNSWORTH, H.E., 'The surface chemistry of metals and semi conductors' J. Wiley (N.Y.), 21, 1960.

167. WEHNER, G.K., Phys. Rev., 102, 690, 1956.

168. FARNSWORTH, H.E., J. Appl. Phys, 26, 252, 1955.

169. FARNSWORTH, H.E. et al., J. Appl. Phys, 29, 1195, 1959.

170. GOBELI, G.W. and ALLEN, F.W., J. Phys. Chem. Solids, 14, 23, 1960.

171. CHOPRA, K.L., J. Appl. Phys., 37, 3405, 1966.

172. FRANCOMBE, M.H., 3rd Int. Vac. Congress (1964), 52, 1965.

173. GESTENBERG, D. and HALL, P.M., J. Electrochem. Soc., 111, 936, 1964.

174. MELMED, A.J., J. Appl. Phys., 37, 275, 1966.

175. CASWELL, H.L., J. Appl. Phys., 32, 105, 1961.

176. SOSNIAK, J. and HULL, G. W. jr., J. Appl. Phys, 38, 4390, 1967.

177. GERSTENBERG, D., Annalen des Physik, 7, 354, 1963.

178. GERSTENBERG, D. and CALBRICK, Y., J. Appl. Phys, 35, 402, 1964.

179. MICHALAK, E.D., Vacuum, 17, 317, 1967.

180. KRIKORIAN, E. and SNEED, R.J., J. Appl. Phys., 37, 3674, 1966.

181. COOK, H.C., J. Vac. Sci. and Technol., 4, 80, 1967.

182. SOSNIAK, J., J. Vac. Sci. and Technol., 4, 87, 1967.

183. SOSNIAK, J., POLITO, W.S. and ROZONYI. G.A., J. Appl. Phys., 38, 3041, 1967.

184. TOOMBS, P.A.B. and BENNETT, P., J. Appl. Phys., 39, 2948, 1968.

185. MAISSEL, L.I. and SCHAIBLE, P.M., J. Appl. Phys., 35, 237, 1965.

186. OBLAS, D.W. and HODA, H., J. Appl. Phys., 39, 6106, 1968.

187. LEE, W.W. and OBLAS, D.W., J. Vac. Sci. and Technology, 7, 130, 1970.

188. SACHSE, H.P. and NICHOLS, G.G., J. Appl. Phys., 41, 4237, 1970.

189. MATTOX, D.M. and KOMINIAK, J. J. Vac. Sci. and Technol. 8, 196, 1971.

190. VARNERIN, L.J. and CARMICHAEL, J.H., J. Appl. Phys., 26, 782, 1955.

191. YOUNG, J.R., J. Appl. Phys., 27, 926, 1956.

192. SMEATON, G.P., CARTER, G. and LECK, J.H., Trans 9th Nat. Vac. Symp. AVS, 491, 1962.

193. CARTER, G. and LECK, J.H., Brit. J. Appl. Phys., 10, 364, 1959.

194. COLLIGON, J.S. and LECK, J.H., Trans 8th Nat. Vac. Symp. AVS. 275, 1961.

195. CARMICHAEL, J.H. and KNOLL, J.S., Trans. 5th Nat. Vac. Symp. AVS. 18, 1958.

196. JENKINS, R.O. and TRODDEN, W.G., Vacuum, 10, 319, 1960.

197. BROWN, F. and DAVIES, J.A., Canadian J. Phys., 41, 844, 1963.

198. KORNELSON, E.V., Canadian J. Phys., 42, 364, 1964.

199. JAMES, L.H., LECK, J.H. and CARTER, G., Brit. J. Appl. Phys., 15, 681, 1964.

200. JAMES, L.H. and CARTER, G., 9th Nat. Vac. Symp. AVS, 502, 1963.

201. CARMICHAEL, J.H. and WATERS, P.M., J. Appl. Phys., 33, 1470, 1962.

202. WINTERS, H.F., J. Chem. Phys., 43, 926, 1965.

203. WINTERS, H.F., J. Chem. Phys., 44, 1472, 1965.

204. JONES, R.E., WINTERS, H.F. and MAISSEL, L.I., J. Vac. Sci. and Technol., 5, 84, 1967.

205. WINTERS, H.F., RAIMONDI, D.L. and HORNE, D.G., J. Appl. Phys., 40, 2996, 1969.

206. WINTERS, H.F., J. Vac. Sci. and Technol., 7, 262, 1969.

207. WINTERS, H.F. and HORNE, D.E., Surface SCience, 24, 587, 1970.

208. WINTERS, H.F., J. Vac. Sci. and Technol., 8, 17, 1971.

209. RAIMONDI, D.L., WINTERS, H.F. et al., IBM Research Report RJ.826, March, 1971.

210. WINTERS, H.F., Private communication (1969) and (1971).

211. RAIMONDI, D.L. and KAY, E., IBM Research REport RJ.607, September, 1969.

212. WINTERS,H.F. and KAY, E., IBM Research Report, RJ.898, August, 1971.

213. WINTERS, H.F. and KAY, E., IBM Research Report, RJ.900, August, 1971.

214. DUSHMAN, S., 'Scientific Foundations of Vacuum technique' Wiley (N.Y.) 693, 1961.

215. LANGMUIR, I., Phys. Rev., 2, 329, 1913.

216. REDHEAD, P.A., Vacuum, 12, 203, 1962.

217. HARRISON, D.E. Jr. et al., Phys. lett., 8, 33, 1966.

218. (Editor) SUTTON, L.E., 'Tables of Interatomic distances, etc.' The Chemical Society, Burlington House, (LONDON), 1965.

219. WEHNER, G.K., General Mills Report, Office of Naval Research.

220. WEIJSENFELD, C.H. and HOOGENDOORN, A., Proc. 5th Conf. on ioniz. phen. in Gases, Munich, 1, 124, 1962.

221. EHRLICH, G., J. Chem. Phys., 34, 39, 1961.

222. WELCHER, F.W., 'Standard methods of chemical analysis, Chapter 36, Van Nostrand (N.Y.) 1963.

223. GULDNER, W., Anal. Chem. 35, 1744, 1963, and, IEEE. Trans Compts Part CP 11, 1967.

224. VRATNY, J., J. Electrochemical Soc., 114, 505, 1967.

225. HUTCHINS, G.A., 'The electron microprobe' J. Wiley (N.Y.), 390, 1966.

226. SLOAN, R.D., Adv X-ray analy., 5, 512, 1962.

227. HOFFMEISTER, W.& ZUEGAL, M, Thin solid films, 2, 35, 1969.

228. GUTHRIE, JW! Mass spectromic analysis of solids', Elsever (N.Y.) Chapter 14, 1966.

229. BILLS, D.G. and EVETT, A.A., J. Appl. Phys., 30, 564, 1959.

230. Vacuum Generators Technical information Bulletin No.4., 1968.

231. LEWIN, G., 'Fundamentals of Vacuum Science and Technology' McGraw Hill (N.Y.) 69, 1965.

232. Vacuum Generators Technical information Bulletin No.3., 1968.

233. ROBERTS, R.W. 'An outline of Vacuum technology' G.E. Report No. 64-RL-3394. C,33, 1964.

234. Varian Associates 'New large cell Vac-Ion pump instruction manual, 27, 1965

234a. ~~27.~~ Radio Heaters Ltd , Berkshire , Private Comm , 1968.

235. FRANCIS, A.B., and JEPSEN, R.L., Varian Ass. technical reprint, VR. 24.

236. CLAUSING, R.E., Varian Ass. technical reprint, 'A large scale getter pumping experiment using vapour deposited titanium films'.

237. Varian Ass. Instruction manual for dual range ionization gauge, 1965.

238. RIEGERT, R.D., 'Optimum usage of quartz crystal monitor based devices' (Sloan Instruments).

239. JONES and LANGMUIR, I., General Electric Review, 1927.

240. BACHMAN, C., 'Experimental Physics", Chapman Hall (London) 147, 1948.

241. RUARK, J.O.S.A. and R.S.I., 13, 205, 1926.

242. Vacuum Generators Instruction manual on M.6. bakeable leak valve.

243. Varian Ass. Instruction manual on quadrupole residual gas analysers, 1966.

244. GREENLAND, K.M., Vacuum, 2, 216, 1952.

245. BERNDT, K.H., 'Film thickness and deposition rate monitoring devices of thin films', Physics of anion films, No.3, 1966.

246. GREAVES, C., Vacuum, 20, 332, 1970.

247. LANGMUIR, I. and MOTT-SMITH, General Elect. Rev., 2, 449, 1924.

248. CRAIG, R.D. and HARDIN, E.H., Vacuum, 16, 67, 1966.

249. ENGLANDER-GOLDEN, P. and RAPP, D., Lockhead Missiles and Space RLport 1965.

250. VACUUM GENERATORS LTD, Technical Information Bulletin 'Mass Spectrometer Partial Pressure Gauge' 1968.

251. STERN, E. and CASWELL, H.L., J. Vac. Sci. and Technol., 4, 128, 1966.

252. BOVEY, R.E., Vacuum, 19, 497, 1969.

253. REDHEAD, P.A. et al. 'The Physical basis of UHV' Chapman Hall (London) 167, 1968.

254. STUART, R.V. and WEHNER, G.K., J. Appl. Phys., 35, 1819, 1964.

255. KAY, E., J. Appl. Phys., 34, 760, 1963.

256. MITCHELL, I.V. and MADDISON, R.C., Vacuum, 21, 591, 1971.
(Through an error, the carbon monoxide concentration was plotted instead of the nitrogen concentration in Figure 7)

257. TATE, O.T. and SMITH, P.T., Phys Rev., 39, 270, 1952.

258. HARRA, D.J. and HAYWARD, W.H., Suppl. Nuovo Cimento, 5, 56, 1967.

259. Paul, W. and STEINWEDEL, H., Z. Naturforsch , 8a , 448 , 1953.